



Strålsäkerhets
myndigheten

Swedish Radiation Safety Authority

Authors:

Paul Scott
Robert Kurth
Andrew Cox
Rick Olson
Dave Rudland

Research

2010:46

Development of the PRO-LOCA Probabilistic Fracture Mechanics Code,
MERIT Final Report

Title: : Development of the PRO-LOCA Probabilistic Fracture Mechanics Code, MERIT Final Report.
Report number: 2010:46
Author: Paul Scott¹, Robert Kurth¹, Andrew Cox¹, Rick Olson¹ and Dave Rudland²
¹Battelle Columbus, USA , ²Nuclear Regulatory Commission, USA.
Date: December 2010

This report concerns a study which has been conducted for the Swedish Radiation Safety Authority, SSM. The conclusions and viewpoints presented in the report are those of the authors and do not necessarily coincide with those of the SSM.

Background

The MERIT project has been an internationally financed program with the main purpose of developing probabilistic models for piping failure of nuclear components and to include these models in a probabilistic code named PRO-LOCA.

Objectives of the project

The principal objective of the project has been to develop probabilistic models for piping failure of nuclear components and to include these models in a probabilistic code.

Results

The MERIT program has produced a code named PRO-LOCA with the following features:

- Crack initiation models for fatigue or stress corrosion cracking for previously unflawed material.
- Subcritical crack growth models for fatigue and stress corrosion cracking for both initiated and pre-existing circumferential defects.
- Models for flaw detection by inspections and leak detection.
- Crack stability.

The PRO-LOCA code can thus predict the leak or break frequency for the whole sequence of initiation, subcritical crack growth until wall penetration and leakage, instability of the through-wall crack (pipe rupture). The outcome of the PRO-LOCA code are a sequence of failure frequencies which represents the probability of surface crack developing, a through-wall crack developing and six different sizes of crack opening areas corresponding to different leak flow rates or LOCA categories. Note that the level of quality assurance of the PRO-LOCA code is such that the code in its current state of development is considered to be more of a research code than a regulatory tool.

Effects on SSM supervisory and regulatory task

The results of this project will be used by SSM for the assessment of detected cracks in nuclear piping components. It can also be used for guidance of locations in risk-informed procedures for in-service inspection.

Project information

Project leader at SSM: Björn Brickstad

Project number: SSM 2008/37

Project Organization: Battelle Columbus has managed the project with Paul Scott as the project manager. The project has been financed by an international consortium representing Canada, Sweden, South Korea, United States and United Kingdom.

TABLE OF CONTENTS

TABLE OF CONTENTS	i
EXECUTIVE SUMMARY	iii
ACKNOWLEDGMENTS	vi
1.0 INTRODUCTION	1-1
2.0 DESCRIPTION OF PRO-LOCA CODE	2-1
2.1 Probabilistic Framework	2-1
2.2 Geometric Model	2-15
2.3 Time Scale	2-16
2.4 Material Properties	2-16
2.5 Loads and Stresses	2-18
2.6 Pre-Existing Flaws.....	2-24
2.7 Crack Initiation Models	2-30
2.8 Subcritical Crack Growth Models (Dave to Review thoroughly)	2-44
2.9 Crack Coalescence.....	2-56
2.10 Crack Stability.....	2-57
2.11 Leak Rate	2-61
2.12 Credit for Inspections	2-68
2.13 Program Output	2-68
2.14 Graphical User Interface (GUI)	2-71
2.15 References.....	2-71
3.0 Quality Assurance Checks and Sensitivity Analyses	3-1
3.1 Modular QA Checks	3-1
3.2 Sensitivity Analyses	3-19
3.3 Comparison of Results from Monte-Carlo Simulations and the Discrete Probability Method.....	3-46
3.4 References	3-47
4.0 DISCUSSION OF RESULTS	4-1
4.1 Comparison of Results between PRO-LOCA and other PFM Codes.....	4-1
4.2 Discussion of Results from Modular QA Checks	4-7
4.3 Discussion of Results from Sensitivity Analyses.....	4-7

4.4 Key Parameters Affecting LOCA Probabilities	4-17
4.5 Current Limitations and Shortcomings of PRO-LOCA	4-18
4.6 References	4-21
5.0 CONCLUSIONS	5-1
APPENDIX A DETAILS OF THE DEVELOPMENT OF GEOMETRIC SPECIFIC WELD RESIDUAL STRESS DISTRIBUTIONS INCLUDED IN PRO-LOCA	A-1
A.1 Introduction	A-1
A.2 Weld Analysis Procedure	A-2
A.3 Dissimilar Metal Weld Results	A-8
A.4 Stainless Steel Weld Results	A-20
A.5 Summary of Results	A-28
A.6 References	A-31
APPENDIX B OTHER MERIT DELIVERABLES	B-1
B.1 Updated SQUIRT Leak Rate Code	B-1
B.2 Databases	B-1

EXECUTIVE SUMMARY

The MERIT (Maximizing Enhancements in Risk-Informed Technology) program was a 3 year international collaborative research program whose main objective was the further development of the PRO-LOCA probabilistic fracture mechanics (PFM) code. While significant improvements have been made to PRO-LOCA as part of the MERIT program, it is still considered a research code and any use of PRO-LOCA must factor that into consideration.

The membership in MERIT included the US Nuclear Regulatory Commission (NRC), the Electric Power Research Institute (EPRI), SSM in Sweden, Rolls Royce in the United Kingdom, a consortium of interests in Canada, and a consortium of interests in South Korea. The PRO-LOCA PFM code was originally developed for the US NRC as part of their re-evaluation of the emergency core cooling system (ECCS) requirements in 10 CFR 50.46. It was envisioned that PRO-LOCA would be used by the NRC on a periodic basis (i.e., every 10 years) as a tool to re-evaluate the break frequency versus break size curves which formed the technical basis for the transition break size (TBS) definition in the proposed rule change to 50.46, i.e., 10 CFR 50.46a. Other potential uses for PRO-LOCA include: (1) a general purpose PFM code for assisting with leak-before-break (LBB), or extremely low probability of rupture (XLPR), assessments, (2) a flaw assessment tool for helping to evaluate the failure probability of a piping system once a flaw is detected in service, and (3) a tool to help with the prioritization of plant maintenance activities, such in-service inspections (ISI). The PRO-LOCA code incorporates many enhancements in technology developed since some of the earlier probabilistic codes (e.g., PRAISE) were developed. Those enhancements include:

- improved crack stability analyses,
- improved leak rate models,
- new material property data,
- new degradation mechanisms including the addition of primary water stress corrosion cracking (PWSCC) for dissimilar metal welds (DMWs) in pressurized water reactors (PWRs),
- updated crack initiation and growth models,
- updated weld residual stress distributions,
- updated repair schemes,
- additional user defined input parameters, e.g., user defined weld residual stress distributions, user defined crack growth laws, user defined material data, user defined crack morphology parameters, and user defined random seed,
- alternative crack initiation models, e.g., single versus multiple crack initiation analyses and arrival rate models,
- alternative inspection and probability of detection (POD) routines,
- allowing a variable stress distribution around the pipe circumference,
- advanced probabilistic routines, e.g., discrete probability methods, including importance sampling, in addition to Monte Carlo simulation,
- incorporating bootstrap methods for predicting confidence limits to provide insights into the variability of results, and
- an updated graphical user interface (GUI) to reflect the most up-to-date changes to PRO-LOCA.

Section 2 of this report provides a detailed description of the technical basis for PRO-LOCA; both the probabilistic framework and the deterministic modules that make up PRO-LOCA. As part of this description of the technical basis for PRO-LOCA, the enhancements made to PRO-LOCA as part of MERIT are discussed in detail.

Section 3 of this report presents the results from the quality assurance (QA) checks that have been conducted as part of this program and the earlier NRC Large Break LOCA program. Modular QA checks have been conducted on most of the deterministic modules in PRO-LOCA to help ensure that the individual algorithms programmed into PRO-LOCA were programmed correctly. For example, results from the LBB.ENG2 through-wall crack stability module in PRO-LOCA were compared with results from the LBB.ENG2 J-estimation scheme in NRCPIPE, and exact agreement was found. Similar type comparisons were made for most of the deterministic modules in PRO-LOCA, e.g., surface and through-wall crack K-solutions, IGSCC and PWSCC initiation and growth modules, fatigue crack growth modules, surface crack stability modules, and leak rate module, and the agreement in those cases was excellent as well. A number of sensitivity analyses were also conducted. Those results are also presented in Section 3. A base case problem was solved and then individual input parameters were systematically changed to ascertain the effect of each of those input parameters on the resultant break probabilities. These analyses served two purposes. One, they helped identify coding errors in cases where the resultant changes in probabilities make little or no physical sense. Two, they helped identify the major risk factors in these types of probabilistic analyses by identifying which input parameters have the greatest effect on the predicted break probabilities.

Section 4 of this report discusses the results from these QA assessments and sensitivity analyses. Two parameters which seem to have a large effect on the LOCA probabilities are water chemistry for the BWRs and operating temperature of the PWRs. The operating temperature of the PWR was especially significant, where a 22 C (40 F) drop in temperature resulted in a 3 or 4 order magnitude decrease in the LOCA probabilities. Both of these parameters (water chemistry and temperature) effect both crack initiation and crack growth. Static bending stress, which also affects the crack initiation and growth characteristics, also had a significant effect on the LOCA probabilities. For the BWRs increasing the static bending stress from 20 MPa (3 ksi) to 50 MPa (7 ksi) resulted in a 1 ½ order of magnitude increase in the Category 2 LOCAs and a 3 order of magnitude increase in the Category 3 LOCAs. Similarly, doubling the static bending stress for the PWRs resulted in a 1 ½ order of magnitude increase in the Category 2 LOCAs and almost a 2 order of magnitude increase in the Category 3 LOCAs.

While inspection parameters had an effect on the LOCA probabilities, their impact did not seem to be as significant as those parameters which affect crack initiation and growth. Increasing the inspection interval from 10 to 20 years caused an order of magnitude or less increase in the LOCA probabilities. In a similar vein improving the quality of the POD curve caused a reduction in the LOCA probabilities although the impact was not that significant. To achieve a comparable order of magnitude decrease in LOCA probability required reducing the probability of detection by a factor of four. When a more realistic reduction in POD was assumed, the effect on the LOCA probabilities was relatively minor. A related parameter to inspection is leakage detection limit. The results for leakage detection limit are somewhat counter intuitive. For the analyses conducted as part of this effort, leakage detection limit does not seem to have that big of an effect on the resultant LOCA probabilities. This finding deserves further exploration.

In contrast to those parameters which affect crack initiation and crack growth, those parameters which affect crack stability did not seem to have as much of an effect on the LOCA probabilities. Neither material strength nor toughness had much of an affect on the LOCA probabilities. Even when the fracture toughness was decreased by a factor 20, the effect on the LOCA probabilities was relatively minor. Another parameter which would affect crack stability is an earthquake. The addition of an earthquake to the PWR load history resulted in about a one order of magnitude increase in the LOCA probabilities. While this seems significant it was shown that the magnitude of this earthquake was quite severe. With a more representative earthquake, the effect of the

earthquake would be expected to be less. The report concludes with a conclusion section in Section 5.

While PRO-LOCA represents a significant advancement in the technology, there is still work to be done. When PRO-LOCA was initially developed, the plan was to incorporate the latest state-of-art deterministic models into a probabilistic framework. Older deterministic methods such as limit load analyses for crack stability were replaced by the latest, most up to date methods such as J-estimate scheme routines based on elastic-plastic fracture mechanics principles. To facilitate and expedite this approach, the plan called for using legacy codes where available. As such, major sections of such legacy codes as SQUIRT, NRCPIPE and NRCPIPES were incorporated in their entirety into PRO-LOCA. While this sped up the developmental process, it did create a situation where a great deal of extraneous code was embedded within PRO-LOCA. This extraneous code has turned out to be somewhat problematic to the developmental process. Furthermore, some of the legacy variable definition has proved troublesome as the same parameter has a different variable name in different legacy codes. There have also been issues with some of the common block definitions. Finally, this legacy code was found to increase the run times for PRO-LOCA.

A further general limitation with PRO-LOCA is the level of quality assurance behind it. For example, as described in Section 3.1, a number of the deterministic modules in PRO-LOCA were subjected to some QA. However, the level of that QA and the overall QA for PRO-LOCA are not to the level required by ASME NQA-1. Part I of NQA-1-2008, *Quality Assurance Requirements for Nuclear Facility Applications*, is organized as 18 separate requirements to mirror the 18-criteria structure of 10 CFR Part 50 Appendix B, *Quality Assurance Criteria for Nuclear Power Plants and Fuel Reprocessing Plants*, and, as such is intended to meet and implement the requirements of Appendix B. As a result of this lack of QA and the general lack of user experience, PRO-LOCA in its current state of development is considered to be a research code and any use of PRO-LOCA must factor that into consideration.

ACKNOWLEDGMENTS

The MERIT (Maximizing Enhancements in Risk Informed Technology) program was an international cooperative research program conducted at Battelle with assistance from staff at Engineering Mechanics Corporation of Columbus (Emc²). There were a total of six members in this international group. The member countries and their respective Technical Advisory Group (TAG) representatives were:

Canada	Mr. Michael Kozluk
Korea	Dr. Young Choi
Sweden	Dr. Bjorn Brickstad
United Kingdom	Dr. Tracey Cool
United States	
Electric Power Research Institute	Mr. Paul Crooker
Nuclear Regulatory Commission	Dr. Al Csontos

The authors would like to thank not only the MERIT TAG members, but also their numerous colleagues in their individual countries who made many valuable suggestions for improving PRO-LOCA.

1.0 INTRODUCTION

The MERIT (Maximizing Enhancements in Risk-Informed Technology) program is a 3 year multi-client international research program whose main objective was the further development of the PRO-LOCA probabilistic fracture mechanics (PFM) code. The membership in MERIT includes the US Nuclear Regulatory Commission (NRC), the Electric Power Research Institute (EPRI), SSM in Sweden, Rolls Royce in the United Kingdom, a consortium of interests in Canada, and a consortium of interests in South Korea. The PRO-LOCA PFM code was originally developed for the US NRC as part of their re-evaluation of the emergency core cooling system (ECCS) requirements in 10 CFR 50.46. It was envisioned that PRO-LOCA would be used by the NRC on a periodic basis (i.e., every 10 years) as a tool to re-evaluate the break frequency versus break size curves which formed the technical basis for the transition break size (TBS) definition in the proposed rule change to 50.46, i.e., 10 CFR 50.46a. Other potential uses for PRO-LOCA include: (1) a general purpose PFM code for making leak-before-break (LBB), or extremely low probability of rupture (XLPR), assessments, (2) a flaw assessment tool for evaluating the failure probability of a piping system once a flaw is detected in service, and (3) a tool to help with the prioritization of maintenance activities, such as in-service inspections (ISI).

As part of the MERIT program a number of enhancements have been made to the PRO-LOCA code. Section 2 of this report provides a detailed description of the technical basis for PRO-LOCA; both the probabilistic framework and the deterministic modules that make up PRO-LOCA. As part of this description of the technical basis for PRO-LOCA, the enhancements made to PRO-LOCA as part of MERIT and the earlier NRC Large Break LOCA program are discussed. Section 3 of this report discusses the quality assurance (QA) checks and sensitivity analyses that have been conducted as part of this program and the earlier NRC program. Modular QA checks have been conducted on most all of the deterministic modules in PRO-LOCA to ensure that the individual algorithms programmed into PRO-LOCA were programmed correctly. For example, results from the LBB.ENG2 through-wall crack stability module in PRO-LOCA were compared with results from the LBB.ENG2 J-estimation scheme in NRCPIPE, and exact agreement was found. Similar type comparisons were made for most all of the deterministic modules in PRO-LOCA, e.g., surface and through-wall crack K-solutions, IGSCC and PWSCC initiation and growth modules, fatigue crack growth modules, surface crack stability modules, and the leak rate module, and the agreement in those cases was excellent as well. A number of sensitivity analyses were also conducted. As part of the main series of analyses, a base case problem was solved and then individual input parameters were systematically changed to ascertain the effect of each of those input parameters on the resultant LOCA probabilities. These analyses served two purposes. One, they helped identify coding errors in cases where the resultant changes in probabilities made little or no physical sense. Two, they helped identify the major risk factors in these types of probabilistic analyses by identifying which input parameters had the greatest effect on the predicted break probabilities. Section 4 of this report discusses the results from the QA assessments and the various sensitivity analyses conducted. Finally, the major conclusions reached regarding PRO-LOCA are discussed in Section 5.

In addition, there are two appendices to this report. Appendix A provides the details of the development of the geometric specific weld residual stress distributions included in PRO-LOCA. Appendix B is a brief description of the other major deliverables (other than PRO-LOCA, its GUI (graphical user interface) and its Users Manual) delivered as part of the MERIT program. These other deliverables include an updated SQUIRT leak rate code. SQUIRT was updated as part of this program to address a number of known issues with SQUIRT that had been identified with its increasing use. In addition, a new transition flow model to handle the flow regime between the single phase orifice flow regime and the two-phase flow regime governed by the Henry-Fauske model was developed and incorporated in SQUIRT. This transition flow model is discussed in

Section 2 of this report. Other deliverables from the MERIT program are an updated CIRCUMCK pipe fracture experiment database and a new leak rate experiment database.

2.0 DESCRIPTION OF PRO-LOCA CODE

This section of the report provides the technical basis for the PRO-LOCA code.

2.1 Probabilistic Framework

The user of the PRO-LOCA code has the option of a number of different probabilistic simulation schemes to choose from. In addition to the traditional Monte-Carlo simulation, the user of PRO-LOCA also has the option of using discrete probability methods, including importance sampling, when they want to predict very low probability events (on the order of 10^{-8} events).

2.1.1 Monte-Carlo Simulation

Monte-Carlo simulation (MCS) is a numerical scheme which solves a statistical problem by generating multiple deterministic scenarios of a model by repeatedly sampling values from the probability distributions for the uncertain variables and observing that fraction of the scenarios satisfying a relevant performance function or functions. The method is useful for obtaining numerical solutions to problems that are too complicated to solve analytically and can be used for any number of random parameters.

For the large break LOCA (LB-LOCA) problem, consider a generic n -dimensional random vector, $\mathbf{X} = \{X_1, X_2, \dots, X_n\}^T$, which characterizes uncertainty in all system parameters, such as geometry, material properties, inspection scheduling, load, initial flaws, etc. Figure 2.1 shows a schematic of the relationship between input vector \mathbf{X} and the i th performance indicator (output) function $g_i(\mathbf{X})$. The details of this output function are described in Section 2.13.



Figure 2.1 Relationship between the input random vector \mathbf{X} and the vector of output performance function $g_i(\mathbf{X})$

To determine the occurrence probability of the i th performance indicator $g_i(\mathbf{X})$, the MCS method involves the following three steps: (1) generation of independent samples of the input random variables from their probability distributions, (2) calculation of a relevant performance function of the LOCA system, and (3) evaluation of the probability of occurrence of the performance function.

2.1.1.1 Step 1 – Sampling Phase

Let $\mathbf{x}^{(1)}, \mathbf{x}^{(2)}, \dots, \mathbf{x}^{(N)}$ denote independent realizations (samples) of random input \mathbf{X} , where N is the sample size for MCS. For simplicity, consider the i th component X_i of input vector \mathbf{X} with the cumulative probability distribution function, $F_{X_i}(x_i)$. Let Z_i be a random variable uniformly distributed in the interval $[0,1]$ and has the cumulative probability distribution function $F_{Z_i}(z_i) = z_i$. For a probability preserving transformation with the distribution functions of X_i and Z_i being equal, the realization x_{i_s} of random variable X_i , can be obtained as

$$x_i = F_{X_i}^{-1}(z_i) \quad (2.1)$$

A two-step simulation technique can be developed based on this transformation. The steps are

- A sample z_i of Z_i is generated, e.g., by using a standard random number generator available in any computer, and
- A sample x_i of X_i can be obtained from Equation 2.1. Thus, by generating independent samples of Z_i , one can obtain from Equation 2.1 independent samples of X_i .

Hence, any random variable with any known distribution function can be easily generated using the transformation in Equation 2.1. For illustration purposes, transformation equations for random variables with *normal* and *log-normal* probability distributions are described below.

Normal Distribution: $N \sim (\mu_i, \sigma_i^2)$

$$\text{PDF: } f_{X_i}(x_i) = \left[1 / (\sqrt{2\pi} \sigma_i) \right] \exp \left[-0.5 \{ (x_i - \mu_i) / \sigma_i \}^2 \right] \quad (2.2)$$

Parameters: μ_i = mean; σ_i = standard deviation

$$\text{CDF: } F_{X_i}(x_i) = \int_{-\infty}^x f_{X_i}(x_i) dx_i = \Phi \left[(x_i - \mu_i) / \sigma_i \right] \quad (2.3)$$

Φ is the CDF of standard normal random variable

$$\text{Transformation: } x_i = \mu_i + \sigma_i \Phi^{-1}(z_i) \quad (2.4)$$

Log-normal Distribution: $LN \sim (\mu_i, \sigma_i^2)$

$$\text{PDF: } f_{X_i}(x_i) = \left[1 / (\sqrt{2\pi} x_i \tilde{\sigma}_i) \right] \exp \left[-0.5 \{ (\ln x_i - \tilde{\mu}_i) / \tilde{\sigma}_i \}^2 \right] \quad (2.5)$$

Parameters: μ_i = mean; σ_i = standard deviation; $V_i = \sigma_i / \mu_i$

$$\text{CDF: } F_{X_i}(x_i) = \int_{-\infty}^x f_{X_i}(x_i) dx_i = \Phi \left[(\ln x_i - \tilde{\mu}_i) / \tilde{\sigma}_i \right] \quad (2.6)$$

$$\tilde{\sigma}_i = \sqrt{\ln(1 + V_i^2)}; \quad \tilde{\mu}_i = \ln \mu_i - \tilde{\sigma}_i^2 / 2$$

Φ is the CDF of standard normal random variable

$$\text{Transformation: } x_i = \exp \left[\tilde{\mu}_i + \tilde{\sigma}_i \Phi^{-1}(z_i) \right] \quad (2.7)$$

In the original version of PRO-LOCA, external subroutines such as RNSET, RNGET, DRNUNF, DRNNOF, DRNWIB, and DSCAL from IMSL were used for random number generation. These routines have all been replaced by sampling procedures written at Battelle Memorial Institute so that a wider variety of distributions can be used and so that IMSL licenses are not an issue for any user.

A couple notes should be made about the sampling phase.

- Sampling occurs:
 - At the beginning of each Monte-Carlo simulation, and
 - At times during the plant history when a critical node is removed from service due to inspection or leak detection.

- From the sampling, a timeline history of cracks initiated and loads on the critical node can be formed. The sampled variables include:
 - Material properties
 - Yield, tensile, Ramberg-Osgood, J-R curve, and
 - Fatigue and SCC growth exponents and coefficients
 - Occurrence of transients
 - Cracks and Detection
 - Fatigue and SCC time to initiations (and fatigue crack sizes),
 - Pre-existing defects,
 - POD, and
 - Leak rate detection limit.

2.1.1.2 Step 2 – Repeat Evaluations

Following generation of input samples $\mathbf{x}^{(1)}, \mathbf{x}^{(2)}, \dots, \mathbf{x}^{(N)}$, let $g_i^{(1)}, g_i^{(2)}, \dots, g_i^{(N)}$ denote the corresponding samples of the i th performance function (output) $g_i(\mathbf{X})$ of the LB-LOCA system that can be obtained from

$$g_i^{(j)} = g_i(\mathbf{x}^{(j)}); j = 1, 2, \dots, N \quad (2.8)$$

Hence, all output samples of $g_i(\mathbf{X})$ can be obtained by conducting repeated deterministic evaluation of the performance function $g_i(\mathbf{X})$, as schematically described in Figure 2.1.

2.1.1.3 Step 3 – Determining Probabilities

Define N_f as the number of trials (analyses) that are associated with occurrence of the i th performance indicator function. Then, the probability of occurrence of the performance indicator P_i can be estimated by

$$P_i \equiv \Pr[g_i(\mathbf{X})] \cong \frac{N_f}{N} ; i = 1, 2, \dots, m, \quad (2.9)$$

which approaches the exact value when N approaches infinity. In general, the minimum required number of trials (analyses) N must be at least $10/P_i$ for a 30-percent coefficient of variation of the estimator.

2.1.2 Discrete Probability Distribution Method

Classically importance sampling methodologies have been employed in Monte Carlo simulations to assess low probability events. More recently adaptive methodologies for transformed density functions have been developed (Refs. 2.1, 2.2). Importance sampling methods for Monte Carlo become nearly intractable for complex engineering systems because it becomes increasingly difficult to remove the weighting function from the response sample. Adaptive methodologies provide fast, accurate answers for analytic functions. Unfortunately most engineering analysis does not employ analytic functions. In those cases, the standard practice is to employ response surfaces (Ref. 2.3) and analyze this approximation. The response surface will introduce a (usually) unquantifiable source of uncertainty unless one performs a Monte Carlo analysis to assess the uncertainty. In that case the adaptive methodology is useful if it is going to be employed for various distribution types and parameters.

A third option is the use of discrete probability distributions (DPDs). In this analysis, the input distribution, if it is analytically described, is discretized into a finite number of values, each value having an associated probability. If the number of discrete values is denoted as N_{BIN} and there are N_V inputs to the analysis then to obtain the response DPD would require $(N_{\text{BIN}})^{N_V}$ calculations. For 100 discrete values and five input variables this would lead to 10,000,000,000 calculations. Clearly this would be no more efficient than the Monte Carlo analysis. However, if one treats the discrete space in the same manner as the continuous space one can employ a Monte Carlo sampling of the discrete space to obtain an estimate of the response DPD. In fact, the same statistical analysis procedures used for polling can be used (Ref. 2.4). The distinct advantage that this method has over polling is that one knows, *a priori*, what the value of each discrete point is as well as its probability! The advantage of this procedure in engineering analysis is that the input DPD can be discretized so that the probability of the input value occurring is not made to be equal at each discrete point. For example, the first value and last values of the DPD can be set equal to the 1 in 10,000 value. The placement of the points in between these limits is set according to an optimization algorithm. By placing the lumped probability mass at the interval conditional mean points the error in using the discrete point will be canceled out from the expectation calculations.

One can illustrate the advantages and disadvantages of these methodologies by examining a theoretical example in which the response surface can be analytically calculated and comparisons of the DPD methodology to Monte Carlo and adaptive importance sampling analysis can be made. In this example it is demonstrated how events with probabilities of less than 1 in 1,000,000 can be estimated using 2,000 samples of the discrete space.

The goal of nearly any engineering system analysis is to calculate the response of a system to a variety of input values. One denotes the response of the system as \mathcal{R} , the inputs to the analysis as the vector \mathbf{x} , and the relationship between \mathcal{R} and \mathbf{x} as f . Then

$$\mathcal{R} = f(\mathbf{x}), \quad \mathbf{x} = (x_1, x_2, \dots, x_N) \quad (2.10)$$

The function f may be *or may not* be analytic. Thus f could represent a complex computer analysis, e.g. PROLOCA. The input vector \mathbf{x} may have one, or more, components that are random variables. To begin one uses an overly simplified example to discuss the methods without becoming bogged down in the details of the engineering analysis.

The example selected is the addition of two random variables. Specifically

$$\mathcal{R} = x_1 + x_2 \quad (2.11)$$

If both of the inputs can be represented by a normal distribution with a mean value of μ_k and a standard deviation of σ_k for k equal to 1 and 2 then one can write down the mean and variance for \mathcal{R} immediately.

$$\mu_{\mathcal{R}} = \mu_1 + \mu_2 \quad (2.12)$$

$$\sigma_{\mathcal{R}}^2 = \sigma_1^2 + \sigma_2^2 \quad (2.13)$$

In the classic Monte Carlo analysis one generates a random number, obtain the value of x_1 by inverting the normal distribution Cumulative Density Function (CDF), generate a second random number, obtain the value of x_2 by inverting the normal distribution CDF, and add the two numbers. This will generate a value for \mathcal{R} that one denotes R_1 . One continues to do this many times to generate a vector of responses denoted $\mathbf{R} = (R_1, R_2, \dots, R_M)$. As M approaches infinity the CDF for the response \mathcal{R} will be approached. Of course if one is trying to calculate the extreme tails of the response distribution one will need, on the average, many, many samples. For the addition of two random variables this is not a very severe limit with today's computers so one will ignore this for the moment. It will become critical when one returns to realistic engineering analysis contained in PROLOCA.

An alternative method for generating the response CDF is to limit our calculations to points in the discrete space. In this case one defines a Discrete Probability Density (DPD) function for each of the inputs. Thus

$$x_1 = \{(x_{1,1}, p_{1,1}), (x_{1,2}, p_{1,2}), \dots, (x_{1,N_{BIN}}, p_{1,N_{BIN}})\} \quad (2.14)$$

$$x_2 = \{(x_{2,1}, p_{2,1}), (x_{2,2}, p_{2,2}), \dots, (x_{2,N_{BIN}}, p_{2,N_{BIN}})\} \quad (2.15)$$

The response DPD is constructed by taking all possible combinations of the input DPDs. Thus

$$\begin{aligned} R_1 &= (x_{1,1} + x_{2,1}, p_{1,1} * p_{2,1}) \\ R_2 &= (x_{1,1} + x_{2,2}, p_{1,1} * p_{2,2}) \\ &\dots \\ R_{N_{BIN}} &= (x_{1,1} + x_{2,N_{BIN}}, p_{1,1} * p_{2,N_{BIN}}) \\ R_{N_{BIN}+1} &= (x_{1,2} + x_{2,1}, p_{1,2} * p_{2,1}) \\ R_{N_{BIN}+2} &= (x_{1,2} + x_{2,2}, p_{1,2} * p_{2,2}) \\ &\dots \\ R_{N_{BIN}^2} &= (x_{1,N_{BIN}} + x_{2,N_{BIN}}, p_{1,N_{BIN}} * p_{2,N_{BIN}}) \end{aligned} \quad (2.16)$$

One knows the resulting DPD is a Probability Density Function since

$$\begin{aligned} p_i p_j &\leq 1 \forall i, j \\ \int_{-\infty}^{\infty} P dP &= \sum_{I=1}^{N_{BIN}} \sum_{J=1}^{N_{BIN}} p_I p_J = \sum_{I=1}^{N_{BIN}} p_I \sum_{J=1}^{N_{BIN}} p_J = \sum_{I=1}^{N_{BIN}} p_I = 1 \end{aligned} \quad (2.17)$$

are the two conditions which must be satisfied in order for a function to be a PDF. Let's begin by examining a three point discretization of the normal distribution.

For a mean value of 10.0 and a standard deviation of 1.0 one knows that 33% of the probability lies between negative infinity and $\mu - 0.42\sigma$ (approximately). The next 33% lies between $\mu - 0.42\sigma$ and $\mu + 0.42\sigma$ (again approximately). The remaining 33% lies between $\mu + 0.42\sigma$ and plus infinity. But one must ask where should this probability mass actually be placed. For the mean and standard deviation assumed, the end points are $(-\infty, 9.58)$, $(9.58, 10.42)$, and $(10.42, \infty)$.

Table 2.1 Three point DPD for $N(\mu, \sigma) = N(10, 1)$

x_i	p_i
8.909	0.33334
10.000	0.33333
11.091	0.33334

If the probability mass is placed at these endpoints an artificial bias will be introduced into the response PDF. If one places the probability mass at the *conditional mean of the interval* then, on the average, 50% of the time the value will be too large and 50% of the time the value will be too small, the error canceling out *on the average*.

Three Point Discrete Probability Distribution Comparison to Theoretical Values

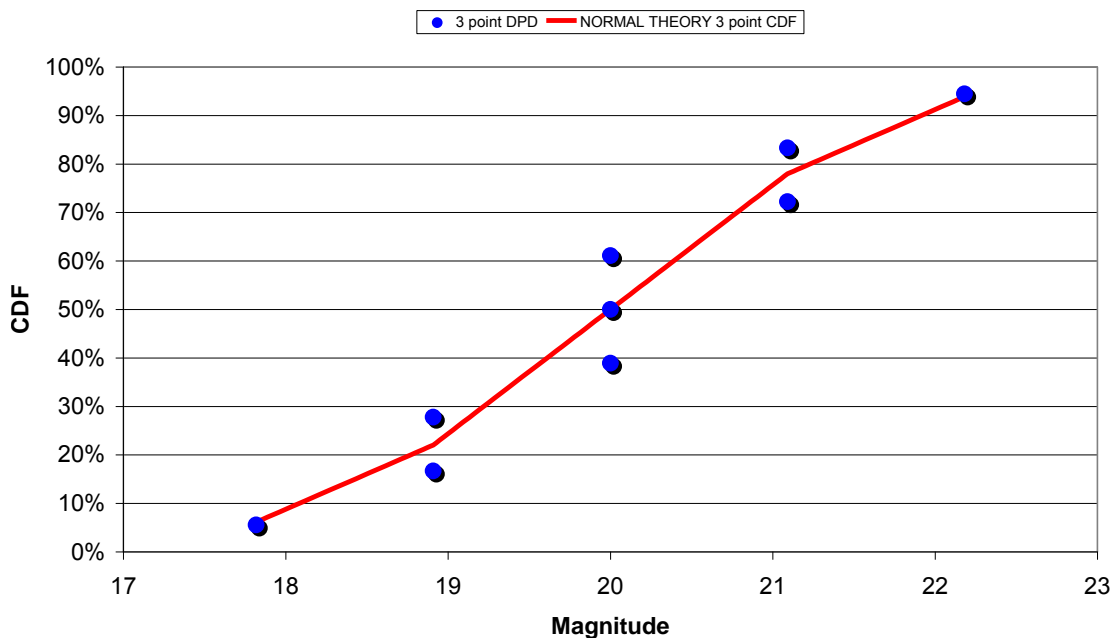


Figure 2.2 Three point DPD calculations

2.1.3 Importance Sampling in the Discrete Space

While the previous example is overly simplified to demonstrate the concept there is, theoretically, no upper limit to the number of bins that are used to define the individual DPD. Thus one could use 1,000,000 discrete intervals leading to $1,000,000^2$ or 1,000,000,000,000 points in a two variable problem. In the case of N input variables and M bins there would be M^N possible responses. For a simple problem, in which there are less than 100 bins and only two variables the entire PDF of the response can be calculated. However, for more complex problems where there may be 10 variables and 100 bins describing the PDF one would have 10^{20} (100^{10}) possible outcomes. In this case one can use the identical strategy used in Monte Carlo analysis but instead of sampling from the continuous space one samples from the discrete space, i.e. from the 10^{20} values.

Because the number of values is finite (albeit a large finite number) one can use the same theory used to do census sampling to obtain the PDF of the response to as high an accuracy as desired. (see for example Reference 2.4).

Even more importantly one can change the way in which the individual DPD's for the input PDF is generated. Rather than using *equal* probability intervals one uses *unequal* probability intervals to perform importance sampling. The following section provides an example.

2.1.4 Sample Calculation of Importance Sampling Calculations

A simple example is the addition of two normal distributions. In this case we know that the response mean is equal to the sum of the two input mean values and the variance of the response is equal to the sum of the input variances. Thus the theoretical distribution of the response CDF can be calculated analytically and then compared with the DPD methodology output and the Monte Carlo output.

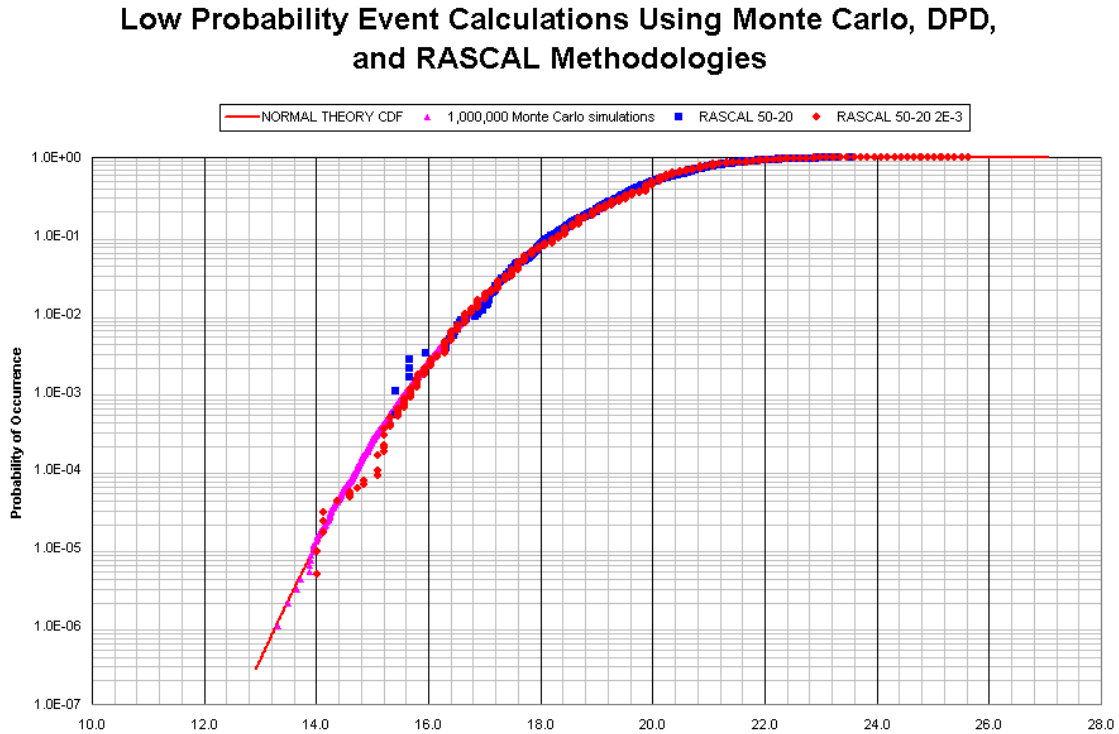


Figure 2.3 Comparison of the response CDF as calculated by Monte Carlo and RASCAL to theory

One adds two random variables with a mean of 10 and a standard deviation of 1.0. One can calculate the response CDF theoretically. One compares this theoretical prediction to

1. Monte Carlo analysis using 1,000,000,000 samples
2. RASCAL analysis using 50 bins of equal probability and 20 samples
3. RASCAL analysis using the first and last bin of 2.0×10^{-3} .

Figure 2.3 shows the resulting calculations. Looking at the entire CDF does not give a very good picture and so one examines the tails of the distribution. In this case the CDF look very similar. Therefore, Figure 2.4 shows the tails of the distribution. In this figure one can see that the use of bin weighting for the DPD method allowed accurate estimates of the tails of the distribution using 1,000 less calculations.

Low Probability Event Calculations Using Monte Carlo, DPD, and RASCAL Methodologies

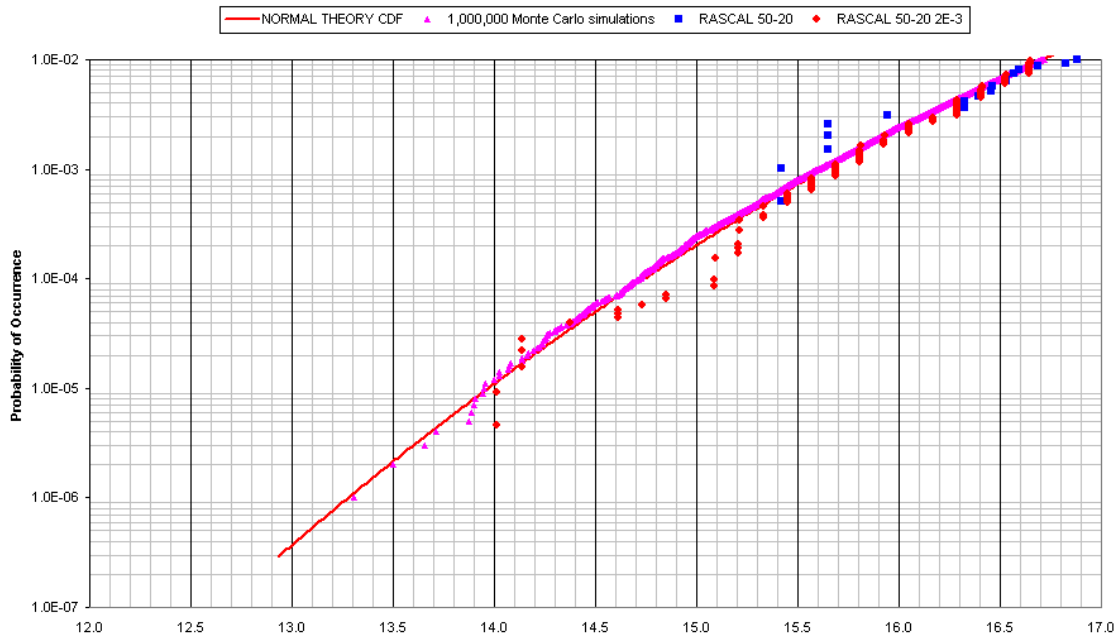


Figure 2.4 Tails of the distribution for Monte Carlo and RASCAL analyses comparison to theory

2.1.5 Alternative Distributions

PROLOCA 2008 has been updated from the 2005 version by allowing the user to input additional distribution types. These distributions are described below and in Table 2.2.

The choice of distributions include:

- Constant
- Uniform
- Normal
- Lognormal
- Weibull
- Exponential
- Extreme Value Type II

Table 2.2 Description of distributions included in PRO-LOCA

Distribution	PDF	CDF	Mean	Variance
Uniform	$f(x) = \frac{1}{b-a}$ $a \leq x \leq b$ $f(x) = 0$ $x < a \text{ or } x > b$	$F(x) = 0$ $x < a$ $F(x) = \frac{x-a}{b-a} \quad a \leq x \leq b$ $F(x) = 1$ $x > b$	$\mu = \frac{a+b}{2}$	$\sigma^2 = \frac{(b-a)^2}{12}$
Normal	$f(x) = \frac{1}{\sigma\sqrt{2\pi}} e^{-\frac{(x-\mu)^2}{2\sigma^2}}$	$F(x) = \frac{1}{2} \left(1 + \operatorname{erf} \left(\frac{x-\mu}{\sigma\sqrt{2}} \right) \right)$	μ	σ
Lognormal	$f(x) = \frac{1}{x\sigma\sqrt{2\pi}} e^{-\frac{(\ln(x)-\mu)^2}{2\sigma^2}}$	$F(x) = \frac{1}{2} + \frac{1}{2} \operatorname{erf} \left[\frac{\ln(x)-\mu}{\sigma\sqrt{2}} \right]$	$\mu = e^{\left(\frac{\mu+\sigma^2}{2} \right)}$	$\sigma^2 = (e^{\sigma^2} - 1)e^{(2\mu+\sigma^2)}$
Weibull	$f(x) = \frac{\beta}{\eta} \left(\frac{x}{\eta} \right)^{\beta-1} e^{-\left(\frac{x}{\eta} \right)^\beta}$	$F(x) = 1 - e^{-\left(\frac{x}{\eta} \right)^\beta}$	$\mu = \eta \Gamma \left(1 + \frac{1}{\beta} \right)$	$\sigma^2 = \eta^2 \left\{ \Gamma \left(1 + \frac{2}{\beta} \right) - \Gamma^2 \left(1 + \frac{1}{\beta} \right) \right\}$
Exponential	$f(x) = \lambda e^{-\lambda x}$	$F(x) = 1 - e^{-\lambda x}$	$\mu = \frac{1}{\lambda}$	$\sigma^2 = \frac{1}{\lambda^2}$
Extreme Value Type II	$f(x) = \alpha x^{-1-\alpha} e^{-x^{-\alpha}}$	$F(x) = e^{-x^{-\alpha}}$	$\mu = \Gamma \left(1 - \frac{1}{\alpha} \right) \quad \alpha > 1$	$\sigma^2 = \Gamma \left(1 - \frac{2}{\alpha} \right) - \left(\Gamma \left(1 - \frac{1}{\alpha} \right) \right)^2 \quad \alpha > 2$

2.1.5.1 Uniform Distribution

Probability Density Function

$$f(x) = \frac{1}{b-a} \quad a \leq x \leq b$$

$$f(x) = 0 \quad x < a \text{ or } x > b$$

Cumulative Distribution Function

$$F(x) = 0 \quad x < a$$

$$F(x) = \frac{x-a}{b-a} \quad a \leq x \leq b$$

$$F(x) = 1 \quad x > b$$

Mean

$$\mu = \frac{a+b}{2}$$

Median

$$\rho = \frac{a+b}{2}$$

Variance

$$\sigma^2 = \frac{(b-a)^2}{12}$$

2.1.5.2 Normal Distribution

Probability Density Function

$$f(x) = \frac{1}{\sigma\sqrt{2\pi}} e^{\left(-\frac{(x-\mu)^2}{2\sigma^2}\right)}$$

Cumulative Distribution Function

$$F(x) = \frac{1}{2} \left(1 + \operatorname{erf} \left(\frac{x-\mu}{\sigma\sqrt{2}} \right) \right)$$

Mean

$$\mu$$

Median

$$\rho = \mu$$

Variance

$$\sigma^2$$

2.1.5.3 Lognormal Distribution

Probability Density Function

$$f(x) = \frac{1}{x\sigma\sqrt{2\pi}} e^{\left[-\frac{(\ln(x)-\mu)^2}{2\sigma^2}\right]}$$

Cumulative Distribution Function

$$F(x) = \frac{1}{2} + \frac{1}{2} \operatorname{erf} \left[\frac{\ln(x) - \mu}{\sigma\sqrt{2}} \right]$$

Mean

$$\mu = e^{\left(\frac{\mu + \sigma^2}{2}\right)}$$

Median

$$\rho = e^{\mu}$$

Variance

$$\sigma^2 = (e^{\sigma^2} - 1)e^{(2\mu + \sigma^2)}$$

2.1.5.4 Weibull Distribution

Probability Density Function

$$f(x) = \frac{\beta}{\eta} \left(\frac{x}{\eta}\right)^{(\beta-1)} e^{-\left(\frac{x}{\eta}\right)^\beta}$$

Cumulative Distribution Function

$$F(x) = 1 - e^{-\left(\frac{x}{\eta}\right)^\beta}$$

Mean

$$\mu = \eta \Gamma\left(1 + \frac{1}{\beta}\right)$$

Median

$$\rho = \eta \ln(2)^{\frac{1}{\beta}}$$

Variance

$$\sigma^2 = \eta^2 \left\{ \Gamma\left(1 + \frac{2}{\beta}\right) - \Gamma^2\left(1 + \frac{1}{\beta}\right) \right\}$$

Since there is no analytic solution to invert the formulas for the η and β parameters one resorts to a Newton iteration method to calculate these values. Newton's method is:

$$x_{n+1} = x_n - \frac{f(x_n)}{\left(\frac{\partial f(x_n)}{\partial x}\right)}$$

One defines z as $1/\beta$ and write for $f(z)$:

$$f\left(\frac{1}{\beta}\right) = f(z) = (\eta - l)^2 \Gamma(1 + 2z) - (\eta - l)^2 \Gamma^2(1 + z) - \sigma^2$$

One now notes the following derivative relationships:

$$\frac{\partial \Gamma(z)}{\partial z} = \psi(z) \Gamma(z)$$

$$\frac{\partial \eta}{\partial z} = \frac{-\mu \psi(z)}{\Gamma(z)}$$

where ψ is the digamma function and Γ is the gamma function. After much algebraic manipulation one finds

$$\frac{\partial f(z)}{\partial z} = -\mu^2 \left(\frac{\psi(1+2z)\Gamma(1+2z)}{\Gamma^2(1+z)} + 2\psi(1+z) \right)$$

$$x_{n+1} = x_n + \frac{(\eta-l)^2 \Gamma(1+2z) - (\eta-l)^2 \Gamma^2(1+z) - \sigma^2}{\mu^2 \left(\frac{\psi(1+2z)\Gamma(1+2z)}{\Gamma^2(1+z)} + 2\psi(1+z) \right)}$$

The value of x_{n+1} provides a new estimate for $1/\beta$. One can then calculate η from

$$\mu = \eta \Gamma \left(1 + \frac{1}{\beta} \right)$$

All of these calculations assume that ℓ is known. This is because one is only using two equations (for the mean and standard deviation) so only two unknowns, η and β , can be calculated.

2.1.5.5 Exponential Distribution

Probability Density Function

$$f(x) = \lambda e^{-\lambda x}$$

Cumulative Distribution Function

$$F(x) = 1 - e^{-\lambda x}$$

Mean

$$\mu = \frac{1}{\lambda}$$

Median

$$\rho = \frac{\ln(2)}{\lambda}$$

Variance

$$\sigma^2 = \frac{1}{\lambda^2}$$

2.1.5.6 Extreme Value Type II (Fréchet) Distribution

Probability Density Function

$$f(x) = \alpha x^{-1-\alpha} e^{-x^{-\alpha}}$$

Cumulative Distribution Function

$$F(x) = e^{-x^{-\alpha}}$$

Mean

$$\mu = \Gamma \left(1 - \frac{1}{\alpha} \right) \quad \alpha > 1$$

Median

$$\rho = \left(\frac{1}{\ln(2)} \right)^{\frac{1}{\alpha}}$$

Variance

$$\sigma^2 = \Gamma \left(1 - \frac{2}{\alpha} \right) - \left(\Gamma \left(1 - \frac{1}{\alpha} \right) \right)^2 \quad \alpha > 2$$

2.1.6 User Defined Random Seed

The random seed can be input as a fixed number by the user allowing the code to reproduce the same calculations or it can be randomly selected by the system clock. These routines are supplied in the INTEL compiler.

2.1.7 Random Variables In PRO-LOCA

Not every variable in PRO-LOCA is random. The variable selected to be treated as random variables are shown in Table 2.3.

Table 2.3 PROLOCA random variables

Number	Parameter	Mean	Standard Dev	Distribution
1	Yield Strength	YIELDM	YIELDS	BYIELDDIST
2	Ultimate Strength	UTSM	UTSS	BUTSDIST
3	Ramberg-Osgood exponent	QNM	QNS	BNDIST
4	Ramberg-Osgood Coefficient	FM	FS	BNDIST
5	J_{lc}	JIM	JIS	WJIDIST
6	m	QMM	QMS	WMDIST
7	C	ACONTM	ACONTS	WACONTDIST
8	User Fatigue C (FCGCOEF)	AMEAN_F	STDV_F	IFCGDIST
9	User SCC C (SCGCOEF)	AMEAN_S	STDV_S	ISCGDIST
10	Fatigue crack length	FLAWMEANLEN	FLAWSLEN	IFLAWDISTLEN
11	Fatigue crack depth	FLAWMEANDEPTH	FLAWSDEPTH	IFLAWDISTDEPTH
12	Weld residual stress SIGORS	SIGORS_M	SIGORS_S	ISIGOTYP
13	Weld residual stress XC	XC_M	XC_S	IXCTYP
Crack morphology parameters				
14	Global roughness	GROUGH_M	GROUGH_S	ITYPGROUGH
15	Local roughness	LROUGH_M	LROUGH_S	ITYPLROUGH
16	Global length	GLFACT_M	GLFACT_S	ITYPGLFACT
17	Local length	LLFACT_M	LLFACT_S	ITYPLLFACT
18	Number of turns	NTL_M	NTL_S	ITYPNTL
19	SCLPAR	WEIMEANTHETA	WEISDTHETA	IWEIDISTTHETA
20	WEISLP	WEIMEANB	WEISDB	IWEIDISTB
21	Initiation time distributions			
	Weibull distribution	SCLPAR	WEISLP	4 (Weibull)
	Non-Weibull distribution	XTHETA	XBETA	ITIMEDIST
22	A182	YIELDMA182	YIELDSA182	WYIELDDIST
23	Leak Detection	Leakdetm	Leakdets	2 (Normal)

Each of the variables in Table 2.3 can be set to a deterministic value (constant —distribution”) or modeled as random via a uniform, normal, lognormal, Weibull, or extreme value distribution.

2.1.8 Parameters Hardwired into PRO-LOCA

In some cases the input parameters for PRO-LOCA can be user defined. In some cases they can be hardwired for the default models. In some cases they can be either. For instance, subunit size, crack length and crack depth are fixed in the default models, but can be input by the user in certain applications, depending on the needs of the problem and the desires of the user. Those parameters which are hardwired for the default models and their associated values are shown in Table 2.4.

Table 2.4 Hardwired parameters included in the default models of PRO-LOCA

Hardwired Parameter	Value
Geometric model	
Subunit size	Percentage of pipe circumference based on 50 mm subunit length for 28-inch diameter pipe
Time scale	
Time scale	1 month
Material Properties	
Material properties – option of using library of default values	Library of default material property values (means and standard deviations) of tensile and fracture toughness properties for both base metals and welds
Loads and Stresses	
For transients; fully reversed loading	R = -1
Weld residual stresses – option of using default weld residual stress solutions	Library of default weld residual stress solutions for 6 geometries; distribution function of distribution of yield strength
Pre-Existing Flaws	
Number of flaws per inch of weld	WinPRAISE (Ref. 2.10) equation
Flaw depths	Statistical distribution of median crack depth, shape parameter, average crack depth, and standard deviation on crack depth from Reference 2.9
Flaw lengths	Distribution on aspect ratio (a/c)
Crack Initiation	
Fatigue parameter K_N	$K_N = 2$
Initiated fatigue crack length	Lognormally distributed with medium value of 3 mm and standard deviation $\ln(b) = 0.85$
Initiated fatigue crack depth (a)	a = 3 mm
PWSCC initiated crack depth (a)	a = 3 mm
PWSCC slope parameter (b)	b = 3
Crack Growth	
Fatigue threshold ΔK_{thres}	$\Delta K_{thres} = 5 \text{ MPa}\cdot\text{m}^{1/2}$
PWSCC threshold K_{thres}	$K_{thres} = 9 \text{ MPa}\cdot\text{m}^{1/2}$
Crack Stability	
Surface crack DPZP –C” parameter	C = 32
Through-wall crack DPZP –C” parameter	C = 18.3
Complex crack DPZP –C” parameter	C = 4.6

2.2 Geometric Model

In this version of PRO-LOCA, only one location or node is analyzed during each run. If the user requires the leak probabilities for the full system, individual runs for each location are required and the probabilities must be summed to get the total probability. Typically, the worst location is used, and the failure probability is conservatively estimated by multiplying the worst-case node failure probability by the number of girth welds in the system.

In all cases, the user is allowed to choose what type of plant is to be analyzed. In the current version of PRO-LOCA, the user has four choices; PWR, BWR, BWR with hydrogen-water chemistry, and CANDU. This choice not only helps define the system to be analyzed but also sets the cracking mechanisms that will occur. In addition, the choice of hydrogen-water chemistry affects active, critical crack growth mechanisms.

The critical node analyzed is assumed to be one pipe diameter of specified size. The user is asked to input the location of the crack in the critical node. The options include base metal, manual arc welds, and inert gas welds. If a weld is chosen, it is assumed that the crack is either in the center of the girth weld or in the heat affected zone (HAZ)¹.

¹ IGSCC in BWRs typically occurs in the HAZ, and the ASME residual stress distribution was based on HAZ measurements.

In order to track the initiation and growth of defects through the plant life, the circumference of the critical node is broken into subunits. For the initial release of the code (June 2004 version), the subunit length was equal to approximately² 10 mm (0.4 inch). Each subunit was treated separately with a predefined location around the circumference. It was also assumed that each subunit experienced an identical stress field, i.e., the stresses imparted on the pipe did not vary around the circumference. For the next released version of PRO-LOCA (December 2005 version), the subunit size was changed to percentage of the pipe circumference. Sensitivity analyses suggested that the subunit size could be increased, thus decreasing the run time proportionately. Based on analysis of the Nine Mile Point IGSCC data, it was decided to fix the subunit length as a percentage of the pipe circumference. The final percentage was established on the basis of a 50 mm (2.0 inch) subunit length for the 28-inch diameter Nine Mile Point recirculation system. In addition as part of the MERIT program, the assumption that each subunit undergoes an identical stress field was changed such that the stresses imparted on the pipe do vary around the pipe circumference. Furthermore, for the user defined arrival rate model for crack initiation that is incorporated into this latest version of PRO-LOCA, the number of subunits is not fixed, but instead is predicated on the number of initiated cracks predicted based on this arrival rate model.

2.3 Time Scale

In the PRO-LOCA code, one month time increments are assumed. The code is structured so that the user can input relevant node conditions, i.e., loads, transients, etc, either before the current plant year in operation, or after the year in operation. The data input before the year in operation is considered deterministic, while the data input after is considered variable. The user can also input the year at the end of license and the year at the end of extended life.

2.4 Material Properties

For inputting material properties, the user is given two options. First they have the option of selecting the default properties from a library of materials. With this option the user will specify the material on each side of the weld. For similar metal welds, the two material selections will be the same, but for a dissimilar metal weld, the user will specify different materials on each side. In the case of a dissimilar metal weld, the user will specify which material selection will govern the tensile properties. In addition to selecting the base materials, the user will also specify the weld type, e.g., Type 304 submerge-arc weld (SAW), Type 304 tungsten-inert-gas (TIG) weld, Inconel 182 weld, etc. A library of default material property values (both means and standard deviations) has been incorporated into the PRO-LOCA code. The library includes both tensile and fracture toughness properties. The default values were based on analysis of existing material property databases, most notably the PIFRAC database (Ref. 2.5) and the database of material property values developed by Argonne National Laboratories (Ref. 2.6). The list of materials, both base metals and weld metals, for which material property values are included in this library, is shown in Table 2.5. For most of these materials, tensile and fracture toughness properties were provided at multiple temperatures. For the cases where specific material data do not exist in the library, e.g., Type 304N or A508 Class II, generic sets of material property values for generic carbon steel, stainless steel, or cast stainless steel were developed and included in the PRO-LOCA library of material properties.

² Note that the number of subunits around the circumference had to be a whole number, so the actual length of a subunit may be slightly greater than or less than 10 mm (0.4 inch) depending on the pipe geometry chosen.

Table 2.5 List of materials included in material property library in the FY05 version of PRO-LOCA

	Base Metals	Weld Metals
Carbon Steels	A106B	A106B SAW
	A106C	A53 Grade A SAW
	A53 Grade A	A516 Grade 70 SAW
	A333 Grade 6	A106C TIG
	A155	STS 410 TIG
	A516 Grade 70	Generic Carbon Steel Weld
	A710 Grade A	
	STS49	
	STS410	
	Generic Carbon Steel	
Stainless Steel	Type 304	Type 304 SAW
	Type 316	Type 304 SAW (annealed)
	Type 316L	Type 304L SAW
	Generic Stainless Steel	Type 316 SAW
		Type 304 TIG
		Generic Stainless Steel Weld
Cast Stainless Steel	CF3	CF8M SAW
	CF3A	Generic Cast Stainless Steel Weld
	CF8	
	CF8A	
	CF8M	
	Generic Cast Stainless Steel	
Nickel Alloy	Alloy 600	Alloy 182 Weld
		Alloy 600 TIG
		Generic Nickel Based Alloy Weld

For all of the material properties, statistical distributions were developed using the available material property test data. A database program was written to input additional data and analyze the data to extract the statistical parameters. For the PRO-LOCA code, all of the available data were used in developing the distributions. Specimen data were binned into 6 temperature categories (20-30C, 31-150C, 151-270C, 271-300C, 301-330C, and 331-350C). For materials and temperatures where less than five experiments existed, distributions were not generated. In these cases, either substitutions occur, or the code defaults to the generic material properties.

The database program written will allow additional data to be added as it is gathered or created. Therefore, as material property data is gathered from other programs, it can be added to the overall database. These database programs currently reside on the Emc² server and can be accessed using the following addresses:

<http://www.emc-sq.com/Emc2MaterialDatabase/TensileTest.php> - Tensile test database

<http://www.emc-sq.com/Emc2MaterialDatabase/JRCurveSummary.php> - Fracture toughness test database.

At this point, the database software is not integral with the PRO-LOCA code, so the material library embedded in PRO-LOCA will have to be manually changed if more data is added to the database.

For the second option, the user inputs their own material property values. For a chosen weld, the user will be asked to input mean values, with corresponding standard deviations, of the following material property values:

- Base metal yield and ultimate strengths,
- Weld metal yield and ultimate strengths,
- Base metal elastic modulus,
- Base metal Ramberg-Osgood coefficients (alpha and n), and
- Weld metal fracture toughness coefficients (J_i , C, and m).

In addition, the user will also specify the distribution type for each of these material property values, i.e., constant, uniform, normal, lognormal, Weibull, exponential, or EV Type 1.

For fracture toughness, the J-R curve is specified by the power law relationship

$$J = J_i + C(\Delta a)^m \quad (2.18)$$

where,

J = Value of J at a given value of crack growth (Δa)

J_i = Value of J at crack initiation

Δa = Amount of crack growth

m = exponent

C = coefficient

These tensile and fracture toughness properties are used in order to make crack stability predictions. It should be noted that the user has the option of either using the default material property coefficients for subcritical crack growth hard wired into the code or providing their own material property coefficients for subcritical crack growth. These parameters will be fully explained in Section 2.8.

It is assumed that the material properties are time independent and contain no correction for strain rate. Thermal aging and dynamic strain aging effects are important in predicting crack behavior and may be included in a future release of this code.

2.5 Loads and Stresses

The loads and associated stresses used in PRO-LOCA are the static loads and stresses, including the weld residual stresses, plus the resultant stresses from both past and future transients.

2.5.1 Normal Operating Loads

The static normal operating load contributions are the result of pipe pressure, temperature, axial loads due to dead weight, static bending loads, plus the weld residual stresses. The axial stress component from the internal pressure (P) and the axial load (F_x) due to dead weight were calculated as:

$$\sigma_{0p} = \frac{PR}{2t} \quad (2.19)$$

and

$$\sigma_{0A} = \frac{F_x}{A} \quad (2.20)$$

where P is the internal pipe pressure, R is the mean pipe radius, and A is the cross-sectional area of the pipe.

The global bending stresses are input by the user as either a stress term, or by inputting the bending moment and torque components. If the user selects the option of inputting bending moments and torques, an effective moment is calculated using Equation 2.21

$$M_{eff} = \sqrt{M_y^2 + M_z^2 + \left[\frac{\sqrt{3}}{2} T \right]^2} \quad (2.21)$$

where,

- M_y = Moment in the y-direction,
- M_z = Moment in the z-direction, and
- T = Torque.

In previous releases of PRO-LOCA it was assumed that the maximum bending stress existed everywhere around the pipe's circumference. As part of MERIT changes were made to the code to address this issue and to allow for an alternative consideration of the effect of secondary stresses. In the FY07 version of PRO-LOCA, the stress at each subunit around the circumference was constant, i.e., each subunit experienced the same maximum stress. In addition, it was assumed that all of the loads on the pipe were primary in nature and fully contributed to the subcritical and critical growth of the cracks. In this most recent revision, the stress at each subunit was modified so that the stress on the subunit was dictated by the location of the subunit relative to the location of maximum bending stress. In each analysis, the maximum stress is assumed to occur at the 0 degree location. Each subunit away from the 0 degree location gets a scaled bending stress based on its location relative to the 0 degree location. This scaling occurs for all normal operating and transient bending stresses. Even though the stress is scaled, and a crack may not occur at the maximum moment location, it is still assumed that all stresses applied provide a Mode I type driving force.

In addition, the primary and secondary stress values (on bending stress only) were separated and are allowed to be input by the user. The user must also input a scaling factor for the secondary stress. This scaling factor allows a portion of the secondary stress to be added for critical crack growth calculations. The following illustrates the current treatment of secondary stresses for subcritical and critical crack growth calculations:

- 1.) For subcritical surface crack growth, all secondary stresses are included as primary stresses,
- 2.) For critical surface cracks calculations, all secondary stresses are included as primary stresses,
- 3.) For through-wall subcritical crack growth, the primary stress plus (secondary stress multiplied by a scaling factor) are included, and
- 4.) For critical through-wall calculations (stability), the primary stress plus (secondary stress multiplied by a scaling factor) are included.

2.5.2 Weld Residual Stresses

For the weld residual stresses the user has the option of inputting their own 4th order polynomial expression as shown below in Equation 2.22 to define the through thickness weld residual stresses,

$$\sigma = \sigma_0 + \sigma_1 \left[\frac{x}{t} \right] + \sigma_2 \left[\frac{x}{t} \right]^2 + \sigma_3 \left[\frac{x}{t} \right]^3 + \sigma_4 \left[\frac{x}{t} \right]^4 \quad (2.22)$$

where t is the wall thickness and x is measured from the inside diameter of the pipe, or they can specify one of a number of geometry specific weld residual stress distributions.

Currently PRO-LOCA has geometric specific weld residual stress distributions for six different geometries. These solutions were developed using detailed finite element analyses. The details of these finite element analyses are provided in Appendix A of this report. The six geometries included in the current version of PRO-LOCA are: two hot leg to reactor pressure vessel (RPV) nozzle dissimilar weld solutions, the surge line to pressurizer nozzle dissimilar metal weld, the pressurizer spray line to pressurizer nozzle dissimilar metal weld, and two stainless-to-stainless weld solutions. The hot leg/RPV

dissimilar weld and the stainless-to-stainless similar weld solutions were developed for both the case of with and without an ID repair weld. For the case of an ID repair weld, the last pass of weld material (~ 15 percent of the wall thickness) on the ID surface was ground out and weld metal was re-deposited in the ground out area. The surge line to pressurizer nozzle weld solutions were only developed for the case of an ID repair weld. Due to size limitations, the spray nozzle solutions were only for the case of no ID repair weld.

For each of the dissimilar weld cases, solutions were developed using the Nickel alloy weld tensile properties as well as the stainless and ferritic steel tensile properties. The Nickel alloy weld tensile properties were used for the analysis of the residual stresses in the weld and buttered regions. The stainless and ferritic steel tensile properties were used in the analysis of the heat-affected-zone and fusion line residual stresses. For each case, solutions were developed for the mean tensile properties as well as the means plus and minus two standard deviation tensile properties. For the weld metal cases, solutions were developed for weld centerline and along paths in the weld metal and buttered region where the residual stresses were the highest. For the stainless and ferritic steel cases, solutions were developed for both the heat-affected-zone (HAZ) as well as along the fusion line.

The maximum weld residual stress in the sensitized region for a particular component was incorporated into the PRO-LOCA code. For example, for the stainless steel recirculation line in a BWR, since the heat affected zone is the sensitized region, which is where stress corrosion cracks will initiated and grow, the maximum stress distribution through the thickness in the heat affected zone was incorporated into the PRO-LOCA code. For the dissimilar weld metal cases, the solutions incorporated into the PRO-LOCA code were the maximum stresses in the weld or buttered region, whichever was greater, which is where pressurized water stress corrosion cracks would most likely initiate and grow. In all cases, the weld residual stresses were normalized by the yield strength of the material and fit to a 4th order polynomial, see Equation 2.23 and Figure 2.5. This normalization will allow the weld residual stresses to be random in nature. Equation 2.23 shows the residual stresses normalized by the yield strength as a function of the normalized distance from the inside surface, where the normalizing parameter is the wall thickness of the component. Table 2.6 shows the coefficients from the curve fitting exercise that are currently incorporated into PRO-LOCA. Figure 2.6 is a plot of the normalized stresses as a function of the normalized distance from the inside surface

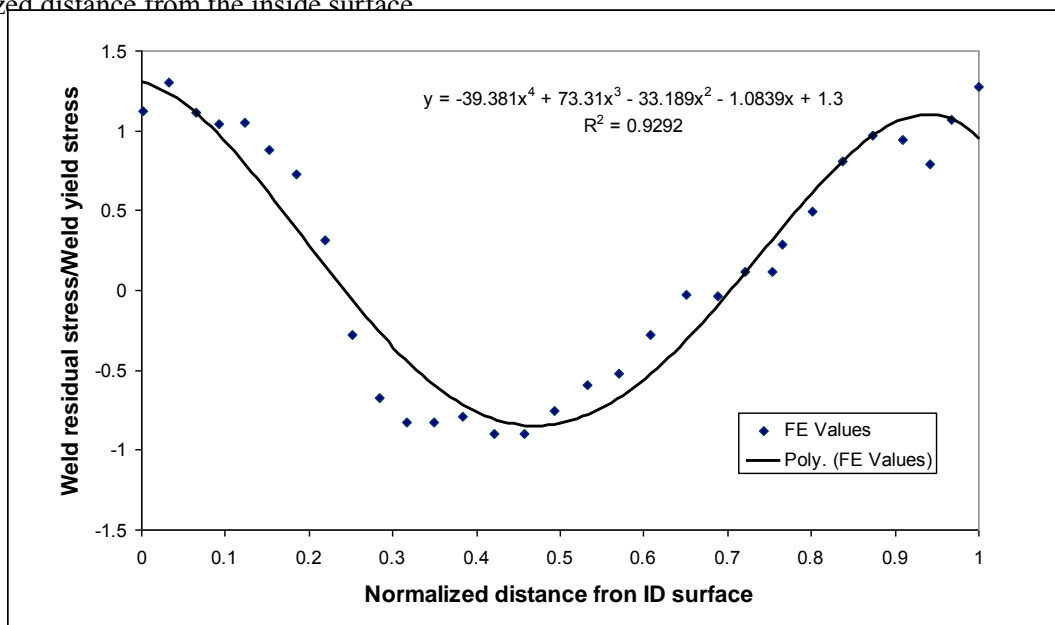


Figure 2.5 Curve fit of weld residual stresses for inclusion into PRO-LOCA

$$\frac{\sigma_{WRS}}{\sigma_y} = \frac{\sigma_0}{\sigma_y} + \frac{\sigma_1}{\sigma_y} \left(\frac{x}{t} \right) + \frac{\sigma_2}{\sigma_y} \left(\frac{x}{t} \right)^2 + \frac{\sigma_3}{\sigma_y} \left(\frac{x}{t} \right)^3 + \frac{\sigma_4}{\sigma_y} \left(\frac{x}{t} \right)^4 \quad (2.23)$$

where,

- σ_{WRS} = Weld residual stress,
- σ_y = Yield strength,
- $\sigma_0, \sigma_1, \sigma_2, \sigma_3,$ and σ_4 = Curve fitting coefficients, and
- x/t = Normalized distance from inside surface.

From Figure 2.5, the highest normalized stresses on the inside surface are for the surge line nozzle bimetal weld with ID repair weld and hot leg/RPV weld with ID repair weld. The surge line nozzle and hot leg/RPV weld stresses are slightly higher on the inside surface than the stainless steel weld with repair weld stresses, but they dissipate much quicker through the thickness than do the stainless steel weld with repair weld stresses. It can be seen from Figure 2.5 that the residual stresses through the inner half of the pipe wall are higher for the cases where ID repair welding was performed than the cases where it was not.

Table 2.6 Coefficients from the curve fitting exercise for weld residual stresses used in PRO-LOCA

Weld Case Description	σ_0/σ_y	σ_1/σ_y	σ_2/σ_y	σ_3/σ_y	σ_4/σ_y	σ_y , MPa
Hot leg - Alloy 182 weld at 324 C (615F), using maximum stress in buttered region	0.75	-9.271	27.71	-32.91	14.98	213.3
Hot leg - Alloy 182 weld at 324 C (615F), using maximum stress in butter region, 15% ID repair weld	1.3	-1.084	-33.19	73.31	-39.38	213.3
Surge line - Alloy 182 weld at 324 C (615F), 15% ID repair weld	1.728	-5.494	-10.65	32.05	-16.53	213.3
Spray line - Alloy 182 weld at 324 C (615F), no ID repair weld	-0.5	-6.427	33.16	-41.32	15.73	213.3
Stainless steel weld at 288 C (550F), using maximum stress in HAZ, no ID repair weld	1.00	-14.04	48.04	-56.32	21.47	160.3
Stainless steel weld at 288 C (550F), using maximum stress in HAZ, ID repair weld	0.800	0.485	-5.007	3.314	0.00	160.3

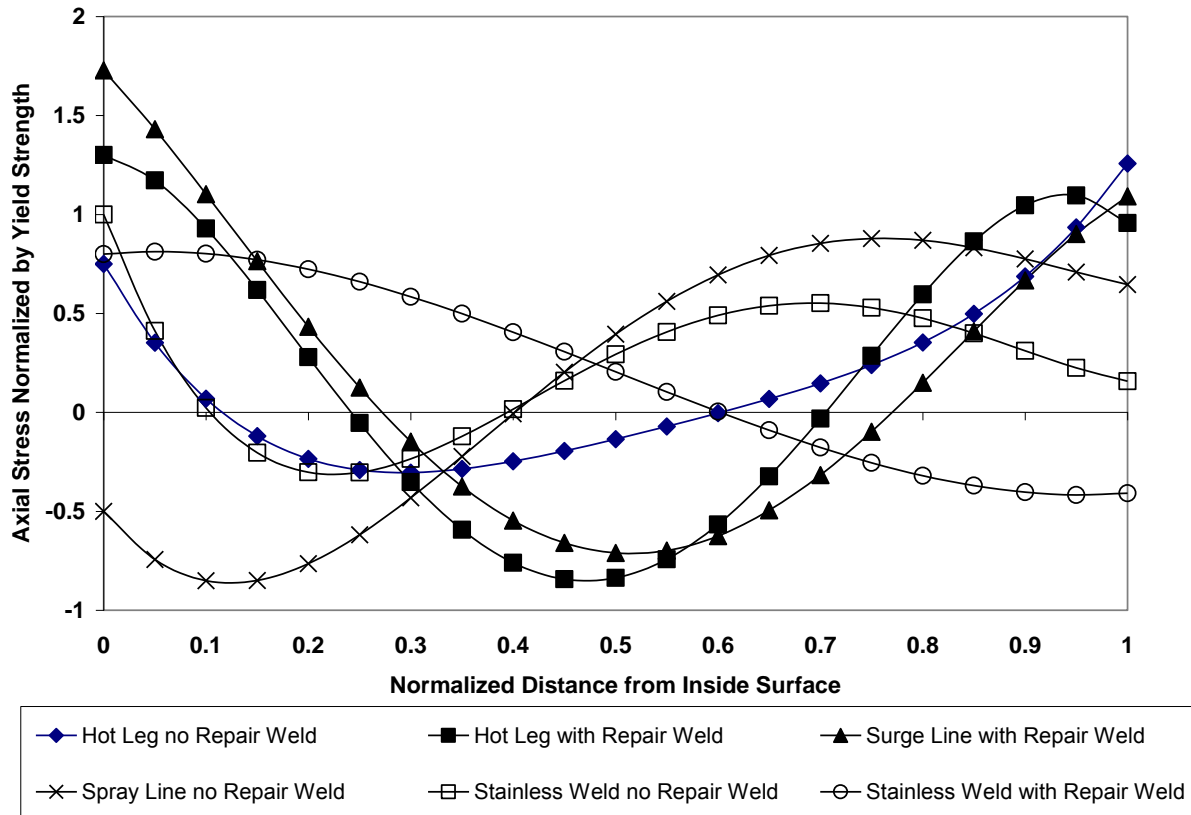


Figure 2.6 Plot of the normalized weld residual stresses as a function of the normalized distance from the inside surface

In the above cases, the variability in the WRS in PRO-LOCA is a function of the variability in the material yield strength. Additional variability in the WRS can be prescribed using the user defined WRS distribution. There are many factors that can contribute to the variability in the welding stress. Therefore the input structure of the user defined welding stress solutions has been modified for this case. The input structure for the user defined welding stress is shown below in Figure 2.7. The user is asked to input the ID stress (mean, standard deviation, and distribution type) and values for the term X_c (mean, standard deviation, and distribution type), i.e., the fractional distance through the thickness where the stress first changes sign. The code then fits a 3rd order polynomial to these sampled values. Using the input ID stress and X_c , the following constraints are applied to generate the residual stress through the thickness:

- The ID stress is defined
- The area under the curve must equal zero (stress equilibrates through the wall thickness)
- The stress on the OD is defined as a uniform random number times the ID stress
- Stress is equal to zero at X_c

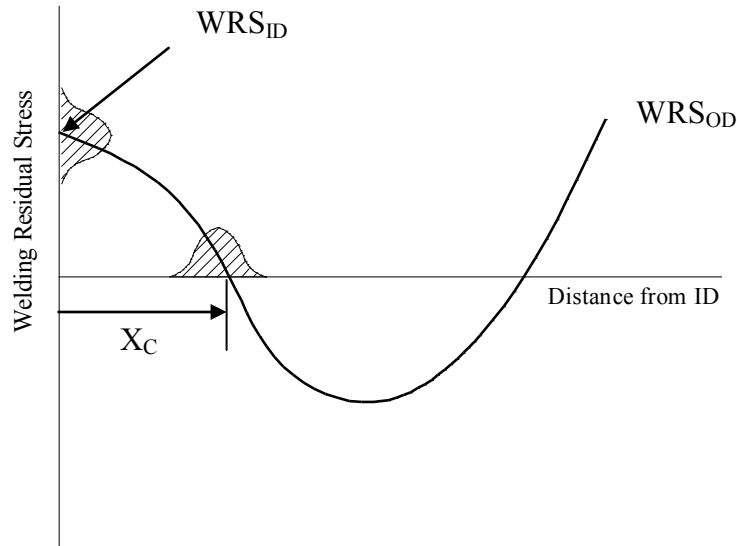


Figure 2.7 User defined welding residual stress schematic

In addition, the current version of PRO-LOCA allows the user to modify the weld residual stress distribution to simulate a repair using either a weld overlay or the mechanical stress improvement process (MSIP). The same user defined weld residual stress schematic as shown in Figure 2.7 is used, where the user inputs the distribution type (uniform, lognormal, etc.), means, and standard deviations for the repaired weld.

2.5.3 Transients

The transients considered in PRO-LOCA include: earthquakes, vibration loadings, generic transients, and startup and shutdown cycles.

2.5.3.1 Earthquakes

The earthquake signatures considered are constant in stress amplitude, with a fixed frequency, under fully reversed loading ($R = -1$). The earthquake signatures are input two different times for each run. For the time up to years in operation, the user inputs the actual earthquake signatures that have occurred up to that point in time. For years greater than the year in operation, a probability per year per earthquake signature is required. If an earthquake is sampled to have happened at a particular time increment, the earthquake was assumed to have happened at the end of that particular year. Earthquakes were assumed to affect not only crack initiation and subcritical crack growth but also crack stability.

2.5.3.2 Vibration Stresses

The inputs for vibration stresses are very similar to earthquake loadings; however, the vibration loading is considered to be continuous over the life of the plant. The vibration stresses are again assumed to be constant amplitude, fully reversed loading with a constant frequency. Axial forces and bending stresses/moments are input as amplitudes which the code adds/subtracts from the normal operating stresses to get the stress range.

2.5.3.3 Generic Transients

Generic transients are cyclic in nature, but do not fit the earthquake or vibration category. As before, the user inputs both the deterministic values (for times less than the years in operation, i.e., past experience) and probabilistic values (for times greater than the years in operation, i.e., future) of the number of cycles, frequency, and probability of occurrence. Unlike the seismic input, the stress ratio for the generic

transients is a user input. For this transient, the user inputs the following values for both the time before the year in operation, and the time after the year in operation:

- Number of transients
- Number of cycles per year
- Rise time, which is used to help define the strain rate dependent properties for the fatigue crack initiation and growth models, much like the frequency does for the earthquake and vibration loadings
- Transient global bending and axial loads (amplitude)
- Transient through thickness stresses (amplitude)
- Stress ratio

2.5.3.4 Start-up and Shutdown Stresses

Start-up and shutdown transient stresses are a bit different than the other transient stresses considered thus far. Instead of acting as a stress amplitude on the normal operating loads, start-up and shutdown loads replace the normal operating loads during the time increment.

2.6 Pre-Existing Flaws

Flaws, which can lead to LOCAs, can either initiate as a result of residual stresses (e.g., stress corrosion cracks) or service loadings (e.g., mechanical or thermal fatigue cracks) or can grow from pre-existing flaws that are introduced into the welds as a result of the welding process and associated imperfections (e.g., lack of fusion, porosity, slag, etc.). In this section, the bases for the distributions of pre-existing flaws are discussed. A number of distributions of pre-existing flaws for a variety of welding processes (arc welding and inert gas welding) for both ferritic and austenitic steels are presented. These distributions came from a review of a number of documents (Refs. 2.7, 2.8, 2.9, 2.10, and 2.11) as well as discussions with experts in the field.

Based on a review of Reference 2.9 and discussions with one of its authors, it was suggested that this reference be used as the basis for estimating the flaw-depth distribution and the flaw frequencies of any pre-existing flaws that might be left in service as a result of welding. In Reference 2.9, the flaw frequencies (number of flaws per inch of weld) are specified in Table 6 for a discrete number of pipe wall thicknesses, i.e., 6.3, 12.7, 19.1, 25.4, 38.1, 50.8, and 63.5 mm. WinPRAISE (Ref. 2.10) on the other hand provides an equation for estimating the number of flaws per inch of weld at the ID surface. As can

be seen in

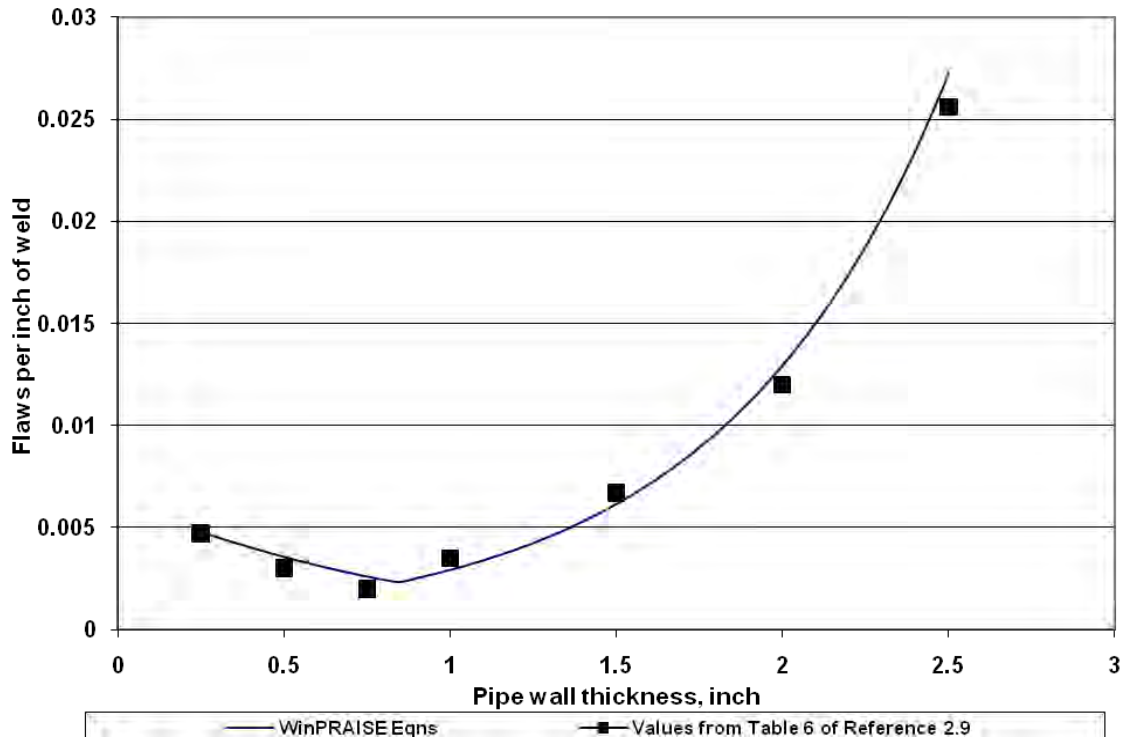


Figure 2.8 the agreement between the tabular values in Reference 2.9 and the WinPRAISE equation is very good. Thus, instead of having to interpolate between the tabular values in Table 6 of Reference 2.9 (as suggested in Reference 2.9), it was decided to use the equation in WinPRAISE directly, see Equation 2.24, to estimate the number of flaws per inch of weld at the inside pipe surface.

$$\# \text{ flaws / inch} = \text{larger} \left[\begin{array}{c} 0.000655 \exp(1.491499h) \\ \text{or} \\ 0.0022h^2 - 0.0066h + 0.0063 \end{array} \right] \quad (2.24)$$

where, h is the pipe wall thickness. Note, this expression is for the case where inspections have been performed. For the case of “noninspections”, the calculated flaw frequencies need to be multiplied by 12.8.

For the flaw depth distribution, Equation 1 in Reference 2.9 specifies a probability density of a lognormal distribution in the form of:

$$\rho(a) = \frac{1}{\mu a \sqrt{2\pi}} \exp \left[\frac{-[\ln(a/a_{50})]^2}{2\mu^2} \right] \quad (2.25)$$

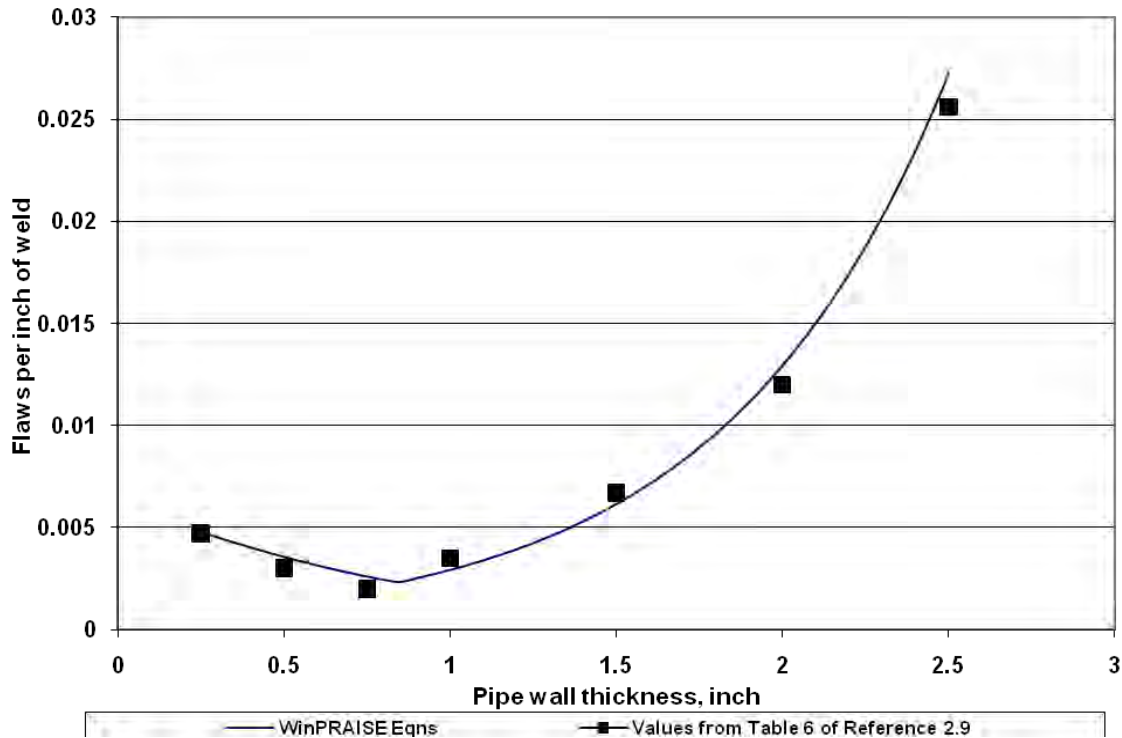


Figure 2.8 Comparison of flaw density as a function of pipe wall thickness between WinPRAISE equations and the values from Table 6 of Reference 2.9

In Equation 2.25, a_{50} is the median crack depth and μ is the shape parameter. The average crack depth (a_{avg}) and the standard deviation of the crack depth (a_{sd}) can be calculated from the median crack depth (a_{50}) and the shape parameter (μ) through the following expressions:

$$a_{50} = a_{avg} \exp \frac{-\mu^2}{2} \quad (2.26)$$

$$\mu = \sqrt{\ln(1 + cov^2)} \quad (2.27)$$

$$cov = \frac{a_{sd}}{a_{avg}} \quad (2.28)$$

The median flaw depth (a_{50}) and the shape parameter (μ) can be calculated using expressions provided in Figures 6 and 7 of Reference 2.9 for both stainless and ferritic steels and for both manual-metal-arc welds (MMAW) and tungsten inert gas (TIG) welds.

The median flaw depth (a_{50}) is:

$$a_{50} = 0.112 - 0.02299h + 0.0001481h^2 \quad (2.29)$$

for stainless steel MMAW welds,

$$a_{50} = 0.1169 - 0.0445h + 0.00797h^2 \quad (2.30)$$

for stainless steel TIG welds,

$$a_{50} = 0.0519h^{(-0.4572+0.0432\ln(h))} \quad (2.31)$$

for ferritic MMAW welds, and

$$a_{50} = 0.0519h^{(-0.8592-0.2467\ln(h))} \quad (2.32)$$

for ferritic TIG welds.

The shape parameter (μ) is:

$$\mu = 0.09733 + 0.3425h - 0.07268h^2 \quad (2.33)$$

for both stainless steel MMAW and TIG welds,

$$\mu = 0.5102 + 0.2294 \ln(h) \quad (2.34)$$

for ferritic MMAW welds, and

$$\mu = 0.5665 + 0.2862 \ln(h) \quad (2.35)$$

for ferritic TIG welds.

As before, “h” is the pipe wall thickness.

When the various parameters, a_{50} , μ , a_{avg} , and a_{sd} , were calculated using the above expressions for the case of a 25.4 mm (1 inch) thick pipe for a stainless steel MMAW, the values for Case #1 in Table 3 of the Reference 2.9 were reproduced exactly. In order to reproduce the smooth curve in Figure 2 of Reference 2.9, one can calculate the lognormal cumulative distribution using Excel®. In order to reproduce the smooth curve in Figure 2 of Reference 2.9, one needs to take 1.0 minus the lognormal cumulative distribution of $-a^2$, see Figure 2.9. This was interpreted to mean that if a flaw exists in this 25.4 mm (1 inch) thick stainless steel MMAW, the probability that the flaw is deeper than 1.3 mm (0.05 inches) is 0.942, deeper than 2.5 mm (0.1 inches) is 0.378, deeper than 6.3 mm (0.25 inches) is 0.0025, and deeper than 12.7 mm (0.5 inches) is 1.3×10^{-6} .

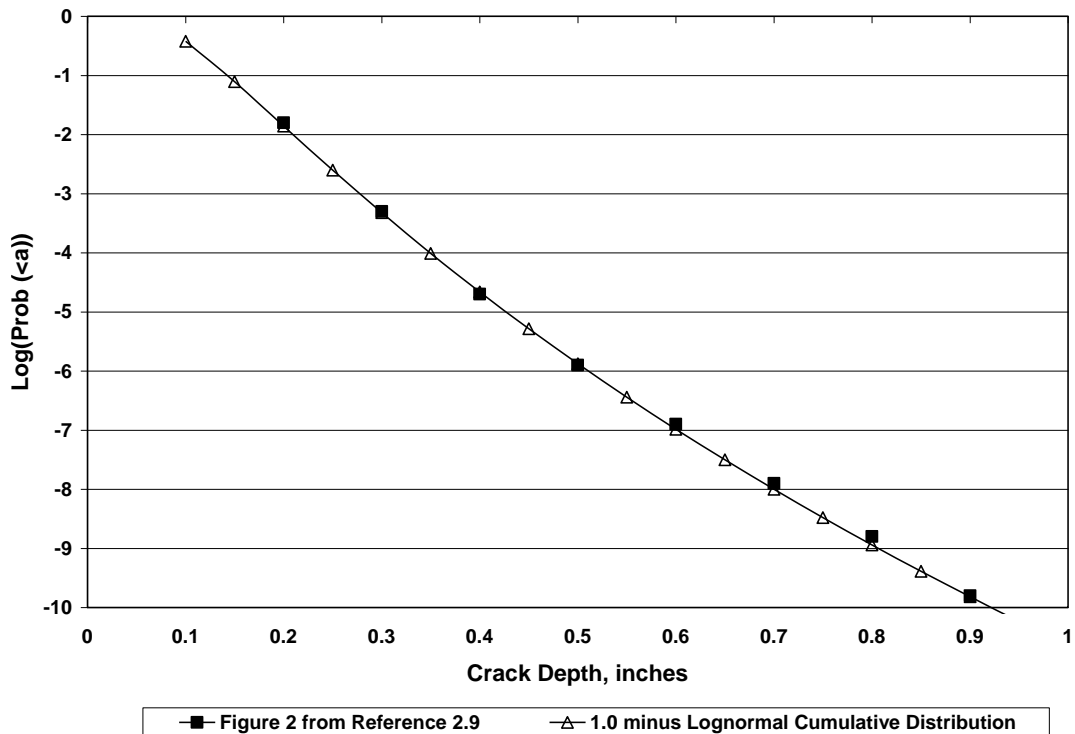


Figure 2.9 Comparison of 1.0 minus the lognormal cumulative distribution of “a” with Figure 2 from Reference 2.9

The final distribution needed is the flaw length or aspect ratio distribution. Reference 2.9 does not address the flaw aspect ratio. However, comparisons have been made of predictions using WinPRAISE and predictions from PRODIGAL and with PNNL data on reactor pressure vessel flaws and it has been found that the WinPRAISE method is in reasonable agreement with the PRODIGAL/PNNL data for relatively small flaws, but overpredicts the aspect ratio for deep flaws (i.e., those approaching the pipe

wall thickness in depth). It has been argued that flaw length rather than aspect ratio is a better way to describe flaws. Flaw length tends to be relatively independent of the flaw depth dimensions. Flaw aspect ratios tend to be smaller as the flaw depth dimension becomes greater. As such, it has been proposed to begin with the WinPRAISE equation to calculate a distribution of flaw aspect ratios and then assume a flaw depth of one or two weld bead thicknesses (say 2.5 to 5.0 mm [0.1 to 0.2 inches]) to calculate a flaw length distribution. It would then be assumed that this length distribution would apply to flaws of all depths.

Based on the above, one could estimate the distribution of aspect ratios ($\beta = b/a$), where b is the half crack length and a is the crack depth, using the lognormal distribution function in Equation 2.36.

$$p(\beta) = \frac{2 \exp \left[- \left(\ln \left(\frac{\beta}{\beta_m} \right) / (\sqrt{2} \lambda) \right)^2 \right]}{\lambda \beta \sqrt{2\pi} \operatorname{erfc} \left(\ln(1/\beta_m) / \sqrt{2} \lambda \right)} \quad (2.36)$$

where β_m and λ are 1.336 and 0.5382, respectively, for the assumption that the proportion of cracks with $\beta > 5$ ($2b/a > 10$) is 10⁻². The expression $\operatorname{erfc}(x)$ in Equation 2.36 is the complementary error function of Abramowitz (Ref. 2.12).

Once the distribution of the aspect ratio, $p(\beta)$, is defined, the distribution of crack lengths ($2b$) for the range of crack depths representative of one to two weld beads, $0.1 < a < 0.2$, can be established. Then this same distribution for crack lengths would be assumed to hold for all crack depths.

In addition to reviewing the various reports and papers and discussing this issue with recognized experts, a separate study was commissioned by the US NRC with PNNL to quantify the distribution of flaws in a number of representative pipe welds supplied to them by Battelle Columbus. The welds supplied to PNNL were all welds made by nuclear certified welders. Battelle Columbus obtained most of these welds from canceled nuclear power plants as part of the Degraded Piping Program (Ref. 2.13) as well as other programs directly with industry.

Two of the welds inspected by PNNL were 8-inch nominal diameter stainless steel pipes with circumferential girth welds made using a combined gas-tungsten-arc and shielded-metal-arc weld (GTAW/SMAW) process. GTAW was used for the root passes and SMAW was used for the fill passes. One of these pipes had a wall thickness of 23 mm (0.91 inches) and one had a wall thickness of 13 mm (0.51 inches). For these welds, a plot of the cumulative flaw density (per square centimeter of fusion zone area) from verified ultrasonic measurements as a function of flaw depth was made. As part of this effort, comparisons were made between these measured flaw densities and predicted densities using the analysis method discussed above. In order to estimate the cumulative densities from the analysis, the flaw frequencies from Equation 2.24 were divided by the area of the fusion zone to get the flaw frequencies per unit area (square centimeter) of fusion zone. This quotient was then multiplied by 1.0 minus the cumulative distribution of the log-normal distribution for various flaw depths. Figure 2.10 shows those comparisons for both the 13- and 23-mm (0.51- and 0.91 inches) wall thickness pipes. For the measured flaw density from the PNNL data, the data from both the 13- and 23-mm (0.51- and 0.91 inches) wall thicknesses stainless steel pipe welds were combined into a single plot. As can be seen in Figure 2.10, the agreement between the analyses predicted densities for the 13-mm (0.51-inch) thick pipe and the cumulative density measured by PNNL is pretty good. There is a little more disagreement for the 23-mm (0.91-inch) thick pipe. On the other hand Figure 2.11 shows a similar comparison for the fusion line region of the bimetallic safe end welds for a series of cold-leg pipes. In this case, the measure density is 2 to 3 orders of magnitude higher than the predicted values from the analysis. Furthermore, for the deeper flaws, this disagreement is getting larger. The fact that these welds had many more flaws than predicted by the analysis may be an artifact of the fact that these were dissimilar welds and the models may not

adequately capture the complexity of these types of welds. Also, for both the 8-inch diameter stainless pipe welds and the bimetallic cold leg pipe welds, the expressions for stainless steel MMAW were used to calculate the median crack depth (a_{50}) and the shape parameter (μ). The questions are should one use the stainless steel or ferritic parameters to describe a flaw distribution for a dissimilar weld and are the expressions for a MMAW suitable to describe the flaw distribution for a shielded-metal-arc weld.

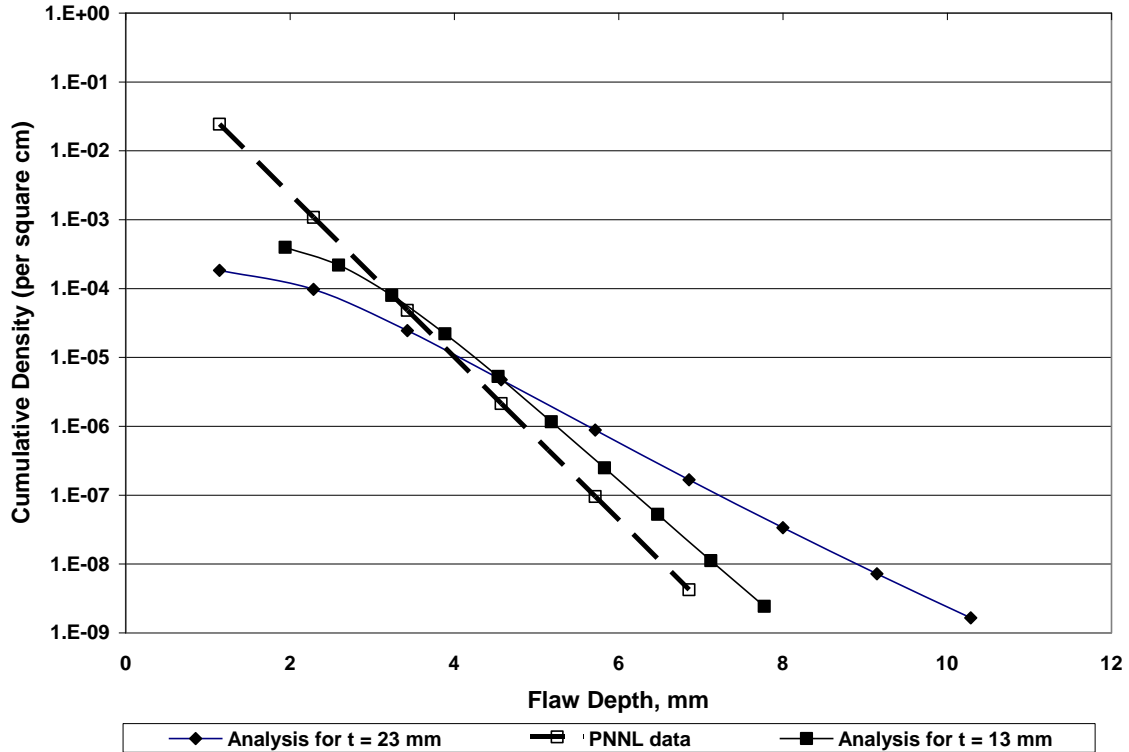


Figure 2.10 Comparisons of cumulative flaw densities from the analysis discussed above with measured densities for two 8-inch diameter stainless steel pipe welds (Measurements made using ultrasonics by PNNL)

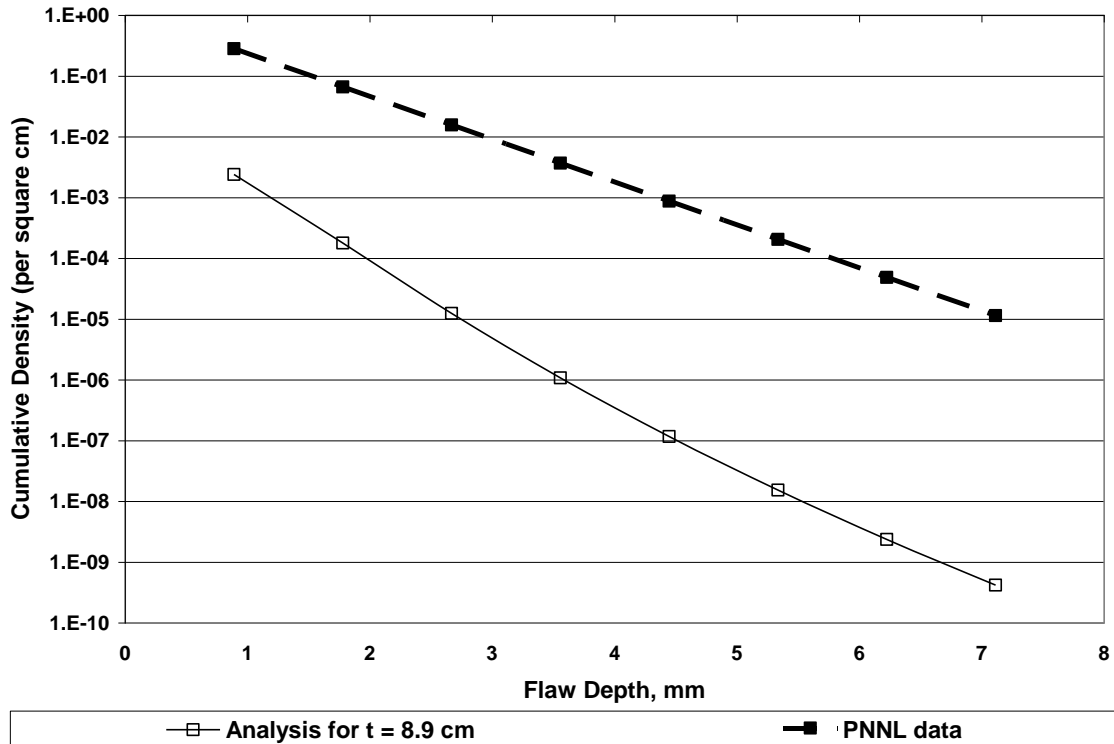


Figure 2.11 Comparisons of cumulative flaw densities from the analysis discussed above with measured densities for two 8-inch diameter stainless steel pipe welds (Measurements made using ultrasonics by PNNL)

2.7 Crack Initiation Models

Currently in PRO-LOCA, the user has the option of choosing default or user defined crack initiation models. The basis of the default crack initiation models included in PRO-LOCA was work performed by Argonne National Laboratories (Ref. 2.14). Some of the constants included in these models were developed specifically for PRO-LOCA, but the actual models were developed in other programs. The default crack initiation models currently included in PRO-LOCA are for fatigue, primary water stress corrosion cracking (PWSCC), and intergranular stress corrosion cracking (IGSCC), and are discussed in Sections 2.7.1, 2.7.2, and 2.7.3, respectively. The user defined crack initiation models are discussed in Section 2.7.4.

2.7.1 Default Air/Corrosion/Thermal Fatigue Model

The default fatigue initiation models are based on a series of experimental strain versus life data sets developed by Argonne and presented in Reference 2.14. This data is for a collection of carbon and low alloy steels, austenitic and stainless steels, and Alloy 600 experiments that were categorized according to material, loading, and environmental conditions. Statistical models were developed and used to estimate the probability of initiating a fatigue crack. Effects of size, geometry, and surface finish on the fatigue initiation life were all accounted for by empirically adjusting the life by a factor, K_N . The parameters included in the models were environment (including dissolved oxygen content and temperature), material (including sulfur content), and the strain amplitude and strain rate.

From Reference 2.14 the number of cycles, $N_i(x)$, corresponding to the x th percentile of probability for crack initiation in carbon steel (CS) and low-alloy steel (LAS) components is expressed by the following equation

$$\ln[N_i(x)] = (6.857 - 0.766I_W) - (0.275 - 0.382I_W)I_S + 0.52F^{-1}[x] - \ln(K_N) - (1.813 + 0.219I_S) \ln(\epsilon_a - 0.080 - 0.014I_S + 0.026F^{-1}[1-x]) - 0.00133T(1 - I_W) + 0.554S^*T^*O^*\dot{\epsilon}^* \quad (2.37)$$

for austenitic stainless steel components by

$$\ln[N_i(x)] = 6.732 + 0.52F^{-1}[x] - \ln(K_N) - 2.032 \ln(\epsilon_a - 0.103 + 0.026F^{-1}[1-x]) - I_W(0.134\dot{\epsilon}^* - 0.359) + 0.382I_{316NG} \quad (2.38)$$

and for Alloy 600 components by

$$\ln[N_i(x)] = 6.969 + 0.52F^{-1}[x] - \ln(K_N) - 1.814 \ln(\epsilon_a - 0.107 + 0.026F^{-1}[1-x]) + 0.498I_T - 0.401I_W \quad (2.39)$$

and for Alloy 182 welds, the Alloy 600 number of cycles is divided by 2

where,

I_W	=	1 for water and 0 for air
I_S	=	1 for CS and 0 for LAS
I_T	=	0 for temps <150C (300F) and 1 for temps between 150 and 350C (300 and 660 F)
K_N	=	4
ϵ_a	=	applied strain amplitude in %
T	=	Temperature in C
S^*	=	Sulfur content, S ($0 < S \leq 0.015$ wt.%)
S^*	=	0.015 ($S > 0.015$ wt.%)
T^*	=	0 ($T < 150$ C [300 F])
T^*	=	$T - 150$ ($T = 150 - 350$ C [300-660F])
O^*	=	0 ($DO < 0.05$ ppm)
O^*	=	Dissolved oxygen, DO ($0.05 \text{ ppm} \leq DO \leq 0.5 \text{ ppm}$)
O^*	=	0.5 ($DO > 0.5$ ppm)
$\dot{\epsilon}^*$	=	0 (strain rate, $\dot{\epsilon} > 1\%/s$)
$\dot{\epsilon}^*$	=	$\ln(\dot{\epsilon})$ ($0.001 \leq \dot{\epsilon} \leq 1\%/s$)
$\dot{\epsilon}^*$	=	$\ln(0.001)$ ($\dot{\epsilon} < 0.001\%/s$)
I_{316NG}	=	1 for Type 361NG SS and 0 otherwise
$F^{-1}[x]$	=	inverse of the standard normal cumulative distribution function – STDEV on life
$F^{-1}[1-x]$	=	inverse of the standard normal cumulative distribution function – STDEV on strain amplitude.

It should be noted that some of the coefficients in these default crack initiation models are still highly debated. According to personal communication with Dr. Omesh Chopra of Argonne, terms like the STDEV of strain amplitude, $0.026F^{-1}[1-x]$, may change to $0.01F^{-1}[1-x]$. However, at this point, the equations in the PRO-LOCA code are taken directly from the published NUREG (Ref. 2.14).

In each of the equations in this section, a strain amplitude threshold for fatigue exists. For example, from Equation 2.37, the term $\ln(\epsilon_a - 0.080 - 0.014I_S + 0.026F^{-1}[1-x])$ describes this threshold. If this term becomes

negative, then the strain is low enough to preclude fatigue crack initiation. Therefore, in the code, if this value becomes negative, fatigue crack initiation will not occur for that loading.

The default fatigue models chosen give a distribution of number of cycles for crack initiation. It was assumed that SCC initiation and fatigue initiation do not interact. During the input/sampling stage of the program, after the cyclic loads are entered, the number of cycles for fatigue crack initiation for each transient loading history is determined separately. Once these are computed, then, during time stepping, Miner's rule is employed to keep track of initiation fatigue damage. Once the damage is greater than 1, initiation occurs.

Initiation will occur if at any time increment Δt if

$$n_{i(VL)}/N_{VL} + n_{i(EQ)}/N_{EQ} + n_{i(GT)}/N_{GT} + n_{i(SD)}/N_{SD} + \text{others...} = 1 \quad (2.40)$$

where

- n_i = number of cycles at that time increment for that cyclic loading history,
- N_{VL} = fatigue initiation cycles for vibration and normal operating loads only,
- N_{EQ} = fatigue initiation cycles for earthquake and normal operating loads only,
- N_{GT} = fatigue initiation cycles for generic transient and normal operating loads only, and
- N_{SD} = fatigue initiation cycles for shutdown loads only.

For the default model, once a fatigue crack initiated, it was assumed to have a lognormally distributed length with a median value of 3 mm (0.125 inch) and a standard deviation of $\ln(b)=0.85$. The depth of the crack is set deterministically at 3 mm (0.125 inch).

While running initial sensitivity studies on the fatigue module in the PRO-LOCA code, it was discovered that in some cases the number of cycles to initiate a fatigue crack appeared very high. This topic was discussed with Bill Shack and Omesh Chopra from Argonne National Labs who originally developed the fatigue crack initiation distributions. They explained that in the development of the equations, the factor, K_N , was placed on the number of cycles to initiation to reduce the value due to differences in size and surface finish between the fatigue specimen and a 228.6 mm (9-inch) diameter pipe component. The use of this term assumes that there is only one crack initiation site in the component. Since the PRO-LOCA code breaks the components circumference into smaller sized subunits, it was felt that the K_N factor needed to be reduced. Discussions with ANL lead to a decision where this factor (K_N) was decreased from a value of 4 to 2. Continued sensitivity studies showed that the difference between the probabilities of first crack initiation with $K_N=4$ and one subunit was about a factor of 3 larger than with $K_N=2$ and 38 subunits at 40 years. If the K_N value was reduced to 1.5, the predictions at 40 years were closer to the one subunit case, but were severely underpredicted at 20 years. Therefore, it was decided to use $K_N=2$ since the sensitivity of the probabilities at 40 years is small relative to the other parameters in the code. It should be realized that this is an unquantified uncertainty in the analysis, and should be further investigated.

It was also noticed during the sensitivity analyses that in some cases, very high or very low number of cycles to fatigue crack initiation were being generated by the PRO-LOCA. The formulation of the equation for the number of cycles to fatigue crack initiation are lognormal in nature, and are therefore driven by the tails of the distribution. The infinite tails on the lognormal/normal distributions may not be realistic in an engineering sense, therefore for these distributions it was decided to cut the tails off at the 5th and 95th percentiles.

2.7.2 Default Primary Water Stress Corrosion Cracking (PWSCC) Initiation Model

Despite extensive research on PWSCC of Alloy 600, primarily for steam generator tubing, no consensus has formed on the mechanism of PWSCC initiation, although the phenomenology has been fairly well

characterized (Ref. 2.15). There is a strong influence of temperature with an activation energy of 40 to 52 kcal/mole. Stresses near yield are needed for initiation, and the time to initiation is sensitive to the stress level. The stress dependence of the time to initiation is frequently modeled as a power law, i.e., $\sim\sigma^4$. Furthermore, cold work has an important accelerating effect on initiation. In the case of CRDM nozzles, this suggests that fabrication processes such as machining or surface grinding could have important consequences on susceptibility to cracking. Studies with steam generator tubing have shown that carbide morphology plays an important role. Intergranular carbides improve resistance to SCC. Even when stresses, fabrication, water chemistry, and other variables are carefully controlled, it is found that initiation is a statistical process (Ref. 2.16). The most widely used statistical model for crack initiation is the Weibull distribution, (Refs. 2.16, 2.17)

$$F(t) = 1 - \exp\left[-\left(\frac{x}{\theta}\right)^b\right], \quad (2.41)$$

where the Weibull scale parameter θ is the time at which the cumulative probability of a leak is 0.63 (in a rough sense a “typical” time to failure), and b is a parameter that is referred to as the Weibull slope. The Weibull slope, b , characterizes the rate at which the chance of failure is increasing with time ($b = 1$ gives a constant failure rate, $b > 1$ gives a failure rate that is increasing with time). The Weibull distribution arises naturally in some problems where failure is dependent on a “weakest link”, but is also a very flexible statistical model that can be used for purely empirical fits.

It is evident that initiation often involves a size dependence. Physically this size dependence arises due to local variations in microstructure, stress level, etc. In a larger component, there is a greater chance of such unfavorable variations occurring. A size dependence is inherent in the Weibull model. If, for example, a pipe weldment is considered as consisting of n subunits each of which obeys a Weibull distribution with scale factors $\theta_1, \theta_2, \dots, \theta_n$ and slope b , then the behavior of the ensemble of n objects, i.e., the pipe weldments, also can be described by a Weibull distribution with a scale factor θ_e and a slope b :

$$\theta_e = \left[\left(\frac{1}{\theta_1}\right)^b + \left(\frac{1}{\theta_2}\right)^b + \dots + \left(\frac{1}{\theta_n}\right)^b \right]^{-\frac{1}{b}} \quad (2.42)$$

In particular for identical subunits, Equation 2.42 simplifies to

$$\theta_e = \frac{\theta}{n^{\frac{1}{b}}} \quad (2.43)$$

The initiation time for the component θ_c is less than the initiation time for the subunits or small specimens (θ). For a pipe weldment, the total length of weld (i.e., highly stressed material) exposed to primary water is approximately πD_i , where D_i is the diameter of the pipe. One now considers a nozzle to be made up of subunits with lengths of highly stressed material of length ℓ . The total number of subunits n_ℓ is then

$$n_\ell = \frac{\pi D_i}{\ell}. \quad (2.44)$$

The scaling rules in Equations 2.42 through 2.44 let us combine data from different diameter weldments and in theory extrapolate from small specimen data to weldment data. For PWSCC it is found that $b \approx 3$ (Refs. 2.16, 2.17). This implies that if one is interested in the initiation of cracking of large diameter weldments in times of 15–60 years, then the corresponding times to failure of small (25.4-mm {1-inch} wide) specimens under corresponding conditions would be on the order of 60 to 240 years, i.e., much longer times than is expected in laboratory tests on small specimens.

In addition to the scaling due to size, it is also possible to consider the effect of changes in stress and temperature. Laboratory testing and field experience with PWSCC suggest that the temperature dependence is Arrhenius with an activation energy Q of about 50 kcal/mole. A stress dependence of σ^4 is often observed. Thus θ can be written as

$$\theta = A\sigma^{-4}e^{-\frac{Q}{RT}} \quad (2.45)$$

where A is a term that depends on material properties and component size, and R is the universal gas constant (1.103×10^{-3} kcal/mole-°R). However, there are difficulties with this approach to account for the effects of stress because most of the available data are from short-term tests. For example, consider the initiation data shown in Figure 2.12 for Alloy 182 weld metal (Ref. 2.18).

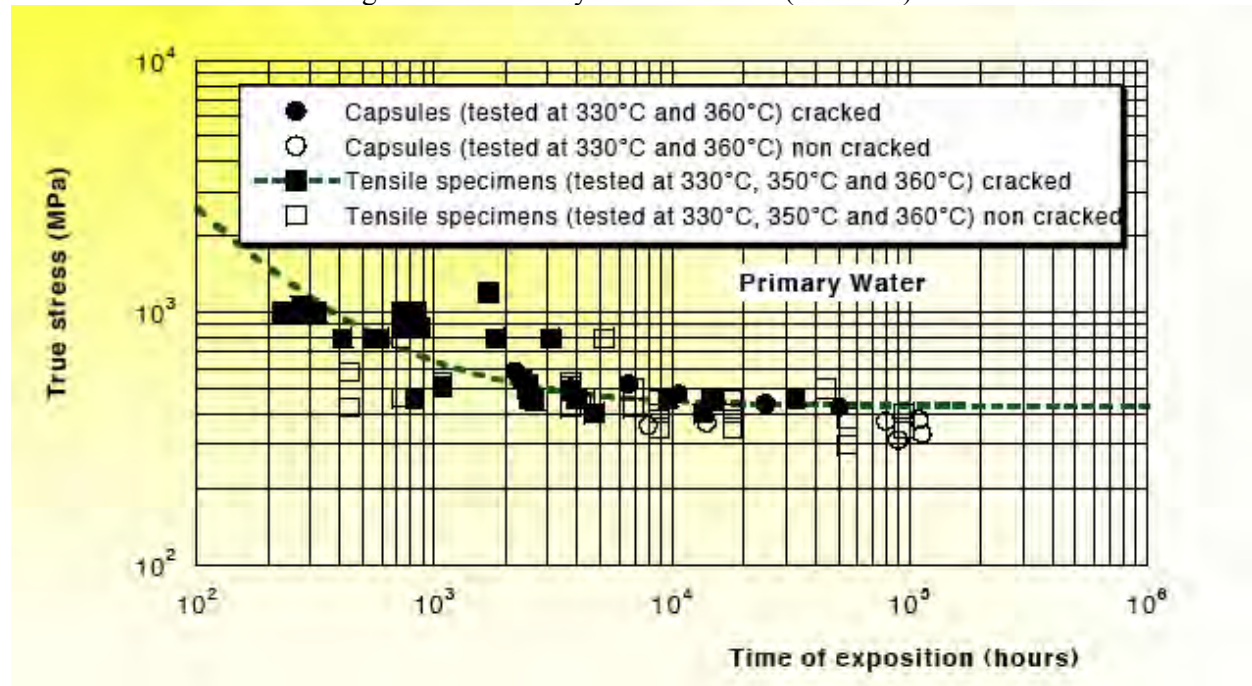


Figure 2.12 Initiation time as a function of applied stress for Alloy 182 weld material (Ref. 2.18)

To get realistic estimates of cracking for large weldments, the initiation time for a unit specimen with an effective active length³ of 25.4 mm (1 inch) will have to be about 100 years (about 10^6 h), i.e., the region of interest is an order of magnitude further out in time than the longest tests ever run in the laboratory.

In Figure 2.13, it can be seen that on the laboratory time scale, the stress behavior is similar to the σ^{-4} often assumed. A Scott-type stress model of the form $(\sigma - \sigma_0)^{-m}$ where m is closer to 1 and σ_0 is a threshold stress is much more appropriate in the region of interest. Because the quantitative results are based on only one data set, the particular values may not be the most appropriate. Based on a broader review of data, a value of m around 1.5 may be appropriate for a Scott-type model. The parameter σ_0 will have a value in the range of 250 to 330 MPa (36 to 48 ksi). However, the flatness of the curve suggests that in this region life is not really stress controlled. Like high cycle fatigue, there is a lot of scatter in life due to minor microstructural variations, surface finish, etc. The variations in life may be

³ A 25.4-mm (1-inch) subunit length was arbitrarily chosen.

due as much or more to variations in σ_0 , which is affected by surface treatment, prior strain history, etc., as in variations in σ . Because the threshold stress is near yield, it is clear that design stresses alone would have little effect on initiation. Higher residual stresses from welding, forming, grinding, etc. are generally needed to cause cracking.

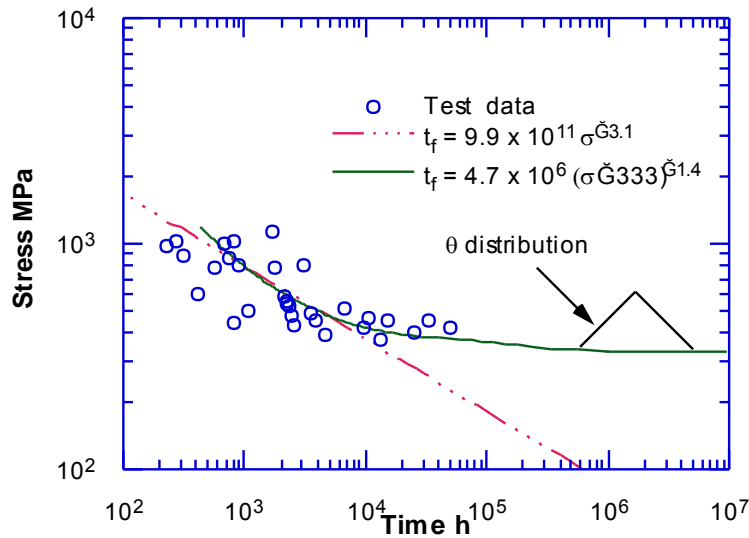


Figure 2.13 Power law and Scott-type fits to Amzallag et al. data

Because of the limited field data available on cracking in hot-leg weldments, initial estimates for the Weibull scale parameter θ to be used in PRO-LOCA (for the default model) were obtained from the analysis of leakage data from CRDM nozzles. Data on the inspection results for the vessel heads of 30 US nuclear plants were analyzed to obtain maximum likelihood estimates for the distribution of the Weibull scale parameter for Alloy 600 nozzles (Ref. 2.19). The distribution for θ was obtained in terms of a log-triangular distribution. The parameters that describe the distribution at 315 C (600°F) are given in Table 2.7.

Table 2.7 Lower and upper limit and peak location for log-triangular distributions for values of the Weibull scale factor θ of a CRDM nozzle at 315 C (600°F) for b=3, 3.5, 4

	Lower Limit	Peak Location	Upper Limit
b=3	3.38	3.46	6.94
b=3.5	3.33	3.37	6.23
b=4	3.28	3.30	5.74

The value $b = 3$ is widely used and gives somewhat more conservative results (earlier failures) than the higher values of b . Thus, a value of $b=3$ is used in the PRO-LOCA code for the default PWSCC initiation model. In order to apply these results to other systems, it is convenient to express the results in terms of θ values for a subunit of width⁴ 25.4 mm (1-inch). At 315 C (600°F), the distribution of the θ of a subunit is given in Table 2.8 using an estimated value of 14.5 subunits for a CRDM nozzle.

Table 2.8 Lower and upper limit and peak location for log-triangular distributions for values of the Weibull scale factor θ of a 25.4-mm (1-inch) subunit at 315 C (600°F) for b=3, 3.5, 4.

	Lower Limit	Peak Location	Upper Limit
b=3	4.27	4.35	7.83
b=3.5	4.09	4.13	6.99
b=4	3.95	3.97	6.41

Table 2.8 are adjusted for temperature using Arrhenius extrapolation. The values are also representative of the values of residual stress and residual plastic strain typical of CRDM nozzles. If it is determined that in other applications the stresses differ systematically from those in the nozzles, the values could be adjusted using a stress adjustment parameter $\Sigma(\sigma)$

$$\Sigma(\sigma) = \begin{cases} \left(\frac{\sigma_{\text{noz}}}{\sigma} \right)^n \\ \left(\frac{\sigma_{\text{noz}} - \sigma_0}{\sigma - \sigma_0} \right)^m \end{cases} \quad (2.46)$$

based on the behavior observed in small specimen test. For the current version of the PRO-LOCA code, it is assumed that $\sigma_{\text{noz}}/\sigma = 0.75$ for the default PWSCC initiation model.

The values in Table 2.7 and Table 2.8 are based on *initiation of leaks* in CRDM nozzles. They are thus nonconservative for the *initiation of cracks*. Based on some initial calculations of the time for growth of through-wall cracks,⁵ it would be reasonable to decrease the scale factors for initiation of cracking in

⁴ The subunit length of 25.4 mm (1 inch) was chosen as an arbitrary value to demonstrate the subunit applicability. In the PRO-LOCA code, scale factors are expressed for a subunit size of 10 mm by using Equations 2.42, 2.43, and 2.44.

⁵ D. Rudland, Emc² to W. J. Shack, Personal Communication, March 12, 2004.

nozzles in Table 2.7 by about 4-5 years. There would be a corresponding decrease in the scale factors for the subunits in Table 2.8. However, field data also suggest that the time to initiation of Alloy 182 is greater than that for Alloy 600 materials (Ref. 2.20). Thus the values in Table 2.7 and Table 2.8 may be used directly to describe initiation of cracking in Alloy 182 weldments. To test these results, the distribution for θ given in Table 2.8 was used to estimate the number of cracks expected to date in PWR hot legs. There are some uncertainties in these calculations, since the hot-leg metal temperatures are not known for all PWRs. It is also not clear exactly which PWRs have Ni-alloy weld metal butters on the hot leg, although it is known that 63 percent do. The results of the Monte Carlo calculations for the expected number of leaks are summarized in Table 2.9. The calculations were done for all Westinghouse PWRs, and then the results reduced by a factor of 0.63.

Table 2.9 Number of cracks expected in hot legs of US PWRs to date based on scaling of the current CRDM nozzle data

Σ	Average number of cracks	St. Dev.
1.0	24.3	1.5
3.2	13.2	1.9
7.7	3.0	1.3
16.0	0.5	0.5

There are only a two reported instances of hot-leg cracking, although without complete inspection information, the actual number is unknown. A value of Σ must be about 7.7 to match the reported cracking. Of course, this assumes that the Weibull scaling is perfect and that the only reason for a difference in the results is a difference in the average stresses in the nozzles and the hot leg. Other factors may be important such as the actual metal temperature. The calculations in Table 2.9 assume a metal temperature of 327 C (620°F). Lowering the metal temperature to 315 C (600°F) reduces the number of cracks from 24 to 8 for a Σ of 1. For the default PWSCC initiation model in the PRO-LOCA code, Σ is assumed to be 3.2 ($\sigma_{noz}/\sigma = 0.75$)

2.7.3 Default IGSCC initiation Model

Initiation of IGSCC in BWRs is also assumed to be statistical process described by Weibull statistics. Thus again cracking of subunits can be related to cracking of weldments of any diameter through Equations 2.42 through 2.44. Values for the Weibull scale parameter and slope can also be estimated from available plant data by Maximum Likelihood Estimation.

The likelihood function for the incidence of cracking in weldments of diameter D reported in NUREG/CR-4792 Volume 3 (Ref. 2.21) is of the form:

$$\ln(L) = \sum_{i=1}^N \ln \left(\int_0^{\infty} p(\theta_i) \frac{N_i!}{n_{f_i}!(N_i - n_{f_i})!} \left\{ W(t_i, \theta_{D_i}, b)^{n_{f_i}} [1 - W(t_i, \theta_{D_i}, b)]^{N_i - n_{f_i}} \right\} d\theta_i \right) \quad (2.47)$$

where N_i is the total number of units in bin i , n_{f_i} is the number of failures in bin i , D_i is the diameter of the welds in bin i , and W is the cumulative Weibull probability function. Using Equations 2.42 through 2.44, the likelihood can be expressed in terms of a single distribution for the Weibull scale factor for the subunit. The distribution is chosen to maximize the likelihood. The scaling laws can be used to determine the Weibull scale factor for any other subunit size.

Volume 3 of the PRAISE report NUREG/CR-4792 (Ref. 2.21) has some field data on cracking in BWRs (Table 5 page 66). This is presumably early 1980s vintage data and hence applicable to BWRs with normal water chemistry (with relatively high impurity levels) and Type 304 SS piping. The data are

highly aggregated. Ideally, what one would like is the number of incidences of cracking per heat at various times. However, these data are aggregated by pipe size for all plants for three inspection times. Thus, when a heat characteristic is picked from a distribution, it applies to all small pipes, or intermediate pipes, or large pipes. It is not clear how this crude binning affects results.

The likelihood is maximized for a Weibull slope of $b = 1$ with θ_ℓ given by a log-triangular distribution with a lower limit of 4.23, a peak location of 8.33, and an upper limit of 8.34. This corresponds to median lives of roughly 68, 4,163, and 4,174 years. As expected, the likelihood maximum is very broad. Shifting the location of the peak value from 8.33 to 7.96 (4,163 to 2,850 years) changes the likelihood function by less than a factor of two.

Having determined a distribution for θ_ℓ , Monte-Carlo samples were generated to estimate the number of leaks that would occur if in fact the weldments were drawn from the distribution. Samples were run for 1, 2, 5, and 10 heats of material. The predicted number of cracks and the standard deviation are shown in Table 2.10.

Table 2.10 Predicted total number of cracks in BWR piping weldments. The observed number is 328

Number of heats of material	Average number of cracks	Standard deviation
1	619	198
2	624	133
5	610	86
10	612	63

These values are about a factor of two higher than the number of cracks used to develop the distribution. The discrepancy may be due to the forced aggregation discussed previously, but the values still seem like a reasonable starting point for analysis.

- The slope value in this case is much smaller than is generally observed for the case of PWSCC in PWRs. However, Eason and Shusto (Ref. 2.22) did a Weibull analysis of cracking for piping in BWRs and also obtain values of b close to 1. The review by Staehle (Ref. 2.23) also cites numerous situations in which investigators have found values of b close to 1 for SCC.

The model above describes conditions that are not very representative to modern BWRs. All BWRs have taken one or more mitigation measures to reduce susceptibility to IGSCC. Ongoing inspections show a marked decrease in the incidence of cracking in BWR piping. Laboratory testing suggests that times to failure (which in the laboratory tests would track closely with times to initiation) are increased by a factor or 20 or more (Ref. 2.23). The most conservative approach to develop an initiation model more representative of modern BWRs would be to use the distribution developed on the field data from the 1970s and 80s as a prior distribution, and then use inspection results for BWRs since that time to do a Bayesian update on the prior distribution. This essentially gives “credit” for the improved performance in actual operation, but ignores the evidence from laboratory testing that the factors of improvement are actually greater, but there has simply not been enough time to observe the full improvement by looking solely at operational data.

An alternate approach would be to consider the current results as a base case (Type 304 stainless steel with low purity normal water chemistry) with a corresponding crack growth rate (CGR) model (SCC and

corrosion fatigue). Reasonable (conservative) factors of improvement could be assigned to the other chemistry and material combinations:

- a factor of 2-5 in initiation for Type 304 stainless steel with high-purity normal water chemistry,
- a factor of 5-10 in initiation for Type 304 stainless steel with hydrogen water chemistry and Type 316NG with normal water chemistry, and
- a factor of 15-20 in initiation for Type 316NG stainless steel with hydrogen water chemistry.

At this point in time, this may be the best approach for estimating the initiation of cracks due to IGSCC in hydrogen water chemistry. These factors were incorporated into the default IGSCC initiation model in the PRO-LOCA code. The bigger change in this activity is allowing the user to change the water chemistry during the life of the plant. Currently, the water chemistry must remain constant during the life of the plant. The development of the deterministic model to address these effects is now complete. At this time the deterministic model merely needs to be incorporated into PRO-LOCA. (Note, under the Damage Tab in the PRO-LOCA GUI there is a window labeled Water Chemistry where the user can input the dissolved oxygen (in terms of parts per million) and water conductivity, however, this tab only affects the fatigue crack initiation model. It has no affect on SCC initiation or growth.)

These factors were incorporated into the PRO-LOCA code, and several example problems were run to investigate their affect on the failure probabilities. The BWR1 case developed in the FY05 effort was used as a case study. The only modification made was that in-service inspections were eliminated. The results of these runs are shown in Figure 2.14. In this figure, the blue diamonds represent the base case.

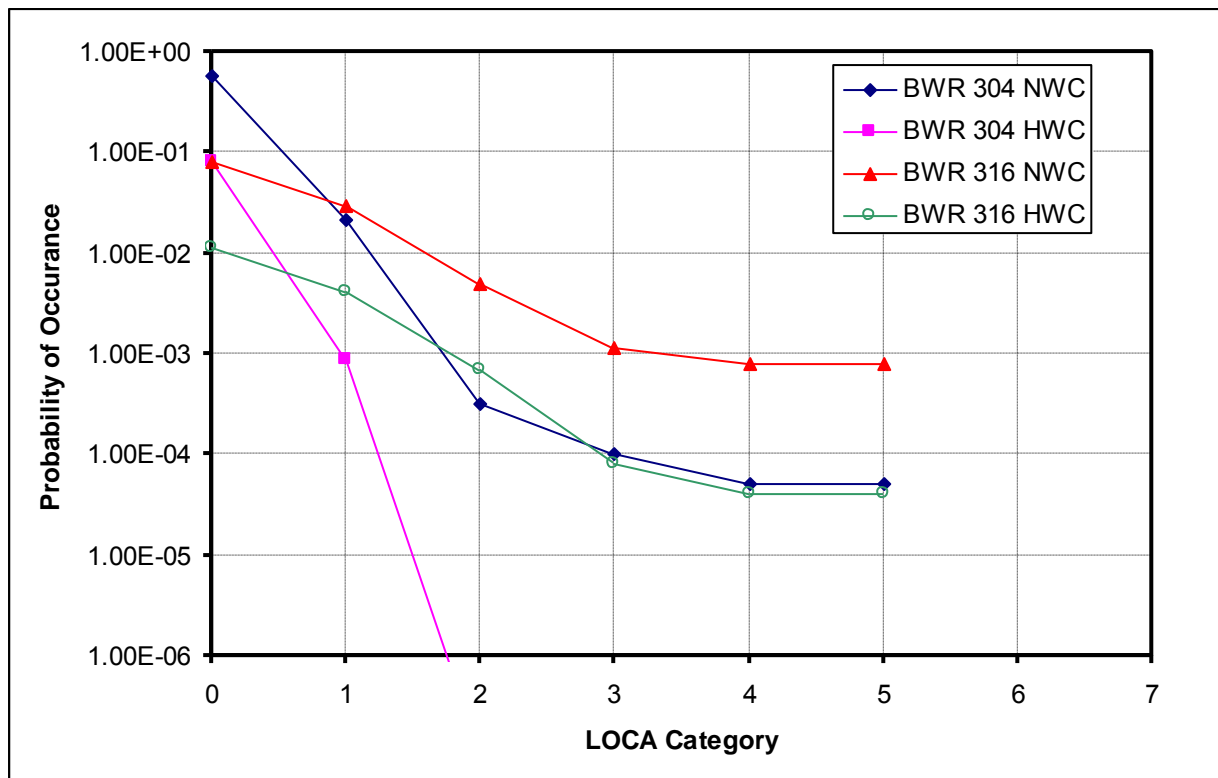


Figure 2.14 Probability of occurrence versus LOCA category for different BWR water chemistries for both Type 304 and Type 316 stainless steel

For time to develop a through-wall crack (i.e., LOCA Category 0), the trends between the cases look appropriate. However, for the larger size LOCAs, the Type 316 material with normal water chemistry appears to have a higher probability of occurrence than the Type 304 with normal water chemistry. On

the surface this is not consistent with the trends for these materials, i.e., Type 316 is supposed to be more resistant to IGSCC than Type 304. However, with further examination, it was discovered that this inconsistency could be attributed to the fact that the inspections were removing defects from the analyses, thus making it only appear that the Type 304 material was more resistant to IGSCC than the Type 316 material.

2.7.4 User Options for Crack Initiation

In the earlier versions of PRO-LOCA, default crack initiation models were used for both fatigue and SCC. As part of the MERIT program, user defined crack initiation models were added to PRO-LOCA as an option. Several options, each with multiple sub-options, are now available to the user:

- Single crack model – only one crack initiates during the plant lifetime
 - Default time to initiation,
 - Default time to initiation, with variable lengths and depths,
 - User inputs a distribution for the time to initiation, with variable lengths and depths
- Number of cracks per year model
 - Default time to initiation, fixed lengths and depths
 - Poisson arrival rate model, variable lengths and depths
- Multiple crack initiation model
 - Default time to initiation,
 - Default time to initiation, with variable lengths and depths,
 - User inputs a distribution for the time to initiation, with variable lengths and depths

For the multiple crack initiation models, cracks are initiated and placed randomly around the circumference. A crack location biasing option is also available with the multiple crack initiation models. The details of that location biasing routine can be found in Reference 2.24.

For the user defined options, the user inputs a distribution for the crack length and the crack depth. The distributions can be:

- Constant
- Uniform
- Normal
- Lognormal
- Weibull
- Exponential
- Extreme Value Type II

2.7.4.1 Single Crack Analyses with User Defined Weibull Parameters

For this selection, the distribution type, the mean, and the standard deviation of the crack length and crack depth must be supplied. However, a constant “distribution” was added so that it is possible to perform the analysis with a single crack of fixed length and depth (initially). For this analysis only one subunit exists and the subunit with the crack is assumed to be centered at the location where the bending moment is a maximum.

The results of using this option are shown in Figure 2.15. Since there is only a single crack, using the initiation data from the earlier version of PRO-LOCA leads to lower initiation times. This is because of the subunit scaling. If the results are rescaled for the number of subunits then Figure 2.16 shows the results. Both of these runs used 10,000 simulations to reduce the run times.

Monte Carlo Simulation Results for PROLOCA 2007

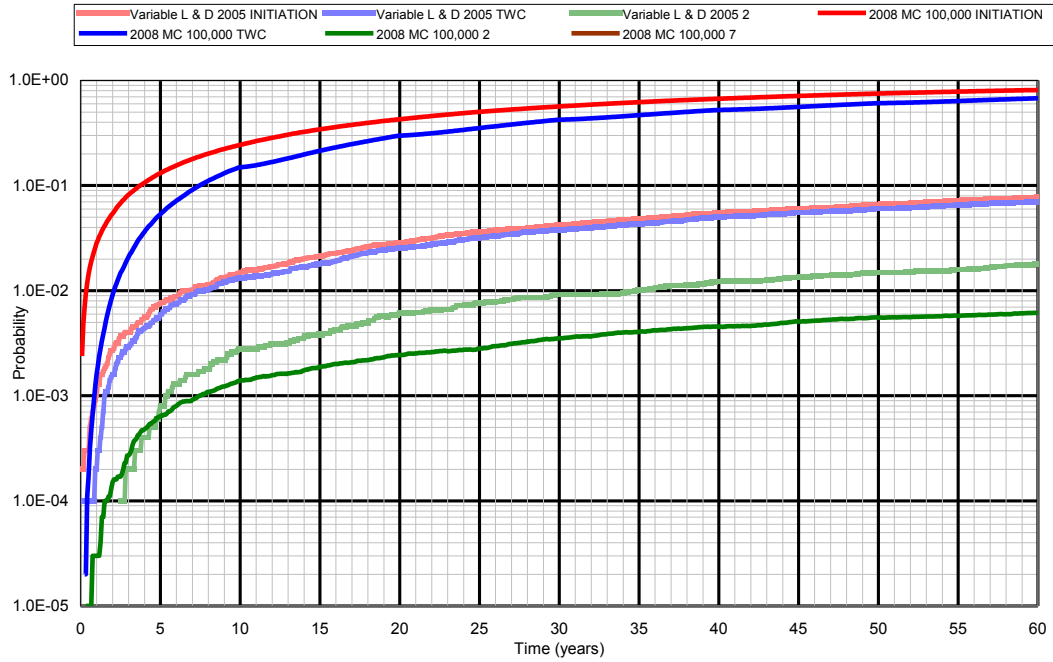


Figure 2.15 Results for a single crack with fixed length and depth (initially)

Monte Carlo Simulation Results for PROLOCA 2007

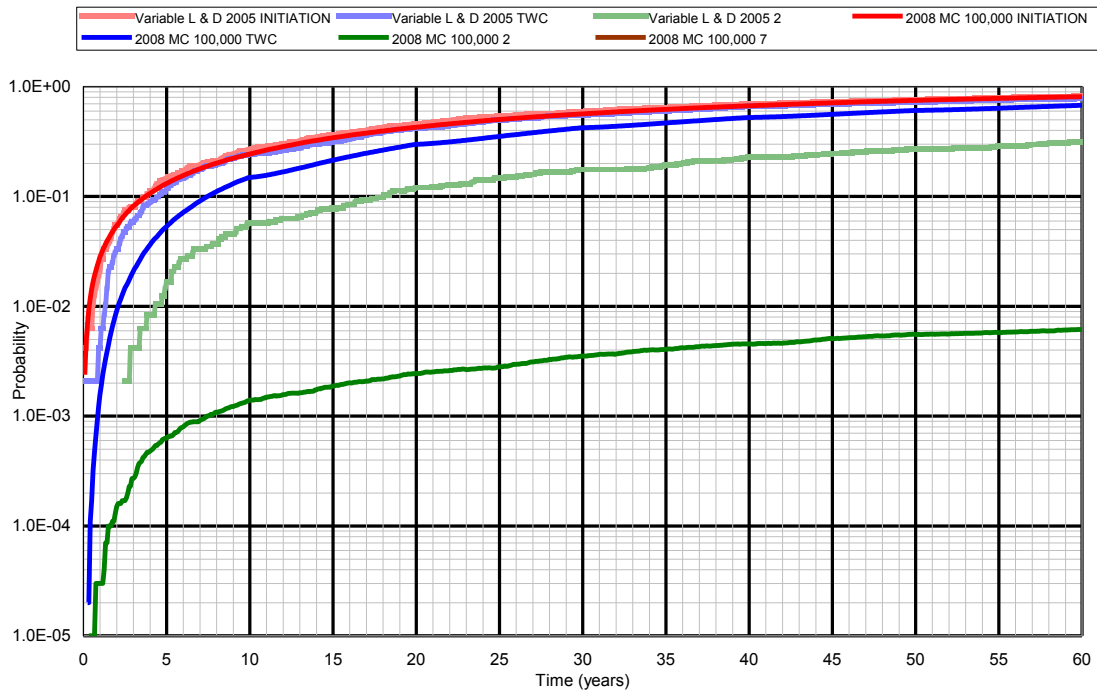


Figure 2.16 Results from Figure 2.15 analysis but with results rescaled for the number of subunits

2.7.4.2 Number of Cracks per Inch of Susceptible Material

Perhaps one of the most important aspects in the development of a probabilistic fracture mechanics (PFM) code for predicting large break loss-of-coolant accidents (LOCAs) is the consideration of the initiation of subcritical cracks, and in particular the proper characterization of multiple crack initiation sites. One approach for introducing multiple initiated cracks into the analyses is an arrival rate model. An arrival rate model for entering the number of cracks per inch of susceptible material per year was developed and incorporated into PRO-LOCA as part of MERIT. For this Poisson's arrival rate model the number of subunits is not fixed, but instead is a variable predicated on the number of initiated cracks predicted by this model. When choosing this arrival rate model, the user selects a distribution type along with means and standard deviations for both the initiated crack lengths and depths. A sample result of the first 100 simulations for such an analysis is shown in Figure 2.17.

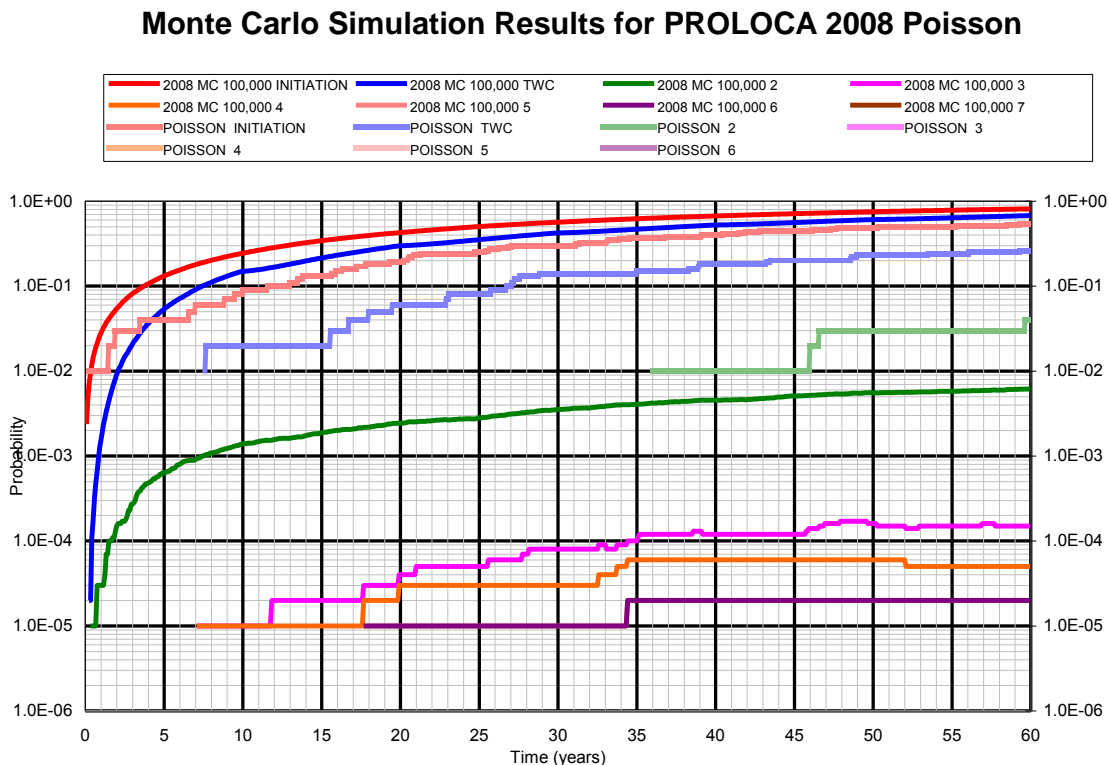


Figure 2.17 Results from cracks per inch of susceptible material for first 100 simulations

2.7.4.3 Multiple Stress Corrosion Crack Initiation Sites

If a single crack were to initiate and grow by typical fatigue mechanisms, then that crack growth in a pure membrane stress is dependent on the aspect ratio (length/depth) of the crack. If the crack length is short with respect to the depth, then the influence functions are higher in the length direction than in the depth direction such that the crack growth rate is higher in the length direction than in the depth direction. However, once a crack grows to a size that its length is greater than its depth, then the influence functions are higher in the depth direction than in the length direction and the crack growth rate in the depth direction becomes higher than in the length direction. Such cracks would tend to grow through-wall before they could reach a critical size. Such cracks would readily be detected by leakage and would not realistically contribute to the probability of a large break LOCA occurring. On the other hand, long surface cracks that do not leak prior to the occurrence of a transient loading event are the more realistic contributor to the probability of a large break LOCA. Such long surface cracks could occur with a high

stress gradient through the thickness, or possibly as a result of multiple cracks initiating and growing together to form one long surface crack. Stress corrosion cracks typically initiate in a high residual stress field, such as at a girth weld. Since the residual stresses are the dominant stress (over the normal operating stresses) leading the crack initiation and growth, and have gradients through the thickness, there is the propensity for multiple cracks to initiate, with each of those cracks growing more in the length direction than in the depth direction. Understanding this propensity for multiple cracks initiating and linking together is of key importance for developing an improved and realistic probabilistic code for predicting large break LOCA events. While analyzing cracks found in service it was found that if one SCC crack initiates, there is a 90 percent chance that other cracks will initiate in the same weld, so the initiation of a second crack is not purely random.

In the FY04 version of the PRO-LOCA code, the critical node being analyzed was broken down into subunits of length 10 mm. Each of these subunits had the probability of initiating an SCC crack that followed the distribution described in the previous section. Since it may not have been realistic to assume that these cracks occur randomly, a simplistic model for predicting multiple SCC initiations was developed. Each of the “n” subunits at the critical node had an individual time of SCC initiation, t_1, t_2, \dots, t_n , that followed the Weibull probability distribution described in the previous section. Next a uniformly distributed random number (R_{check}) between 0 and 1 was generated. If R_{check} was greater than P_{50} , which represents the probability that multiple cracks will initiate at a time, it was assumed that the SCCs at n subunits would initiate at the timings, t_1, t_2, \dots, t_n , previously generated. For the FY04 version, P_{50} was hard coded to 50 percent (i.e., 0.5).

If R_{check} is less than P_{50} , then another uniformly distributed random number (C_{10}) between 0 and 1 was generated and multiplied by 10 percent. This number represents the number of cracks that will initiate, and was always less than 10% of the total number of subunits⁶.

For illustration, assume $R_{check} < P_{50}$, $n = 30$, and $C_{10} = 0.1$. Then at time t_1 , ($30 \times 0.1 = 3$) SCCs will form. The times for the first three initiating cracks (from the Weibull distribution) are set to the first initiating crack's time ($t_1 = t_2 = t_3$) = t_1 . At the next initiation time, t_4 , ($27 \times 0.1 = 3$) SCCs will form. The times for the fourth, fifth, and sixth initiations were set to the time of the fourth initiation. This process continued through the rest of the time history. The location of the initiated cracks corresponded to the initial distribution set by the Weibull distribution. For instance, the locations of the first three initiated cracks were at the locations marked t_1, t_2 , and t_3 in Figure 2.18, but all occurred at time t_1 .

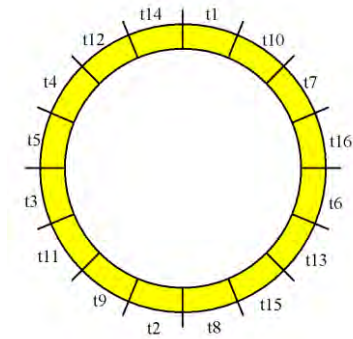


Figure 2.18 Initiation times per subunit

If a crack, which is initiated by some other mechanism (such as fatigue or initial flaw), already exists at the location of the subunit, then SCC initiation was ignored in that subunit. Clearly, this was a simplistic approach for predicting multiple crack initiation sites. As such a more robust analysis scheme was

⁶ This number was chosen as a best guess at the number of subunits that may initiate at the same time.

developed. This more robust methodology, which was incorporated into the FY05 version of PRO-LOCA replaced this previously developed FY04 method.

For the FY05 version of the PRO-LOCA code, IGSCC cracking data from the Nine Mile Point plant was used to aid in developing an improved IGSCC time to crack initiation distribution and a more realistic crack biasing routine. For the current version of PRO-LOCA the user has the option of turning this biasing option on or off if they chose a multiple crack initiation analysis with the user defined initiation time distribution. (For the single crack initiation analysis or the multiple crack initiation analysis with the default initiation time distribution, this biasing option is not available.) Sensitivity studies have shown that this location biasing has only a minimal affect on the probabilities of leakage (~10%).

2.8 Subcritical Crack Growth Models

The subcritical crack growth models were not developed as part of this program. Argonne National Lab has conducted years of research in developing crack growth models for nuclear grade piping steels at operating conditions. Therefore, it was prudent to use these models. The crack growth models have been fully documented in references by Argonne and therefore only a summary is presented in this section.

2.8.1 K-Solutions

In order to make proper crack growth predictions, accurate stress intensity factor solutions are needed. Over the years, many researchers have developed K-solutions for circumferential and axial surface and through-wall cracks in cylindrical vessels based on finite element parametric analyses. Researchers such as Atluri and Kathiresan (Ref. 2.25), McGowan and Raymond (Ref. 2.26), Raju and Newman (Ref. 2.27), Chapuliot and Lacire (Ref. 2.28), and Anderson et al. (Ref. 2.29) have all used three-dimensional finite element analyses to infer stress-intensity factor solutions along a semi-elliptical crack front in cylindrical vessels. In all cases, the K-solutions were developed using the principle of superposition.

The principle of superposition states that the solution for a multiple load case is equal to the sum of the results from the individual load cases. If one considers an arbitrary body subjected to a far-field normal stress, a traction at the desired crack plane exists. If a crack was present at that location, superposition could be used, as shown in Figure 2.19, to calculate the stress intensity factor. In short, the stress intensity factor for a far-field load is equal to the stress intensity with a crack face load equal to the normal stress at the crack location in absence of the crack.

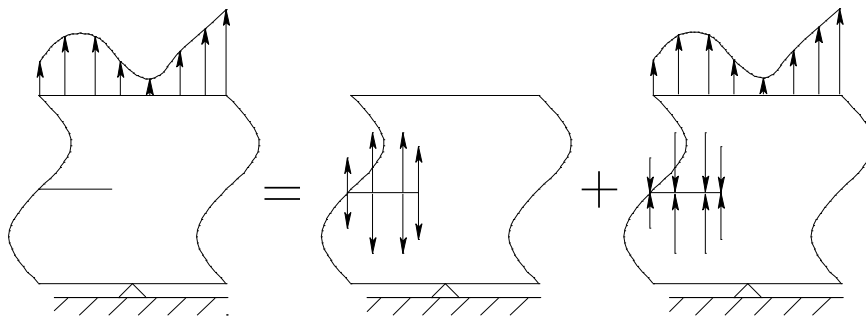


Figure 2.19 Application of superposition showing stress intensity simplification

In all cases, researchers have run parametric finite element analyses using power-law crack-face pressure to infer stress intensity factors from far-field arbitrary loading. The form of the crack-face pressure is as follows.

$$p(x) = p_n \left[\frac{x}{a} \right]^n \quad (2.48)$$

where x is the local coordinate measured from the mouth of the crack, a is the crack depth, and p_n is the stress at $x = a$.

If a through-wall stress distribution in an uncracked cylinder can be represented by a polynomial of the form

$$\sigma(x) = \sigma_0 + \sigma_1 \left[\frac{x}{t} \right] + \sigma_2 \left[\frac{x}{t} \right]^2 + \sigma_3 \left[\frac{x}{t} \right]^3 + \sigma_4 \left[\frac{x}{t} \right]^4 \quad (2.49)$$

and if a crack is introduced into this stress field then,

$$K_I = \left(\sigma_0 G_0 + \sigma_1 G_1 \left[\frac{a}{t} \right] + \sigma_2 G_2 \left[\frac{a}{t} \right]^2 + \sigma_3 G_3 \left[\frac{a}{t} \right]^3 + \sigma_4 G_4 \left[\frac{a}{t} \right]^4 + \sigma_5 G_5 \right) \sqrt{\frac{\pi a}{Q}} \quad (2.50)$$

where Q is the surface-crack shape parameter and G_i are the influence functions⁷, which are nondimensional representations of K . The individual G values are inferred from the power-law crack-face-pressure finite-element runs and then summed using the principle of superposition.

In order to generate the influence functions, the five different power-law load cases would have to be individually run to obtain the influence functions. For the magnitude of R/t , a/c , and a/t values required to fully characterize the stress intensities for cracked cylinders, the number of finite element runs becomes unreasonable. In fact, many researchers limited the number of solutions by only considering lower-order stress terms and limited crack and cylinder geometries.

However, current researchers have used weight functions to limit the number of analyses needed to fully characterize this problem. The basis for the weight function approach is a reciprocal theorem that states that given two arbitrary and independent linear elastic solutions for the same body the following equation is valid:

$$F_i(a) * u_i(b) = F_i(b) * u_i(a) \quad (2.51)$$

where F_i are the applied forces, u_i are the displacements at the same points, and a and b are different loading histories.

The weight function separates the influences of stress field and geometry of a cracked body on the stress intensity factor. Once the weight function for a particular body is developed, the stress intensity can be determined for any loading by integrating the product of the loading and the weight function. One must be careful in utilizing generic weight functions in complex geometries. The functions are usually given for crack-face tractions, and are affected by the presence of any fixed-displacement boundary conditions. When utilizing the weight functions, the resulting K will reflect the fixed-displacement condition used in generating the weight functions. Therefore care must be taken when applying the weight-function approach to a complex geometry.

Some of the earlier K -solutions generated were limited in crack size and location, i.e., limited crack-depth-to-length ratios, and wall-thickness-to-vessel-radius ratios. However, the Anderson solutions contain influence functions for both internal and external semi-elliptical circumferential cracks in cylinders for a variety of R/t , crack length, and crack depth values. In addition, Anderson has circumferential through-wall-crack solutions for similar pipe geometries. Therefore, it was decided to use these solutions in the PRO-LOCA code.

⁷ Note that σ_3 is the global in-plane bending stress, and G_3 is the influence function for this stress.

2.8.1.1 Circumferential Surface Cracks

Andersons K-solutions for a circumferential surface crack on the inside pipe diameter are given in Reference 2.29. The solutions in this report were generated for R/t values from 3 to 100, c/a values from 1 to 32 and a/t values from 0.2 to 0.8. Anderson generated influence functions G_0 and G_1 as given in Equation 2.50, and G_5 which corresponds to global in-plane bending. The influence function G_2 , G_3 , and G_4 are inferred from the weight function formulas given in Reference 2.29.

The influence functions were generated for any location along a semi-elliptical crack front as defined in Figure 2.20. However, in this code, it is assumed that the crack remains semi-elliptical as it grows, therefore the only crack front locations of interest are at the deepest point and at the free surface. Using the definitions in Figure 2.20, the deepest point is defined at $N = 90$ degrees and the surface point is defined at $N = 0$ degrees.

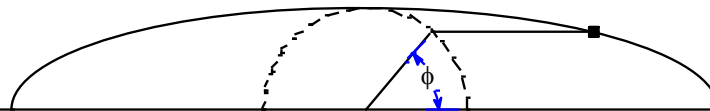


Figure 2.20 Definition of crack-front angle

Using the tables of influence functions in Reference 2.29, curve fits were performed. The curve fits were optimized to minimize the difference between the curve fit and FE value. For the influence functions at the deepest point ($N = 90$ degrees), the maximum error was about 5 percent. However, due to the inconsistency of the surface influence functions ($N = 0$ degrees), the maximum error was about 20 percent.⁸ An example of the curve fit compared to the FE results is shown in Figure 2.21.

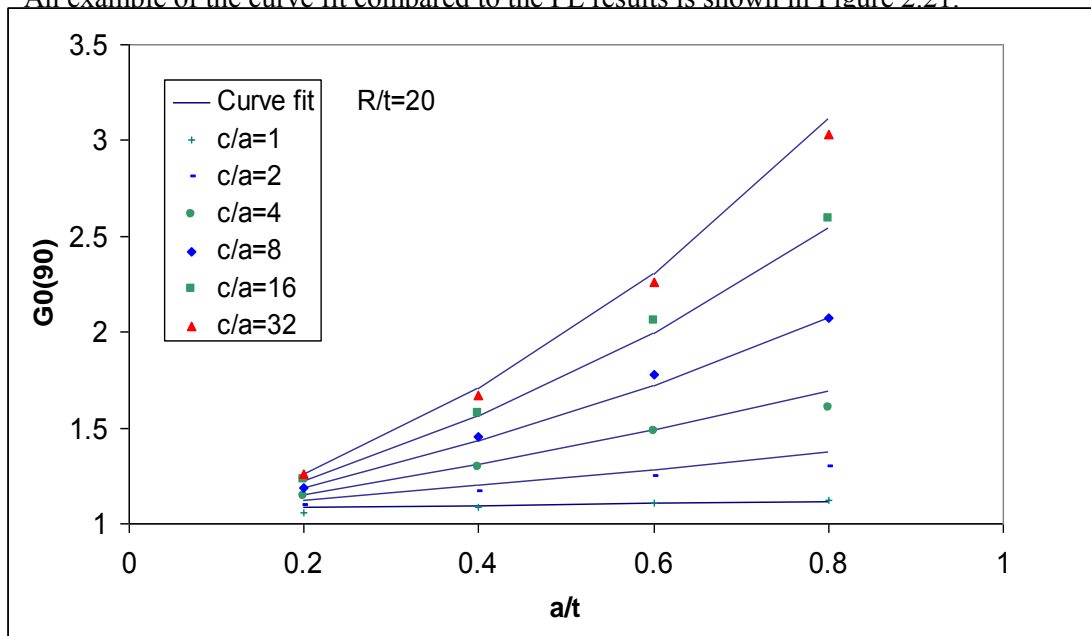


Figure 2.21 Comparison of curve fit and FE solutions for influence function G_0 at the deepest point of a circumferential surface crack in pipe with $R/t=20$

⁸ Note that the largest errors occurred for the longest cracks, which have the smallest influence functions. Therefore, even with a 20 percent error, the absolute difference in the influence functions was small.

As shown from Figure 2.21, there are several shortcomings of the Anderson solutions. First, the influence functions were only generated for a/t values from 0.2 to 0.8. This becomes a problem when trying to predict crack behavior from initiation to failure. Therefore, several assumptions were made. First, when the crack becomes a through-wall crack an equivalent area approach is used to establish the length of the resultant through-wall crack. Secondly, a solution by Chapuliot (Ref. 2.28) was developed for $a/t = 0$. These results were incorporated and linear interpolation was used between these values and Anderson's results at $a/t = 0.2$.

In addition to the elliptical surface crack results, Anderson also generated K solutions for $a/c = 0$ (infinitely long surface crack). Since long surface crack K -solutions are currently not available, it was assumed in this code that for surface cracks with c/a greater than 32, the K solution at the free surface is equal to the K -solution at $c/a = 32$ and at the deepest point, the K -solutions equals that of the K -solution for $a/c = 0$. This assumption is conservative in the length direction, because as the crack length gets longer, the influence functions (hence the K -solution) at the free surface tends toward zero. By using the K -solution at the free surface equal to $c/a = 32$, slightly larger crack growths will occur, producing conservative leak probabilities.

2.8.1.2 Circumferential Through-Wall Cracks

The Anderson K -solutions for a circumferential through-wall crack in a pipe are given in Reference 2.30. These solutions were generated for R/t values from 1 to 100 and to crack lengths of about 66 percent of the circumference. The solutions were generated for both the inside and outside surface of the through-wall crack, however; only the G_0 , G_1 and G_5 influence functions are available. At this time, the weight function solutions for a TWC are not available.

Similar through-wall-crack solutions were generated for through-wall cracks in pipes in Reference 2.31. These solutions are similar to those generated from Sanders (Ref. 2.32) but curve fit through 1 at a zero crack length. A comparison of the NURGER/CR-4572 (Ref. 2.31) results with the Anderson solutions is shown in Figure 2.22. In this figure, the Anderson solution is averaged though-wall, and is shown to be slightly higher than the solution in NUREG/CR-4572.

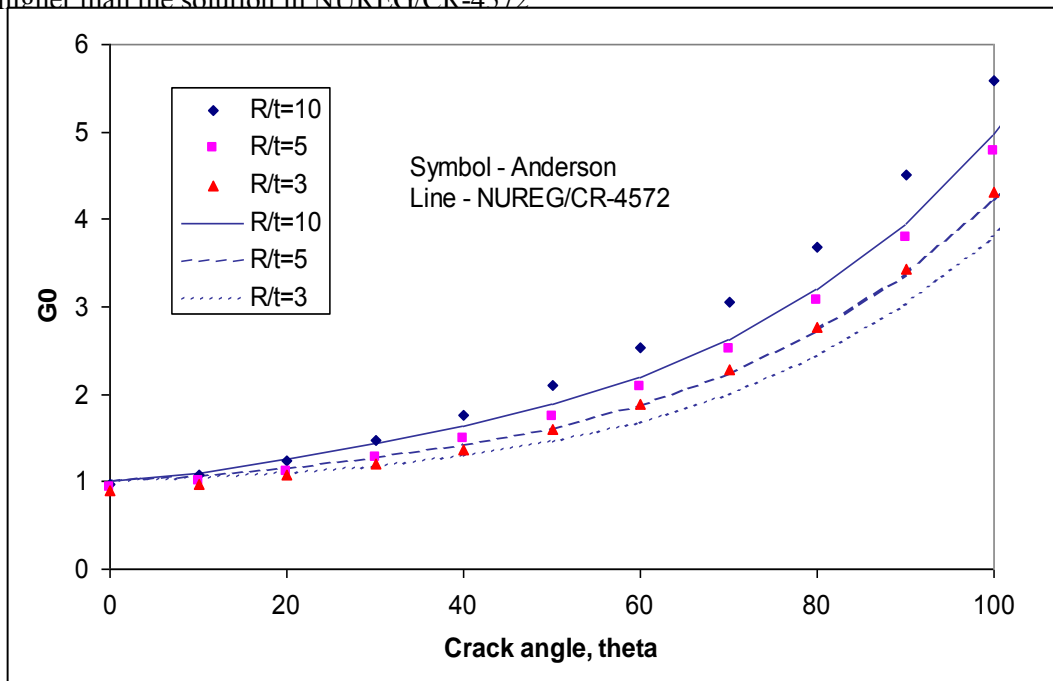


Figure 2.22 Comparison of Anderson solution and the solution in NUREG/CR-4572. Note G_0 is for axial membranes loading only

The Anderson solution was chosen for use in the PRO-LOCA code because of its larger range of R/t values and its modeling of linear through thickness stress distribution. In Reference 2.30, the through-wall crack K solutions were curve fit and the coefficients were presented for R/t values of 1, 3, 5, 10, 20, 60, and 100. These coefficients were programmed in PRO-LOCA and linear interpolation was used to predict the coefficients for other R/t values. The influence function on both the inside and outside surface of the through-wall crack are calculated, and then averaged to get the K-solution for through-wall-crack growth.

2.8.2 Default Air/Corrosion/Thermal Fatigue Crack Growth Model

The default fatigue crack growth models used in the PRO-LOCA code were developed by Argonne. Fatigue crack growth rates are highly sensitive to a range of environmental conditions. The collection of environments considered in this model is summarized in Table 2.11.

Table 2.11 Materials and environments for consideration

Type 304 stainless steel BWR normal water chemistry
Type 304 stainless steel BWR hydrogen water chemistry
Type 316NG stainless steel BWR normal water chemistry
Type 316NG stainless steel BWR hydrogen water chemistry
Type 304 SS PWR primary water chemistry
Alloy 600 PWR primary water chemistry

The problem of environmental effects on fatigue crack growth rates is treated in detail in Reference 2.33. There can be environmental effects on fatigue even for material and environmental combinations that do not produce classical SCC. The three term superposition formulation proposed in Reference 2.33 is descriptive over a wide range of conditions and is in good agreement with the results of the PLEDGE code⁹ for comparable water chemistries, but may be unnecessarily complex for a probabilistic fracture mechanics code. An alternate approach is taken here. Only two terms, a SCC and a corrosion fatigue term, are used. Corrosion fatigue contributions are computed using a version of PLEDGE that was modified to base cyclic crack growth rates on the ASME Section XI correlations developed by James and Jones (Ref. 2.34). The modified PLEDGE code was benchmarked against the crack growth models in Reference 2.33 and the original version of PLEDGE. The calculations were done for cyclic loadings corresponding to rise times of 1, 10, 100, 1,000, and 10,000 seconds with R values of 0.7, 0.5, and 0.3. The resulting crack growth rates were then divided by the ASME Section XI results for the same loading conditions to get an environmental effects coefficient, E. As expected, some material and environmental combinations show little enhancement. The largest enhancement is for conventional Type 304 stainless steel in a relatively low purity normal BWR water chemistry—a condition that essentially no longer exists in the US. The resulting distributions for E are approximately lognormal in the sense that the results for the proposed 95th, 50th, and 5th percentiles were in reasonable agreement with those expected for a lognormal distribution. The environmental coefficients are in general functions of the rise time (or frequency). The log-means and log-standard deviations of the distributions for E can be expressed with good accuracy by simple power laws of the rise time.

The James and Jones correlation for austenitic stainless steels is

⁹ PLEDGE is a General Electric code for predicting environmentally assisted crack growth rates.

$$\frac{da}{dN} = C(T)S(R)\Delta K^{3.3} \quad (2.52)$$

where the R correction S(R) is given by

$$S(R) = \begin{cases} 1 + 1.8R & R \leq 0.8 \\ -43.35 + 57.97R & R > 0.8 \end{cases} \quad (2.53)$$

da/dN is in m/cycle with ΔK in MPa-m^{1/2}, and the temperature term C(T) is

$$C(T) = 1.154 \times 10^{-3} \exp(a_1 + a_2 T + a_3 T^2 + a_4 T^3) \quad (2.54)$$

for T in degrees F where the coefficients a_k are given in Table 2.12:

Table 2.12 Temperature coefficients for James-Jones air fatigue correlation

a ₁	-1.99E+01
a ₂	8.12E-04
a ₃	-1.13E-06
a ₄	1.02E-09

James and Jones do not give a threshold value for ΔK . Literature values range from 5.5–8 MPa-m^{1/2} (5.0–7.3 ksi-inch^{1/2}), Ref. 2.35, but the database is pretty sparse and the effect of the environment has not been studied. The use of a ΔK threshold of 5.5 MPa-m^{1/2} (5.0 ksi-inch^{1/2}) is implemented into the PRO-LOCA code for the default fatigue model for austenitic stainless steels.

It is well known that in low alloy steels, there is a threshold crack growth rate for environmental effects. Below this threshold the crack growth rate drops back to close the air rate. Above the threshold the crack growth rate can jump to a much higher rate. The work of Kassner et al. (Ref. 2.36) suggests that there is also a threshold for environmental effects on fatigue crack growth rates for austenitic materials, but the conservative assumption is made here that the threshold for environmental enhancement is the same as for fatigue crack growth in air.

James and Jones also do not give a distribution for C(T). A cursory review of their data suggests a factor of 4 to get the 5th–95th percentile bounds would be appropriate. Again, it is not clear from their paper just how many heats were included in the database so it is not clear whether the factor of 4 is primarily data scatter or actually represents the true heat-to-heat variability that should be captured. Therefore, for this version of the PRO-LOCA code, C(T) is assumed to be deterministic for the default fatigue model. A multiplier E that depends on the material environment combination and the rise time T_R of the loading cycle is introduced to account for the environment.

$$\frac{da}{dN} = E(T_R, \text{material, chemistry})C(T)S(R)\Delta K^{3.3} \quad (2.55)$$

E also incorporates the variability in the crack growth rates in air so that C(T) is a deterministic variable given by Equation 2.54. E is lognormally distributed. The log-mean (μ) and log-standard deviation (σ) of E for the different environment and material combinations are given as functions of the rise time (in seconds) in Table 2.13.

Table 2.13 Values for the log–mean (μ) and log–standard deviation (σ) for the environmental correction factor E. For rise times shorter than 1 s, use $T_R = 1$

	$\exp(\mu)$	$\exp(1.645\sigma)$
Type 304 stainless steel BWR normal water chemistry	$1.7 T_R^{0.26}$	$4.0 T_R^{0.18}$
Type 304 stainless steel BWR hydrogen water chemistry	$1.7 T_R^{0.07}$	$4.0 T_R^{0.07}$
Type 316NG stainless steel BWR normal water chemistry	$1.7 T_R^{0.14}$	$4.0 T_R^{0.11}$
Type 316NG stainless steel BWR hydrogen water chemistry	1.7	4.0
Type 304 stainless steel PWR primary water chemistry	$1.7 T_R^{0.19}$	4.0

The results in Table 2.13 suggest that for long rise times, the growth per cycle can increase markedly, although the time-based crack-growth rate decreases monotonically with increasing rise times. There is relatively limited data on corrosion fatigue of Type 304 SS in PWR primary water. Recent data by Wire (Ref. 2.37) suggest that the behavior is similar to that proposed in Reference 2.33 for BWR environments with 0.2 ppm dissolved oxygen. Based on these results, the NUREG/CR–6176 (Ref. 2.33) correlation along with the proposed factor of 4 for the air fatigue da/dN was used to develop an E term for the PWR environment. In contrast to the BWR environments in which the total crack growth rate is the superposition of the fatigue crack growth rate and an SCC term, there is no SCC term for austenitic stainless steels in a PWR environment.

A similar approach was taken to the corrosion fatigue of Alloy 600 and 690 and Alloy 182. Expressions for fatigue in air and some results on corrosion fatigue for Alloy 600 and 690 are presented in NUREG/CR–6383 and –6721 (Refs. 2.38, 2.39). In air, the nickel data has been fit with a general form similar to Equation 2.52:

$$\frac{da}{dN} = C_A(T)S_A(R)\Delta K^{4.1} \quad (2.56)$$

where the R correction $S_A(R)$ is of the form:

$$S_A = (1 - 0.82 R)^{-2.2} \quad (2.57)$$

and the temperature term C_A is a third-order polynomial:

$$C_A = 4.835 \times 10^{-14} + 1.622 \times 10^{-16} T - 1.490 \times 10^{-18} T^2 + 4.355 \times 10^{-21} T^3 \quad (2.58)$$

In Equation 2.58, the temperature is in degrees C. The crack growth rate is in m/s and K is in $\text{MPa}\cdot\text{m}^{1/2}$.

The data are too limited to develop a distribution for C_A . Equations 2.56 through 2.58 have been assumed to define median values of the fatigue life and a factor of 4 is assumed to describe the distribution of crack growth rates similar to what was found for the austenitic stainless steels in air. In NUREG/CR–6721 (Ref. 2.39) the correlation $\text{CGR}_{\text{air}} + 4.4 \times 10^{-7} \text{CGR}^{0.33}$ has been found to describe the behavior of Alloy 600 in 288°C (550 F) BWR environments and the behavior of susceptible heats of Alloy 600 in 320°C (608 F) PWR environments. In the tests, it was found that a number of heats showed little enhancement, while a susceptible heat gave the crack growth rates described by the correlation. Thus it is probably overly conservative to assume that the correlation describes the median behavior of Alloy 600. Instead it is assumed that the crack growth rate given by the correlation with the environmental term doubled and the air crack growth rate at its 95th percentile value defines the 95th percentile and that the 5th percentile value is close to the air line. The median value is then the square

root of the product. These assumptions can then be used to develop an environmental factor E fit by a power law.

$$\frac{da}{dN} = E(T_R)C_A(T)S_A(R)\Delta K^{4.1} \quad (2.59)$$

The factor E is again lognormal with log-mean (μ) and log-standard deviation (σ):

$$\begin{aligned} \exp(\mu) &= 1.7T_R^{0.25} \\ \exp(1.645\sigma) &= 4.0T_R^{0.10} \end{aligned} \quad (2.60)$$

Reference 2.39 also reviews the more limited data on the corrosion fatigue of Alloy 182. The data indicate that crack growth rates in Alloy 182 are higher than those in Alloy 600 in both air and PWR environments. It is assumed that reasonable estimates can be made by doubling the factor C_A and the mean environmental correction:

$$\begin{aligned} C_{182} &= 2C_A \\ \exp(\mu_{182}) &= 3.4T_R^{0.25} \end{aligned} \quad (2.61)$$

The results for the distribution of the factor E given in Equations 2.59 through 2.61 are for 320°C (608 F). E is thermally activated with an activation energy of 30 kcal/mole.

2.8.3 Default IGSCC Growth Model

Detailed phenomenological models have been developed to describe cracking in BWR environments (Refs. 2.40, 2.41, 2.42, and 2.43). However, such detailed models need not be incorporated in a probabilistic code to predict pipe failures. The primary reason for variability in crack growth rates that needs to be considered in the code is material variability and variability in water chemistry conditions. Even if a detailed model were available, the analyst would still need to come up with distributions describing water chemistry conditions and material variability. This perhaps could be done with enough resources, but would be difficult. The approach that has been taken has been to use expert judgment to define water chemistry conditions and material variability that need to be addressed. Detailed phenomenological models are then used to compute the corresponding range of expected crack growth rates, and it is these ranges in crack growth rates that are used as input for the probabilistic model. A first cut at such an approach is outlined in Table 2.14. Water chemistry conditions are defined in terms of conductivity and electrochemical potential (ECP). Under normal water chemistry conditions, the ECP value for the severe water chemistry (200 mV) would actually include a contribution from possible higher oxygen values at startup/shutdown leading to an average value of 200 mV. The lower ECP (140 mV) could correspond for example to a BWR with stringent shutdown oxygen control. The conductivities similarly range from very good impurity control to relatively poor control by modern standards. The electrochemical potentiokinetic reactivation (EPR) values are nominally meant to represent the degrees of sensitization that might be found in different materials, but could also be more generally assumed to represent material variability.

The conditions in the table are probably somewhat conservative compared to the operating conditions for a modern BWR. This is partly because it is easier to reach consensus that these conditions are conservative than it would be to identify the most representative conditions, and partly because the conditions are intended to reflect in some average way that over some portion of the operating cycle will differ from the nominal operating conditions. For hydrogen-water chemistries (HWC), the crack growth rates are dominated by the time the HWC system is actually available. Again a range of values is chosen that bracket the range of values that actually occur in service. The variability is almost purely epistemic. It arises from our lack of knowledge about the exact water chemistry and material conditions. The corresponding crack growth rates have been computed using PLEDGE or the BWRVIP correlation. Independent review of the PLEDGE code shows that it gives good agreement with virtually all the

available SCC data (Ref. 2.44) and is taken here as the best estimate for a given set of conditions. Once the 5th and 95th percentiles are defined, the distribution is assumed to be lognormal. The assumption of lognormality was checked by comparing the exact median of a lognormal distribution = $CGR_{95} * CGR_5)^{0.5}$ with the crack growth rates determined directly from the “most likely” conditions. The average (rather than the median) crack growth rate for Type 304 stainless steel in normal-water chemistry conditions is 3.23×10^{-10} m/s (1.3×10^{-8} inch/s) consistent with values used in disposition analyses. The calculations are carried out for a nominal K of 27 MPa-m^{0.5} (25 ksi-inch^{0.5}). The general form of the crack-growth rate law is assumed to be

$$\frac{da}{dt} = CK^{2.2} \quad (2.62)$$

and the corresponding C value can be evaluated since the crack growth rate and K are known (admittedly in mixed units involving m/s and ksi in^{0.5}). Knowing the 5 and 95th percentile values, one can determine the mean (m) and the standard deviation (σ) of the lognormal distribution for C as shown in Table 2.14.

Table 2.14 Definition of water chemistry and material variability to determine 5 and 95 percentiles of the crack growth rate distribution using PLEDGE

K ksi in^{0.5}	EPR C/cm²	Conductivity μS/cm	T°C	ECP mV	Pledge m/s	HWC available	95/50/5 m/s	(95*5)^{0.5}	C=CGR/K^{2.2}
304 stainless steel									
NWC									
25.0	30	0.2	289	200	1.16e-09		1.16e-09		9.75e-13
25.0	15	0.15	289	150	1.81e-10		1.81e-10	1.45e-10	1.22e-13
25.0	5	0.1	289	140	1.82e-11		1.82e-11		1.53e-14
HWC									
25.0	30	0.2	289	-200	6.12e-11	0.70	3.91e-10		3.29e-13
25.0	15	0.15	289	-240	2.67e-12	0.80	3.84e-11	4.16e-11	3.49e-14
25.0	5	0.1	289	-300	2.00e-12	0.85	4.42e-12		3.71e-15
316L stainless steel									
NWC									
25.0	10	0.2	289	200	1.81e-10		1.81e-10		1.52e-13
25.0	5	0.15	289	200	4.73e-11		4.73e-11	4.25e-11	3.57e-14
25.0	0	0.1	289	200	9.95e-12		9.95e-12		8.36e-15
HWC									
25.0	10	0.2	289	-200	3.32e-12	0.70	5.67e-11		4.77e-14
25.0	5	0.15	289	-240	2.24e-12	0.80	1.13e-11	1.32e-11	1.11e-14
25.0	0	0.1	289	-300	1.88e-12	0.85	3.09e-12		2.60e-15

Table 2.15 Definition of water chemistry and material variability using BWRVIP correlation

K ksi in^{0.5}	EPR C/cm²	Conductivity μS/cm	T°C	ECP mV	BWRVIP m/s	HWC available	95/50/5 m/s	(95*5)^{0.5}	C=CGR/K^{2.2}
304 stainless steel									
NWC									
25.0	30	0.2	289	200	2.20e-10		2.20e-10		1.85e-13
25.0	15	0.15	289	150	1.27e-10		1.27e-10	1.19e-10	1.00e-13
25.0	5	0.1	289	140	6.44e-11		6.44e-11		5.41e-14
HWC									
25.0	30	0.2	289	-200	5.18e-11	0.70	1.02e-10		8.60e-14
25.0	15	0.1	289	-240	1.63e-11	0.80	3.84e-11	4.61e-11	3.88e-14
25.0	5	0.1	289	-300	1.31e-11	0.85	2.08e-11		1.75e-14

Table 2.16 Mean and standard deviation for the lognormal distribution of the crack growth rate coefficient C for different water chemistries and materials

Material	Chemistry	Mean	Standard deviation
304	NWC	-29.735	1.264
304	HWC	-30.985	1.362
316NG	NWC	-30.964	0.882
316NG	HWC	-32.130	0.885

A similar approach can be developed using the results based on the BWRVIP correlation shown in Table 2.15. Because the BWRVIP correlations do not include any way to account for material variability (except in terms of data scatter), there is less variability in the results. The bulk of the available data are in better agreement with the PLEDGE predictions than the BWRVIP results. The results in Table 2.16 together with Equation 2.62 provide the input needed for the probabilistic analysis. Because lognormal distributions have infinite tails that lead to physically unrealistic crack growth rates, log-triangular distributions, which are very similar to lognormal distributions except for the extreme tails, may be preferred. A log-triangular distribution with a lower bound of $m-2.406\sigma$, a peak value of m , and an upper bound value of $m+2.406\sigma$ will have 5th and 95th percentile values identical to those of the corresponding lognormal distribution and will differ only slightly from the lognormal distribution over the 0.05 to 0.95 range (rms error 0.9%). Currently, for the default IGSCC growth model in the PRO-LOCA code, both a lognormal and a log-triangular definition are coded. The default is set to lognormal.

2.8.4 Default PWSCC Growth Model

Data on the crack growth rate of Alloy 600 materials relevant to CRDM nozzles (i.e. not SG tubes) have been collected and analyzed in Reference 2.45. The data were fit to a correlation for the crack growth rate, da/dt of the form

$$\frac{da}{dt} = A(K - 9)^{1.16} \quad (2.63)$$

proposed by Scott (Ref. 2.46) where K , the stress intensity, is in $\text{MPa}\cdot\text{m}^{1/2}$ and da/dt is in m/s . Unlike Equation 2.62 the correlation predicts a "threshold" at $K = 9 \text{ MPa}\cdot\text{m}^{1/2}$ ($8 \text{ ksi}\cdot\text{inch}^{1/2}$). The behavior at low values of K is difficult to determine experimentally. Whether or not a true threshold value exists may depend on the patience of the experimenter. It is also not clear at what value of crack depth it can be assumed that fracture mechanics controls the crack growth rate. It is widely recognized in fatigue that cracks shorter than about $200\mu\text{m}$ can have crack growth rates considerably higher than those predicted by fracture mechanics extrapolations from conventional crack growth rate testing. To avoid these difficulties, it is assumed that initiation results in a macroscopic crack 3 mm (0.12 inch) deep for the default PWSCC model.

In Reference 2.45, values of A in the population of heats in service were assumed to be represented by a log-normal distribution. At 325°C (617°F) the log-mean of the log-normal distribution is -27.34 and the log-standard deviation is 1.02 (with the crack growth rate in units of m/s and K in $\text{MPa}\cdot\text{m}^{1/2}$). For other temperatures appropriate values of A are obtained by Arrhenius extrapolation using an activation energy for crack growth of 130 kJ/mole (31.0 kcal/mole). The value of A varies by about a factor of 100 over the entire population of materials. At 316°C (600°F) for a typical K value of $27.5 \text{ MPa}\cdot\text{m}^{1/2}$ ($25 \text{ ksi}\cdot\text{inch}^{1/2}$), $da/dt = 18 \text{ mm/year}$ (0.7 inch/year) for the worst heat.

Because the infinite tails of the log-normal distribution are unrealistic, it may again be preferable to represent the distribution as a log-triangular distribution with a lower bound value $m-2.406\sigma$, a peak value m , and upper bound value $m+2.406\sigma$. As before, for the default PWSCC model, both lognormal and log-triangular distributions are coded in the current version of the PRO-LOCA code. The lognormal option is the default.

An MRP working group is developing a crack growth rate distribution for Alloy 182 materials. The crack growth rates in Alloy 182 on average are a factor of 2 to 3 higher than in Alloy 600. The variability in crack growth rate also does not appear to be as large. Until the MRP group completes its analysis, the crack growth rates for Alloy 182 at 325°C (617°F) are represented in terms of a lognormal distribution with log mean of -25.47 and log standard deviation of 0.46 for the corresponding log-triangular distribution. For other temperatures, an activation energy for crack growth of 130 kJ/mol (31.0 kcal/mol) is again used.

2.8.5 Fatigue and SCC Growth Interaction

In many conditions, environmental fatigue and SCC may interact and both add to the crack growth at a particular time increment. For a particular time increment, the crack growth from fatigue and SCC are treated separately as given below

$$\Delta a_{\text{fat}_{\Delta t}} = \left. \frac{da}{dN} \right|_{\text{fatigue}} (N_i)_{\text{fat}_{\Delta t}} \quad (2.64)$$

$$\Delta a_{\text{SCC}_{\Delta t}} = \left. \frac{da}{dt} \right|_{\text{SCC}} (\Delta t)_i \quad (2.65)$$

The contribution to the total crack growth per time increment is then the sum of the components as shown below.

$$\Delta a_{\Delta t} = \Delta a_{\text{fat}_{\Delta t}} + \Delta a_{\text{SCC}_{\Delta t}} \quad (2.66)$$

2.8.6 User Defined Crack Growth Laws with User Controlled Damage Parameters

As part of MERIT, user defined crack growth laws were implemented into the PRO-LOCA code. In order to make this change, the form of the laws had to be held constant. The following laws were chosen,

- SCC – $da/dt = C(K-K_{th})^m$ with both a K plateau in which the crack growth does not increase with further increase in K and a K threshold defined for no crack growth
- Fatigue – $da/dN = C(\Delta K)^m$ with a ΔK threshold defined for no crack growth

In each of these cases, only the crack growth coefficients (C) are input as distributed variables. The crack growth exponent (m), the stress intensity (K) plateau, and the K (SCC) and ΔK (fatigue) thresholds are deterministic. In addition, flags were added to the code so that the user has the ability to turn on and off both the SCC and fatigue crack growth. In addition, the user can set the flags so that the default fatigue and SCC laws can be used.

2.9 Crack Coalescence

Crack coalescence is an important part of guaranteeing that the cracks that developed in this code are representative of the long surface cracks found in service. For circumferential surface cracks, as shown in Figure 2.23, when the distance between the surface cracks becomes less than two times the deepest surface crack depth, the cracks will coalesce. The depth of the new crack is equal to the deepest surface crack and the length is equal to the sum of the lengths of each crack

plus the distance between them. This criterion is based on Section XI, Article IWA-3000 of the ASME Boiler and Pressure Vessel code.

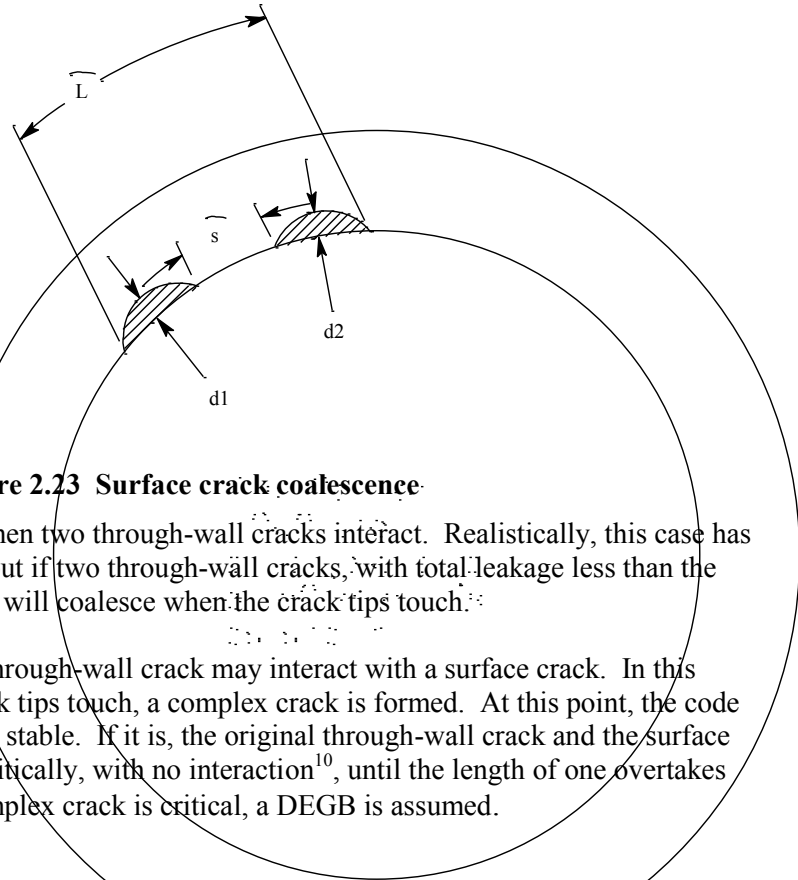


Figure 2.23 Surface crack coalescence

Another case of coalescence is when two through-wall cracks interact. Realistically, this case has a low probability of occurrence, but if two through-wall cracks, with total leakage less than the tech. spec. limit, are present, they will coalesce when the crack tips touch.

There is also a possibility that a through-wall crack may interact with a surface crack. In this case, it is assumed that if the crack tips touch, a complex crack is formed. At this point, the code will check if the complex crack is stable. If it is, the original through-wall crack and the surface crack will continue to grow subcritically, with no interaction¹⁰, until the length of one overtakes the length of the other. If the complex crack is critical, a DEGB is assumed.

2.10 Crack Stability

The PRO-LOCA code checks both surface-crack and through-wall-crack stability when appropriate. The methodologies behind the surface crack and through-wall crack failure criteria have been developed elsewhere and are fully published in the open literature. The descriptions in this section are meant to give an overview of the criteria, with the details left to the references. In previous versions of PRO-LOCA, when a stability analysis was needed, the PRO-LOCA code first checked stability using the Dimensionless Plastic Zone Parameter (DPZP) analysis. If this simple¹¹ criterion failed, then a more detailed stability criterion was used. For surface crack stability, the SC.TNP1 analysis method was used. For through-wall crack stability, the LBB.ENG2 analysis method was used. PRO-LOCA also uses the GE/EPRI through-wall crack J-estimation scheme, but only for crack opening displacement (COD) assessments. These two methods (SC.TNP1 and LBB.ENG2) were chosen in that they agreed best with the full-scale pipe fracture experiments conducted previously (Refs. 2.47 and 2.48). Originally, the PRO-LOCA code contained all of the J-estimation schemes for both through-wall and surface-cracked pipe programmed into NRCPIPE and NRCPIPES, respectively. As part of the MERIT program it was decided to streamline these stability routines by eliminating extraneous code (i.e., coding for SC.ENG, LBB.NRC, etc.), with the goal of hopefully speeding up the code. However, as part of

¹⁰ Note that this is an assumption since K-solutions for complex cracks are not available.

¹¹ This criterion was used as a screening criterion for stability since it is a simple formulation and would take only a small amount of CPU time to complete.

this effort a number of issues were found with the SC.TNP1 routine, especially with the combined pressure and bending solutions. (Note, it had long been recognized that there were issues with the applied J formulation in SC.TNP1, but these issues were offset by using L-C oriented Compact(Tension), C(T), specimen data to predict the fracture resistance of a crack growing through the thickness of the pipe, i.e., in the higher toughness L-R orientation.) In addition, as part of this streamlining effort, numerous discrepancies were uncovered between what was coded into NRCPIPE and the applicable equations in Reference 2.49. As a result, it was decided to forego using the SC.TNP1 methodology for predicting stability for surface-cracked pipe, and instead to use the simpler DPZP method. In addition, the DPZP method would still be used as a screening criterion for through-wall crack stability. When used as a screening tool, the DPZP predicted failure loads were multiplied by a factor of 0.8 to ensure a degree of conservatism in the screening process. If the applied loads are greater than 80 percent of the DPZP predicted failure load for a through-wall crack in a pipe, then the PRO-LOCA code would use the more rigorous LBB.ENG2 method for assessing the stability of that through-wall crack.

2.10.1 DPZP Analysis for Surface Crack Stability

The Dimensionless Plastic-Zone Parameter (DPZP) analysis is a semi-empirical procedure developed by Battelle (Refs. 2.50 and 2.51) and is used to analyze cracked pipe under bending and tension loads. In this analysis, a fully plastic condition is assumed to occur when the Irwin plastic-zone size (Ref. 2.52) equals the remaining tensile ligament length. The ratio of the maximum predicted stress (on the basis of the DPZP analysis) to the calculated Net Section Collapse (NSC) stress (see Figure 2.24) is expressed as a function of the DPZP as

$$\sigma = \sigma_{nsc} [2 / \pi] \arccos \{ \exp [- C (DPZP)] \} \quad (2.67)$$

where

$$DPZP = 2EJ_i / \left(\pi^2 \sigma_f^2 D \right) \quad (2.68)$$

σ	=	total failure stress,
σ_{nsc}	=	NSC predicted tension and bending stress,
E	=	elastic modulus,
J_i	=	J at crack initiation,
σ_f	=	flow stress $(\sigma_y + \sigma_u)/2$,
σ_y	=	yield stress,
σ_u	=	ultimate stress,
D	=	nominal pipe diameter, and
C	=	statistically based curve-fit parameter.

The C-parameter was determined from statistically fitting experimental pipe tests results. This parameter is different for circumferential through-wall cracks, circumferential surface cracks, and circumferential complex cracks. These parameters had been refined over the years as more experimental data became available, and the values used in PRO-LOCA are given below.

- For circumferential through-wall cracked pipes, the C-parameter was last updated in Reference 2.51 to be 18.3.
- For circumferential surface cracked pipes, the C-parameter was last updated in Reference 2.53 to be 32.
- For circumferential complex-cracked pipe, the data from Reference 2.54 was used to calculate a C-parameter value of 4.6.

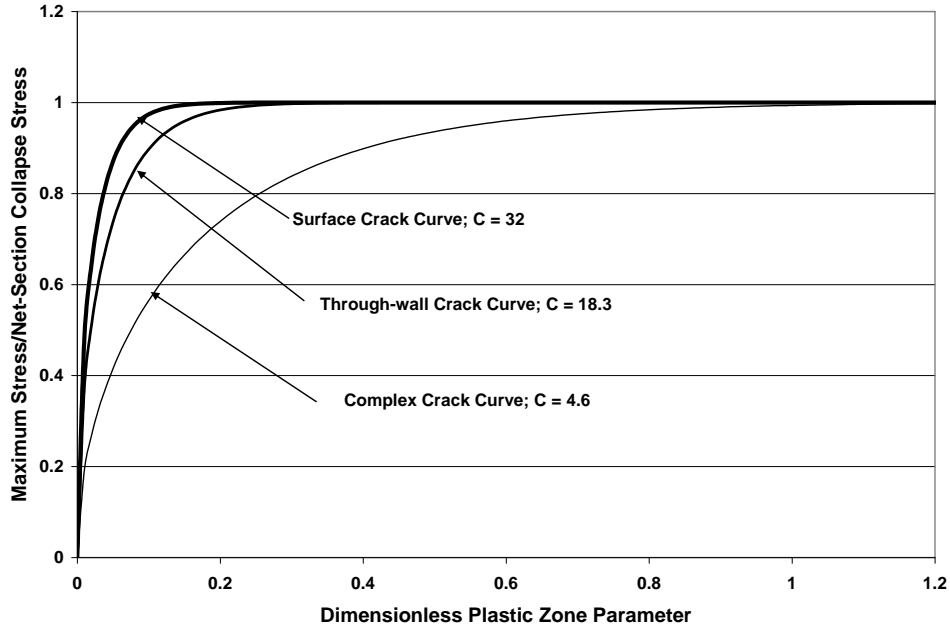


Figure 2.24 Dimensionless Plastic Zone Parameter Analysis

2.10.2 LBB.ENG2 Method for Through-Wall Crack Stability

The LBB.ENG2 estimation method proposed by Brust and Gilles (Ref. 2.48) for evaluating the J-integral of cracked tubular members subjected to combined tensile and bending loads is used in the PRO-LOCA for assessing the stability of through-wall cracks. The method of analysis is based on (1) classical deformation theory of plasticity, (2) a constitutive law characterized by a Ramberg-Osgood model, and (3) an equivalence criteria incorporating a reduced thickness analogy for simulating system compliance due to the presence of a crack in a pipe. The method is general in the sense that it may be applied in the complete range between elastic and fully plastic conditions. Since it is based on J-tearing theory, it is subject to the usual limitations imposed upon this theory, e.g., proportional loading, etc. This has the implication that the crack growth must be small, although in practice, J tearing methodology is used far beyond the limits of its theoretical validity with acceptable results.

The LBB.ENG2 method was selected because of its computational efficiency and it was found to be slightly conservative yet reasonably accurate when compared with experimental data. In the development of a J-estimation scheme, the crack-driving force, J, admit additive decomposition into elastic and plastic components is given by

$$J = J_e + J_p \quad (2.69)$$

where the subscripts "e" and "p" refer to the elastic and plastic contributions, respectively. The elastic component, J_e , and the plastic component, J_p , of the total energy release rate, J, can be readily obtained. In Reference 2.48 detailed derivations of J_e and J_p are provided.

2.10.2.1 Elastic Solution

The elastic component of J, J_e , is given by

$$J_e = \left[\frac{K_I^T + K_I^B}{E} \right]^2 \quad (2.70)$$

where E is the modulus of elasticity and K_I^T and K_I^B are the tensile and bending stress-intensity factors in which plane stress conditions are assumed. From the theory of linear-elastic fracture mechanics, K_I^T and K_I^B can be obtained from

$$K_I^T = \frac{P}{2\pi R_m t} F_T(\theta) \sqrt{\pi R_m \theta} \quad (2.71)$$

$$K_I^B = \frac{(M + Pe)}{\pi R_m^2 t} F_B(\theta) \sqrt{\pi R_m \theta} \quad (2.72)$$

where P is the load, M is the applied moment, e is the eccentricity of the load, and $F_T(\theta)$ and $F_B(\theta)$ are the tension and bending geometry functions with explicit definitions given in Appendix A of Reference 2.55.

2.10.2.2 Plastic Solution

The plastic component of J, J_p , is given by

$$J_p = \left[\frac{\alpha}{E\sigma_0^{n-1}} \right] \left[\frac{\pi R_m}{2(n+1)} \right] H_T(n, \theta) L_T(n, \theta) I_T(\theta) \left[\frac{P}{2\pi R_m t} \right]^{n+1} \\ + \left[\frac{\alpha}{E\sigma_0^{n-1}} \right] \left[\frac{\pi R_m}{2(n+1)} \right] H_B(n, \theta) L_B(n, \theta) I_B(\theta) \left[\frac{M + Pe}{\pi R_m^2 t} \right]^{n+1} \quad (2.73)$$

where σ_0 is the reference stress, and α and n are Ramberg-Osgood parameters characterizing the stress-strain curve of the material,

$$H_T(n, \theta) = \left[\frac{4\theta F_T(\theta)^2}{I_T(\theta)} \right] + \left[\frac{1}{L_T(n, \theta)} \right] \left[\frac{\partial L_T(n, \theta)}{\partial \theta} \right] \quad (2.74)$$

$$L_T(n, \theta) = \left[1 - \left(\frac{\theta}{\pi} \right) - \left(\frac{2}{\pi} \right) \sin^{-1} \left(\frac{1}{2} \sin(\theta) \right) \right]^{1-n} \quad (2.75)$$

$$I_T(\theta) = 4 \int_0^\theta \theta F_T(\theta)^2 d\theta \quad (2.76)$$

and

$$H_B(n, \theta) = \left[\frac{4\theta F_B(\theta)^2}{I_B(\theta)} \right] + \left[\frac{1}{L_B(n, \theta)} \right] \left[\frac{\partial L_B(n, \theta)}{\partial \theta} \right] \quad (2.77)$$

$$L_B(n, \theta) = \left[\frac{\pi}{4 \left\{ \cos \left(\frac{\theta}{2} \right) - \frac{1}{2} \sin \theta \right\}} \right]^{n-1} \left[\frac{\pi}{4\hat{K}} \right]^n \quad (2.78)$$

$$I_B(\theta) = 4 \int_0^\theta \theta F_B(\theta)^2 d\theta \quad (2.79)$$

$$\hat{K} = \left(\frac{\sqrt{\pi}}{2} \right) \left[\frac{\Gamma \left(1 + \frac{1}{2} n \right)}{\Gamma \left(\frac{3}{2} + \frac{1}{2} n \right)} \right] \quad (2.80)$$

with

$$\Gamma(u) = \int_0^{\infty} \xi^{u-1} \exp(-\xi) d\xi \quad (2.81)$$

as the gamma function. Explicit functional forms of $I_B(\Theta)$ and $I_T(\Theta)$ are also given in Appendix A of Reference 2.55.

2.10.3 Complex Crack

The PRO-LOCA code uses the LBB.ENG2 method for calculating the maximum load (maximum bending stress) for complex crack stability calculations. If the applied bending stress is less than the maximum calculated bending failure stress, the complex crack is stable. The complex crack is modeled using the LBB.ENG2 method as a through-wall crack with a reduced wall thickness.

2.11 Leak Rate

The PRO-LOCA code allows the user to input the leak-detection limit as a normally distributed value. A mean value and standard deviation of the leak rate detection limit are input through the PRO-LOCA graphical user interface (GUI). If the current leak rate through an existing crack is greater than this sampled leak detection limit, it is assumed that the leak would be detected and the critical node is removed from the analysis. The time increments are continued with newly sampled critical node parameters.

The PRO-LOCA code uses the Henry-Fauske model for two-phase flow through a crack that was used in the SQUIRT code for calculating leak rates for pipes with through-wall cracks. The PRO-LOCA leak rate model used the Henry-Fauske model for cases where the ratio of the flow path length (i.e., wall thickness) to the hydraulic diameter (t/D_h) is greater than 15. For larger openings, where the ratio of the flow path length to the hydraulic diameter is less than 0.5, an orifice flow model is assumed in PRO-LOCA. Recently, an improved transition flow model to bridge the two flow regimes was developed and implemented into SQUIRT, but has not yet been incorporated into PRO-LOCA. References 2.56 and 2.57 describe the SQUIRT model and code in detail. A brief description of the models and limitations follows.

SQUIRT, which stands for Seepage Quantification of Upsets In Reactor Tubes, is a computer program that predicts the leakage rate for cracked pipes in nuclear power plants. In all cases the fluid in the piping system is assumed to be water at a given temperature and pressure. The development of the SQUIRT computer model enables licensing authorities and industry users to conduct the leak-rate evaluations for leak-before-break (LBB) applications in a more efficient manner. The SQUIRT code also includes technical advances that are not available in other computer codes currently used for leak-rate estimation.

Development of leak-rate estimation methodology was initiated in response to intergranular stress corrosion cracking in boiling water reactor (BWR) piping. Further interest in this area was stimulated by investigations into the application of a leak-before-break (LBB) philosophy to piping integrity safety analyses instead of assuming a double-ended guillotine break. Adoption of an LBB philosophy requires reliable leak-detection systems and verified leak-rate estimation techniques. The development of a verifiable leakage rate assessment methodology is critical to LBB evaluations. Regulatory implications include the elimination of pipe-whip restraints and jet-impingement shields, as well as changing requirements for equipment qualification for the case of steam released from a break. In addition, accurate leak-rate prediction requires correlation of crack size and shape, and is necessary to evaluate the ability of normal makeup systems to handle potential leakage.

2.11.1 Flow Models in SQUIRT

A review (Ref. 2.56) of existing thermal-hydraulic models indicated that the Henry-Fauske model was the best currently available representation of fluid flow through tight cracks in a piping system. This model allows for non-equilibrium vapor generation rates as the fluid flows through the crack. The rate at which vapor is formed approaches the equilibrium value using an exponential relaxation correlation, with the correlation coefficients determined from the experimental data of Henry. In addition to the uncertainty associated with specifying the non-equilibrium vapor generation rate, other uncertainties in the analysis arise due to incomplete knowledge of the flow path losses, the friction factors for tight cracks, and the potential for particulate plugging.

The SQUIRT thermal-hydraulic model predictions were compared with the experimental data for two-phase flow through long tubes, two-phase flow through slits, and two-phase flow through actual cracked pipe. The details of some of these comparisons are provided in Section 3.1 (Modular QA) of this report.

While the Henry-Fauske two phase model for tight cracks for subcooled liquid is the default model in PRO-LOCA, there are two other models depending on the size of the opening and the thermodynamic state of the fluid inside the pipe. The other two models are:

1. Single-phase liquid model. This model predicts the leakage rate through a pipe crack when the fluid inside the pipe is under pressure, but the fluid temperature is below the saturation temperature corresponding to the ambient pressure outside of the pipe. In this case the fluid remains a liquid as it flows through the pipe crack and as it is discharged. This model solves the flow equations associated with non-compressible fluid flow.
2. Superheated single-phase steam model. This model predicts the leakage rate through a pipe crack when the fluid inside the pipe is superheated steam. By definition, superheated steam has a steam quality of 100%. In this case, the fluid remains a gas as it flows through the pipe crack and as it is discharged. This module solves the flow equations associated with compressible gas flow.

Previously, the SQUIRT module in PRO-LOCA automatically adjusted the thermo-hydraulic model as described next. If the temperature of the fluid inside the pipe was less than or equal to the saturation temperature of the fluid at the ambient pressure, then the single-phase liquid flow model was used to calculate a leakage rate. Alternatively, if the crack depth (pipe wall thickness) to hydraulic diameter ratio (t/D_h) was less than 0.5^{12} , then the single-phase liquid model was used because the fluid is assumed to pass through the crack as a liquid before it has time to flash to a two-phase mixture.

If the temperature of the fluid inside the pipe was greater than the saturation temperature of water at the pipe operating pressure, then the superheated steam fluid flow model was used to calculate the leakage rate. Under these circumstances, the steam quality was assumed to be 100 percent throughout the flow path, and the fluid was modeled using the single-phase compressible gas flow equations.

¹² As part of the MERIT program this ratio of the crack depth to hydraulic diameter for which the single phase orifice equations were used was changed from 0.5 to 4.6 as part of the development process of the transition flow model.

Finally, if the crack depth (pipe wall thickness) to hydraulic-diameter ratio was greater than 30¹³ (tight crack) and the fluid inside the pipe was a liquid at a temperature less than the saturation temperature of the fluid inside the pipe, the fluid would flash to a two-phase mixture at the ambient pressure, and the Henry-Fauske two-phase flow model in SQUIRT was used to calculate the flow rate. Figure 2.25 shows the critical pressure ratio (ratio of the pressure at the crack opening on the outside of the pipe (i.e., exit plane pressure), P_c , and the pressure inside the pipe, P_o) as a function of the crack depth (pipe wall thickness) to hydraulic diameter ratio (t/D_h) for two-phase flow. This figure also shows the region on the plot where the Henry-Fauske model was considered to be valid. This model is only theoretically valid for ratios of the pipe thickness (t) to hydraulic diameter (D_h) greater than about 30. For (t/D_h) ratios less than 30, the assumptions used to generate the Henry-Fauske model begin to breakdown. Fauske conducted tests for (t/D_h) ratios less than 30, and found that the critical pressure ratio (P_c/P_o), where P_c is the pressure at the crack opening on the outside of the pipe (i.e., exit plane pressure) and P_o is the pressure inside the pipe, was no longer constant for (t/D_h) ratios less than 12. Figure 2.25 also shows the region on the plot where the single-phase liquid model may be used to approximate the leakage rate.

The prior versions of SQUIRT did not have a transitional two-phase flow model to handle pipe cracks with depth (pipe wall thickness) to hydraulic diameter ratios between 4.6 and 30. As part of the MERIT program, a new transitional flow model was developed to address flow conditions in this flow regime.

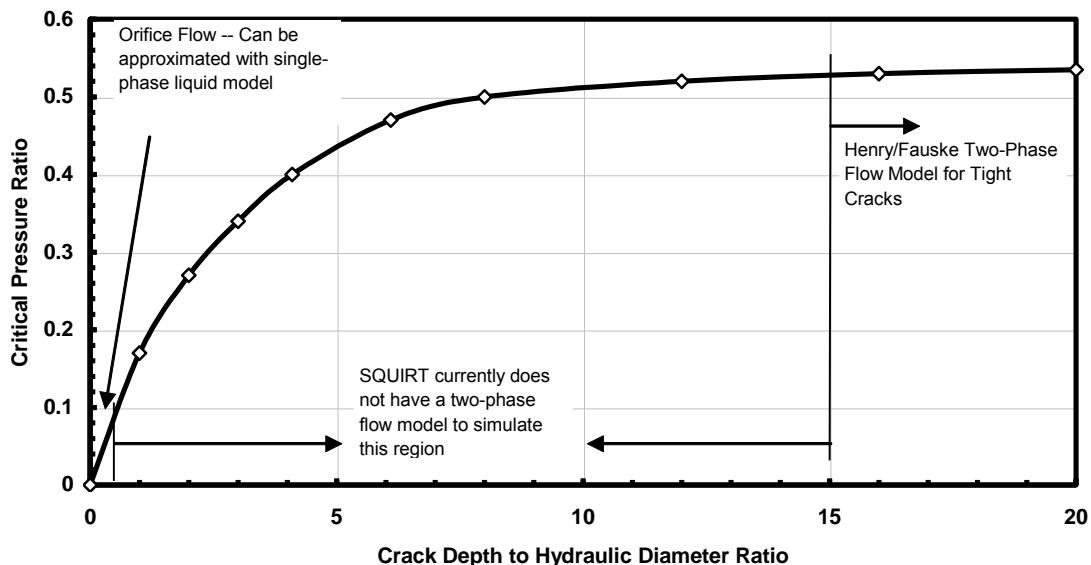


Figure 2.25 Plot of critical pressure ratio as a function of crack depth to hydraulic diameter ratio showing when the leak rate models in SQUIRT are valid (Ref. 2.58)

¹³ While a ratio of 30 appears to be the theoretical limit of the Henry-Fauske model, a practical limit of 15 was used in earlier versions of SQUIRT and PRO-LOCA in that the associated error with using the Henry-Fauske model to this lower limit was not felt to be significant.

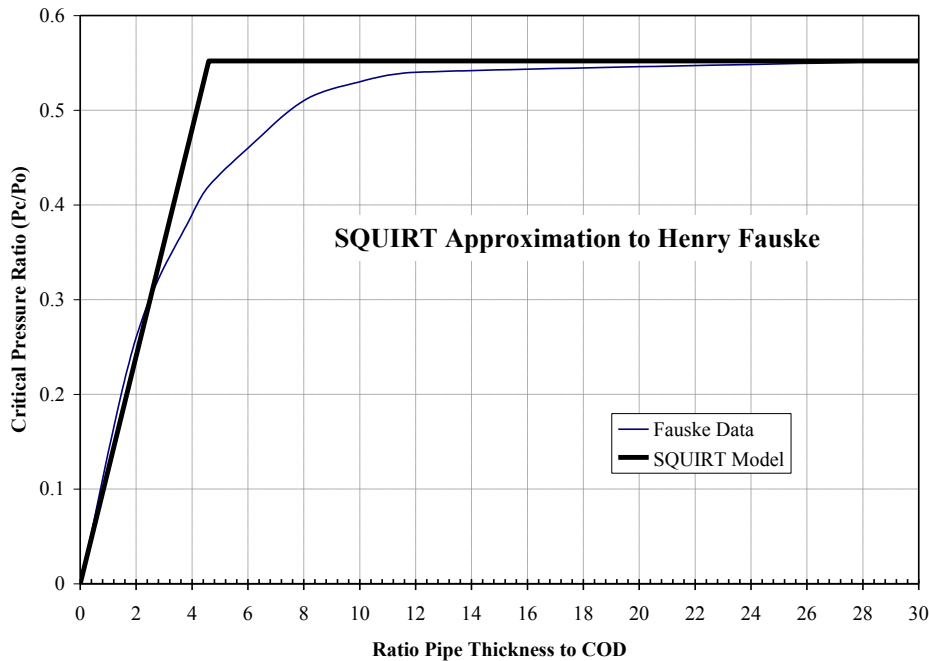


Figure 2.26 Transition flow model

The new transition flow model in SQUIRT, see Figure 2.26, calculates the mass flux of the two-phase steam-water flow using the Henry-Fauske model at (t/D_h) ratio of 30, and assumes this mass flux is constant between $12 \leq (t/D_h) < 30$. For $4.6 < (t/D_h) < 12$, the leakage rate is calculated as an interpolation between an orifice-type flow equation at $(t/D_h) = 4.6$ and the Henry-Fauske model prediction at $(t/D_h) = 12$. For $(t/D_h) \leq 4.6$, the critical pressure ratio is assumed to be a linear function of (t/D_h) as shown in the above figure, and the leakage rate is calculated using an orifice-type flow equation with the fluid properties evaluated at the average pressure condition $(P_o + P_c)/2$ in the crack.

The new SQUIRT transition flow model allows leakage rates to be calculated for (t/D_h) ratios > 30 where the Henry-Fauske model is valid, for (t/D_h) approximately zero where the orifice flow equations are valid, and for intermediate ratios, $0 < (t/D_h) < 30$ using experimental data and the above interpolation methods. This new transition flow model has been incorporated into the latest version of SQUIRT, but at this time still needs to be incorporated into PRO-LOCA.

In comparing the prior version of SQUIRT (no transition flow model) with the latest version of SQUIRT (with transition flow model), it can be seen that the differences in predicted leakage rates at t/D_h values of 15 (the lower limit on where two-phase flow solutions were obtainable in the prior version of SQUIRT) are approximately 30 to 45 percent, depending on the crack morphology assumed. Conversely, in this same flow regime, the differences in crack opening areas for comparable leak rates are in the range of 25 to 30 percent, depending on the crack morphology assumed in the analyses.

As an illustration of the size of cracks that fall into these flow regimes, if considering a 14-inch diameter Schedule 160 surge line case, the crack opening area for a t/D_h value of 5 is on the order of 650 mm^2 (1 inch^2) while the crack opening area for a t/D_h value of 30 is on the order of 125 mm^2 (0.2 inch^2). Both of these areas fall between the crack opening areas for the first two bins of crack sizes outputted by PRO-LOCA.

2.11.2 Crack Morphology Parameters

As a fluid passes through a crack, significant pressure losses occur when the fluid changes direction along the flow path. The surface roughness, the number of turns along the flow path,

and the actual crack path length are the crack morphology parameters that need to be characterized in order to determine these pressure losses. A brief description of each parameter and how they affect the pressure loss is given below.

2.11.2.1 Surface Roughness

This parameter defines the roughness of the crack face, and is used in calculating the pressure losses due to friction. Surface roughness is characterized by making measurements of the difference between the flow path centerline and the peaks/valleys of the profile. It was determined in Reference 2.55 that the appropriate surface roughness that affects the flow is a function of the crack-opening displacement (COD), i.e., large values of COD correspond to a global roughness (μ_G) while small values of COD correspond to local values (μ_L), see Figure 2.27.

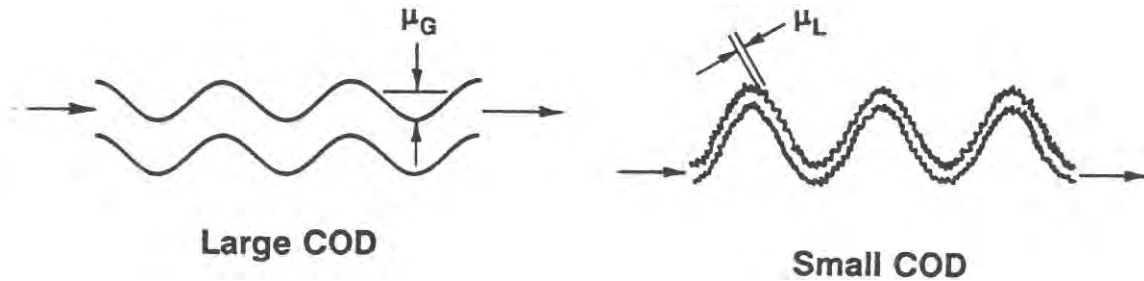


Figure 2.27 Local and global surface roughness

2.11.2.2 Number of Turns

As illustrated in Figure 2.27, what was the waviness in the flow path for large COD values becomes a major change in flow direction for small COD values. These turns in the flow path can account for up to one half of the pressure loss across the crack. Thus, the pressure loss is a function of the number of 90-degree turns in the flow path, which corresponds to one velocity head loss.

2.11.2.3 Actual Crack Path/Wall Thickness

Through an examination of service cracks, it was determined that most cracks do not grow perpendicular to the wall thickness, see Figure 2.28. Therefore, a parameter was developed that represents the true path of the crack or flow path length.

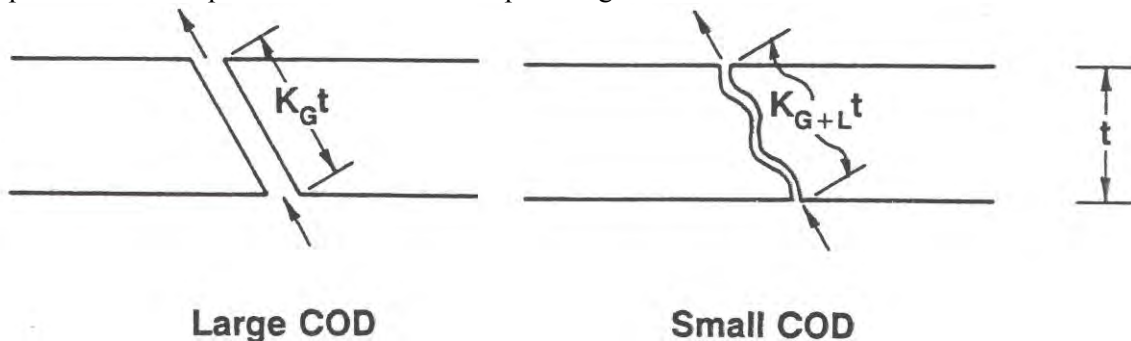


Figure 2.28 Global and local path deviations from straightness

2.11.2.4 PRO-LOCA Crack Morphology Parameters

The leak rate module in PRO-LOCA gives the users the option of using either the default crack morphology parameters incorporated in SQUIRT or inputting their own values (both means and standard deviations). The default parameters in SQUIRT were first developed for air fatigue,

corrosion fatigue and intergranular stress corrosion cracking (IGSCC) as part of the NRC's Short Cracks in Piping and Piping Welds program and were documented in NUREG/CR-6004 (Ref. 2.55). These default values (means and standard deviations) were based on measurements from actual cracks removed from service. Subsequently, as part of the NRC's Large Break LOCA program, default values (means and standard deviations) were obtained from measurements of primary water stress corrosion cracks (PWSCC) removed from service (Ref. 2.59).

Table 2.17 gives the default mean values and standard deviations of the crack morphology parameters for the three different crack mechanisms (corrosion fatigue, IGSCC, and PWSCC) embedded in PRO-LOCA as determined from measurements on cracks removed from service. If both fatigue and SCC are active mechanisms, the initiation mechanism dictates the crack morphology if the default crack morphologies are chosen. For SCC, the code distinguishes between PWSCC and IGSCC by the reactor type chosen, i.e., PWSCC morphologies are used for PWR plants and IGSCC morphologies are used for BWR plants.

Table 2.17 Mean and standard deviation of default crack morphology parameters

Crack Morphology Variable	Corrosion Fatigue		IGSCC		PWSCC – Base		PWSCC – Weld ^(a)	
	Mean	Standard Dev	Mean	Standard Dev	Mean	Standard Dev	Mean	Standard Dev
$\mu_L, \mu\text{m}$	8.814	2.972	4.70	3.937	10.62	9.870	16.86	13.57
$\mu_G, \mu\text{m}$	40.51	17.65	80.0	39.01	92.67	65.26	113.9	90.97
n_L, mm^{-1}	6.730	8.070	28.2	18.90	8.043	2.043	5.940	4.540
K_G	1.017	0.0163	1.07	0.100	1.060	0.095	1.009	0.011
K_{G+L}	1.060	0.0300	1.33	0.170	1.327	0.249	1.243	0.079

(a) Crack growth parallel to long direction of dendritic grains.

If the user of PRO-LOCA chooses to input their own crack morphology parameters, they have the option of further specifying a crack-opening displacement (COD) dependent model of these crack morphology parameters, see Figure 2.29. Prior to the publication of NUREG/CR-6004, the crack morphology parameters discussed above were considered to be independent of COD. However, as part of NUREG/CR-6004 it was hypothesized that the appropriate roughness should be large (global) or small (local) depending on whether the COD is large or small, respectively, see Figure 2.29. As part of NUREG/CR-6004, the dependence of surface roughness, μ , with COD (δ) was achieved by assuming a piecewise linear function given by Equation 2.82.

$$\mu = \begin{cases} \mu_L, & 0.0 < \frac{\delta}{\mu_G} < 0.1 \\ \mu_L + \frac{\mu_G - \mu_L}{9.9} \left[\frac{\delta}{\mu_G} - 0.1 \right], & 0.1 < \frac{\delta}{\mu_G} < 10 \\ \mu_G, & \frac{\delta}{\mu_G} > 10 \end{cases} \quad (2.82)$$

Where μ_L is the local surface roughness, μ_G is the global surface roughness, and δ is the center-crack-opening displacement. Figure 2.29 shows the schematic variation of μ with respect to COD (δ).

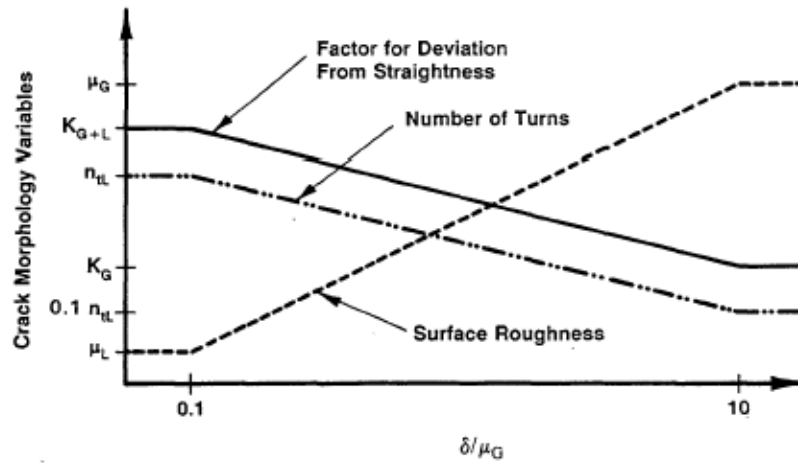


Figure 2.29 Crack morphology variables versus normalized COD

In a similar vein, Figure 2.29 shows the schematic variation of the number of turns and flow path length with respect to δ , see Equations 2.83 and 2.84.

$$n_t = \begin{cases} n_{tL}, & 0.0 < \frac{\delta}{\mu_G} < 0.1 \\ n_{tL} - \frac{n_{tL}}{11} \left[\frac{\delta}{\mu_G} - 0.1 \right], & 0.1 < \frac{\delta}{\mu_G} < 10 \\ 0.1 n_{tL}, & \frac{\delta}{\mu_G} > 10 \end{cases} \quad (2.83)$$

$$\frac{L_a}{t} = \begin{cases} K_{G+L}, & 0.0 < \frac{\delta}{\mu_G} < 0.1 \\ K_{G+L} - \frac{K_{G+L} - K_G}{9.9} \left[\frac{\delta}{\mu_G} - 0.1 \right], & 0.1 < \frac{\delta}{\mu_G} < 10 \\ K_G, & \frac{\delta}{\mu_G} > 10 \end{cases} \quad (2.84)$$

It should be noted that Equations 2.82 through 2.84 provide an approximate correction to account for the COD dependency of these crack morphology parameters. More recent analyses as part of the NRC's Barrier Integrity Program (Ref. 2.60) indicate that the upper limit on the ratio of the crack opening displacement to global roughness (δ/μ_G) is more like 5 than 10. At this time, however, the limit in both SQUIRT and PRO-LOCA is still set to 10.

2.12 Credit for Inspections

As with the loading history, the times for inspections are input for both the time to year in operation and for future time. For the time up to the year in operation, the inspections are handled as a deterministic input, and the user is asked to input the number of inspections that have occurred and the months of the inspection (since the start of plant operations) in which they occurred, and a probability of detection (POD) curve for each inspection. In addition, the user can input whether or not any leaks have been observed during the past operating experience. For the future inspections, the user is asked to input basically the same information, i.e., when the inspections are expected to occur (since the start of operating) and a probability of detection (POD) curve for each inspection. Note, in each case, the inspection occurs at the end of that time period, e.g., at the end of the 10th year or 120th month.

The inspection technique accuracy is based on either a Weibull or piece-wise linear distribution of a probability of detection (POD) curve. This curve gives the probability of detection as a function of crack depth. At this time crack length detection is assumed to be deterministic. The user specifies the detectable crack length. Once a crack is detected, it can be replaced with a similar material, it can be replaced by a non-susceptible material, or it can be repaired using either a weld overlay or mechanical stress improvement process (MSIP). For this later case, the weld residual stress distribution is manually modified by the user to reflect an improved residual stress distribution due to the repair. If a crack leaks, the affected segment is replaced with either a similar material or a non-susceptible material. The choice of replacement material is a user input. As part of the MERIT program the following inspection options have been added to the PRO-LOCA code

1. Defined future inspection times - modifications were made to allow the user to define individual times for each inspection throughout the life of the plant.
2. POD per inspection – modifications were made so that the user can define a different POD for each inspection.
3. Repair/replace option – modifications were made so that the user has three options
 - a. Replace with same material
 - b. Modify weld residual stress to simulate a weld repaired with either a weld overlay or by the mechanical stress improvement process (MSIP)
 - c. Replace with SCC resistant material
4. Credit for leaks in past – for previous operating history where no leaks have been observed, logic was added to remove any simulations that predict leakage. This allows the simulation to match experience.
5. Dependent inspections – At this time no changes have been made to the code to address dependent inspections due to uncertainty of what was desired here.

2.13 Program Output

In the current version of the PRO-LOCA code, the program is capable of outputting many of the variables so that sensitivity studies and benchmarking can be performed. However, the extensive amount of outputting does cause the code to run inefficiently. Therefore, for runs that include many Monte-Carlo increments, only limited data is written to file. The user has the option to

write additional data to file if needed. The data that is normally output to file includes crack size probabilities as a function of time (output samples of $g_i(\mathbf{X})$).

The probabilities are grouped into nine bins according to crack size. These bins include first occurrence of crack initiation, first occurrence of a through-wall crack (TWC) and the following crack opening area (COA) sizes:

- Any TWC with a COA less than 93.5 mm² (0.145 inch²)
- Any TWC with a COA less than 1,406 mm² (2.18 inch²)
- Any TWC with a COA less than 4,690 mm² (7.27 inch²)
- Any TWC with a COA less than 23,477 mm² (36.39 inch²)
- Any TWC with a COA less than 100,645 mm² (156.0 inch²)
- Any TWC with a COA less than 503,225 mm² (780.0 inch²)
- Any TWC with a COA greater than 503,225 mm² (780.0 inch²)

The crack-opening area sizes shown were derived from effective opening diameters that correspond to PWR leak rates as shown in Table 2.18.

Table 2.18 Crack-opening area definitions

COA, mm ² (inch ²)	Effective Opening Diameter, mm (inch)	PWR leak rate, lpm (gpm)
93.5 (0.145)	10.9 (0.43)	380 (100)
1,406 (2.18)	42.42 (1.67)	5,680 (1,500)
4,690 (7.27)	77.2 (3.04)	18,900 (5,000)
23,477 (36.39)	173 (6.81)	94,700 (25,000)
100,645 (156.0)	358 (14.1)	380,000 (100,000)
503,225 (780.0)	800 (31.5)	1,900,000 (500,000)

As part of the MERIT program the user was given the option of specifying confidence bounds on the program outputs. This option was incorporated into PRO-LOCA for several different response outputs using a bootstrap methodology. Currently confidence intervals are calculated for:

1. Maximum Crack Length
2. Maximum Crack Depth
3. First Crack Initiation Time
4. Time for First Coalescence
5. Time for First Through Wall Crack
6. Time for First Complex Crack
7. Crack Length at First Leak
8. Crack Opening at First Leak
9. Crack Opening Area for each of the seven LOCA categories

Because of the complexity of the PRO-LOCA code and the fact that up to seven different distribution types can be used for many of the random variables, it was decided that the best tool for these types of confidence bound calculations is the bootstrap method. This methodology was added to PRO-LOCA, together with a Newton iteration for user specified levels. Figure 2.30 shows examples of some of the confidence bands calculations. In this figure the mean and 90% confidence bands for the (maximum) crack length, (maximum) crack depth, crack length at leak, crack opening at leak, and time to initiation are shown. The abscissa is the number of

simulations. Around 7,500 simulations there is an increase in the crack length at leak and opening area because a significantly large leak is predicted.

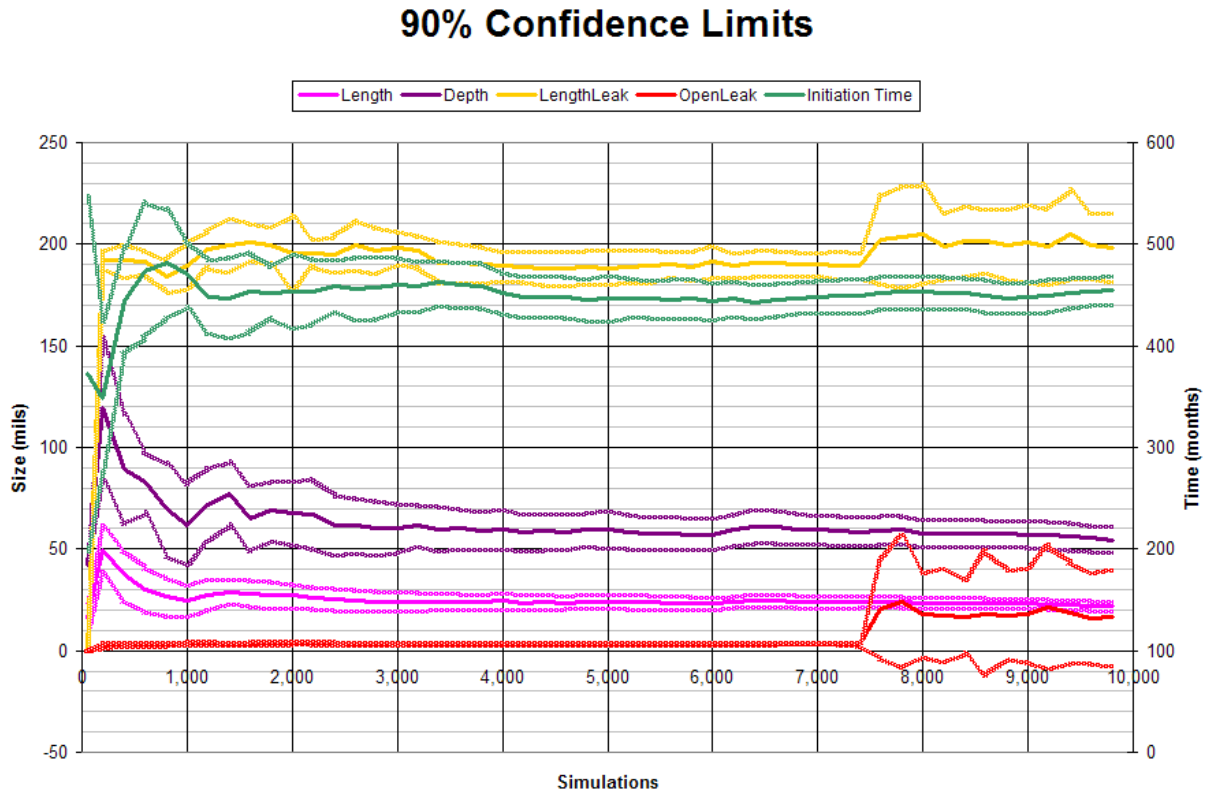


Figure 2.30 90% Confidence Bands as a Function of the Number of Simulations

It is important to note that these means and confidence bands are conditional. That is, the crack length at leak is only calculated for those cases in which a leak occurs. Otherwise, the calculated crack lengths would be essentially zero since there is a small probability of leakage and most simulations would have a zero length.

Figure 2.31 shows a snapshot of the output screen. The probability of initiation, TWC, and the seven LOCA category leaks are still output, but now the confidence bands on the physical quantities of interest and the LOCA category opening sizes are also shown.

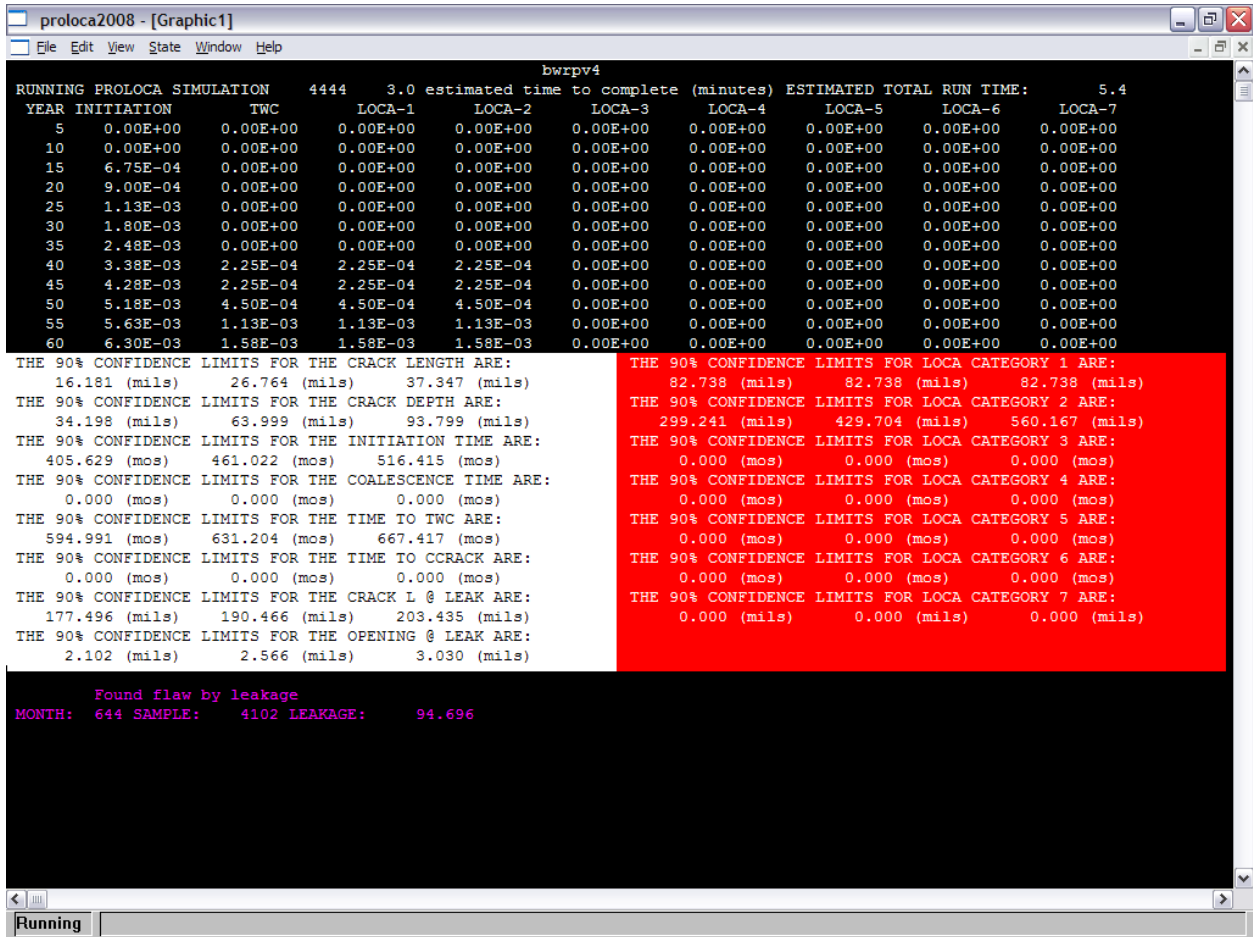


Figure 2.31 PROLOCA 2008 Output Screen with Confidence Band Calculations

2.14 Graphical User Interface (GUI)

The graphical user interface (GUI) has been significantly reorganized as part of the MERIT program to address the many changes made to the PRO-LOCA code and to reflect the desires of the TAG membership to the extent possible. The organization and structure of the GUI are discussed in detail in the PRO-LOCA Users Manual (Ref. 2.61).

2.15 References

2.1 Hopkins, D.A., Chamis, C.C., *Probabilistic Structural Analysis methods: SSME Propulsion Components*, Advanced Earth-to-Orbit Propulsion Technology, 1, NASA Conference Publication 2436, 1986

2.2 Madsen, H.O., Krenk, S., and Lind, N.C., *Methods of Structural Safety*, Prentice-Hall, 1986

2.3 Box, G.E.P., and Draper, N.R., *Empirical Model-Building and Response Surfaces*, John Wiley & Sons, USA, 1987

2.4 Deming, W. E., *Some Theory of Sampling*, Dover Publishing, 1966, Library of Congress Catalog number 66-30538

- 2.5 Wilkowski, G., and others, —~~Shor~~Cracks in Piping and Piping Welds – Seventh Program Report March 1993 – December 1994,” NUREG/CR-4599, Vol. 4, No. 1, April 1995.
- 2.6 Chopra, O. K., Sather, A., and Bush, L. Y., —~~Long~~Term Embrittlement of Cast Duplex Stainless Steels in LWR Systems – Semiannual Report April – September 1989,” NUREG/CR-4744, Vol. 4, No. 2, June 1991.
- 2.7 Harris, D. O. and Dedhia, D., —~~A~~Probabilistic Fracture Mechanics Code for Piping Reliability Analysis (pcPRAISE code),” NUREG/CR-5864, 1992.
- 2.8 Chapman, O. J. V., and Simonen, F. A., —~~R~~PRODIGAL – A Model for Estimating the Probabilities of Defects in Reactor Pressure Vessel Welds,” NUREG/CR-5505, August 1998.
- 2.9 M. Khaleel, Vic Chapman, Dave Harris, and Fred Simonen —~~F~~law Size Distribution and Flaw Existence Frequencies in Nuclear Piping” PVP Vol. 386, 1999
- 2.10 Harris, D. and Dedhia, D., —~~W~~PRAISE 98 PRAISE Code in Windows,” April 1998.
- 2.11 Khaleel, M., Simonen, F., Phan, H., Harris, D., and Dedhia, D., —~~F~~igue Analysis of Components, for 60-Year Plant Life,” NUREG/CR-6674, June 2000.
- 2.12 Abramowitz, M., and Stegun, I., *Handbook of Mathematical Functions*, National Bureau of Standards Applied Mathematics Series 55, Washington, DC, 1964.
- 2.13 Wilkowski, G., and others, —~~D~~egraded Piping Program – Phase II,” Summary of Technical Results and Their Significance to Leak-Before-Break and In-Service Flaw Acceptance Criteria, March 1984 – January 1989, NUREG/CR-4082, Vol. 8, March 1989.
- 2.14 Keisler, J., Chopra, O.K, and Shack W.J., —~~F~~atigue Strain–Life Behavior of Carbon and Low–Alloy Steels, Austenitic Stainless Steels, and Alloy 600 in LWR Environments,” NUREG/CR-6335, ANL-95/15, June 1995.
- 2.15 P. M. Scott, —~~P~~rediction of Alloy 600 Component Failures in PWR Systems,” Proceedings of the CORROSION/96 Research Topical Symposia 1996, National Association of Corrosion Engineers (NACE), Houston (1996).
- 2.16 R. Staehle, —~~B~~ases for Predicting the Earliest Penetrations Due to SCC for Alloy 600 on the Secondary Side of PWR Steam Generators,” NUREG/CR-6737 (2001).
- 2.17 J. Gorman, R. Staelhe, and K. D. Stavropoulos, —~~S~~tatistical Analysis of Steam Generator Tube Degradation,” EPRI NP-7493, EPRI, Palo Alto (1991).
- 2.18 C. Amzallag, J. M. Boursier, C. Pagès C. Gimond, —~~S~~tress Corrosion Life Assessment of 182 and 82 Welds Used in PWR Components,” Tenth International Conference on Environmental Degradation of Materials in Nuclear Power Systems— Water Reactors, August 5–9, 2001, Harveys Resort and Casino Lake Tahoe Lake Tahoe, Nevada, CD-ROM NACE (2002).
- 2.19 W. J. Shack, —~~P~~arametric Studies of the Probability of Failure of CRDM Nozzles,” NUREG/CP–0180, Proceedings of the Vessel Penetration Inspection, Crack Growth, and Repair Conference, Gaithersburg, MD, Sept. 29-Oct. 2, 2003 (2004)
- 2.20 W. H. Bamford and J. F. Hall, NUREG/CP–0180, —~~A~~ Review of Alloy 600 Cracking in Operating Nuclear Plants: Historical Experience and Future Trends,” Proceedings of the Vessel Penetration Inspection, Crack Growth, and Repair Conference, Gaithersburg, MD, Sept. 29-Oct. 2, 2003 (2004)
- 2.21 D. O. Harris, D. D. Dedhia, E. D. Eason, and S. D. Patterson, —~~P~~robability of Failure in BWR Reactor Coolant Piping,” NUREG/CR-4792 v3, UCID-20914 v3 (1986).

- 2.22 E. D. Eason and L. M. Shusto, —Analysis of Cracking in Small Diameter BWR Piping,” EPRI NP-4394 (1986)
- 2.23 J. Alexander, C. Briant, W. Clarke, R. Davis, C. Jewett, J. Kass, J. Lemaire, H. Solomon, R. Tunder, and M. Wang, —Alternate Alloys of BWR Pipe Applications,” EPRI NP-2671-LD (1982).
- 2.24 Wilkowski, G., Xu, H., Rudland, D., and Scott, P, —Statistical Characteristics Analysis and Simulation of Circumferential IGSCC Cracks for a BWR Plant,” PVP2006-ICPVT11-93966, Proceedings of ASME-PVP 2006: 2006 ASME Pressure Vessels and Piping Division Conference, July 23-27, 2006, Vancouver, BC, Canada.
- 2.25 Atluri, S.N., and Kathiresan, K., —Outer and Inner Surface Flaws in Thin-Walled Pressure Vessels,” Transactions of the Fourth International Conference on Structural Mechanics in Reactor Technology, San Francisco, Cal. 1977.
- 2.26 McGowan, J.J., and Raymond, M., —Stress Intensity Factor Solutions For Internal Semi-Elliptical Surface Flaws in a Cylinder Under Arbitrary Loading,” Fracture Mechanics, ASTM STP 677, American Society for Testing and Materials, 1979, pp. 365-380.
- 2.27 Raju, I.S., and Newman, J.C., —Stress-Intensity Factors for Internal and External Surface Cracks in Cylindrical Vessels,” Journal of Pressure Vessel Technology, Vol. 104, pp 293-298, November 1982.
- 2.28 Chapuliot, S., Lacire, M.H and Le Delliou P., —Stress Intensity Factors for Internal Circumferential Cracks in Tubes Over a Wide Range of Radius over Thickness Ratios,” PVP-Vol. 365, Fatigue, Fracture and High Temperature Design Methods in Pressure Vessels and Piping, American Society of Mechanical Engineering, 1998.
- 2.29 Anderson, T.L., Thornwald, G., Revelle, D.A., and Lanaud, C., —Stress Intensity Solutions for Surface Cracks and Buried Cracks in Cylinders, Spheres, and Flat Plates,” Structural Reliability Technology final report to The Materials Property Council, Inc., March 14, 2000.
- 2.30 Anderson, T.L., —Stress Intensity and Crack Opening Area Solutions for Through-wall Cracks in Cylinders, and Spheres,” Structural Reliability Technology final report to The Materials Property Council, Inc., January 29, 2003.
- 2.31 Klecker, R., Brust, F., and Wilkowski, G., —NRC Leak-Before-Break (LBB/NRC) Analysis Method for Circumferentially Through-Wall Cracked Pipes Under Axial Plus Bending Loads, NUREG/CR-4572, BMI-2134, May 1986.
- 2.32 Sanders, J.L., Jr. —Circumferential Through-Crack in a Cylindrical Shell Under Combined Bending and Tension,” Journal of Applied Mechanics, March 1983, Vol. 50, p.221.
- 2.33 W. Shack and T. F. Kassner, —Review of Environmental Effects on Fatigue Crack Growth of Austenitic Stainless Steels,” NUREG/CR-6176, ANL-94/1 (1994).
- 2.34 L. A. James and D. P. Jones, —Fatigue Crack Growth Correlation for Austenitic Stainless Steels in Air,” Proc. Conf. on Predictive Capabilities in Environmentally-Assisted Cracking, R. Rungta, ed., PVP Vol. 99, American Society of Mechanical Engineers, NY, pp. 363-414 (1985).
- 2.35 J. M. Barsom and S. T. Rolfe, —Fracture and fatigue control in structures: applications of fracture mechanics,” ASTM, West Conshohocken, PA. (1999).
- 2.36 W. E. Ruther, W. K. Soppet, and T. F. Kassner, —Environmentally Assisted Cracking in Light Water Reactors: Semiannual Report, October 1993 – March 1994,” NUREG/CR-4667 Vol. 18, ANL-95/2, pp. 12-25 (March 1995).

- 2.37 G.L. Wire and W. J. Mills, —“Fatigue crack propagation from notched specimens of 304 SS in an elevated temperature aqueous environment,” American Society of Mechanical Engineers, Pressure Vessels and Piping Division (Publication) PVP, v 439, 2002, p 151-164
- 2.38 W. E. Ruther, W. K. Soppet, and T. F. Kassner, —“Corrosion Fatigue of Alloys 600 and 690 in Simulated LWR Water,” NUREG/CR-6383, ANL-95/37 (1996).
- 2.39 O. K. Chopra, W. K. Soppet, and W. J. Shack, —“Effects of Alloy Chemistry, Cold Work, and Water Chemistry on Corrosion Fatigue and Stress Corrosion Cracking of Nickel Alloys and Welds,” NUREG/CR-6721, ANL-01/07 (2001).
- 2.40 F. P. Ford, —“Quantitative Prediction of Environmentally Assisted Cracking,” Corrosion, 52, pp. 375-395 (1997).
- 2.41 F. P. Ford, D. F. Taylor, P. L. Andresen, and R. Ballinger, —“Corrosion-Assisted Cracking of Stainless and Low-alloy Steels,” EPRI NP-5064s, Electric Power Research Institute, Palo Alto, CA (February 1987).
- 2.42 T. Shoji, —“Quantitative Prediction of Environmentally Assisted Cracking Based on Crack Tip Strain Rate,” Proc. Conf. on Predictive Capabilities in Environmentally-Assisted Cracking, R. Rungta, ed., PVP Vol. 99, American Society of Mechanical Engineers, NY, pp.127-142 (1985).
- 2.43 T. Shoji, S. Suzuki, and R. G. Ballinger, —“Theoretical Prediction of SCC Growth Behavior-Threshold and Plateau Growth Rate,” Proceedings of the Seventh International Symposium on Environmental Degradation of Materials in Nuclear Power Systems—Water Reactors, NACE International, Houston (1996).
- 2.44 W. J. Shack, —“Environmentally Assisted Cracking in Light Water Reactors: Semiannual Report, July-December 1999,” NUREG/CR-4667 Vol. 29, ANL-00/23, pp. 47-64 (2000).
- 2.45 —“Materials Reliability Program (MRP) Crack Growth Rates for Evaluating Primary Water Stress Corrosion Cracking (PWSCC) of Thick-Wall Alloy 600 Materials (MRP-55) Revision 1,” EPRI, Palo Alto, CA, TR-1006695, 2002.
- 2.46 P. M. Scott —“An Analysis of Primary Water Stress Corrosion Cracking in PWR Steam Generators,” Proc. NEA/CSNI-UNIPED Specialist Meeting on Operating Experience with Steam Generators, Paper 5.6, Brussels, 16-20 September 1991.
- 2.47 Scott, P., and Ahmad, J., —“Experimental and Analytical Assessment of Circumferentially Surface-Cracked Pipes Under Bending,” NUREG/CR-4872, April 1987.
- 2.48 Gilles, P., and Brust, F. W., —“Approximate Methods for Fracture Analysis of Tubular Members Subjected to Combined Tension and Bending Loads,” Proceedings of the 8th OMAE Conference, Hague, The Netherlands, 1989.
- 2.49 Krishnaswamy, P., and others, —“Fracture Behavior of Short Circumferentially Surface-Cracked Pipe,” NUREG/CR-6298, November 1995.
- 2.50 Wilkowski, G. M., and Scott, P. M., —“A Statistical Based Circumferentially Cracked Pipe Fracture Mechanics Analysis for Design or Code Implementation,” Nuclear Engineering and Design, Vol. III, pp. 173-187, 1989.
- 2.51 Scott, P. M. and Wilkowski, G. M., —“Development and Application of a Database of Pipe Fracture Experiments,” in Fatigue and Fracture - 1996 - Volume 1, PVP - Vol. 323, July 1996, pp. 13-26.
- 2.52 Broek, D., *Elementary Engineering Fracture Mechanics*, Sythoff and Nordhoff, The Netherlands, 1978.

- 2.53 Wilkowski, G. M., Olson, R. J., and Scott, P. M., —~~Site~~ Site-of-the-Art Report on Piping Fracture Mechanics,” U.S. Nuclear Regulatory Commission report, NUREG/CR-6540, BMI-2196, February 1998.
- 2.54 Kramer, G. and Papaspyropoulos, V., —An Assessment of Circumferentially Complex-Cracked Pipe Subjected to Bending,” NUREG/CR-4687, October 1986.
- 2.55 Rahman, S., Ghadaili, N., Paul, D., and Wilkowski, G., —~~Probabilistic~~ Probabilistic Pipe Fracture Evaluations for Leak-Rate-Detection Applications,” NUREG/CR-6004, April 1995.
- 2.56 Paul, D., Ahmad, J., Scott, P., Flanigan, L., and Wilkowski, G., —~~Evaluation~~ Evaluation and Refinement of Leak-Rate Estimation Models,” NUREG/CR-5128, Rev. 1, June 1994.
- 2.57 —~~Users~~ Users Guide for SQUIRT (Windows Version 1.1),” Battelle Memorial Institute, March 2003.
- 2.58 El-Wakil, M., M., *Nuclear Heat Transport*, International Text Book Company, Copyright 1971, Page 362, Figure 12-21.
- 2.59 Rudland D., Wolterman, R. and Wilkowski, G., —~~Impact~~ Impact of PWSCC and Current Leak Detection on Leak-Before-Break,” Emc² final report to NRC, January 31, 2003
- 2.60 Kupperman, D., Sheen, S., Shack, W., Diercks, D., Krishnaswamy, P., Rudland, D., and Wilkowski, G., —~~Barrier~~ Barrier Integrity Research Program,” NUREG/CR-6861, December 2004.
- 2.61 —~~Users~~ Users Manual for PRO-LOCA Code”, 2009.

3.0 Quality Assurance Checks and Sensitivity Analyses

In this section of the report the quality assurance checks and sensitivity analyses that PRO-LOCA was subjected to are discussed in detail.

3.1 Modular QA Checks

The purpose of this section is to present comparisons between some of the deterministic modules coded in PRO-LOCA and either experimental results and/or other analysis results. For instance, the stability routines, such as DPZP and LBB.ENG, were fully documented and compared with full-scale pipe fracture experimental results developed in other programs. For the PRO-LOCA code, these routines were converted to Fortran subroutines. Therefore this QA check only compares results of the Fortran routines and the published original analysis results. The detailed comparison of the methodology for these codes has already been presented in the references. The SQUIRT2 module in the SQUIRT leak rate code is the basis for the leak rate assessment in PRO-LOCA. As with the stability modules, this SQUIRT2 module has been fully documented and compared with experimental data in other programs. As such, this QA check compares the results from the Fortran routines in PRO-LOCA with results from SQUIRT2 analyses. In addition, the previously conducted comparisons of the SQUIRT2 analysis results with experimental leak rate data are also provided. In addition to the stability modules and the SQUIRT leak rate modules, modular QA checks are also provided for the K-solutions, the crack initiation modules, and the crack growth modules incorporated in PRO-LOCA.

3.1.1 K-Solutions

The Anderson K-solutions for both a surface crack and a through-wall crack were used in this code. As a QA check, the code was modified to output the influence functions as a function of crack size. These results were then compared with the tabular values given in the Anderson references.

3.1.1.1 Surface Crack K-Solutions - For the surface crack solutions, the Anderson (Ref. 3.1) solutions were used for a/t values ranging from 0.2 to 0.8. For a/t values of zero, the Chapuliot results (Ref. 3.2) were used and interpolation was used between a/t of zero and 0.2.

Figure 3.1 shows a comparison of the G_0 influence function at the deepest point of the surface crack from the original reference and output from the PRO-LOCA code. As shown in this figure, the comparison is excellent. Figure 3.2 shows a similar comparison as in Figure 3.1, but at the free surface of the surface crack. The results show that the PRO-LOCA code does a reasonable job of mirroring the FE results from the original references. Note, the curve fits generated have maximum error in the free surface influence function due to some irregularities in the trends generated by the FE solutions. The maximum error is about 20 percent and occurs for the longest cracks, which have the smallest influence functions.

Note from Figure 3.1 that for $c/a = \text{infinity}$, the solutions at the deepest point of the surface crack are very similar to that for $c/a = 32$. In fact, the uncertainty in the curve fits masks any difference between these solutions. Also note that the solution at $c/a=32$ is approaching zero at the free surface. If a surface crack exists that is greater in length than $c/a=32$, using the $c/a=32$ solutions

will slightly overestimate the growth in the length direction, and once the crack breaks through the wall, will give conservative leak-rate predictions.

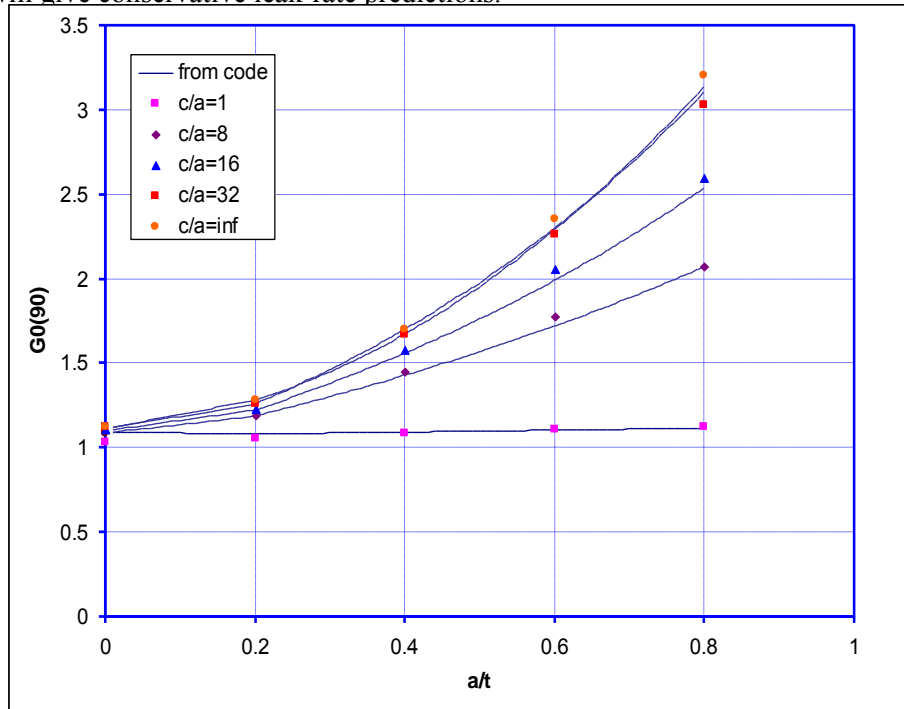


Figure 3.1 Comparison of FE results and PRO-LOCA output for influence function G_0 at the deepest point of the surface crack

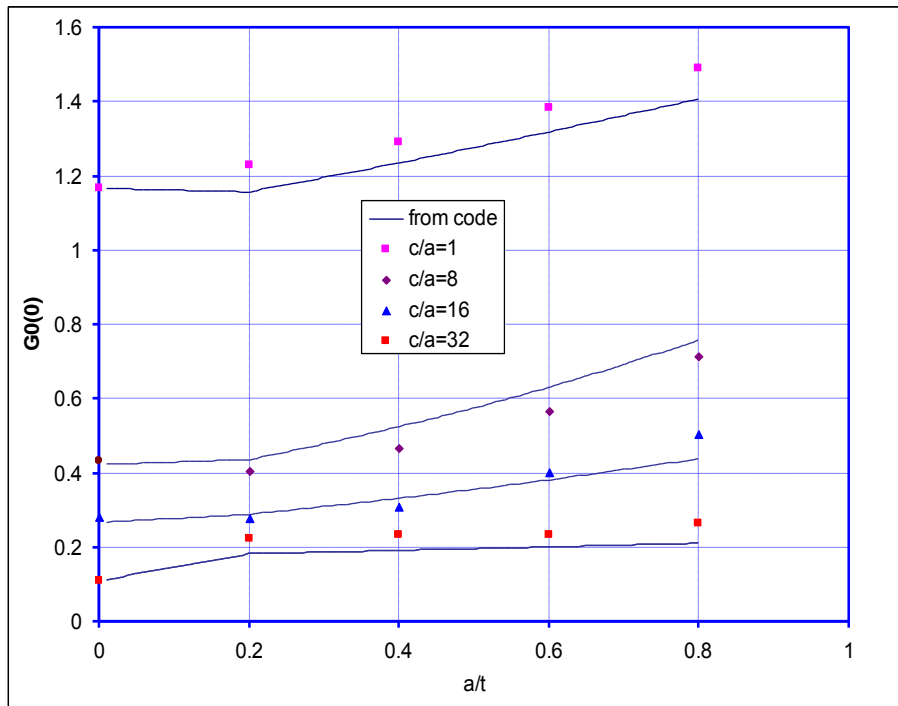


Figure 3.2 Comparison of FE results and PRO-LOCA output for influence function G_0 at the free surface of the surface crack

3.1.1.2 *Through-Wall Crack K-Solutions* - A comparison between the K-solution output from PRO-LOCA and the Anderson solution for through-wall cracks is shown in Figure 3.3. Note, the Anderson solution for TWC was input directly into PRO-LOCA. Intermediate values were calculated using linear interpolation between the tabular Anderson values. Therefore, as expected, the PRO-LOCA code outputs the exact influence functions as is published by Anderson. Also note that the values shown in Figure 3.3 are averaged through the thickness. In Reference 3.3, Anderson presents influence function values both on the inside and outside diameter of the pipe. Since PRO-LOCA does not capture crack variation through the thickness for through-wall cracks, the average influence function values were used to predict the through-wall crack driving force.

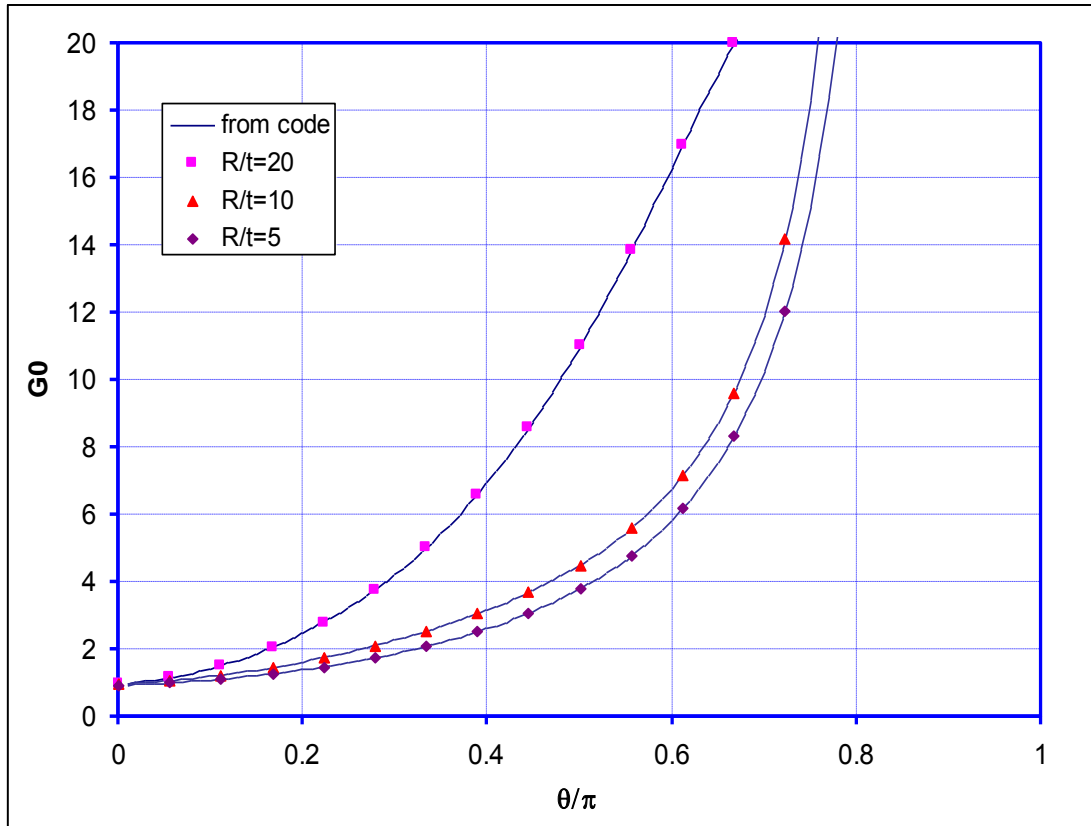


Figure 3.3 Comparison of FE results and PRO-LOCA output for influence function G_0 for a through-wall crack

3.1.2 Crack Stability Modules

The crack stability models used in PRO-LOCA are the DPZP model for surface crack stability and the LBB.ENG2 model for through-wall crack stability. The DPZP through-wall crack model was also used as a screening criterion for through-wall crack stability.

3.1.2.1 *LBB.ENG2* - The through-wall-crack stability calculation module of the PRO-LOCA code, identified as TWCFSDAJ, was written in FORTRAN. It was translated from the NRCPIPE code (Windows Version 3.0), Reference 3.4. The TWCFSDAJ module only utilizes the LBB.ENG2 method of the NRCPIPE code. The LBB.ENG2 method is described in Section 2.11 of this report.

The quality assurance checks in this section of the report compare the results obtained from the PRO-LOCA code (TWCFSDAJ module) with the results obtained from the Windows Version 3.0 of the NRCPIPE code. Table 3.1 lists the input parameters for several cases used for comparing the initiation and maximum bending stresses calculated from the two codes. The cases listed cover different pipe material properties, pipe sizes (diameter and thickness), pipe pressure and various crack lengths.

Table 3.2 shows the calculated initiation and maximum bending stresses obtained from the two codes.

Figure 3.4 (initiation bending stress) and Figure 3.5 (maximum bending stress) show the results of all the cases analyzed. The straight-line plots in Figure 3.4 and Figure 3.5 show a 1 to 1 relation between the Windows Version 3.0 (NRCPIPE) and the PRO-LOCA code (TWCFSDAJ) i.e., the line represents an exact match between the two codes. The data points in Figure 3.4 and Figure 3.5 represent the results from the various cases analyzed. The initiation bending stress and maximum bending stress results obtained from the PRO-LOCA code (TWCFSDAJ module) compare almost exactly with the results from the Windows Version 3.0 of NRCPIPE for the LBI

The
3.4.
of ti
coe

ce
an
a

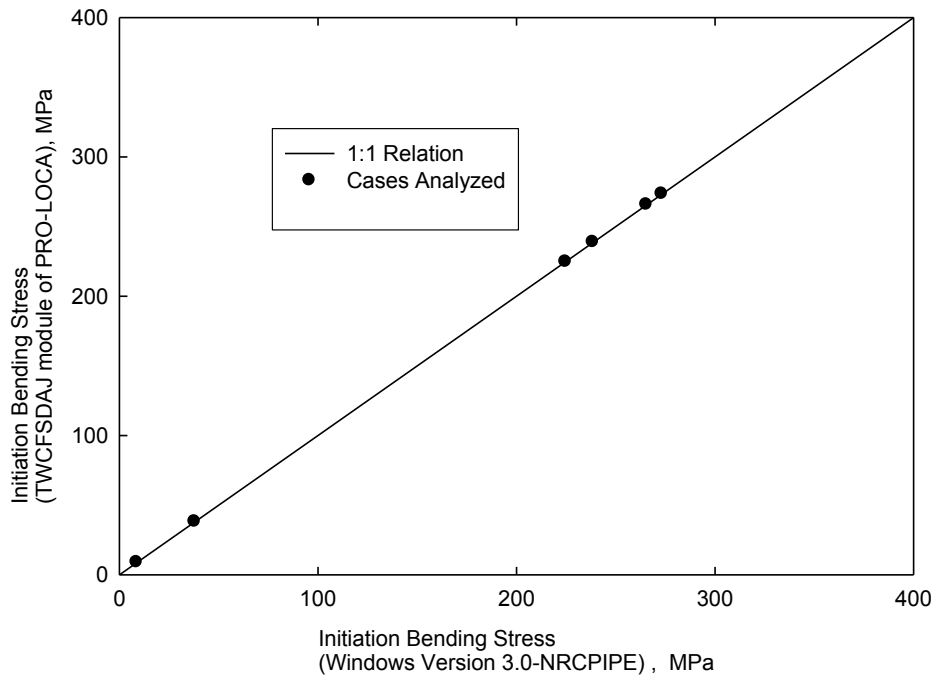


Figure 3.4 Comparison of LBB-ENG2 Initiation bending stress (NRCPIPE and PRO-LOCA)

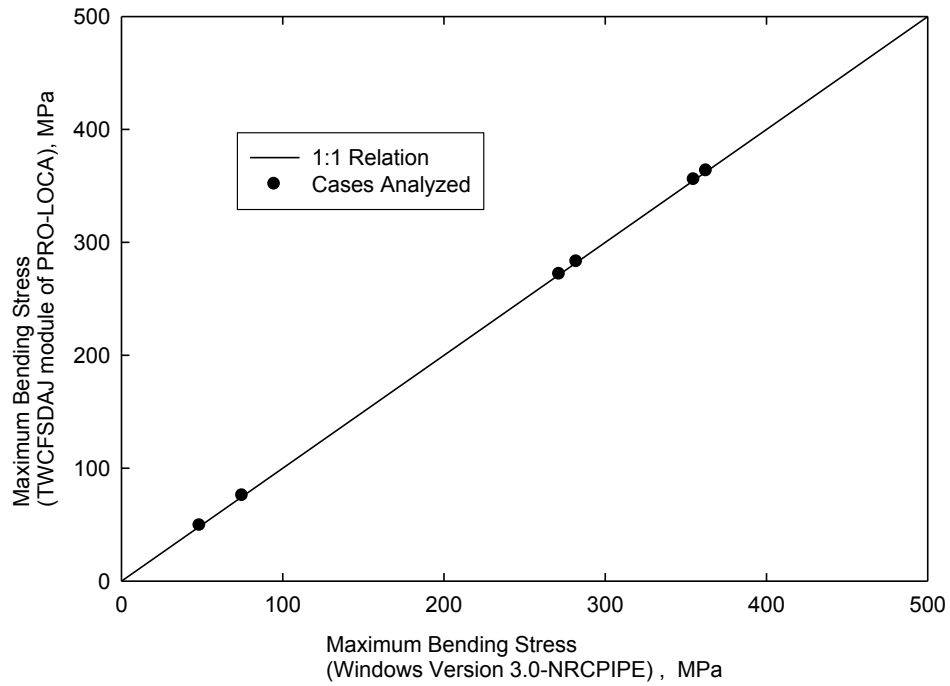


Figure 3.5 Comparison of LBB-ENG2 maximum bending stress (NRCPIPE and PRO-LOCA) (LBB.ENG2 Method) (NRCPIPE and PRO-LOCA)

Table 3.1 Input parameters for comparison between Windows version of NRCPIPE and PRO-LOCA (LBB.ENG2 method)

Case No.	Pipe Outside Diameter mm	Pipe Wall Thick mm	Crack Length mm	Pipe Pressure MPa	Yield Stress MPa	Ultimate Stress MPa	Reference Stress MPa	Reference Strain mm/mm	J at crack Initiation N/mm	Constant for J-R Curve	Exponent for J-R Curve
1	413.5	26.2	447.8	7.0	299.24	739.4	299.24	0.002597	43.41	183.6	0.4448
2	413.5	26.2	447.8	0.0	299.24	739.4	299.24	0.002597	43.41	183.6	0.4448
3	711.2	35.8	179.4	7.239	154.78	442.36	154.78	0.000847	1242.7	344.189	0.7393
4	711.2	35.8	179.4	0.0	154.78	442.36	154.78	0.000847	1242.7	344.189	0.7393
5	812.8	76.2	115.8	15.512	201.05	529.2	201.05	0.0011	300.6	202.1	0.7196
6	812.8	76.2	115.8	0.0	201.05	529.2	201.05	0.0011	300.6	202.1	0.7196

Table 3.2 Output parameters for comparison between Windows version of NRCPIPE and PRO-LOCA (LBB.ENG2 method)

Case No.	Initiation Bending Stress MPa (Windows-NRCPIPE)	Initiation Bending Stress MPa (PRO-LOCA)	Maximum Bending Stress MPa (Windows-NRCPIPE)	Maximum Bending Stress MPa (PRO-LOCA)
1	8.789	8.789	48.782	48.782
2	38.018	38.018	75.253	75.253
3	224.86	224.56	271.82	271.469
4	238.59	238.59	282.439	282.439
5	265.55	265.55	355.187	355.187
6	273.3	273.3	362.95	362.95

3.1.2.2 Surface Crack DPZP - The DPZP surface-crack stability routine incorporated into the PRO-LOCA code, identified as SCFSDAD, was written in FORTRAN. It was translated from the NRCPIPES code (Windows Version 3.0). The Windows Version of the NRCPIPES code was written in Visual Basic. The Windows Version 3.0 was developed from the DOS version 2.0a, which was released in March 1995. The NRCPIPES code is described in detail in Reference 3.5. The SCFSDAD module only utilizes the DPZP method of the NRCPIPES code. The DPZP method is described in Section 2.11 of this report.

The quality assurance checks in this section of the report compare the results obtained from the PRO-LOCA code (SCFSDAD module) with the results obtained from the Windows Version 3.0 of the NRCPIPES code. Table 3.3 lists the input parameters for several cases used for comparing the maximum bending stresses calculated from the two codes. The cases listed cover different pipe material properties, pipe sizes (diameter and thickness), pipe pressure and various crack sizes (length and crack depth). Table 3.4 shows the maximum bending stresses obtained from the two codes.

Figure 3.6 (maximum bending stress) shows the results of all the cases analyzed. The straight-line plot in Figure 3.6 shows a 1-to-1 relation between the results from the Windows Version 3.0 of NRCPIPES and the PRO-LOCA code (SCFSDAD) i.e. the line represents an exact match between the two codes. The data points in Figure 3.6 represent the results from the various cases analyzed. The maximum bending stress results obtained from the PRO-LOCA code (SCFSDAD module) compare nearly exactly with the results from the Windows Version 3.0 of NRCPIPES for the DPZP method.

The accuracy of the surface-crack DPZP analysis compared with full-scale experimental pipe fracture data at LWR temperatures with bending or combined pressure and bending is given in Reference 3.6. For the combined pressure and bending cases, the mean value of the ratio of the experimental stress to the predicted stress at failure was 1.05 with a coefficient of variance of 12.4 percent.

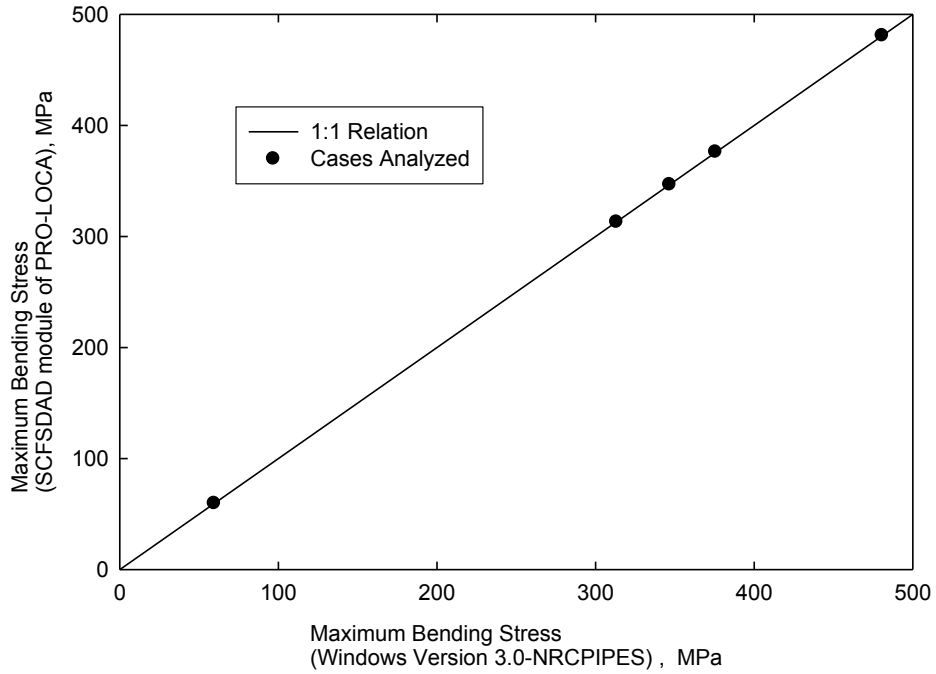


Figure 3.6 Comparison of DPZP on Maximum Bending Stress (NRCPIPES) and (PRO-LOCA) (DPZP Method)

Table 3.3 Input parameters for comparison of surface crack results between Windows version of NRCPIPES and PRO-LOCA

Case No.	Pipe Outside Diameter mm	Pipe Wall Thick mm	Crack Length mm	Crack Depth mm	Pipe Pressure MPa	Yield Stress MPa	Ultimate Stress MPa	Young's Modulus MPa	J at crack Initiation N/mm
1	929.64	81.88	240.0	40.64	15.513	344.7	620.5	199947	87.56
2	421.0	28.37	653.7	28.37	0.0	170.9	428.8	182688	43.41
3	711.2	35.38	179.4	10.26	7.000	154.8	442.4	182741	1242.7
4	680.0	40.00	534.3	20.00	7.000	160.9	461.6	182727	206.4
5	812.8	76.2	115.8	16.256	15.513	201.1	529.20	182727	300.6

Table 3.4 Output parameters for comparison of surface crack results between Windows version of NRCPIPES and PRO-LOCA

Case No.	Failure Bending Stress MPa (Windows-NRCPIPES)	Failure Bending Stress MPa (PRO-LOCA)
1	346.68	346.69
2	59.537	59.59
3	375.62	376.05
4	313.2	313.0
5	480.710	480.83

3.1.2.3 Through-Wall Crack DPZP - The DPZP through-wall-crack analysis was used as a screening criterion (for failure) in the PRO-LOCA code. The PRO-LOCA module, identified as TWCFSAD, was written in FORTRAN. It was translated from the NRCPIPE code (Windows Version 3.0). The Windows Version of the NRCPIPE code was written in Visual Basic. The Windows Version 3.0 was developed from the DOS version 2.0a, which was released in March 1995. The NRCPIPE code is described in detail in Reference 3.4. The TWCFSAD module only utilizes the DPZP method of the NRCPIPE code. The DPZP method is described in Section 2.11 of this report.

The quality assurance checks in this section of the report compare the results obtained from the PRO-LOCA code (TWCFSAD module) with the results obtained from the Windows Version 3.0 of the NRCPIPE code for the DPZP method. Table 3.5 lists the input parameters for several cases used for comparing the maximum bending stresses calculated from the two codes. The cases listed cover a wide variety of pipe material properties, pipe sizes (diameter and thickness), pipe pressure and crack sizes (crack length and depth). Table 3.6 shows the predicted maximum bending stresses obtained from the two codes.

Figure 3.7 shows the results of all the cases analyzed. The straight-line plot in Figure 3.7 shows a 1 to 1 relation between the Windows Version 3.0 (NRCPIPE) and the PRO-LOCA code (TWCFSAD), i.e., the line represents an exact match between the two codes. The data points in Figure 3.7 represent the results from the various cases analyzed. The maximum bending stress results obtained from the PRO-LOCA code (TWCFSAD module) compare nearly exactly with the results from the Windows Version 3.0 of NRCPIPE for the DPZP method.

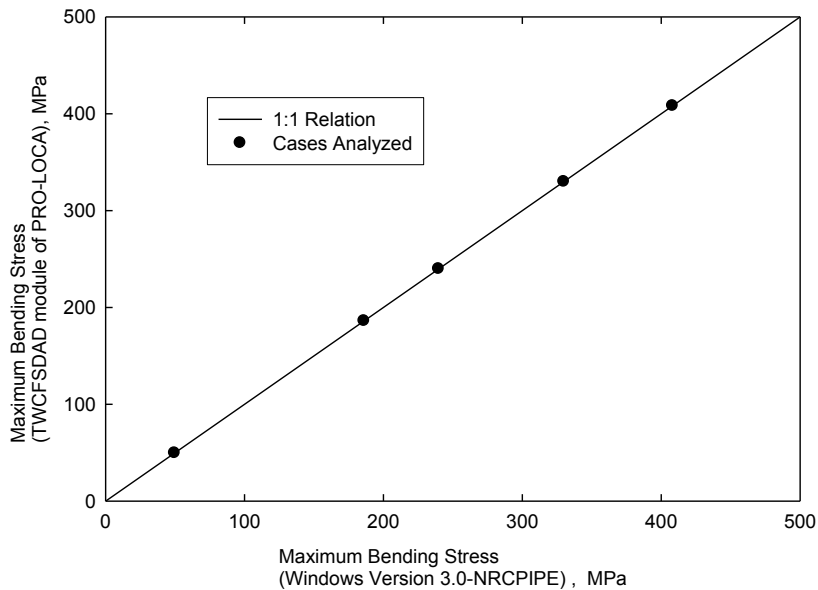


Figure 3.7 Comparison of Maximum Bending Stress (NRCPIPE and PRO-LOCA) (DPZP Method)

Table 3.5 Input parameters for comparison of through-wall crack results between Windows version of NRCPIPE and PRO-LOCA (DPZP method)

Case No.	Pipe Outside Diameter mm	Pipe Wall Thick mm	Crack Length mm	Pipe Pressure MPa	Yield Stress MPa	Ultimate Stress MPa	Young's Modulus MPa	J at crack Initiation N/mm
1	929.64	81.28	222.1	15.513	344.7	620.5	199947	87.56
2	421.0	28.37	653.7	0.0	170.9	428.8	182688	43.41
3	711.2	35.38	179.4	7.000	154.8	442.4	182741	1242.7
4	680.0	40.00	534.3	7.000	160.9	461.6	182727	206.4
5	812.8	76.2	115.8	15.513	201.1	529.20	182727	300.6

Table 3.6 Output parameters for comparison of through-wall crack results between Windows version of NRCPIPE and PRO-LOCA (DPZP method)

Case No.	Failure Bending Stress MPa (Windows-NRCPIPE)	Failure Bending Stress MPa (PRO-LOCA)
1	239.75	239.81
2	49.65	49.65
3	329.84	329.84
4	186.06	186.06
5	408.17	408.17

3.1.3 SQUIRT Leakage Rate Module

The leak-rate module of the PRO-LOCA code, identified as SQFSDA, was written in FORTRAN. It was translated from the SQUIRT2 module of the Windows Version 1.1 of the SQUIRT code. The Windows Version of the SQUIRT code was written in Visual Basic. The Windows Version 1.1 was developed from the DOS version 2.0a, which was released March 1995. The SQUIRT code is described in detail in Reference 3.7. The leak-rate model is described in Section 2.12 of this report.

Reference 3.8 describes in detail the validation of the SQUIRT2 thermo-hydraulic model where the results obtained from the SQUIRT2 module are compared with both the results from other leak rate codes as well as experimental results. Figure 3.8 shows a comparison of leak rate predictions from both the SQUIRT code and the LEAK-RATE code developed by Ontario Hydro in Canada. Figure 3.9 shows a comparison of the SQUIRT predicted leak rates and some experimental leak rate data developed by Ontario Hydro (Ref. 3.9). As can be seen, the agreement with both the LEAK-RATE code and the experimental data is quite good.

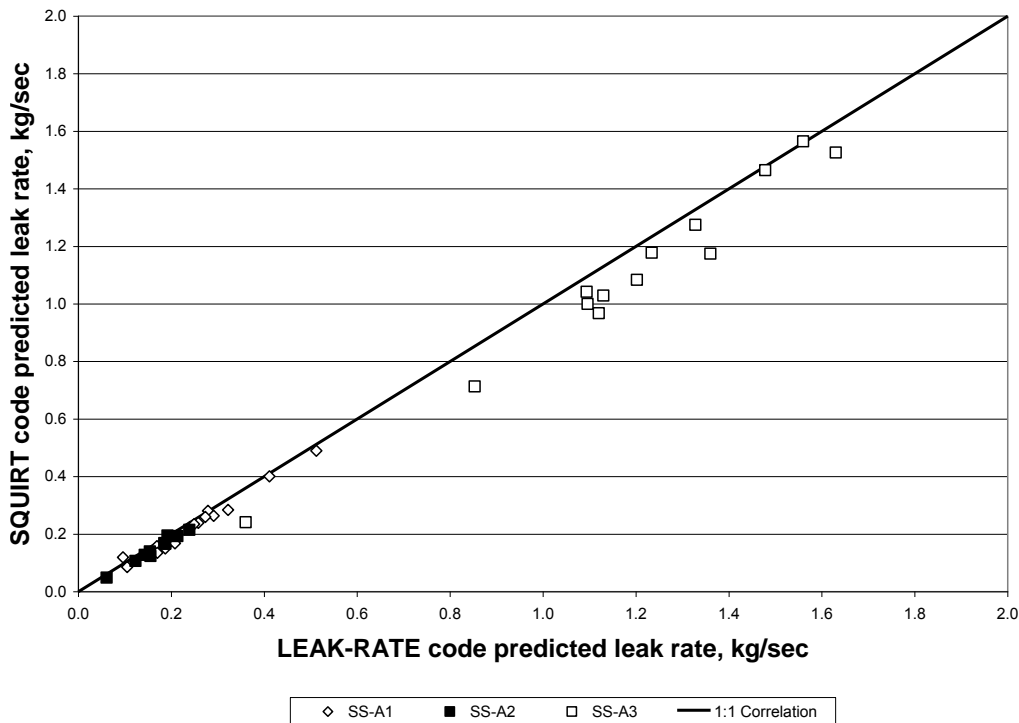


Figure 3.8 Comparison of predicted leak rates from SQUIRT and LEAK-RATE computer programs

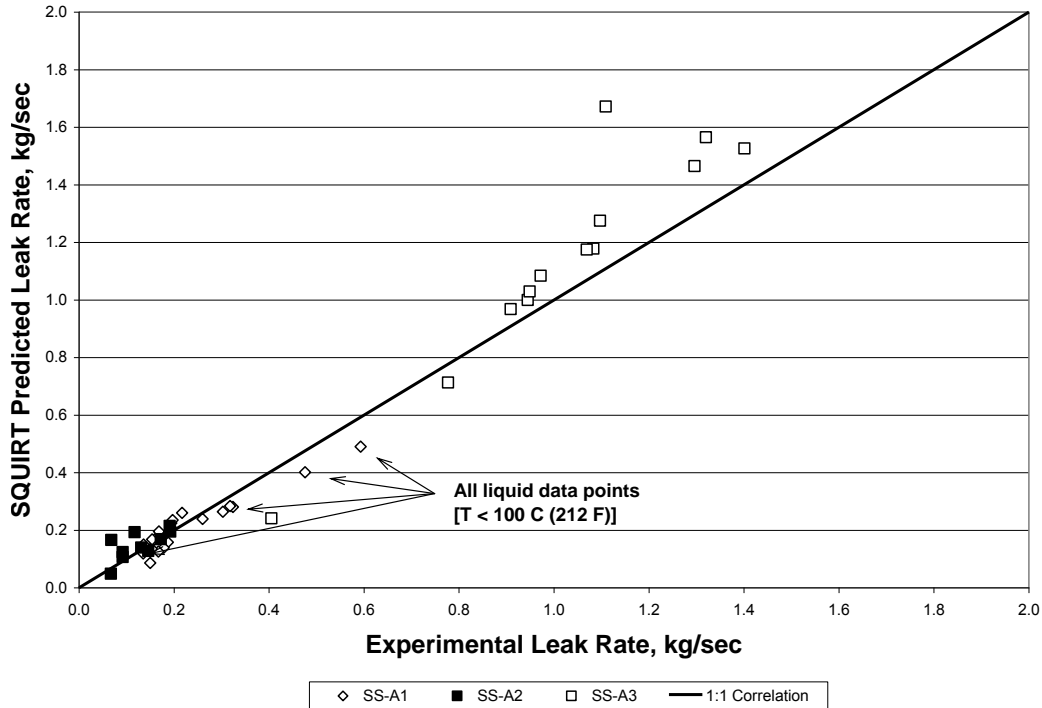


Figure 3.9 Comparison of SQUIRT predicted leak rates versus experimentally measured leak rates for Ontario Hydro experiments

The quality assurance checks in this section of the report compare the results obtained from the PRO-LOCA code (SQFSDA module) with the results obtained from the Windows Version 1.1 of the SQUIRT code (SQUIRT2 module). Table 3.7 lists the input parameters for several cases used for comparing volumetric leak rates from the two codes. The cases listed cover a variety of cracking mechanisms (IGSCC, Fatigue and PWSCC), pipe sizes (diameter and thickness), crack sizes (length and crack-opening displacement), and thermodynamic fluid conditions (temperature, pressure, and fluid state). Table 3.8 shows the volumetric leak rates obtained from the two codes.

Figure 3.10 shows the results of all the cases analyzed. The straight-line plot in Figure 3.10 shows a 1 to 1 relation between the Windows Version 1.1 (SQUIRT2) and the PRO-LOCA code (SQFSDA), i.e., the line represents an exact match between the two codes. The data points in Figure 3.10 represent the results from the various cases analyzed. The leak rate results obtained from the PRO-LOCA code (SQFSDA module) compare almost exactly with the results from the Windows Version 1.1 of SQUIRT2.

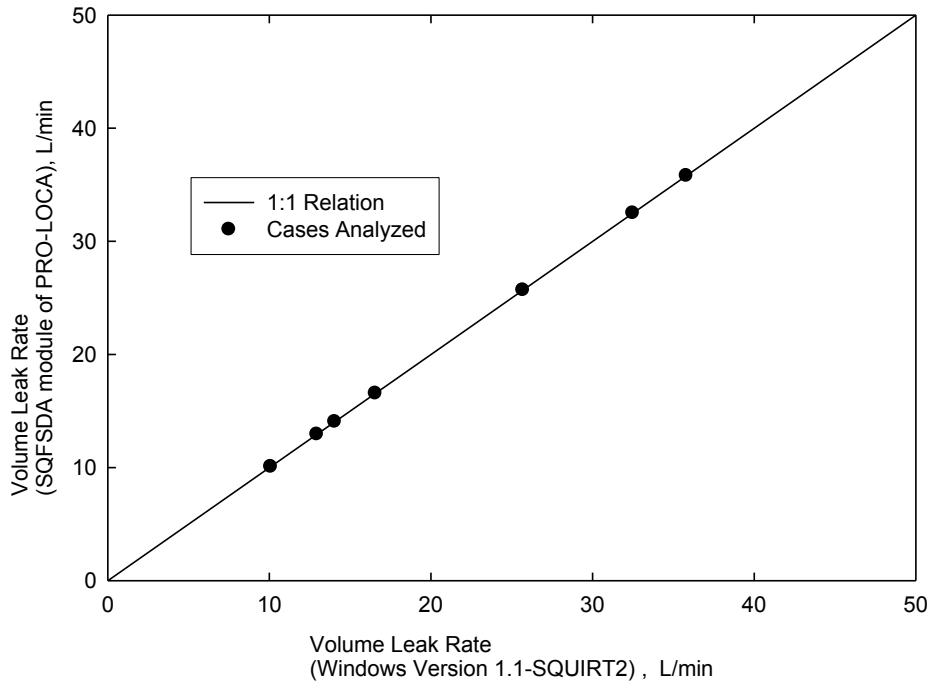


Figure 3.10 Comparison of Calculated Leak Rates (SQUIRT and PRO-LOCA)
 Figure 4.3.2.1 Comparison of Calculated Leak Rates (SQUIRT and PRO-LOCA)
 (SQUIRT and PRO-LOCA)

Table 3.7 Input parameters for comparison of leak rates between Windows version of SQUIRT and PRO-LOCA

Case No.	Pipe Outside Diameter mm	Pipe Wall Thickness mm	Cracking Mechanism	Crack Length mm	Crack Gap mm	Pipe Pressure kPa	Temperature °C	Fluid Condition
1	413.512	26.187	IGSCC	50.8	0.564	15513.2	287.8	SUBC
2	413.512	26.187	Fatigue	50.8	0.564	15513.2	287.8	SUBC
3	413.512	26.187	PWSCC	50.8	0.564	15513.2	287.8	SUBC
4	413.512	26.187	IGSCC	50.8	0.800	15513.2	287.8	SUBC
5	413.512	26.187	IGSCC	70.8	0.564	15513.2	287.8	SUBC
6	413.512	26.187	IGSCC	70.8	0.800	15513.2	287.8	SUBC
7	680.0	40.000	IGSCC	137.0	0.4	15513.2	287.8	SUBC
8	680.0	40.000	IGSCC	137.0	1.700	15513.2	287.8	SATL

SUBC = Subcooled water
 SATL = Saturated liquid

Table 3.8 Output parameters for comparison of leak rates between Windows version of SQUIRT and PRO-LOCA

Case No.	Volume Leak Rate L/min (Windows)	Volume Leak Rate L/min (PRO-LOCA)
1	10.0811	10.0807
2	32.4874	32.4865
3	16.5589	16.5583
4	25.6868	25.6881
5	14.0501	14.0496
6	35.8004	35.8016
7	12.9404	12.9398
8	172.581	172.617

3.1.4 Crack Initiation Models

In this section modular QA checks for the crack initiation modules for two of the cracking mechanisms, i.e., IGSCC and PWSCC, considered in PRO-LOCA are discussed.

3.1.4.1 IGSCC - The development of the IGSCC crack initiation model is described in Section 2.8. This model is a Weibull-based model that has been calibrated to leaks in older BWR plants. The model is scaled to the subunit size (approximately 10 mm) and crack initiation times are sampled on a subunit basis. For IGSCC, the Weibull scale factor is a log-triangular distribution that is first sampled for each Monte-Carlo increment and is then used to sample initiation times for each subunit. For this subunit time to initiation, the distributions were programmed into an Excel spreadsheet, and the results of this spreadsheet were compared with the output from PRO-LOCA, see Figure 3.11.

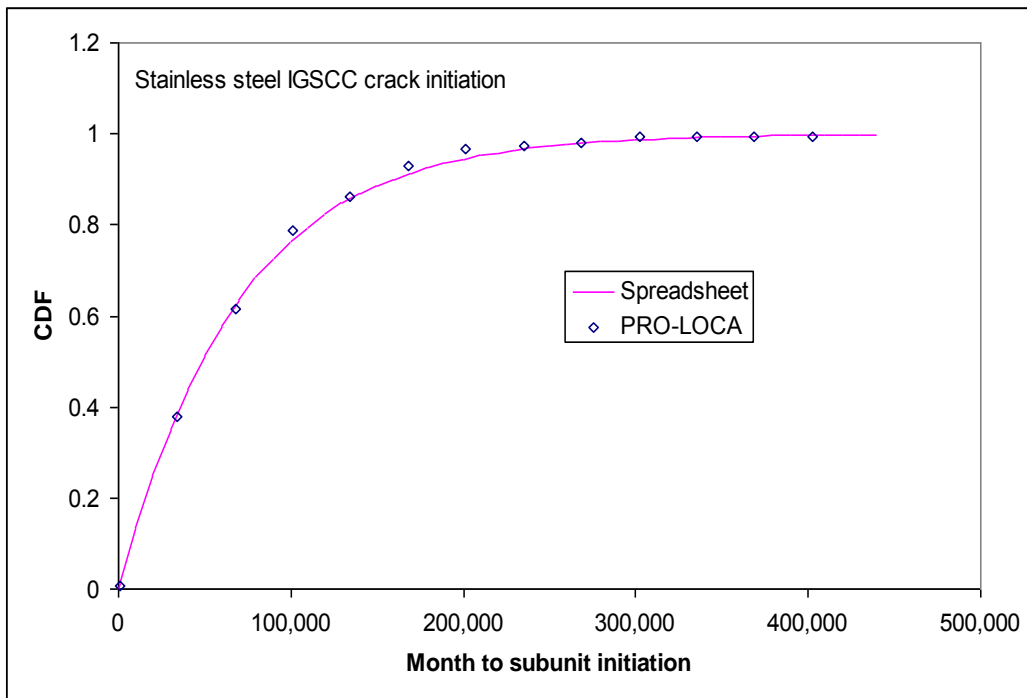


Figure 3.11 Comparison of month to IGSCC subunit crack initiation between spreadsheet formulation and PRO-LOCA code

As shown in this figure, the PRO-LOCA code outputs the cumulative density function for the subunit initiation very similar to the spreadsheet code.

In addition to the subunit initiation, the PRO-LOCA code outputs the probabilities to first crack initiation for the entire pipe cross-section. The same EXCEL spreadsheet is used, but the Weibull scale factor is further scaled to the pipe circumference. This comparison is shown in Figure 3.12. It should be noted that in Figure 3.12 only 1000 Monte-Carlo increments were run. The comparison between the spreadsheet and the PRO-LOCA output is very good and would be exact if more iterations were performed.

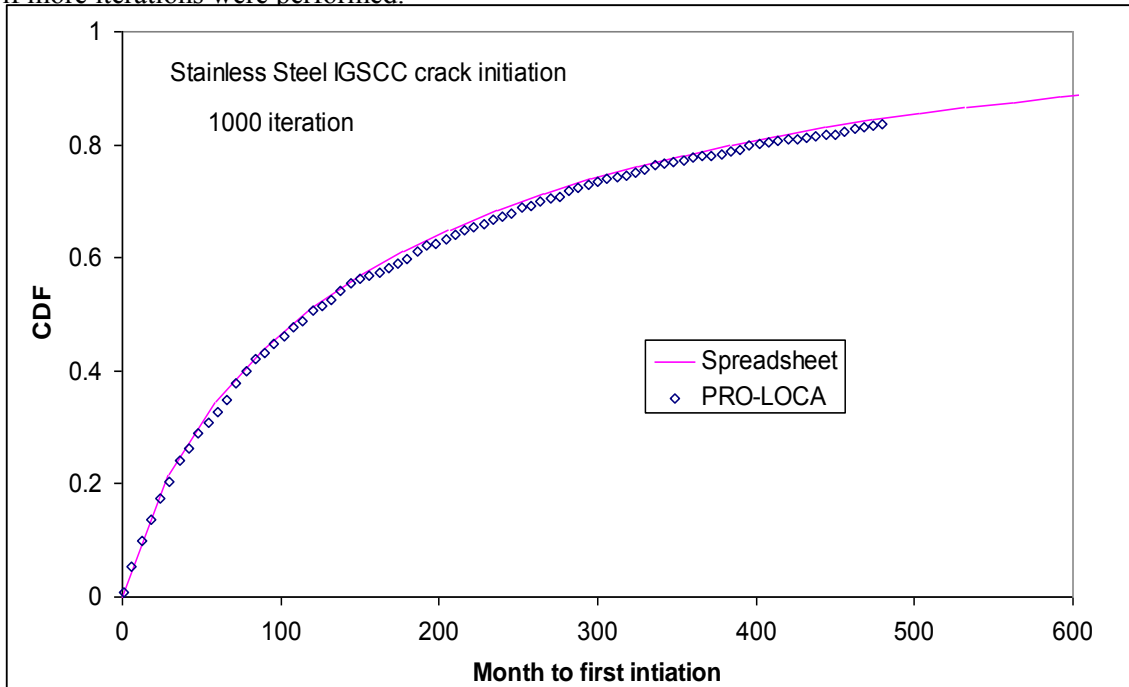


Figure 3.12 Comparison of month to first IGSCC crack initiation for the PRO-LOCA code and spreadsheet formulation

3.1.4.2 PWSCC - The development of the PWSCC crack initiation model is given in Section 2.8. As with IGSCC, the model is based on a Weibull characterization of the initiation time, but because of the limited pipe cracking data due to PWSCC, this model was calibrated to PWSCC cracking in Control Rod Drive Mechanisms (CRDMs). The model was scaled to a subunit size (approximately 10 mm) in a CRDM nozzle tube and was used for the subunit sizes in the analyzed piping segment. The scale factor for the Weibull distribution for the CRDM tubes was developed from inspection results and assumed to follow a log-triangular distribution, see Section 2.8.2 for further discussion. For PWSCC, once the nozzle scale factor is sampled, this is used to calculate the scale factor for the subunit size. The initiation times are then sampled for each subunit from these scale factors. This process was programmed into an Excel spreadsheet for QA purposes. The results from the spreadsheet were then compared to the output from the PRO-LOCA code for each subunit, see Figure 3.13. The comparisons are excellent.

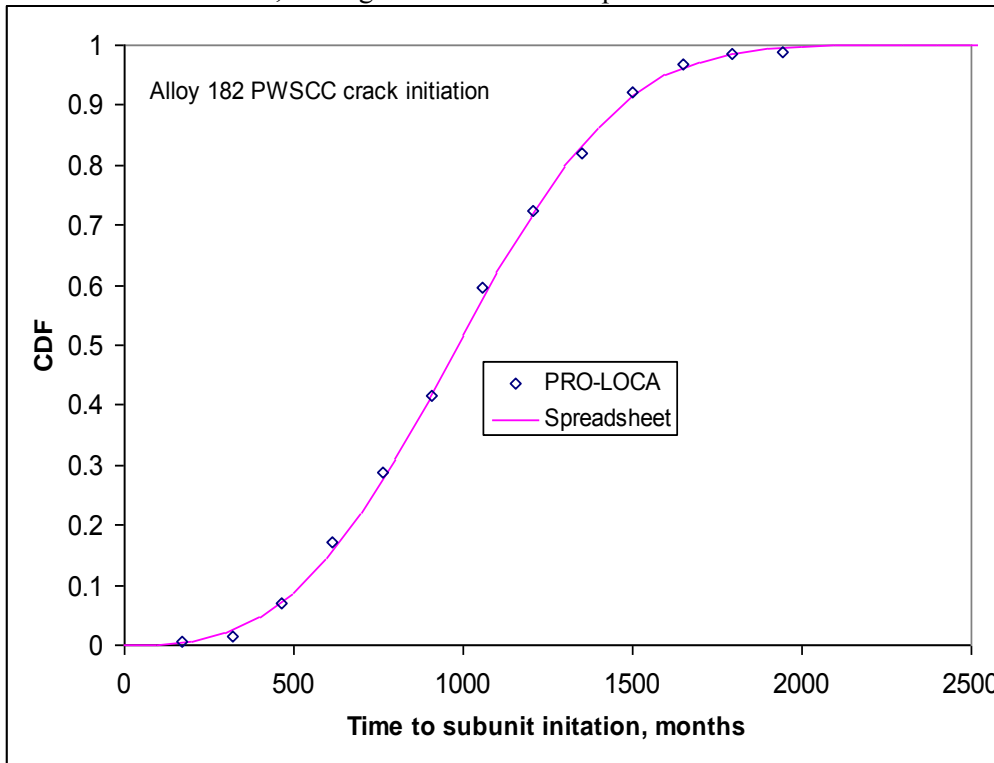


Figure 3.13 Comparison of month to PWSCC subunit crack initiation between spreadsheet formulation and PRO-LOCA code

In addition, the PRO-LOCA code will output the probability of first crack initiation for the entire critical node circumference. The same spreadsheet was used, but the subunit Weibull scale factor was scaled from the 10-mm size to the size of the circumference. The comparison is shown in Figure 3.14. The number of iterations for this comparison was 1000, which provides a good comparison with the spreadsheet results.

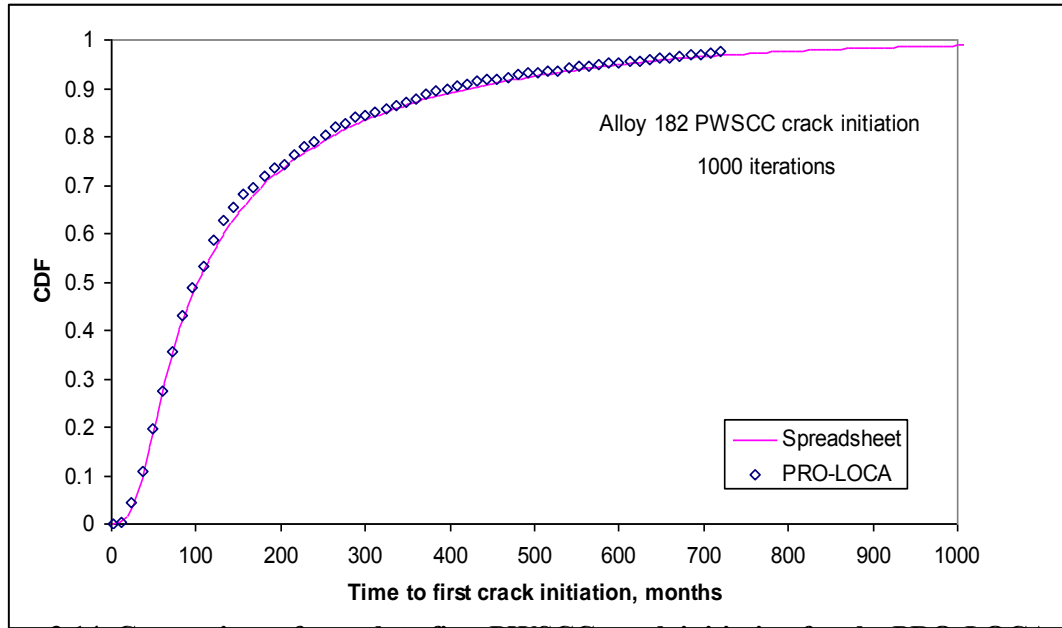


Figure 3.14 Comparison of month to first PWSCC crack initiation for the PRO-LOCA code and spreadsheet formulation

3.1.5 Crack Growth Models

In this section modular QA checks for the crack growth modules for the three cracking mechanisms, i.e., fatigue, IGSCC, and PWSCC, considered in PRO-LOCA are discussed.

3.1.5.1 Fatigue - In order to QA the fatigue crack growth model, a stainless steel weld in a PWR piping weld case was run. In addition to normal operating loads, a vibration load signature was applied. Crack growth from preexisting weld defects was tracked for a single crack. The crack growth equations were programmed into an Excel spreadsheet for comparison purposes. The results of this comparison are shown in Figure 3.15. The PRO-LOCA code and the spreadsheet show very similar results.

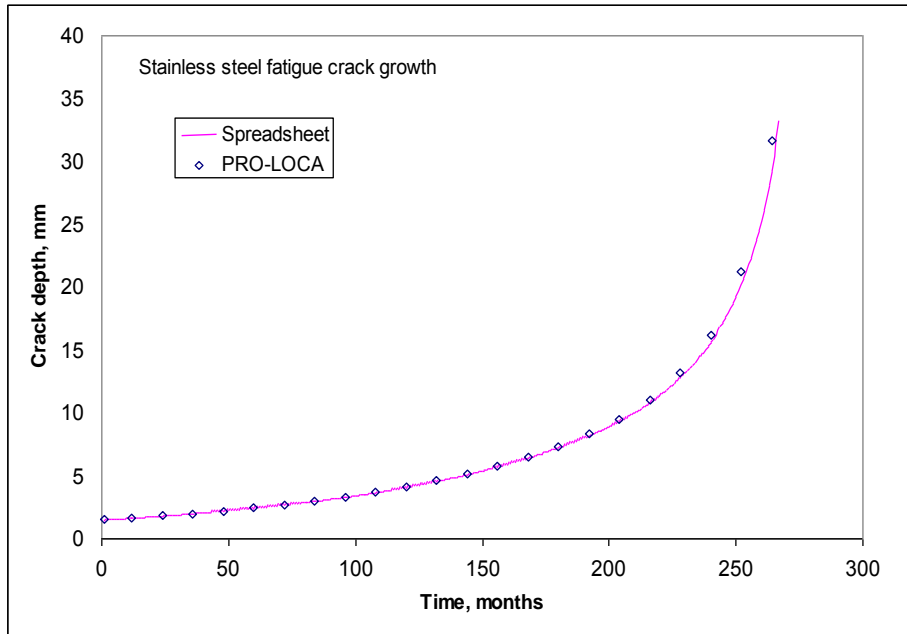


Figure 3.15 Stainless steel fatigue crack growth prediction comparison

3.1.5.2 IGSCC - A similar case was run for a BWR stainless steel piping system. In this case, however, no vibrations loads and only operating pressure (axial stress = 24 MPa [3.5 ksi]) was applied. The flaws were allowed to initiate from IGSCC and grow under these loads. The crack growth equations were programmed into an Excel spreadsheet for comparison purposes. A comparison of the output from PRO-LOCA and the spreadsheet code are shown in Figure 3.16. Because the only driving force in this example was pressure loading, the amount of growth was limited, but as shown in Figure 3.16, the comparisons were excellent.

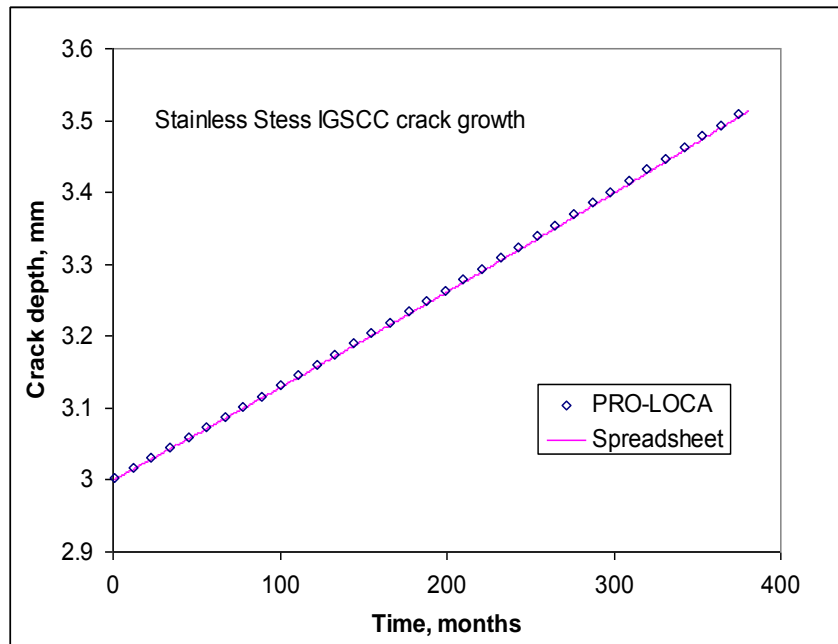


Figure 3.16 Stainless steel IGSCC crack growth prediction comparison

3.1.5.3 PWSCC - For the case of PWSCC, a similar case was run, but an additional axial stress (total axial stress = 150 MPa [21.7 ksi]) was added to induce more crack growth than in the IGSCC case. The flaws were allowed to initiate from PWSCC and grow under these loads. The crack growth equations were programmed into an Excel spreadsheet for comparison purposes. A comparison of the output from PRO-LOCA and the spreadsheet code are shown in Figure 3.17. The results in the figure show an excellent comparison between the two cases.

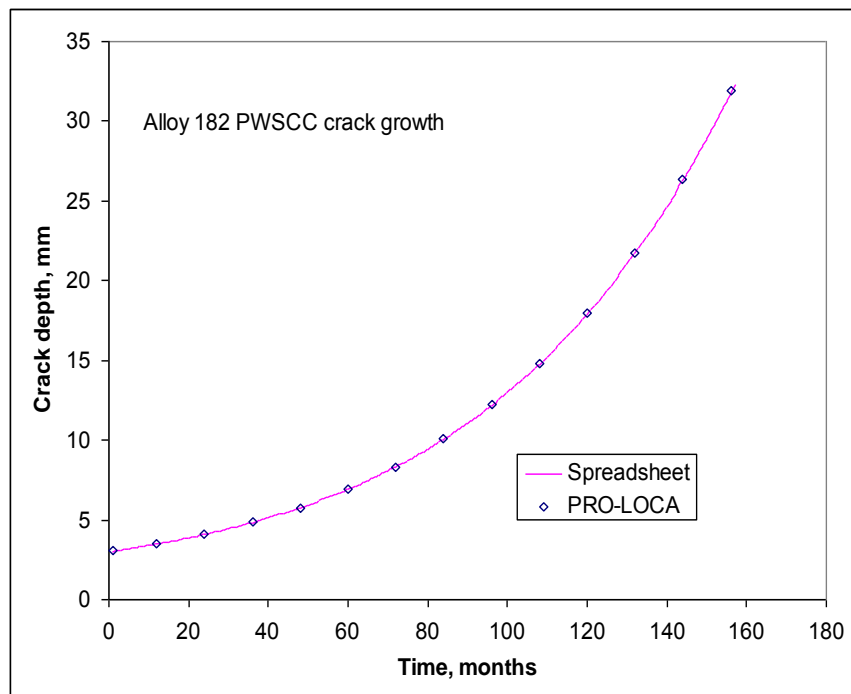


Figure 3.17 Alloy 182 PWSCC crack growth prediction comparison

3.2 Sensitivity Analyses

In this section of the report the results from a series of sensitivity analyses are presented. For the first series of analyses, a base case problem was solved and then individual parameters were individually changed in order to see the effect of changing this single parameter on the results of the analyses. The objectives of these analyses were two-fold. One was a sanity check to ascertain whether the specific input parameter change resulted in a logical change to the resultant probabilities, e.g., does increasing the inspection interval (time between inspections) increase the resultant probabilities as one would expect. As part of this assessment, different parts of the code were exercised to ensure that those parts of the code were working properly. The second objective of this parametric study was to assess what input parameters were the major drivers in the probabilities, i.e., changing what parameters resulted in the most significant changes to the resultant probabilities.

3.2.1 Parametric Study

A detailed parametric study was conducted using Version 3.5.30 of PRO-LOCA with a release date of April 24, 2009 to ascertain the effect that specific input parameters had on the resultant LOCA probabilities. As part of this study, a base case was developed and then specific input parameters were changed to investigate the effect those specific changes had on the resultant LOCA probabilities. As discussed above, the objectives of this study were two-fold: (1) a sanity check to ascertain whether the specific input parameter changes had a logical effect on the resultant LOCA probabilities and (2) to ascertain the major drivers associated with the resultant probabilities. A major outcome of these sanity checks was to identify any coding errors associated with PRO-LOCA. A number of such errors were identified as part of this process and subsequently corrected. Table 3.9 presents the input parameters for the BWR base case problem while Table 3.10 presents the input parameters for the PWR base case problem. In order to facilitate these analyses, constant deterministic input parameters were used as much as possible.

Figure 3.18 and Figure 3.19 show the results for the BWR and PWR base cases, respectively. These figures show the probability of occurrences as a function of years of plant operations for various size LOCAs. The top curve in these figures represents the probability of occurrences for crack initiation. The next curve represents the probability of occurrence for the development of a through-wall crack. The remaining curves represent various size LOCA events. In subsequent figures the same figure format will be followed, except two sets of results will be shown on each figure; one for the reference case (i.e., the base case in some instances) and one for the specific parameter being considered in that particular parametric study. For example, Figure 3.20 shows the effect of static bending stress on the probability of occurrences for various size LOCA events for BWRs. In the following figures and related text only the results are presented. A discussion of those results is deferred to Section 4 of this report.

Table 3.9 Input parameters for BWR base case problem

GUI Screen Tab	Input Parameter	Value
Plant	Reactor type and piping system	BWR recirculation line
	Years in operation and years of end of license and extended life	0, 40, and 60 years
	Outside diameter and wall thickness	711 mm and 30.2 mm
	Leak rate detection	Mean 378 lpm w/zero Std. Dev.
	Weld repair	Replace w/non-susceptible mat'l
	Material1, Weld material, Material2	Type 304, Type 304 SAW, Type 304
	Material at crack location	Stainless steel
Material Properties	Material input property parameters	User input, no correlation
	Elastic modulus	180,000 MPa
	Base metal properties	Yield = 187.8 MPa, Ultimate = 493 MPa, n = 4.2, F = 599
	Weld metal properties	Yield = 240 MPa, $J_i = 570.7 \text{ kJ/m}^2$, m = 0.6, C = 292.3
Static Loads	Global bending input type	Stress
	Secondary stress ratio	0
	Pipe temperature and pressure	288 C and 7 MPa
	Axial and bending loads	$F_x = 100 \text{ kN}$, primary stress = 50 MPa, secondary stress = 0
	Weld residual stresses	Stainless steel weld ground out, re-deposited last pass, heated to 550 F, no load
Past Transients	Earthquake, vibrations, other	None
Future Transients	Earthquake	None
	Vibrations	None
	Other transients	20 cycles/year, 4 second rise time, 0.025 probability/year, $F_x = 0$, primary stress = 172.4 MPa, secondary stress = 0
Initiation	Initial defects	None
	User options/Crack model	Single crack analysis, default crack initiation time model
Damage	Crack morphology	Default
	Water chemistry and sulfur content	0.01 $\mu\text{S/cm}$, 0 ppm, 0.05
	SCC and fatigue crack growth	Default SCC and fatigue cracking model
Inspection	Crack length detection	5,000 mm
	POD curve	BWR28
	Past inspections	None
	Future inspections	Every 10 years
Simulation	Method	Monte Carlo (100,000 simulations)
	Seeding	Fixed 1234 random seed number

Table 3.10 Input parameters for PWR base case problem

GUI Screen Tab	Input Parameter	Value
Plant	Reactor type and piping system	PWR hot leg
	Years in operation and years of end of license and extended life	0, 40, and 60 years
	Outside diameter and wall thickness	914.4 mm and 71.1 mm
	Leak rate detection	Mean 1,890 lpm w/zero Std. Dev.
	Weld repair	Replace w/non-susceptible mat ¹
	Material1, Weld material, Material2	Type 304, A182, A106B (Using Tensile Properties of Type 305)
	Material at crack location	Alloy 182
Material Properties	Material input property parameters	User input, no correlation
	Elastic modulus	180,000 MPa
	Base metal properties	Yield = 187.8 MPa, Ultimate = 493 MPa, n = 4.2, F = 599
	Weld metal properties	Yield = 245 MPa, J _i = 570.7 kJ/m ² , m = 0.6, C = 292.3
Static Loads	Global bending input type	Stress
	Secondary stress ratio	0
	Pipe temperature and pressure	310 C and 15.5 MPa
	Axial and bending loads	F _x = 100 kN, primary stress = 117 MPa, secondary stress = 0
	Weld residual stresses	Hot leg Alloy 182 weld at 615 F, using max stress in weld/butter
Past Transients	Earthquake, vibrations, other	None
Future Transients	Earthquake, vibrations, other	None
Initiation	Initial defects	None
	User options/Crack model	Single crack analysis, default crack initiation time model
Damage	Crack morphology	Default
	Water chemistry and sulfur content	0.01 μS/cm, 0 ppm, 0.05
Inspection	SCC and fatigue crack growth	Default SCC cracking model; fatigue disabled
	Crack length detection	5,000 mm
	POD curve	HotLegPOD
	Past inspections	None
	Future inspections	Every 10 years
Simulation	Method	Monte Carlo (100,000 simulations)
	Seeding	None

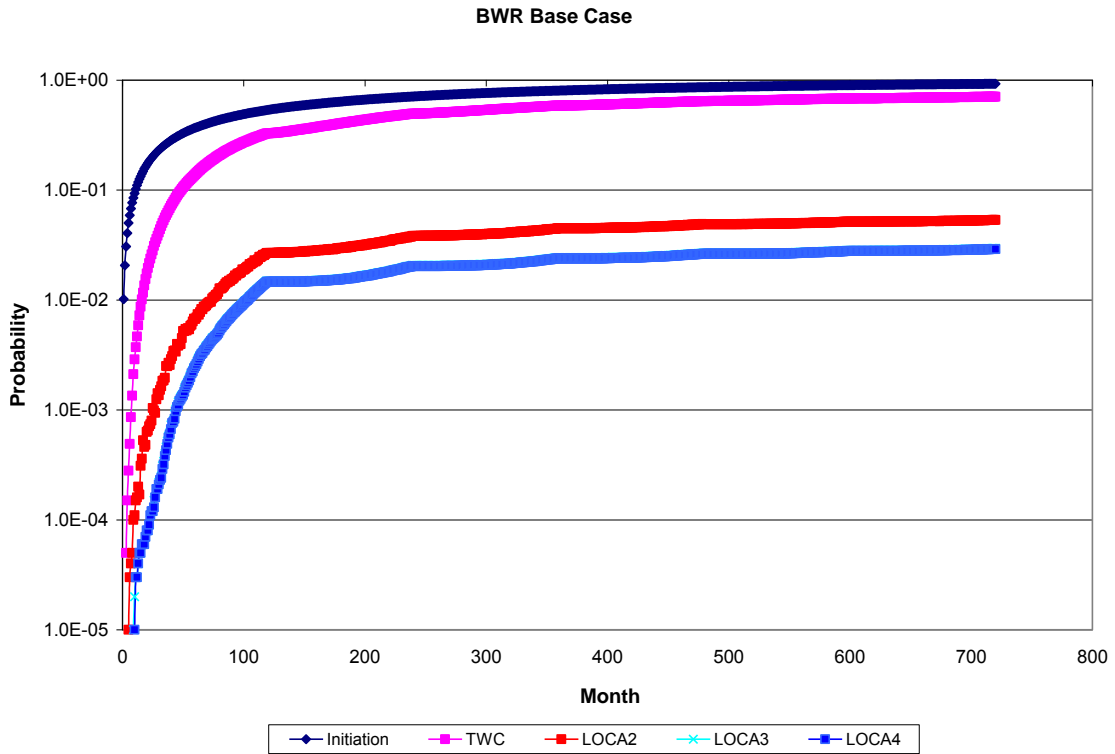


Figure 3.18 BWR base case results

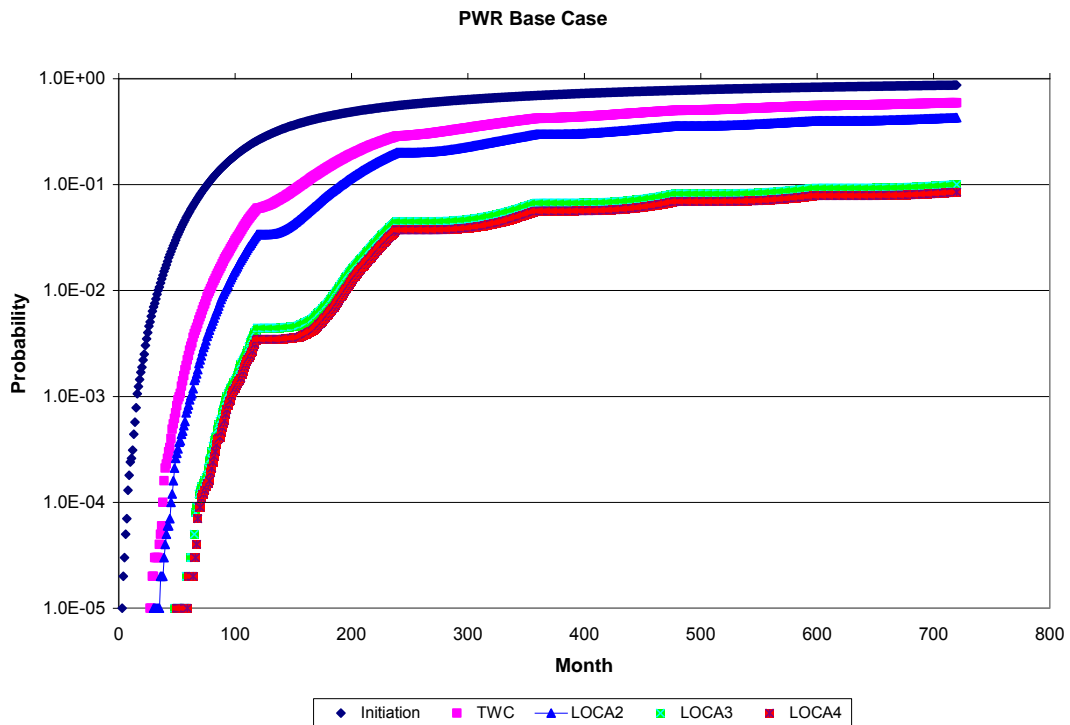


Figure 3.19 PWR base case results

3.2.1.1 BWR Results - Figure 3.20 shows the effect of static bending stress on the BWR LOCA probabilities. Figure 3.20 shows the effect of lowering the static bending stress from 50 MPa (7 ksi) to 20 MPa (3 ksi). The change had little or no effect of the probability of a through-wall crack occurring. Conversely, the decrease in the static bending stress caused almost a two order of magnitude decrease in the probability of a Category 2 LOCA and almost a three order of magnitude decrease in the probability of a Category 3 LOCA.

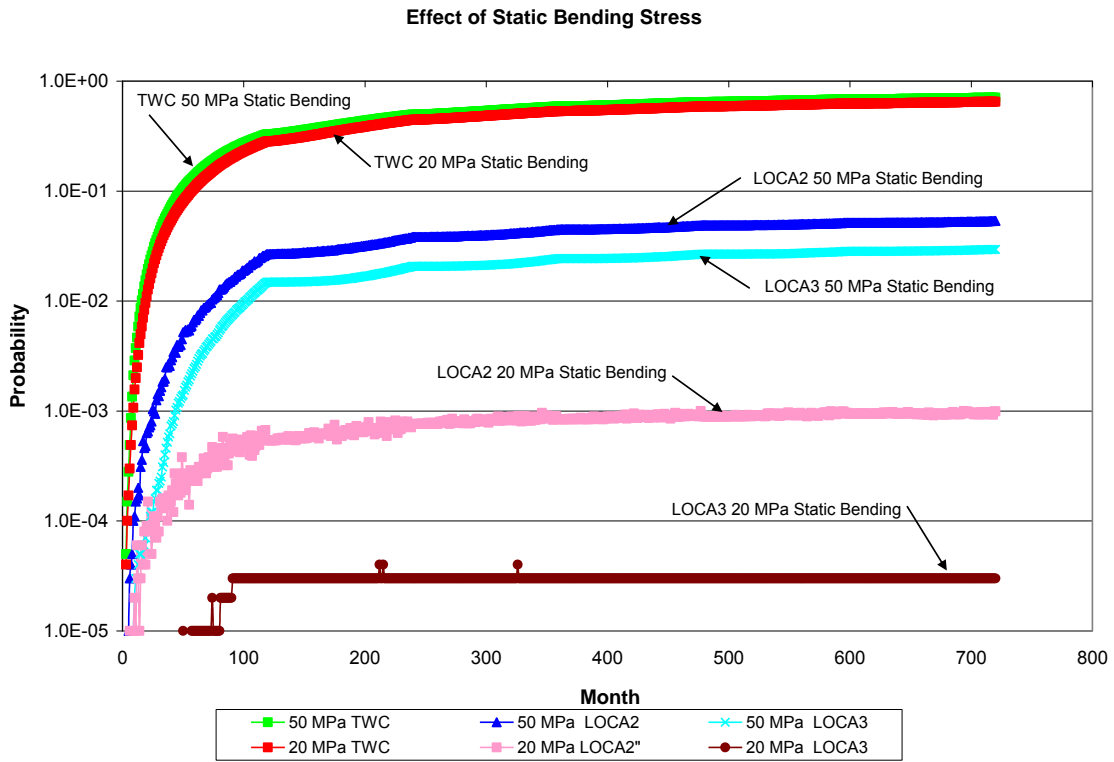


Figure 3.20 Effect of static bending stress on BWR LOCA probabilities

Figure 3.21 shows the effect of weld residual stress on the BWR LOCA probabilities. The user defined weld residual stress input with a constant distribution was used in both cases. In one case the inside surface stress was 70 MPa (10 ksi) while in the other the inside surface stress was 210 MPa (30 ksi). In both cases the X_c value (through-wall location where stress first changes sign) was set to a value of 0.3. The higher ID stress caused a slight increase in the through-wall crack probabilities, and a slight decrease of the Category 3 LOCA probabilities. The Category 2 LOCA probabilities were basically unchanged with this increase in the ID weld residual stress.

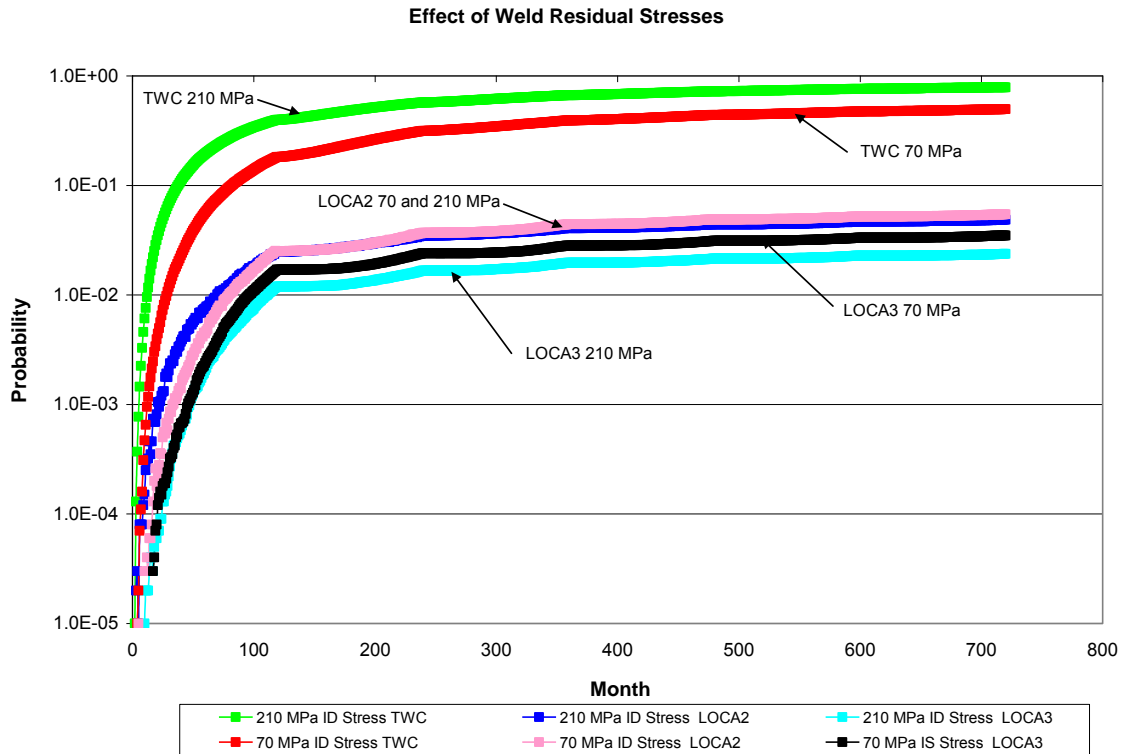


Figure 3.21 Effect of weld residual stress on BWR LOCA probabilities

Figure 3.22 shows the effect of a second transient on the BWR LOCA probabilities. As can be seen the second transient had little effect on any of the probabilities. The Category 2 and 3 LOCA probabilities increased very slightly while the through-wall crack probabilities were unaffected. Figure 3.23 shows the effect of excluding the transient from the base case scenario. As was the case for the previous figure, the inclusion, or exclusion, of this transient had little effect on any of the LOCA probabilities.

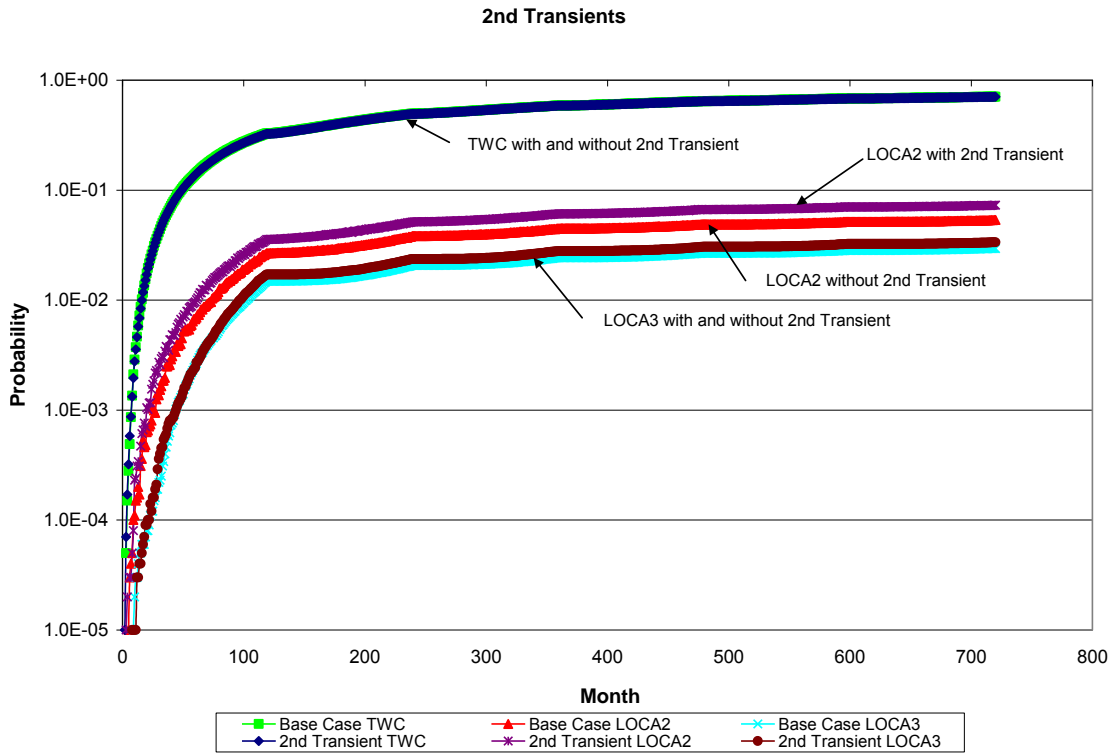


Figure 3.22 Effect of 2nd transient on BWR LOCA probabilities

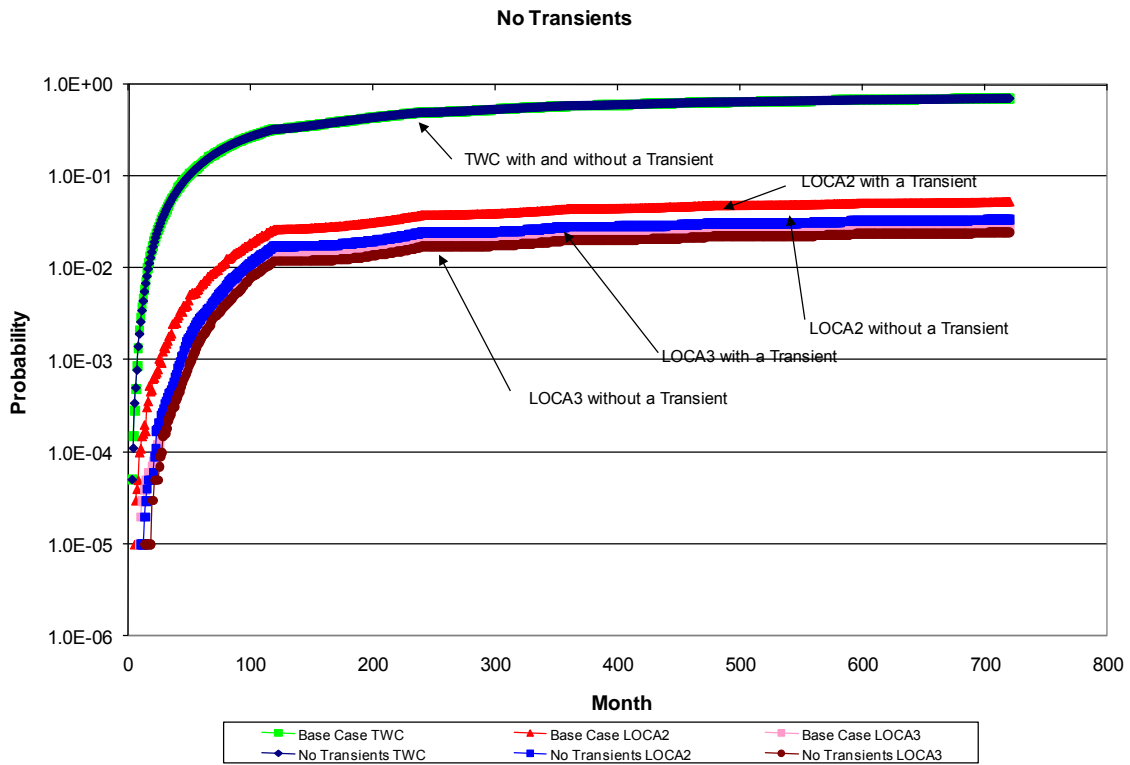


Figure 3.23 Effect of a transient on the BWR LOCA probabilities

Figure 3.24 shows the effect of the inspection interval on the BWR LOCA probabilities. As can be seen in this figure increasing the inspection interval from 10 to 20 years (i.e., fewer inspections) resulted in about a half order of magnitude increase in LOCA2 and LOCA3 probabilities. Conversely, increasing the inspection interval had little effect on the through-wall crack probabilities.

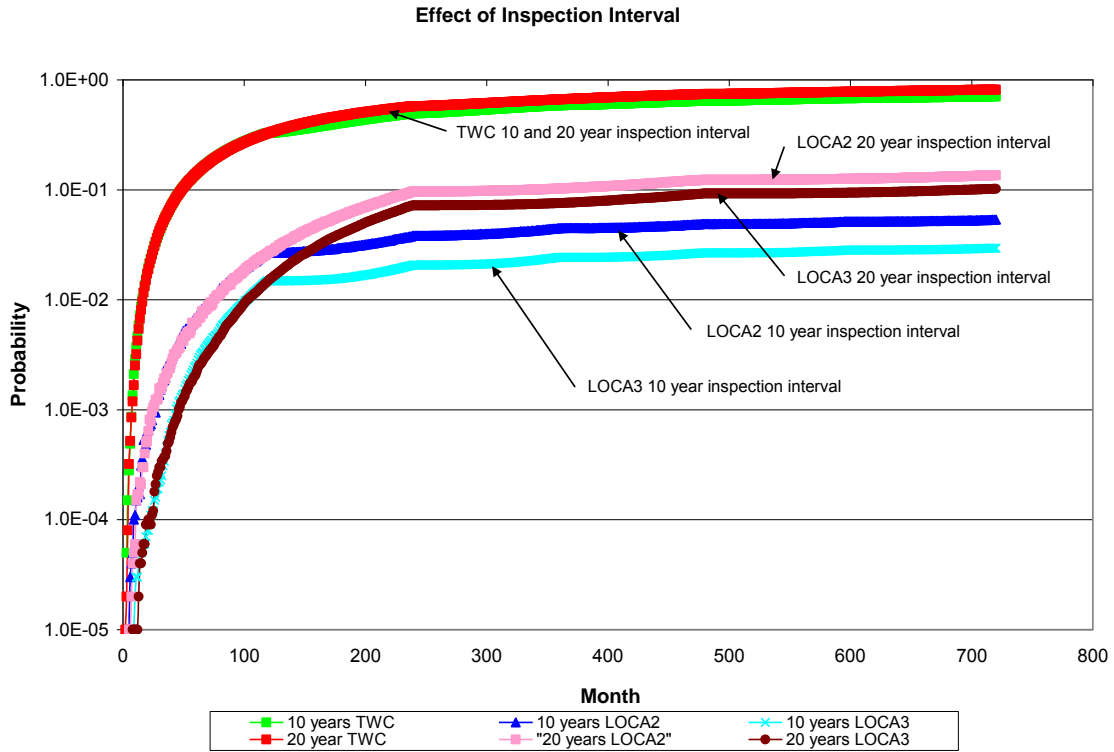


Figure 3.24 Effect of inspection interval on BWR LOCA probabilities

Figure 3.25 shows the effect of water chemistry on the BWR LOCA probabilities. As can be seen in this figure changing the water chemistry from BWR normal water chemistry to BWR hydrogen water chemistry had a significant effect on the LOCA probabilities. There was approximately an order of magnitude decrease in the probability for the through-wall cracks and the Category 2 LOCAs and almost a two order of magnitude decrease for the Category 3 LOCAs for hydrogen water chemistry when compared with normal water chemistry.

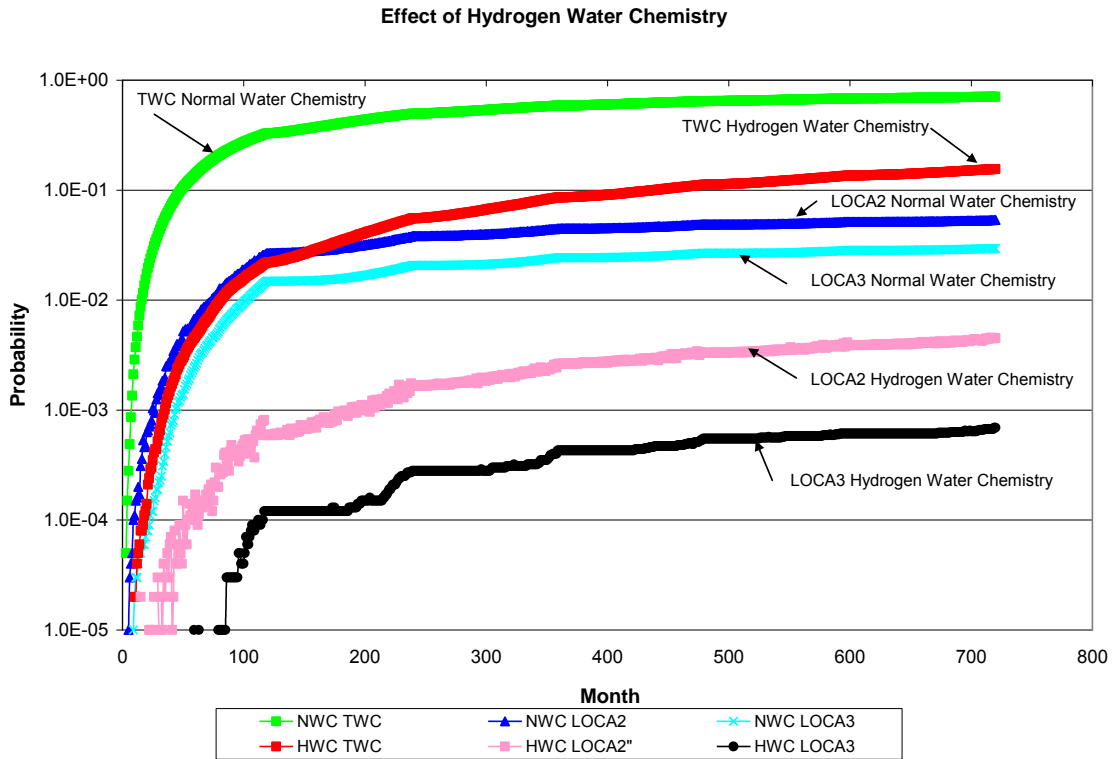


Figure 3.25 Effect of water chemistry on BWR LOCA probabilities

Figure 3.26 shows the effect of the leakage detection limit on the BWR LOCA probabilities. The results in this figure are all for the case of hydrogen water chemistry. Similarly, Figure 3.27 shows the effect of the leakage detection limit on the BWR LOCA probabilities, except all of these results are for the case of normal water chemistry. As would be expected leakage detection limit had no effect on the through-wall crack probability, regardless of water chemistry. Increasing the leakage detection limit from 1.89 lpm (0.5 gpm) to 378 lpm (100 gpm) resulted in about an order of magnitude decrease in the Category 2 LOCAs. Conversely, this same increase caused about an order of magnitude increase in the Category 3 LOCAs. These trends were evident for both the hydrogen and normal water chemistry cases.

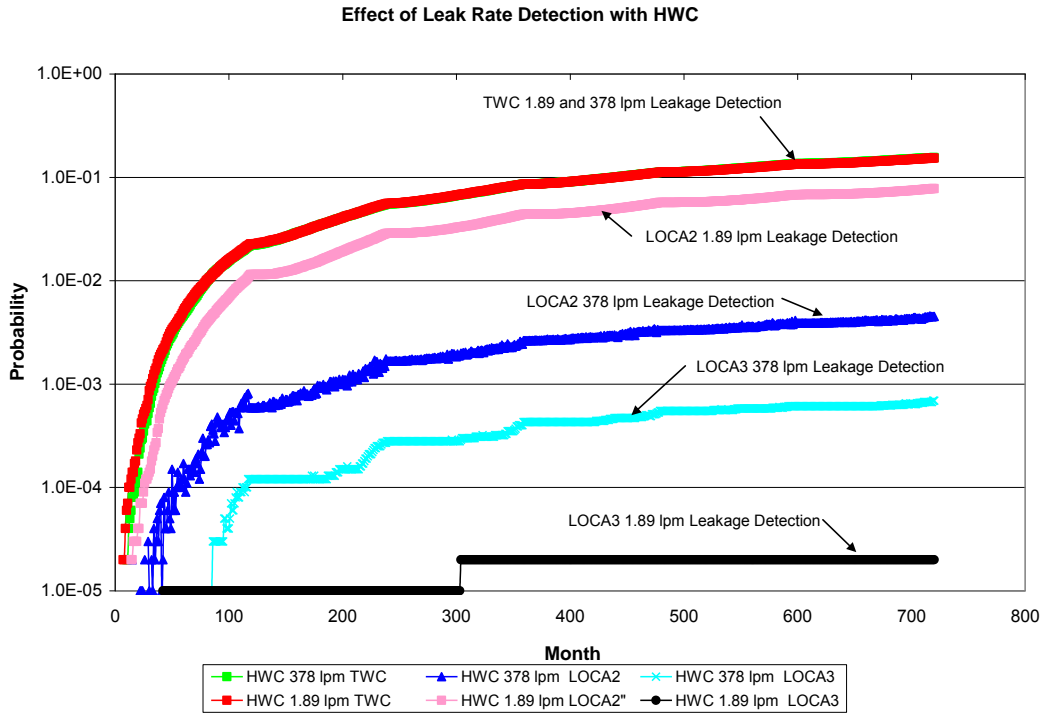


Figure 3.26 Effect of leak rate detection limit with hydrogen water chemistry on BWR LOCA probabilities

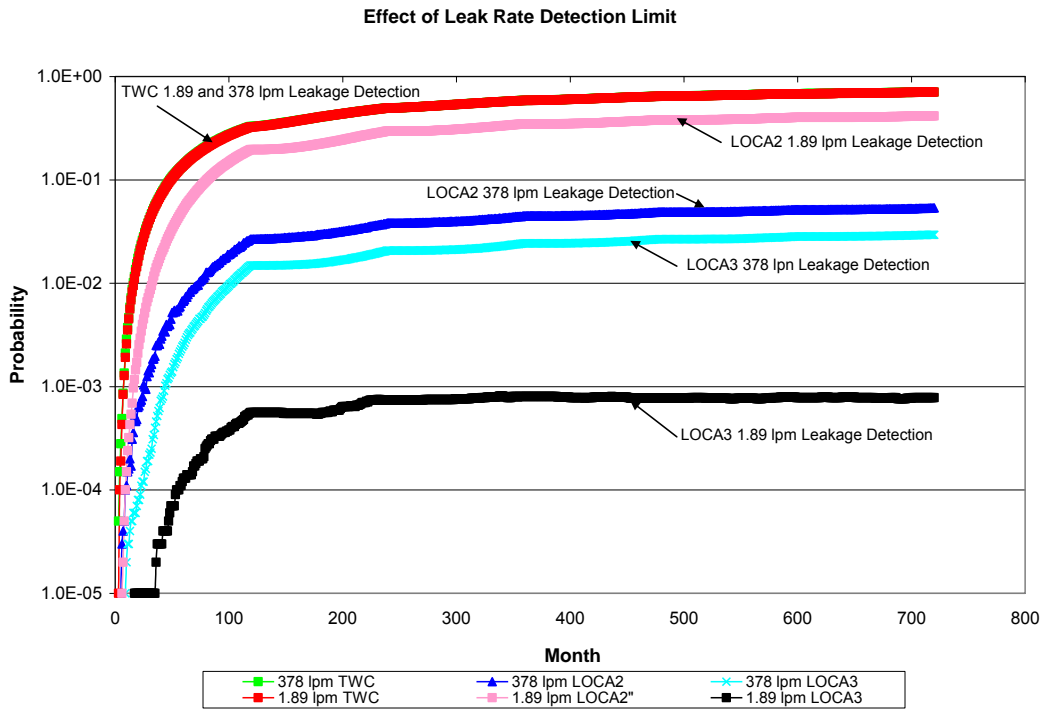


Figure 3.27 Effect of leak rate detection limit with normal water chemistry on BWR LOCA probabilities

Figure 3.28 shows the effect of crack initiation model on the BWR LOCA probabilities. For through-wall cracks, the effect was minimal. Even for the LOCA2 and LOCA3 probabilities, the effect was not that significant. The multiple crack initiation model (using the default time and crack size distributions) resulted in about a half order of magnitude increase in the LOCA2 and LOCA3 probabilities with respect to the single crack initiation model (again using the default time and crack size distributions).

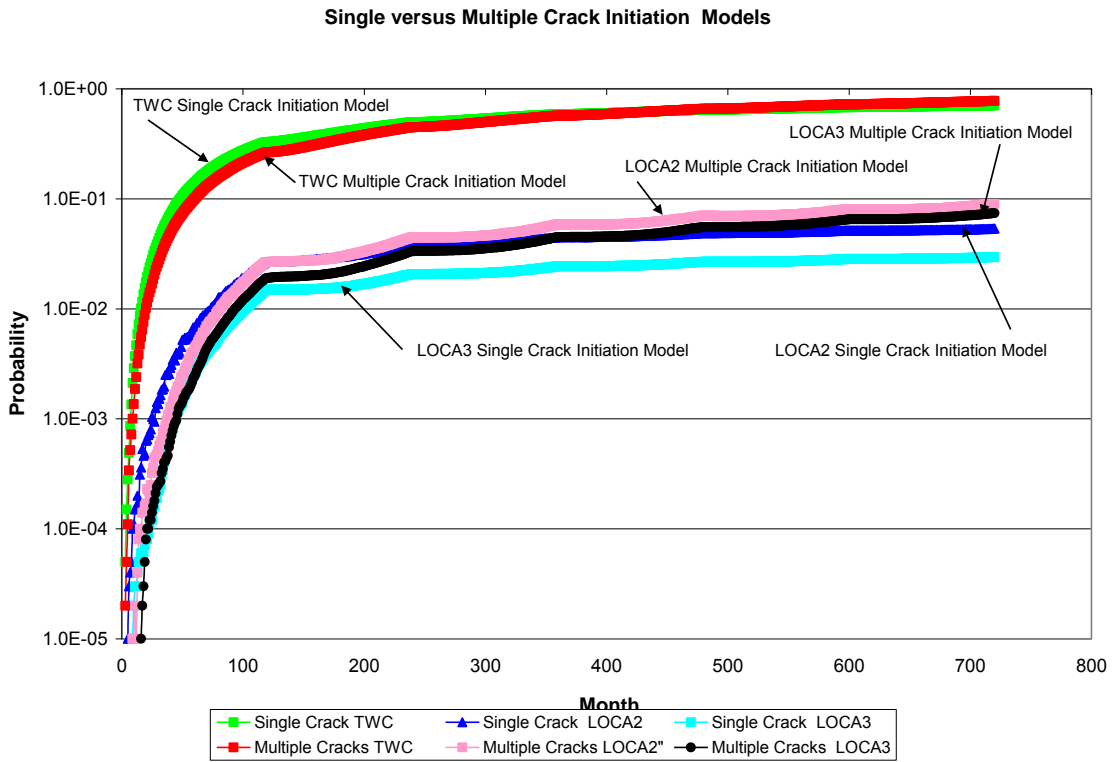


Figure 3.28 Effect of crack initiation model on BWR LOCA probabilities

Figure 3.29 shows the effect of arrival rate on the BWR LOCA probabilities. Two different arrival rates were considered, i.e., 0.01 cracks per year and 1 crack per year. The through-wall crack probabilities for the 1 crack per year arrival rate are about a half order of magnitude higher than the through-wall crack probabilities for the 0.01 cracks per year arrival rate. Similarly the LOCA2 and LOCA3 probabilities are slightly higher for the 1 crack per year arrival rate than they are for the 0.01 cracks per year arrival rate.

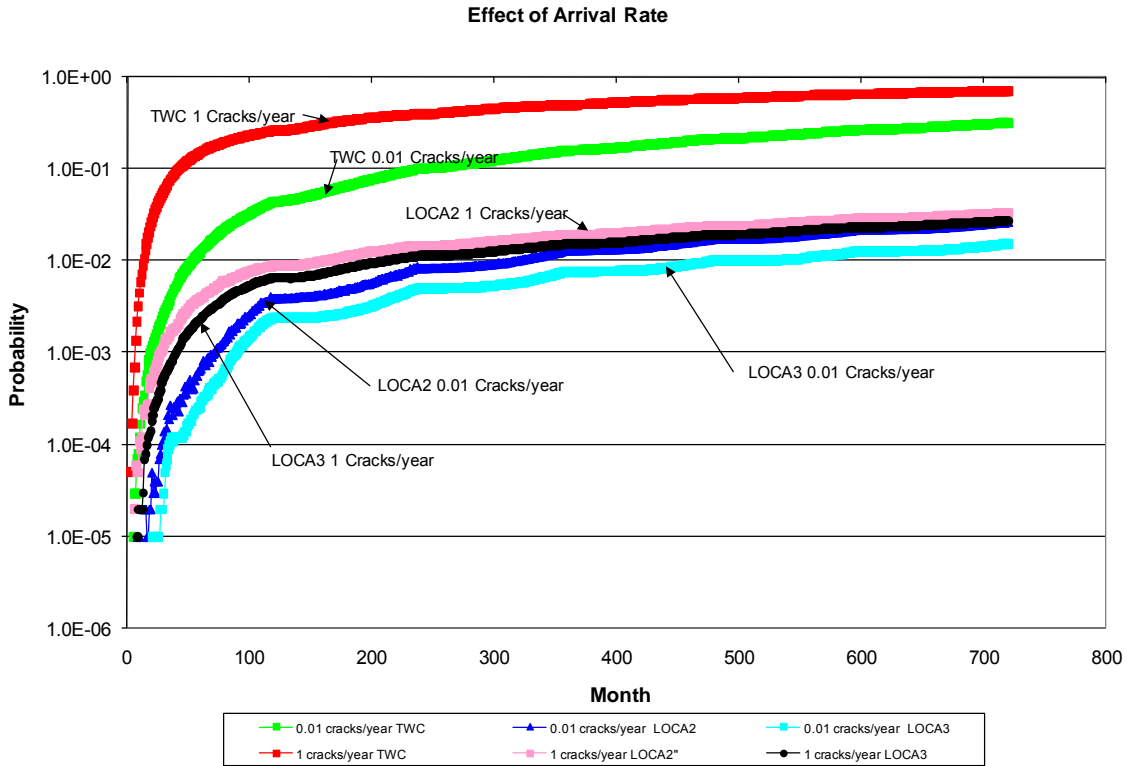


Figure 3.29 Effect of arrival rate on BWR LOCA probabilities

3.2.1.2 PWR Results – Figure 3.30 shows the effect of temperature on the PWR LOCA probabilities. In PWRs primary water stress corrosion cracking of dissimilar metal welds is a temperature dependent phenomenon. As can be seen in Figure 3.30 lowering the operating temperature 22 C (40 F) from 310 C (590 F) to 288 C (550 F) resulted in a significant reduction in the LOCA probabilities. The through-wall crack probabilities decreased 2 to 3 orders of magnitude. At 30 years the decrease approached 3 orders of magnitude while at 60 years the decrease was closer to 2 orders of magnitude. A similar decrease was evident for the Category 4 LOCAs.

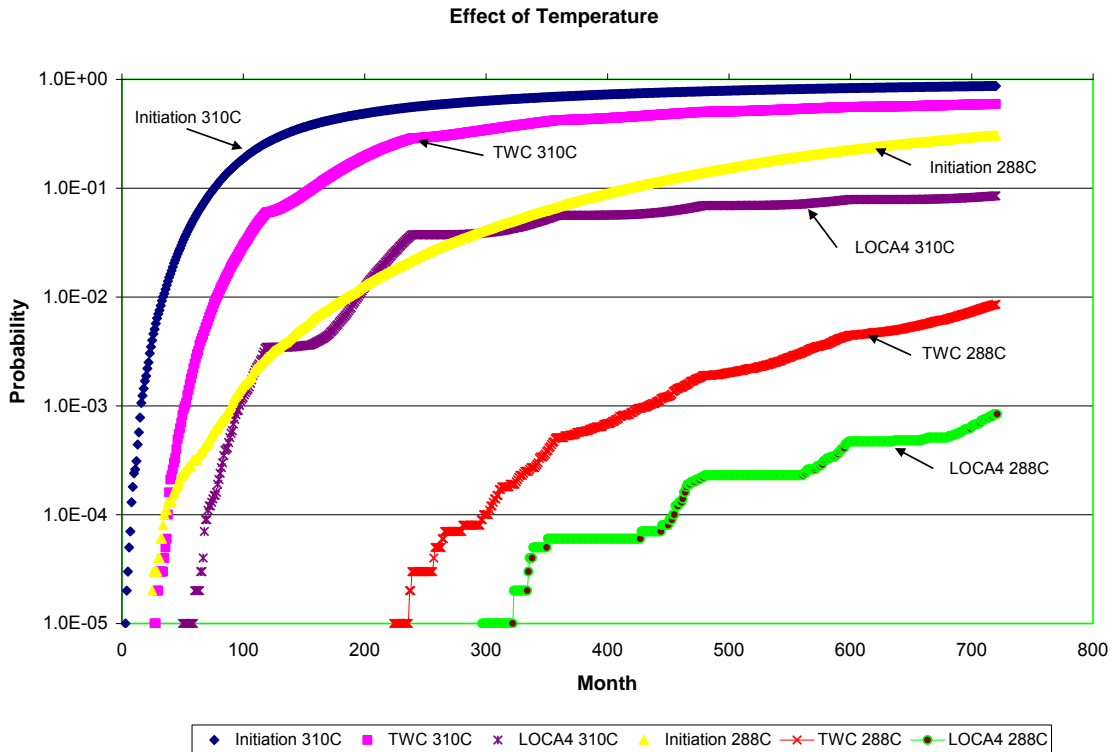


Figure 3.30 Effect of temperature on PWR LOCA probabilities

Figure 3.31 shows the effect of the static bending stress on the PWR LOCA probabilities. The 1X stress in Figure 3.31 was 117 MPa (17 ksi) while the 2X stress was 235 MPa (34 ksi). For each case the operating temperature was 288 C (550 F). As can be seen in this figure doubling the static bending stress caused a 1 to 1.5 order of magnitude increase in the resultant LOCA probabilities.

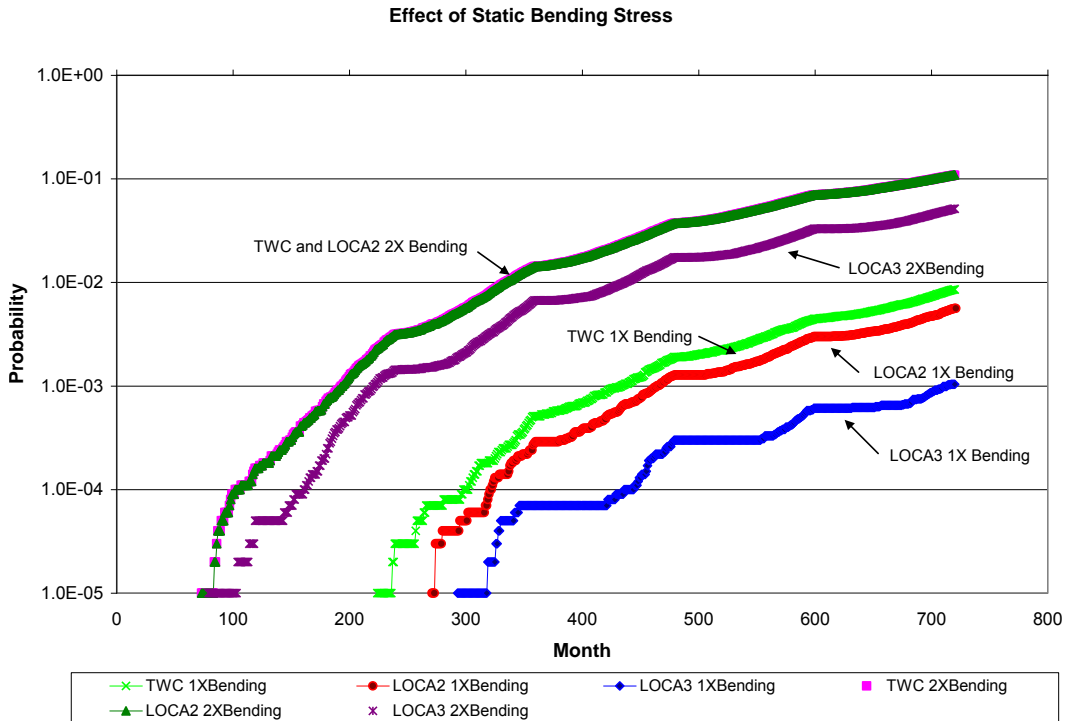


Figure 3.31 Effect of static bending stress on PWR LOCA probabilities

Figure 3.32 shows the effect of the weld residual stresses on the PWR LOCA probabilities. The inside surface residual stress for the high stress case was 200 MPa (29 ksi) while the inside surface residual stress for the low stress case was 35 MPa (5 ksi). For each case the X_c term was 0.3. While reducing the weld residual stresses resulted in a reduction in the LOCA probabilities, the reduction was typically less than an order of magnitude, with the most significant reductions being for the through-wall crack probabilities.

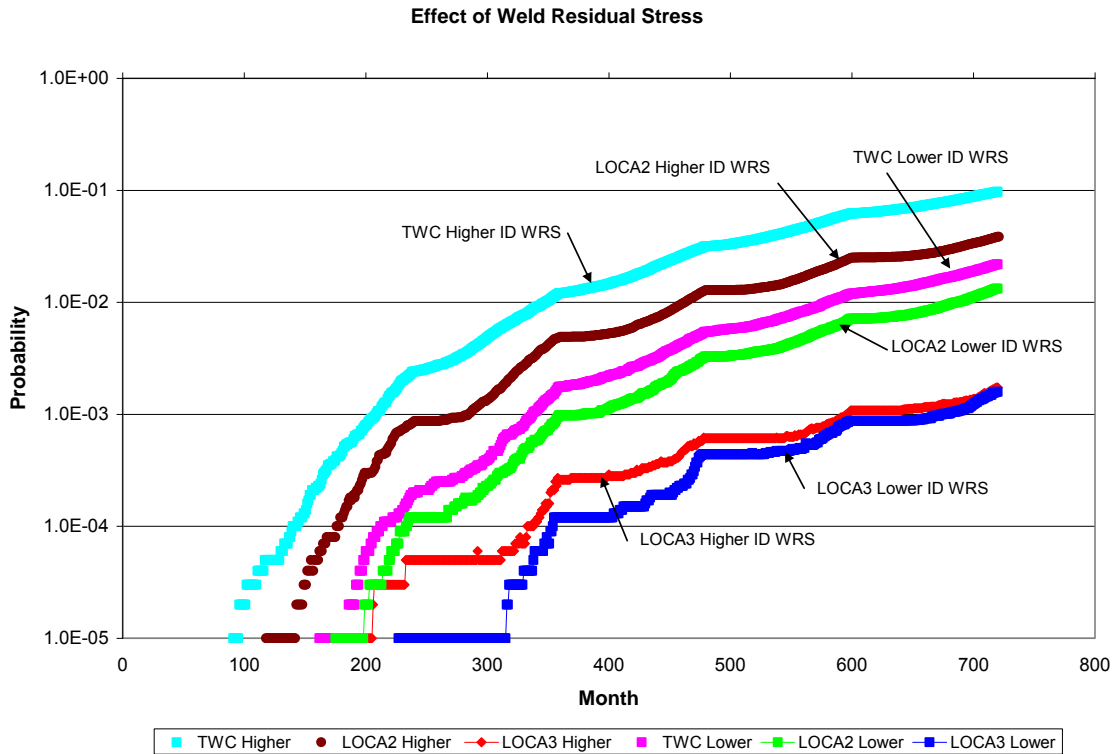


Figure 3.32 Effect of weld residual stress on PWR LOCA probabilities

Figure 3.33 shows the effect of an earthquake on the PWR LOCA probabilities. The earthquake was a 15 second, 4 hertz earthquake (60 total cycles) with a probability of occurrence per year of 0.025 with a primary global bending stress of 105 MPa (15 ksi). The addition of an earthquake resulted in about a one order of magnitude increase in the through-wall crack and Category 2 LOCA probabilities and about a half order of magnitude increase in the Category 3 LOCA probabilities.

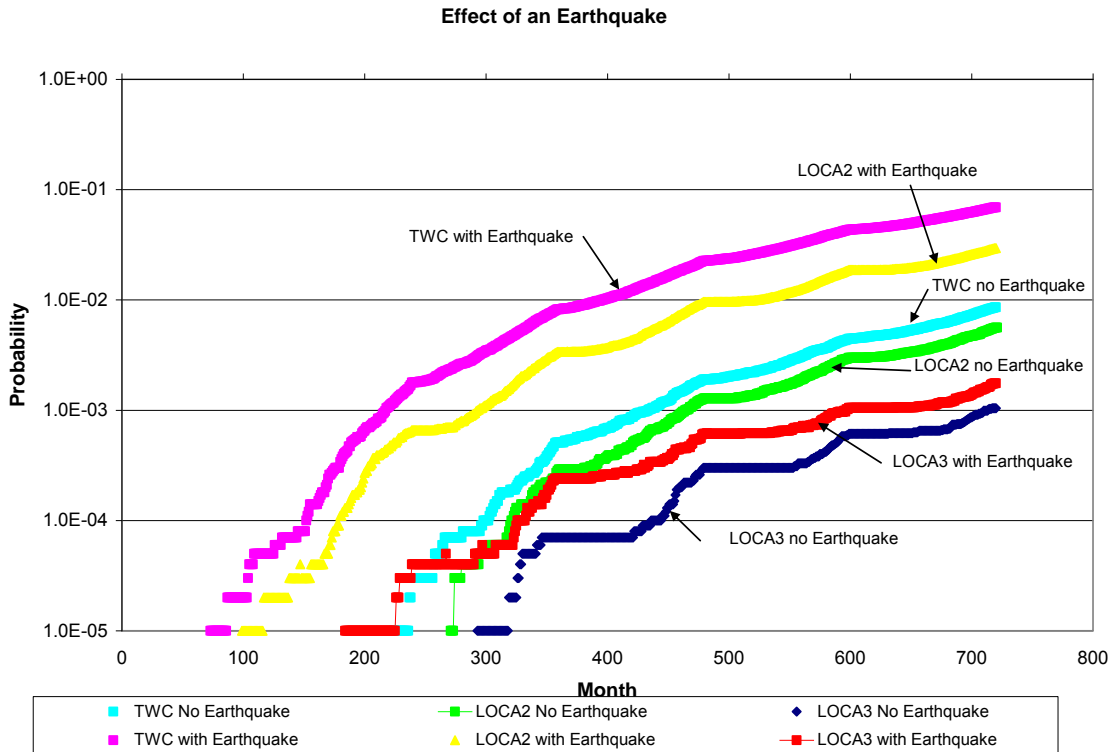


Figure 3.33 Effect of an earthquake on PWR LOCA probabilities

Figure 3.34 shows the effect of the number of cycles in the earthquake on the PWR LOCA probabilities. The nominal case included a total of 60 cycles in each earthquake (15 second duration at 4 hertz) while the additional earthquake cycle case included a total of 240 cycles in each earthquake (60 second duration at 4 hertz). The additional cycles had almost no effect of the through-wall crack and Category 2 LOCAs. In both cases the probability of occurrence per year for the earthquake was 0.025 and the primary bending stress was 105 MPa (15 ksi) and the secondary bending stress was 35 MPa (5 ksi). While the effect on the Category 3 LOCAs was more significant, the effect was still not all that significant. The additional cycles only resulted in about a half order of magnitude increase in the LOCA3 probabilities.

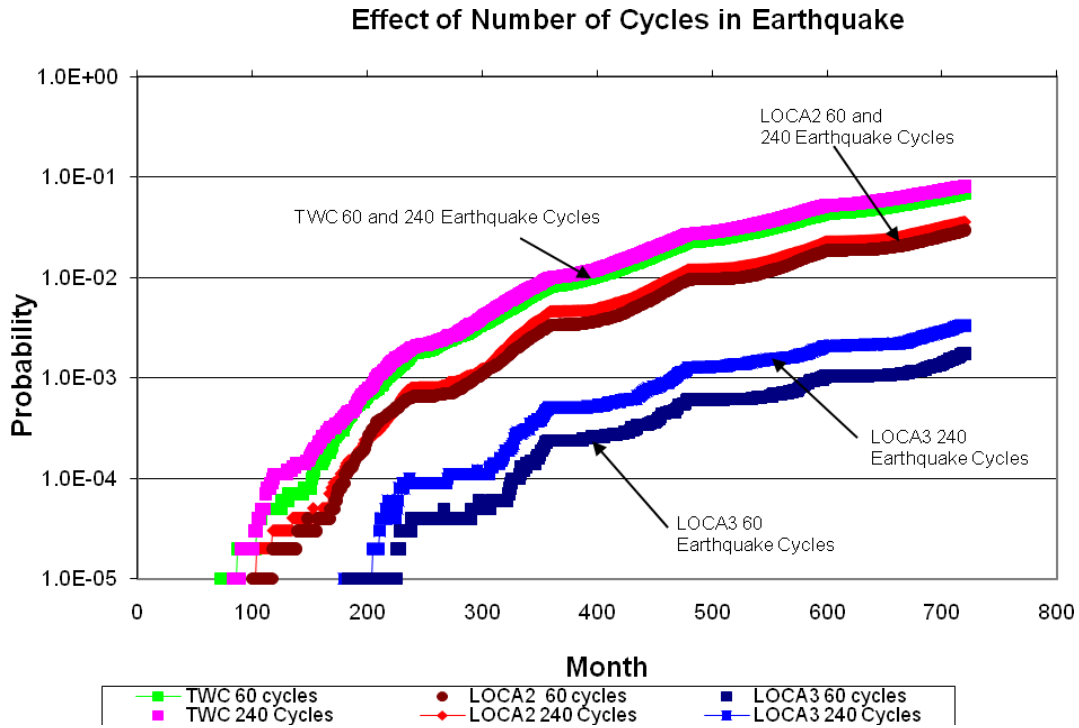


Figure 3.34 Effect of the number of cycles in an earthquake on the PWR LOCA probabilities

Figure 3.35 shows the effect of the magnitude of the earthquake on the PWR LOCA probabilities. The primary and secondary global bending stresses for the nominal case was 105 MPa (15 ksi) and 35 MPa (5 ksi), respectively, while they were 300 MPa (43 ksi) and 100 MPa (14.3 ksi), respectively, for the higher load case. The higher earthquake loads resulted in a half to one order of magnitude increase in the resultant LOCA probabilities.

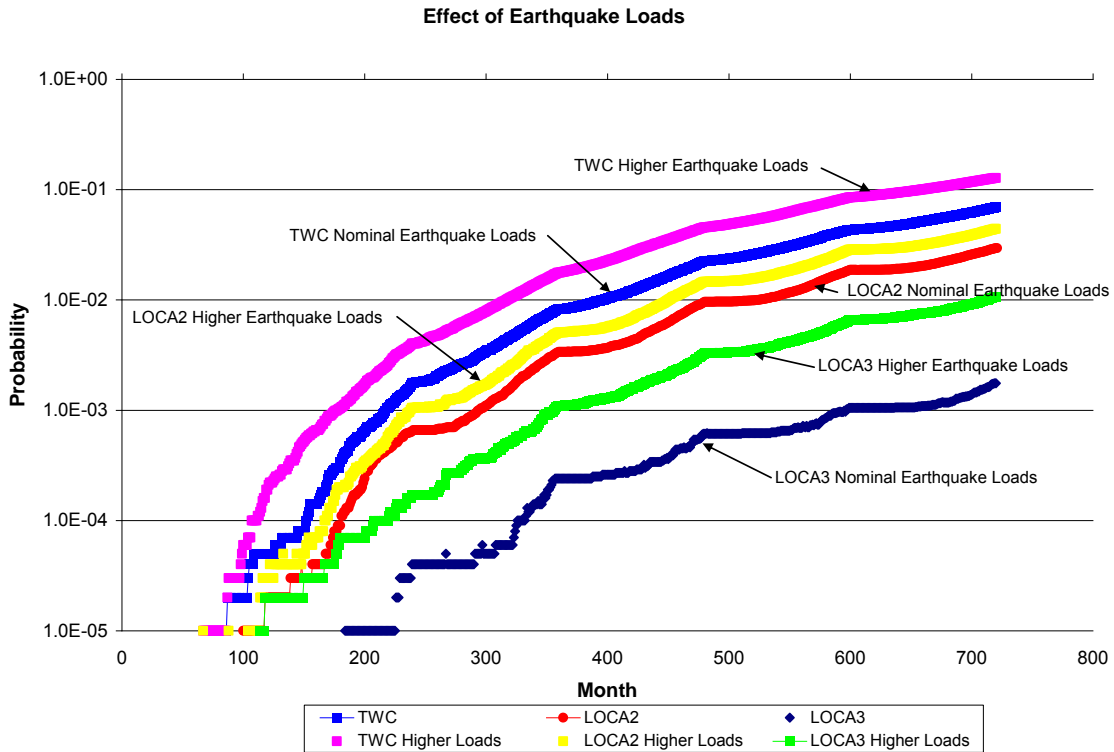


Figure 3.35 Effect of earthquake magnitude on the PWR LOCA probabilities

Figure 3.36 shows the effect of increasing the material strength properties on the PWR LOCA probabilities. The nominal yield and ultimate strengths for the base metal were 188 MPa (27.3 ksi) and 493 MPa (71.5 ksi), respectively. The higher strength yield and ultimate strengths for the base metal were 240 MPa (34.8 ksi) and 660 MPa (95.7 ksi), respectively. This almost 30 percent increase in strength had almost no effect on the resultant LOCA probabilities.

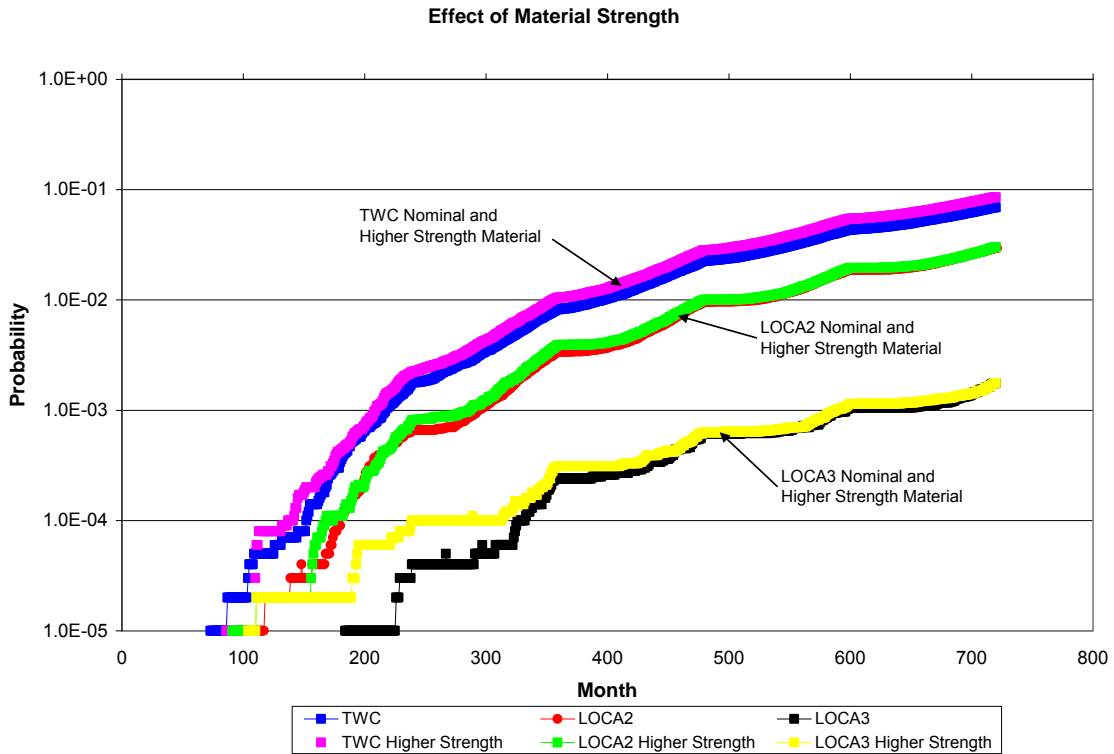


Figure 3.36 Effect of material strength on the PWR LOCA probabilities

Figure 3.37 shows the effect of material toughness on the PWR LOCA probabilities. The toughness for the higher toughness case was almost 20 times higher than the toughness for the nominal toughness case. Even with this level of increase in toughness the effect on the LOCA probabilities was almost non-existent.

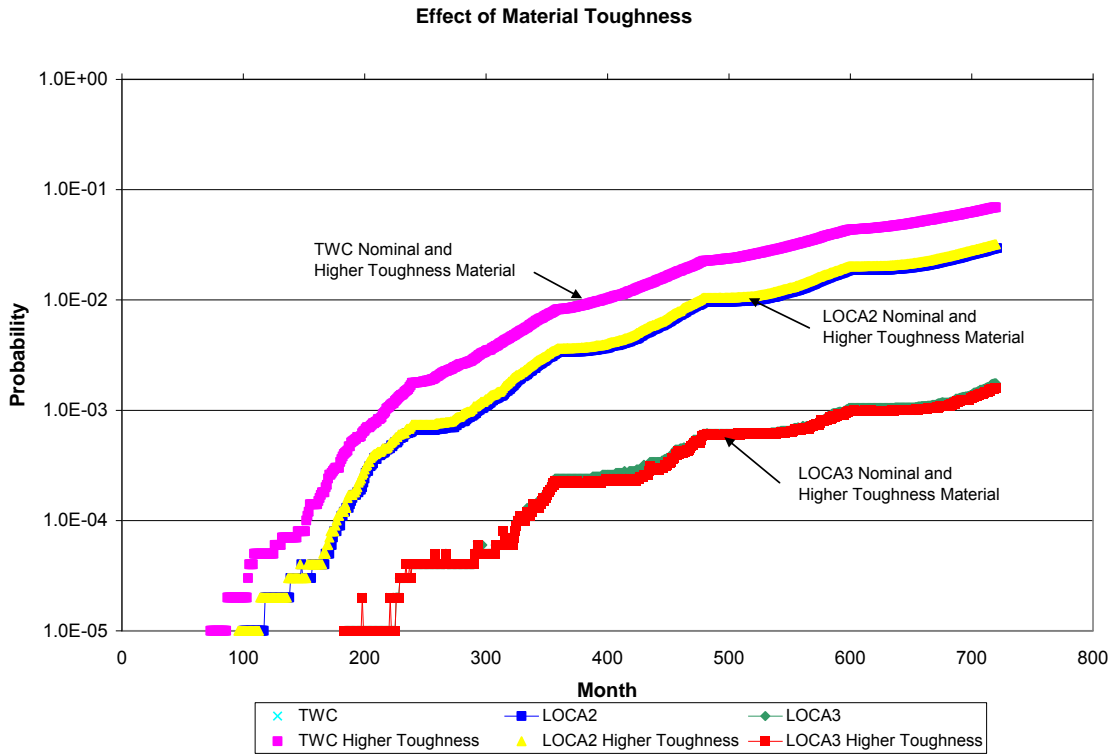


Figure 3.37 Effect of material toughness on PWR LOCA probabilities

Figure 3.38 shows the effect of inspection interval on the PWR LOCA probabilities. Increasing the inspection interval from 10 to 20 years (i.e., less inspections) resulted in approximately an order of magnitude increase in the PWR LOCA probabilities.

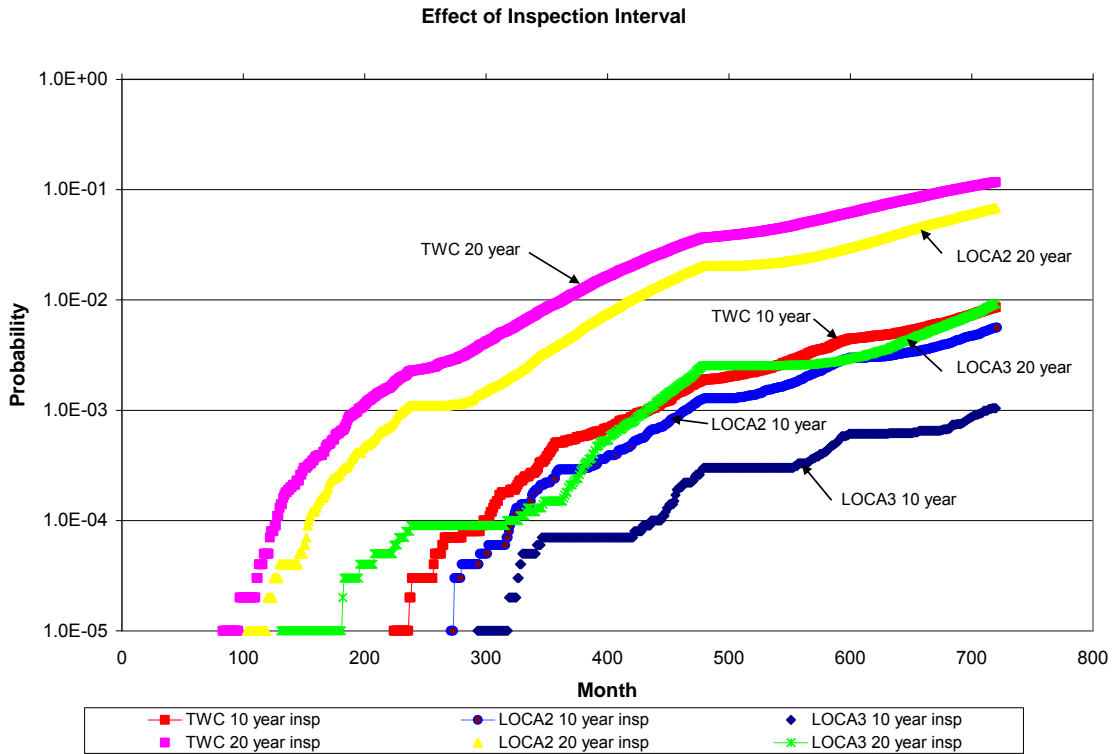


Figure 3.38 Effect of inspection interval on PWR LOCA probabilities

Figure 3.39 shows the effect of the probability of detection (POD) curve on the PWR LOCA probabilities. The differences between the “poor” and “better” POD curves are shown in Figure 3.40. As can be seen, the better POD curve resulted in slightly lower LOCA probabilities, although the effect of this change in inspection quality (i.e., POD) was minimal.

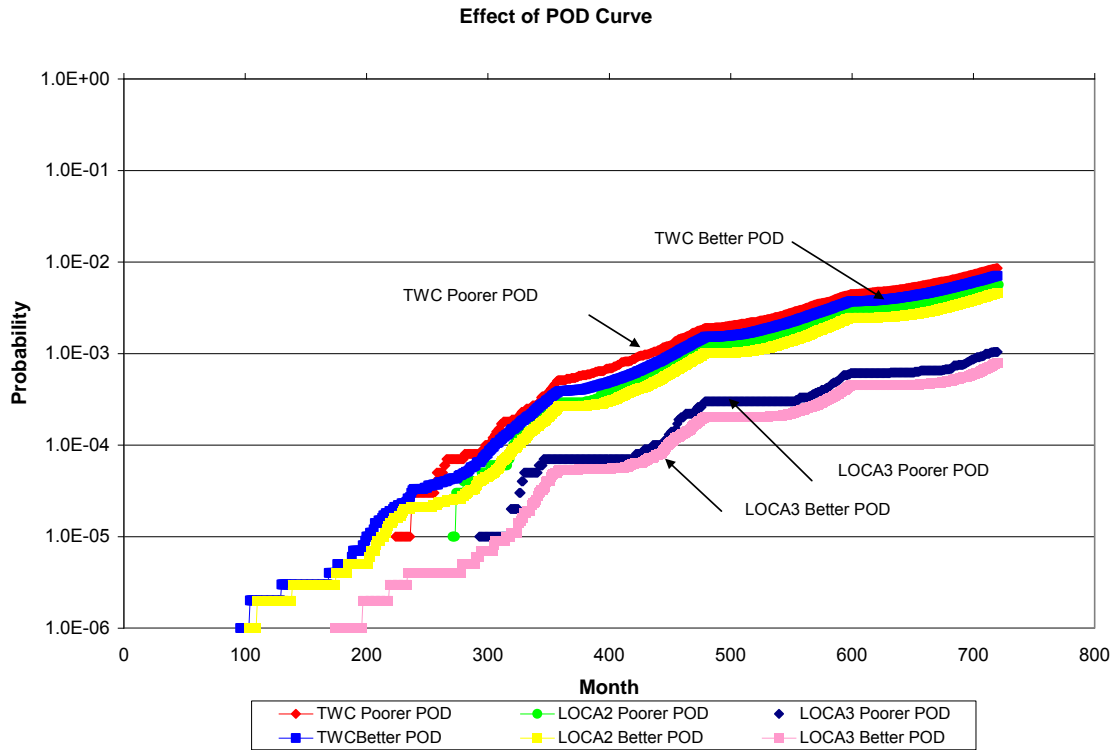


Figure 3.39 Effect of POD quality on PWR LOCA probabilities

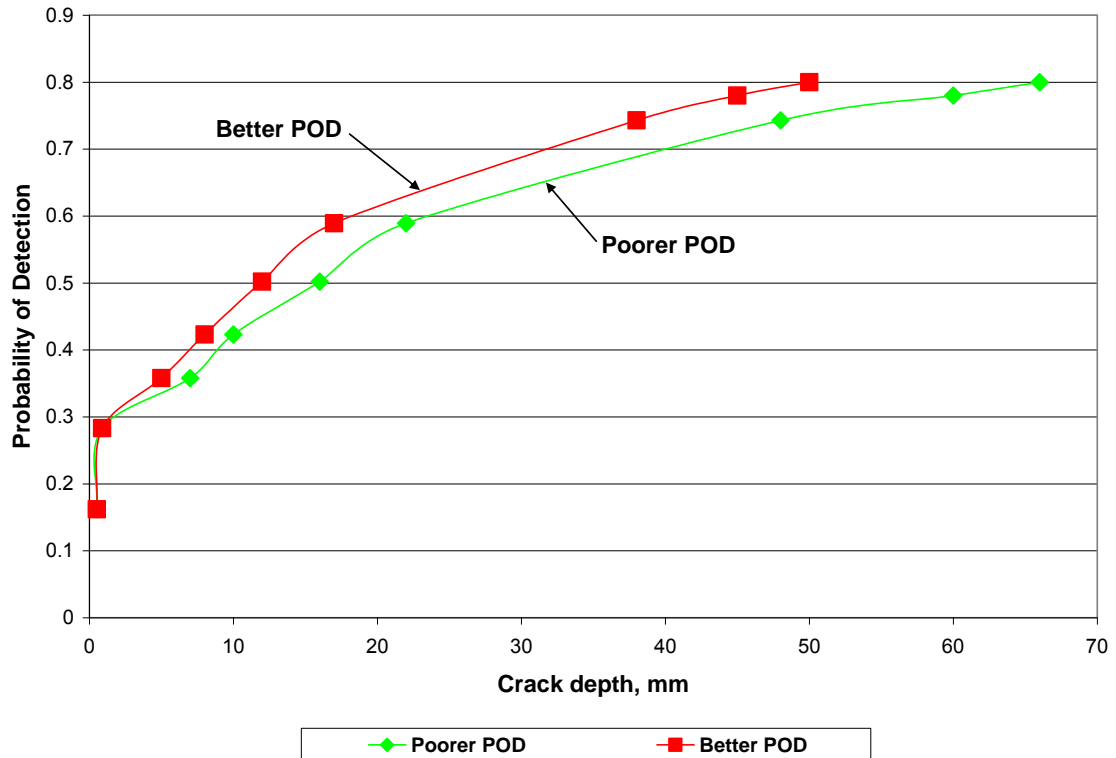


Figure 3.40 Comparisons between "poorer" and "better" POD curves

Figure 3.41 shows the effect of the plant's leakage detection limit on the PWR LOCA probabilities. Increasing the leakage detection limit from 1.89 lpm (0.5 gpm) to 1,890 lpm (500 gpm), a 1,000 fold increase, had absolutely no effect on the PWR LOCA probabilities.

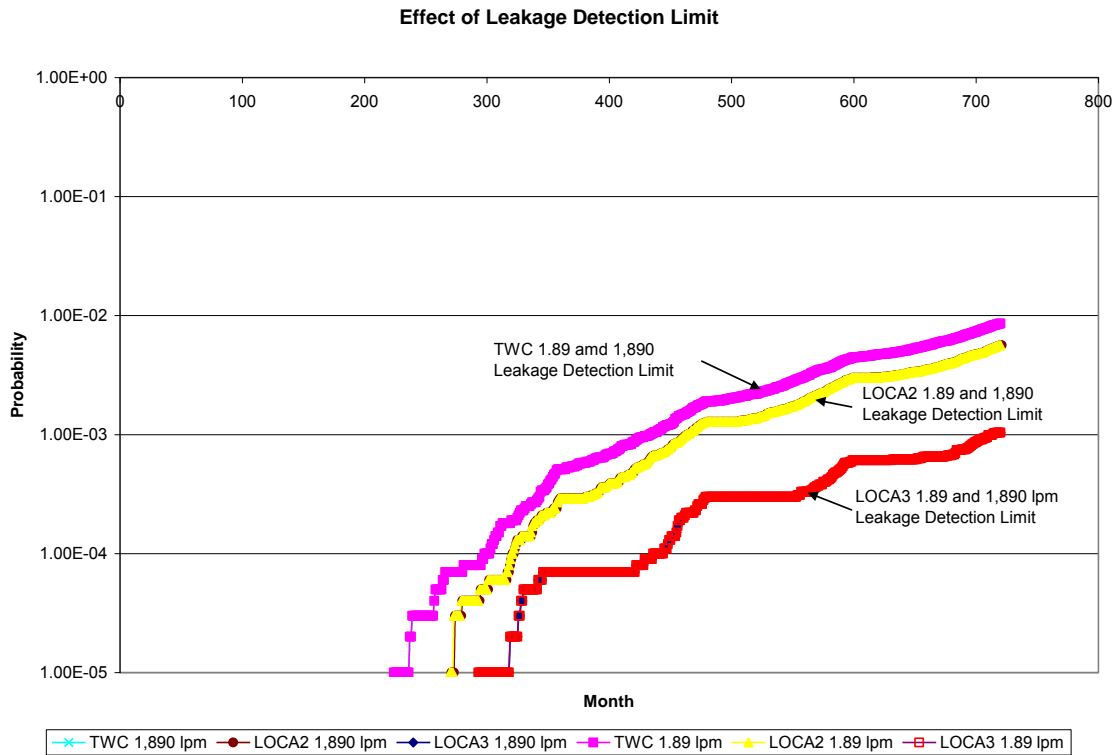


Figure 3.41 Effect of leakage detection limit on PWR LOCA probabilities

Figure 3.42 shows the effect of crack morphology on the PWR LOCA probabilities. Decreasing the crack face surface roughness by a factor of 10 (i.e., smoother crack morphology) had almost no effect on the through-wall crack and Category 2 LOCA probabilities. However, the reduction in surface roughness did lower the Category 3 LOCA probabilities by about a half order of magnitude.

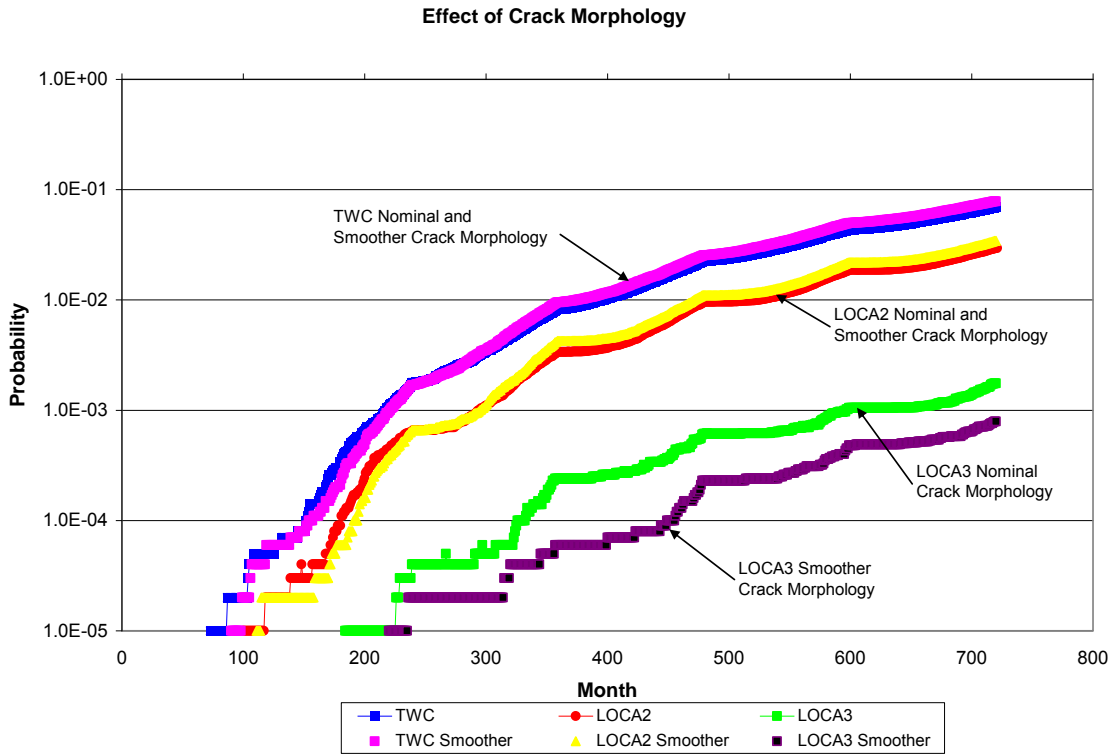


Figure 3.42 Effect of crack morphology on PWR LOCA probabilities

Figure 3.43 shows the effect of the differences between the single crack and multiple crack initiation models on the PWR LOCA probabilities. In both cases the default crack initiation time and crack size models were invoked. The multiple crack initiation model resulted in slightly lower LOCA probabilities (approximately half order of magnitude) than did the single crack initiation model.

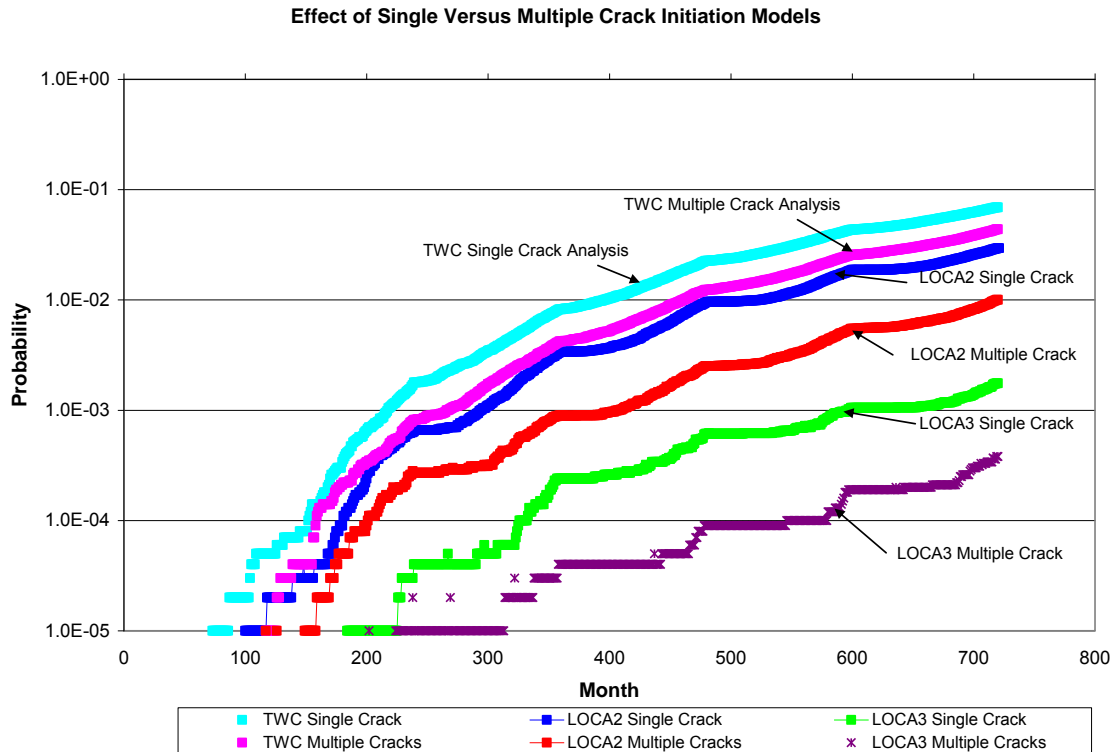


Figure 3.43 Effect of single versus multiple default crack initiation models on PWR LOCA probabilities

Figure 3.44 shows the effect of the arrival rate on the PWR LOCA probabilities. Two different arrival rates were considered as part of these analyses, 0.01 cracks/year and 0.05 cracks/year. Increasing the arrival rate from 0.01 cracks/year to 0.05 cracks/year caused about an order of magnitude decrease in the through-wall crack and Category 2 LOCAs. Similarly this increase in arrival rate also caused a reduction in the Category 3 LOCAs, although a much smaller reduction.

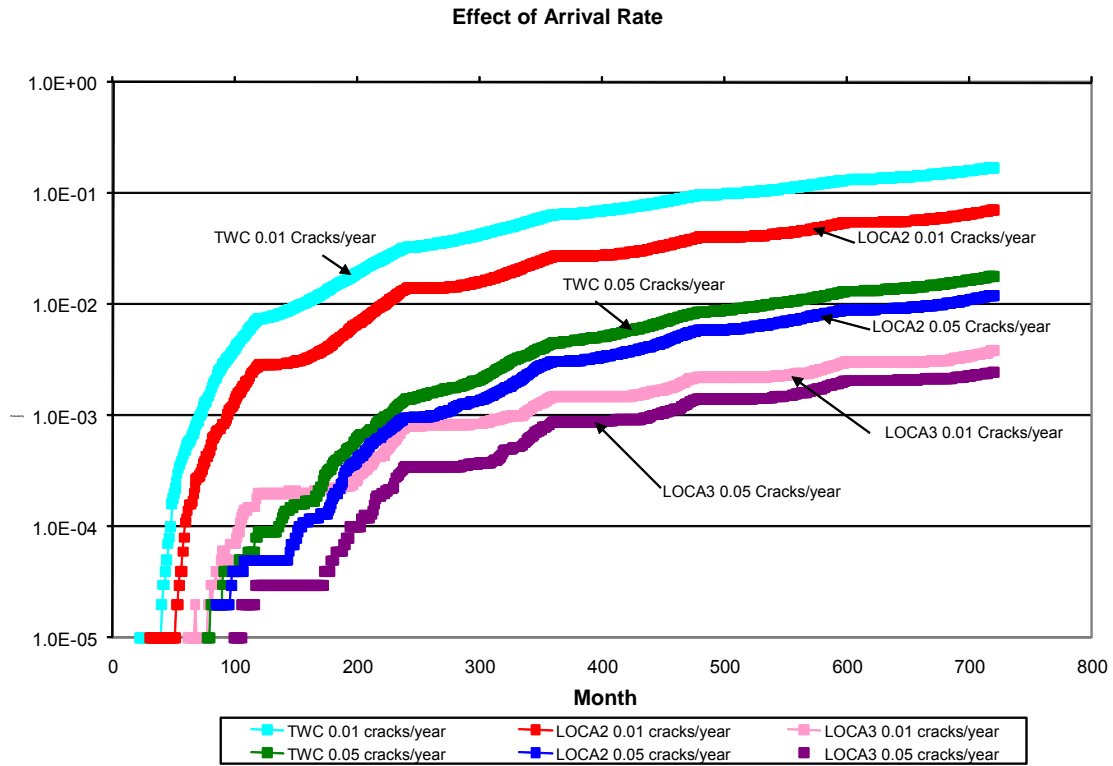


Figure 3.44 Effect of arrival rate on PWR LOCA probabilities

Figure 3.45 shows the effect of the replacement material on the PWR LOCA probabilities. When a crack is detected through in-service inspection, PRO-LOCA offers the user a number of options. The two options considered in this figure are to replace the cracked section with a similar material or to replace the cracked section with a non-susceptible material, i.e., non-susceptible to stress corrosion cracking. As seen in this figure replacing the cracked section with a non-susceptible material results in about an order of magnitude increase in the through-wall crack and Category 2 LOCAs. Conversely, replacing the cracked section with a non-susceptible material results in a slight reduction in the Category 3 LOCAs.

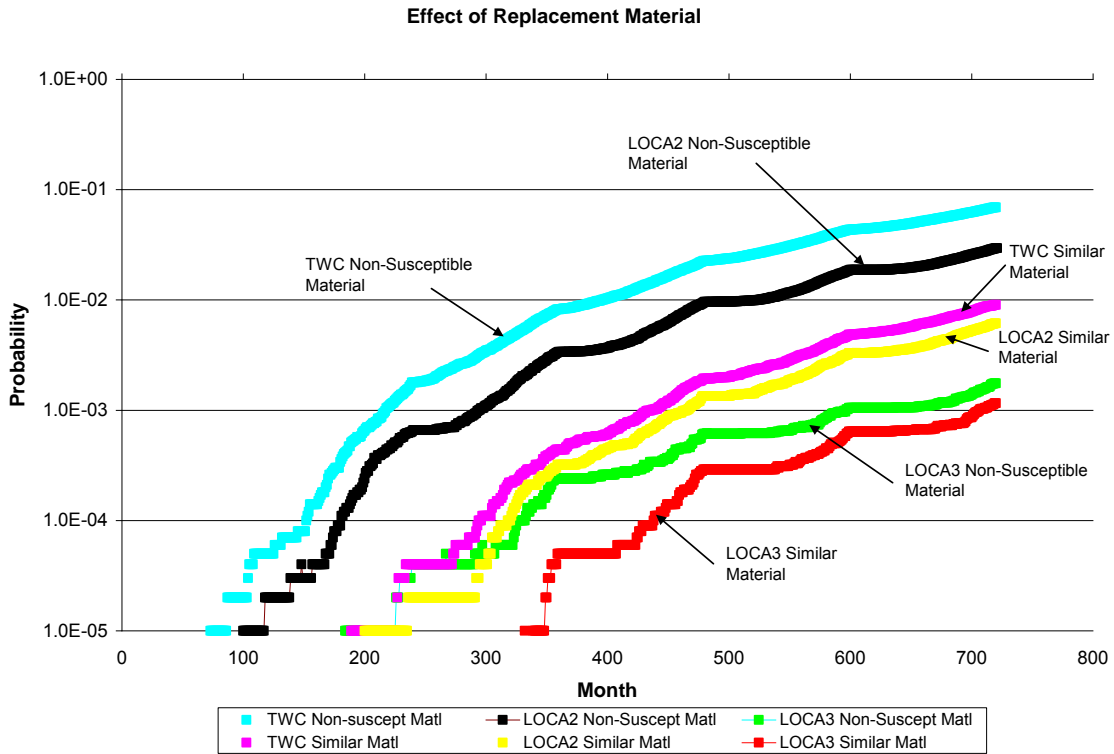


Figure 3.45 Effect of replacement material on PWR LOCA probabilities

The final sensitivity analyses conducted compared the LOCA probabilities for when the loads are based on moment inputs and when they are based on stress inputs, see Figure 3.46. The input decks for the two cases were identical. The only difference was that in one case the load inputs were based on stresses while in the other the load inputs were based on equivalent moments. As can be seen the results for the two cases are identical for all break sizes, i.e., through-wall cracks, LOCA2, LOCA3, and LOCA4.

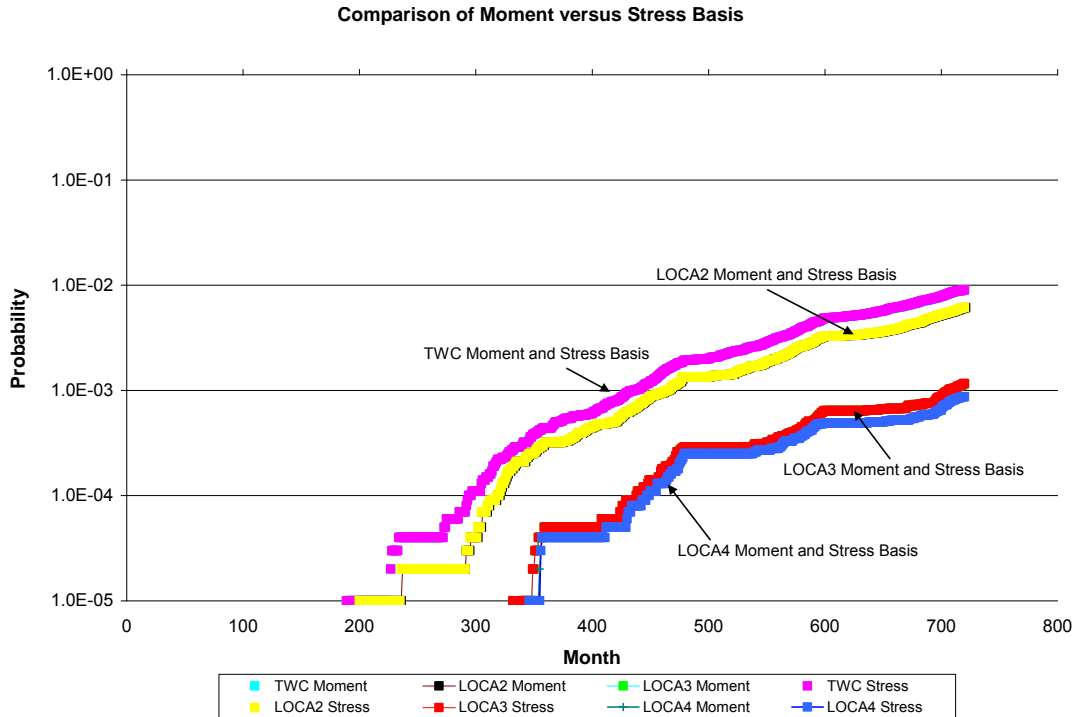


Figure 3.46 Comparison of LOCA probabilities for when loads based on moments versus when based on stress

3.3 Comparison of Results from Monte-Carlo Simulations and the Discrete Probability Method

The Discrete Probability Method (DPM) was added to PRO-LOCA to allow for the assessment of LOCA probabilities for very low probability events (on the order of 10^{-8} or lower) in a reasonable time frame. To achieve 10^{-8} probabilities using Monte Carlo may require on the order of 10^9 simulations. Depending on the problem, such simulations may require weeks if not months of computational time. Thus, the necessity for incorporating the DPM, as described in Section 2.1, as a simulation method into PRO-LOCA.

In order to evaluate the fidelity of this method two separate analyses addressing the same problem were conducted, one using Monte Carlo with 1,000,000 simulations and one using the DPM with importance sampling with the same number of simulations. For these analyses, a dissimilar metal weld at a hot leg outlet nozzle was considered. The material chosen represented an Alloy 82/182 weld joining a Type 316 stainless steel safe end and a SA-508 ferritic nozzle. Primary water stress corrosion cracking was assumed to be the only active degradation mechanism. Figure 3.47 shows the results from the two analyses. As can be seen, the results for the higher probabilities for the smaller break sizes (initiation, through-wall crack, and LOCA2) matched perfectly, while the DPM with importance sampling provided the lower probabilities (less than 10^{-6}) for the larger LOCA sizes (LOCA3 and LOCA4). The agreement at the smaller break sizes indicates that the DPM with importance sampling is working properly.

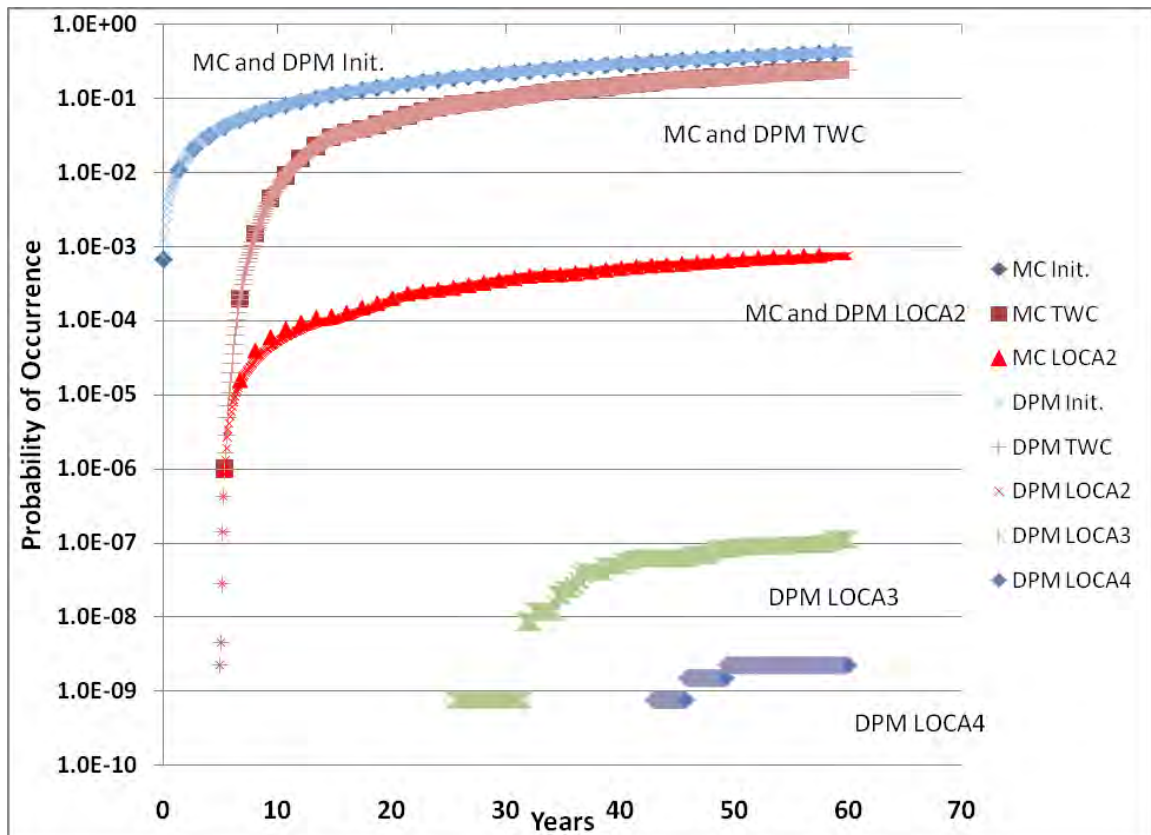


Figure 3.47 Comparison of LOCA probabilities for same problem using both Monte Carlo and Discrete Probability Method with Importance Sampling

3.4 References

- 3.1 Anderson, T.L., Thornwald, G., Revelle, D.A., and Lanaud, C., —Stress Intensity Solutions for Surface Cracks and Buried Cracks in Cylinders, Spheres, and Flat Plates,” Structural Reliability Technology final report to The Materials Property Council, Inc.
- 3.2 Chapuliot, S., Lacire, M.H and Le Delliou P., —Stress Intensity Factors for Internal Circumferential Cracks in Tubes Over a Wide Range of Radius over Thickness Ratios,” PVP-Vol. 365, Fatigue, Fracture and High Temperature Design Methods in Pressure Vess
- 3.3 Anderson, T.L., —Stress Intensity and Crack Opening Area Solutions for Through-wall Cracks in Cylinders, and Spheres,” Structural Reliability Technology final report to The Materials Property Council, Inc., January 29, 2003.
- 3.4 Brust, F., Scott, P, Rahman, S., Ghadiali, N, Kilinski, T., Francini, B., Marschall, C., Miura, N., Krishnaswamy, P., and Wilkowski, G., —Assessment of Short Through-Wall Circumferential Cracks in Pipes,” NUREG/CR-6235, April 1995.
- 3.5 P. Krishnaswamy, P. Scott, S. Rahman, and others —Fracture Behavior of Short Circumferentially Surface-Cracked Pipe,” NUREG/CR-6298, November 1995.

- 3.6 Scott, P., and Wilkowski, G., —Development and Application of a Database of Pipe Fracture Experiments,” PVP Vol. 323, Fatigue and Fracture, Vol. 1, July 1996.
- 3.7 Paul, D., Ahmad, J., Scott, P., Flanigan, L., Wilkowski, G., —Evaluation and Refinement of Leak-Rate Estimation Models,” NUERG/CR-5128, Rev. 1, June 1994.
- 3.8 Scott, P., Ghadaili, N., Paul, D., Morbitizer, R., Wilkowski, G., and Rudland, D., —Letter Report for Subtask 1a - Finalize and QA SQUIRT Code,” March 2003.
- 3.9 Boag, J., Flaman, M., and Mills, B., —Leak Rate Experiments for Through-Wall Artificial Cracks,” International Journal of Pressure Vessel and Piping, Vol. 43, 1990.
- 3.10 Materials Reliability Program (MRP) Crack Growth Rates for Evaluating Primary Water Stress Corrosion Cracking (PWSCC) of Alloy 82, 182, and 132 Welds (MRP-115), EPRI, Palo Alto, CA: 2004. 1006696.

4.0 DISCUSSION OF RESULTS

In this section of the report, the results from Section 3 will be discussed in detail. However, before doing a brief discussion is provided comparing the technical basis of PRO-LOCA with that of the PRAISE PFM code.

4.1 Comparison of Results between PRO-LOCA and other PFM Codes

In this section of the report, the PRO-LOCA code will be compared with PRAISE. Much of this discussion is similar to that provided to the MERIT TAG members when they were provided the December 2005 PRO-LOCA technical basis document which presented the technical basis/status of PRO-LOCA at the start of the MERIT program.

The PRAISE code (Ref. 4.1) was first developed in 1981 by researchers at Lawrence Livermore National Laboratories. Since that time it has been updated on several occasions. The most recent being the version developed for use on a personal computer (pcPRAISE), Ref. 4.2, and the Windows-based version of pcPRAISE, coined WinPRAISE (Ref. 4.3). It has been shown that WinPRAISE and pcPRAISE give the same results for the same problem with the same input.

PRO-LOCA incorporates a number of enhancements to the deterministic models based on NRC-sponsored research conducted over the last 20 years. Some of the more pertinent enhancements include, among other things, new methods for addressing multiple crack initiation sites, new crack growth models, new weld residual stress solutions, new crack stability models, and new methods for accounting for in-service inspections. In addition, new degradation mechanisms, not previously considered in codes such as PRAISE were added. This included the consideration of primary water stress corrosion cracking (PWSCC) for dissimilar welds in pressurized water reactors (PWRs). These enhancements are discussed in the following sections.

4.1.1 Degradation Mechanisms

PRAISE was initially developed in 1981 for the assessment of the influence of seismic events on the failure probability of cracked piping in pressurized water reactors (PWRs). The cracking mechanism originally considered by PRAISE was fatigue crack growth due to cyclic loading of pre-existing crack-like weld defects, introduced during the fabrication process. A major enhancement made to the code in the mid-1980's allowed for the probabilistic treatment of the initiation and growth of intergranular stress corrosion cracks (IGSCC) in sensitized weldments in Type 304 stainless steel piping in boiling water reactors (BWRs). Provisions for analyzing Type 316 NG stainless steel piping were subsequently added.

While the primary focus of PRAISE is on fatigue crack growth from pre-existing defects and IGSCC initiation and growth in sensitized stainless steel weldments in BWRs, PRO-LOCA considers initiation and growth of fatigue, IGSCC, and PWSCC cracks, as well as growth from pre-existing defects.

4.1.2 Multiple Crack Initiation Models

Perhaps one of the most important aspects in the development of a probabilistic pipe fracture mechanics code for predicting larger size LOCA events is the consideration of the initiation of subcritical cracks, and in particular the proper characterization of multiple crack initiations. If a single crack were to initiate and grow by typical fatigue mechanisms, then the crack growth in a pure membrane stress field is frequently as great in the depth direction as in the length direction. Such cracks, once they penetrated the pipe wall thickness, would readily be detected by leakage

and would not realistically contribute to the probability of a large break LOCA occurring. It is the longer surface cracks that do not leak prior to a transient loading event that are the more realistic contributors to a large break LOCA. Such longer cracks could occur where there exists a high stress gradient through the thickness, or where there exists the possibility of multiple cracks initiating and growing together to form one longer surface crack. Stress corrosion cracks typically initiate in a high residual stress field, such as at a girth weld. Since the residual stresses are the dominant stress for IGSCC initiation (over the normal operating stresses), and have a gradient through the thickness, there is the propensity for multiple cracks to initiate, with each of those cracks growing more in the length direction than the depth direction. Hence understanding the possibility of multiple cracks initiating through IGSCC is of key importance for developing an improved and realistic probabilistic piping LOCA code.

The means by which PRAISE captures this process of multiple initiation sites appears to be one of its major limitations, at least from the perspective of predicting the frequencies of larger size LOCA events. Calculations using PRAISE, carried out as part of an expert elicitation process (Ref. 4.4) aimed at predicting various size LOCA events, for a 12-inch diameter stainless steel, unmitigated, recirculation piping system, predicted that the maximum half crack length (b) of a surface crack was only 30 mm (1.2 inches) after 25 years of service. In fact, most of the resultant surface cracks had half crack lengths shorter than 10 mm (0.4 inches), see Figure 4.1. In reality, however, many much longer IGSCC cracks have been found in service with less than 25 years of plant operation. This discrepancy between the PRAISE predictions and service history appears to be the result of how multiple crack initiation sites are modeled in PRAISE. Analysis of IGSCC cracks removed from service has shown that if one IGSCC crack initiates, there is a 90 percent chance that other cracks will initiate in the same weld. Therefore, the initiation of the second crack is not purely a random occurrence, as is currently assumed in PRAISE. Since being able to predict the development of these long surface cracks is critical for the estimating the frequency of larger size LOCAs, an improved model which captures this dependence between initiation sites was deemed crucial for the development of the PRO-LOCA code.

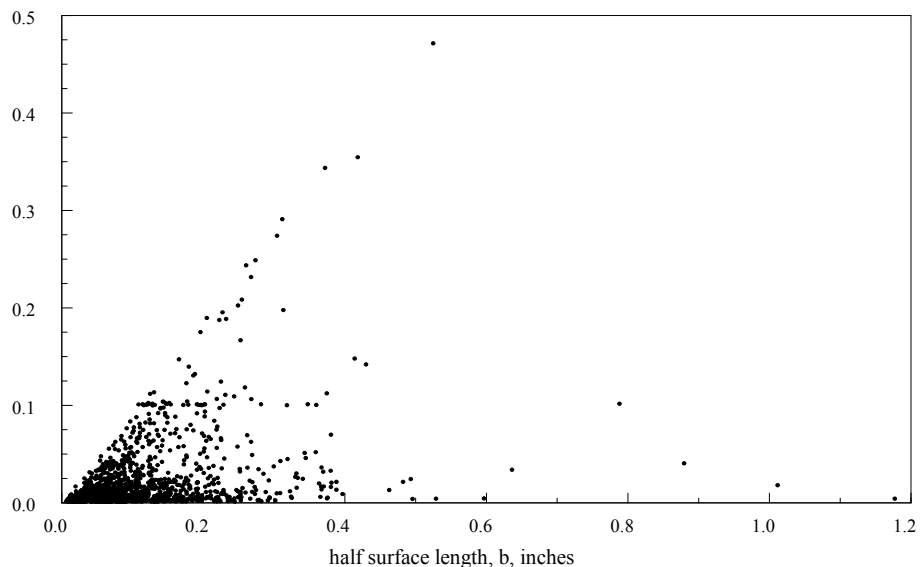


Figure 4.1 PRAISE predicted crack sizes after 25 years of service for the elicitation benchmark case (mean normal operating stress of 83 MPa [12 ksi]) with a weld overlay applied at 20 years

For PRO-LOCA the multiple crack initiation model is likewise based on segmenting the critical node into subunits. In PRO-LOCA the size of the subunits is based on a fix percentage of the pipe circumference. Currently that percentage is approximately based on a 50 mm (2 inch) long subunit for a 28-inch diameter pipe. The user has the option of three distinct multiple initiation models to choose from:

- Default time to initiation, with fixed lengths and depths
- Default time to initiation, with variable lengths and depths, and
- User inputs a distribution for the time to initiation, with variable lengths and depths.

For each of these multiple crack initiation models, cracks are typically initiated and placed randomly around the circumference. However, for the last option where the user inputs a distribution for the time to initiation, a crack location biasing option is also available. If the user chooses to incorporate this location bias into their analysis, subsequent cracks (after the first cracks initiate) will be biased to occur nearer to the site of the previously initiated cracks. If the user chooses not to incorporate this location bias, then the location of the subsequent cracks will be random, much like the approach incorporated in PRAISE. As with PRAISE, if multiple cracks do develop, then they can subsequently coalesce as they grow. For circumferential surface cracks, the coalescence criterion in PRO-LOCA is that when the distance between two surface cracks becomes less than two times the depth of the deepest surface crack, then the cracks will coalesce. The inputs used in generating the results shown in Figure 4.1 were run with the PRO-LOCA code. The resultant crack sizes after 25 years of service are shown in Figure 4.2. Also included with this figure are the bounds of the crack sizes calculated with PRAISE, as shown in Figure 4.1. As is apparent in Figure 4.2, the PRO-LOCA code is able to predict much larger cracks (approximately 3 times longer) than can the PRAISE code.

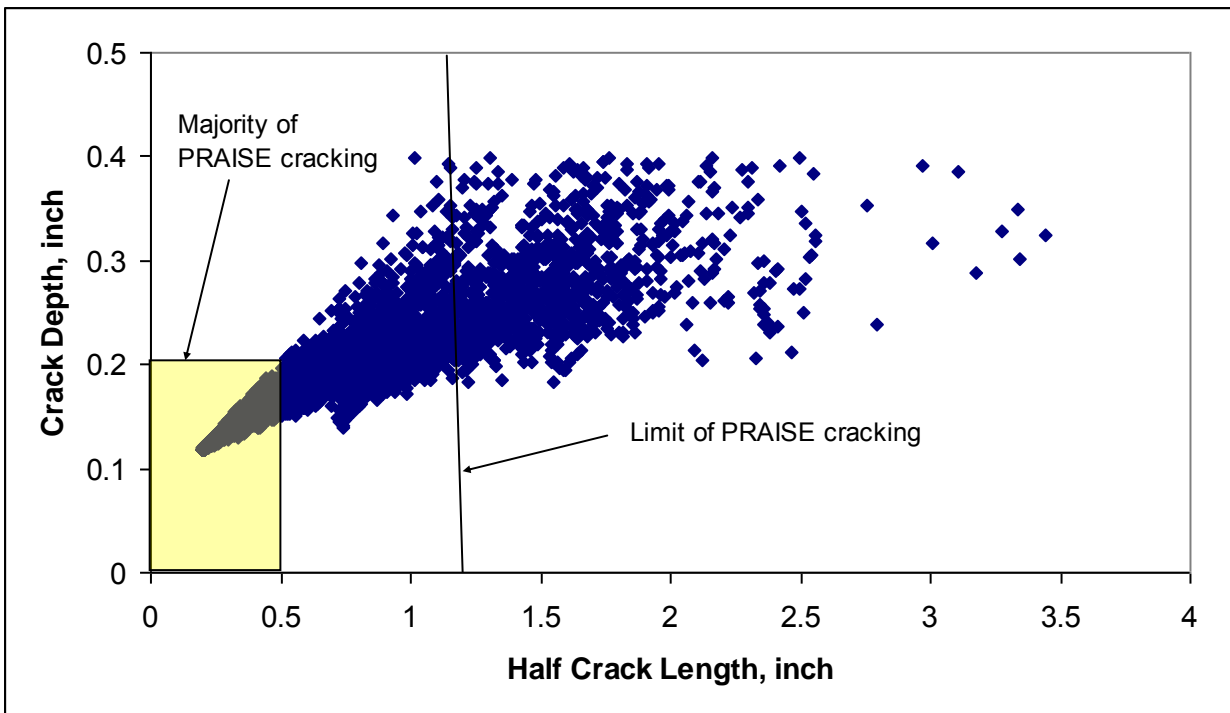


Figure 4.2 Comparison of crack sizes calculated for PRAISE and PRO-LOCA

4.1.3 Crack Growth Models

The stress corrosion crack growth rate relationship incorporated in PRAISE is based on analysis of stress corrosion crack growth rate data for Type 304 and Type 316NG fracture mechanics specimens tested under BWR environmental conditions. Analysis of the data available at the time PRAISE was being developed indicated a linear variation between the log of the crack growth rate ($\log da/dt$) and the stress intensity factor K . The dependence of the crack growth rate on the environment was assumed to be described by the environmental term, f_3 , in the treatment of stress corrosion crack growth, see Equation 4-1

$$\log(da/dt) = C_{10} + C_{11} \{C_{13}[\log(f_3(\text{env.}))]+C_{14}K\} \quad (4-1)$$

For PRAISE, the IGSCC growth is separated into two parts, an early phase based on a constant crack velocity plus a later phase based on fracture mechanics principles.

The subcritical crack growth models incorporated in PRO-LOCA for IGSCC are the latest statistically-based models developed by Argonne National Laboratories (Ref. 4.5). Unlike the PRAISE code, where the log of the crack growth rate was assumed to be a linear function of K , the crack growth relationship embodied PRO-LOCA is assumed to be a power-law function of K , see Equation 4.2.

$$\frac{da}{dt} = CK^{2.2} \quad (4-2)$$

In addition to subcritical crack growth due to IGSCC, PRO-LOCA also includes models for considering subcritical crack growth due to fatigue and PWSCC. Fatigue crack growth, although by different models, was also considered in PRAISE, but PWSCC is an entirely new mechanism not considered in PRAISE.

4.1.4 Weld Residual Stresses

Weld residual stresses are input into the PRAISE code by one of six different options. (There is a seventh option if one considers the case of no residual stresses.) Three of the options are user inputs; in one case the user inputs coefficients for a polynomial curve fit of the residual stresses, in a second case the user defines the residual stresses at the ID and OD surfaces and the code assumes a linear fit through the thickness, and in a third case the mean and standard deviation of stress at the ID surface are input by the user and a self-equilibrating linear variation through the thickness is used.

For the other three options, PRAISE assigns a random distribution to the weld residual stresses. This stress distribution is dependent on the pipe diameter. For the large diameter piping (greater than 20 inch), the distributions were established based on analysis of nine separate experimental data sets. Mean and standard deviations of the curve-fit parameters describing the through-thickness residual stresses in the heat-affected zone of large-diameter austenitic piping were developed and incorporated into PRAISE. For the small (4 to 10 inch) and intermediate (10 to 20 inch) diameter lines, there was very little information available regarding the through-thickness variation of the residual stresses. There was, however, a wealth of data for the weld residual stresses at the inside surface. Data on the axial component of the inside surface residual stresses were compiled for locations approximately 3 mm (0.125 inch) from the weld fusion line where the peak sensitization levels generally occur (Ref. 4.6). These data were used to generate distributions on stress (means and standard deviations) on the inside surface for both small and

intermediate diameter lines. Since insufficient information was available to characterize the through-thickness variation of the residual stresses for these small and intermediate diameter lines, a number of assumptions were made in order to characterize their statistical and spatial residual stress distributions.

In PRO-LOCA, there are a total of eight options the user currently has to choose from. The user can provide their own 4th order polynomial fit of the residual stress distribution through the thickness. Here they can provide their own 4th order polynomial where the variation in residual stress is introduced only through the distribution in the material yield strength or they can provide a user defined weld residual stress distribution with user prescribed distributions on the inner diameter weld residual stress term as well as the distance from the inside surface where the weld residual stress crosses through zero, i.e., the X_c term. Alternatively, there are six default weld residual stress solutions embodied in PRO-LOCA. Four of the solutions are for dissimilar welds while two are for stainless steel welds. Instead of relying on a series of assumptions for defining the through thickness stresses, these solutions were developed using detailed finite element analyses. As a result, the solutions included in PRO-LOCA for the stainless steel weld cases result in much higher residual stresses on the ID surface than what would be the case for the PRAISE code, see Figure 4.3.

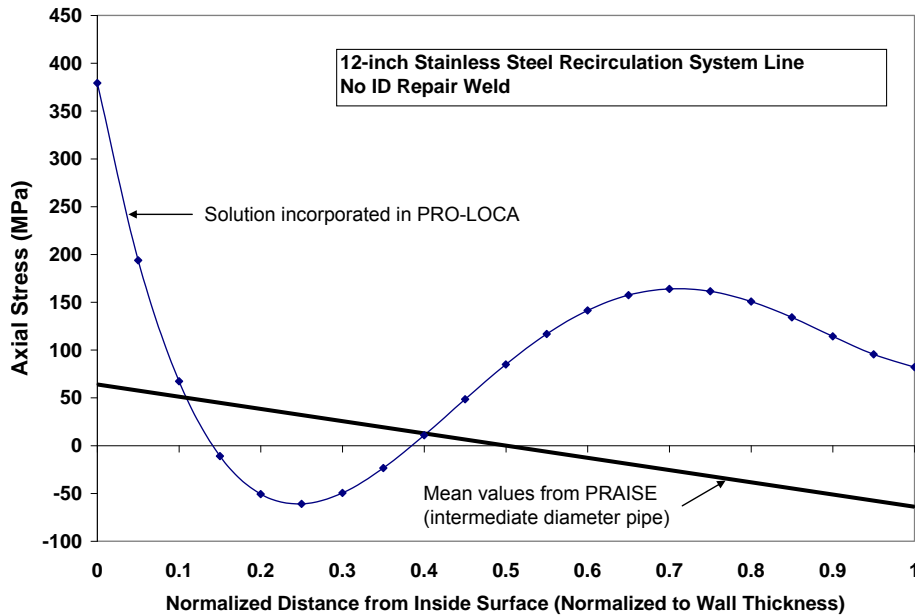


Figure 4.3 Comparison of PRAISE and PRO-LOCA code weld residual stresses for 12-inch diameter stainless steel pipe weld

4.1.1.5 Fracture Stability Analyses

In PRAISE, the user has the option of selecting either a simple limit-load or tearing modulus analyses for the fracture stability analysis. For the tearing modulus analysis, the J-integral is calculated by a method similar to that of the GE/EPR method (Ref. 4.7). The J-R curve used to calculate the tearing modulus of the material (T_{mat}) is assumed to be linear.

In PRO-LOCA, a simple screening criterion based on the Dimensionless-Plastic-Zone-Parameter (DPZP) analysis (Ref. 4.8) is used to initially check for through-wall crack stability. The DPZP

analysis is a semi-empirical analysis method developed by Battelle and is used to analyze either surface or through-wall cracked pipe under bending and tension loads.

For a through-wall crack, if the applied stress is greater than the DPZP failure stress, then the PRO-LOCA code uses the LBB.ENG2 through-wall crack J-estimation scheme (Ref. 4.9) to calculate the maximum bending stress for through-wall crack stability considerations. The LBB.ENG2 method was chosen in that it had been shown to agree best with full-scale through-wall cracked pipe experiments in earlier studies (Ref. 4.10). If the applied bending stress is less than the maximum calculated bending failure stress using the LBB.ENG2 method, then the through-wall crack is considered stable. If not, then the code assumes a DEGB occurs.

Originally, the SC.TNP1 method (Ref. 4.11) was going to be used to ultimately assess the stability of surface cracks in PRO-LOCA since it had been shown previously that the SC.TNP1 method agreed best with full-scale surface cracked pipe experiments (Ref. 4.11). However, as part of the MERIT program a number of issues were identified with SC.TNP1 methodology. As a result, it was decided to use the DPZP method for surface cracks as the surface crack stability criteria in PRO-LOCA. Regardless, however, both the DPZP and LBB.ENG2 methods were considered an improvement over the simple limit load criteria incorporated into PRAISE.

4.1.6 Inspection Details

Pre-service and in-service nondestructive inspections can be considered in PRAISE code analyses. These enter into the analyses through the probability of detecting a defect during the inspection as a function of defect size. If a crack is detected, it is assumed to be repaired, with the repaired joint being defect free. The probability of detection on successive examinations is assumed to be independent. That is, the fact that the crack was missed on an earlier inspection does not influence the probability of detecting it on the next inspection. The inspection detection probability in PRAISE is expressed in terms of the probability of not detecting a crack of area (A), where there are a number of parameters that get input by the user depending on the inspection protocol used and the material being inspected. Some of these parameters also get adjusted depending on whether the detection capabilities are considered “good” or “outstanding”.

In PRO-LOCA there are a number of options for addressing the effects of inspections on the resultant LOCA probabilities. First the user can either specify the probability of detection (POD) curve as either a piece wise linear fit or a Weibull distribution of the probability of detection versus defect size curve. The user can also specify different POD curves for different inspections and can vary the intervals between inspections throughout the life of the plant. Furthermore, the user can specify one set of inspections for past inspections (i.e., inspections that have already been accomplished) and another set of inspections for future inspections (i.e., inspections yet to be performed). In addition, for the past inspections, the user can either take credit or not for the fact that no leaks have been detected during these past inspections. Finally, if a defect is discovered during one of these inspections, the user has the option replacing the node, or weld, with similar material, without defects, much like PRAISE, or they can either (1) repair the node, or weld, with a weld overlay or mechanical stress improvement process (MSIP) or (2) they can replace the weld with a new material not susceptible to cracking. For the repair option, the user defines a new weld residual stress distribution to represent the weld repaired by either a weld overlay or MSIP.

4.2 Discussion of Results from Modular QA Checks

Quality assurance checks were made for many of the deterministic modules in PRO-LOCA. The modules evaluated were the

- Anderson K-solutions for both surface and through-wall cracks,
- crack stability modules for both through-wall and surface cracks,
- leak rate module based on the SQUIRT leak rate code,
- crack initiation models for IGSCC and PWSCC, and
- crack growth models for fatigue, IGSCC, and PWSCC.

In some cases comparisons were made between the output from PRO-LOCA and other computer codes, e.g., results from the LBB.ENG2 through-wall crack stability module in PRO-LOCA were compared with results from the LBB.ENG2 method in the NRCPIPE code. In each case the comparison with these other codes was excellent. For many of these cases, comparisons between these other codes with experimental data had previously been made and the agreement was found to be excellent.

4.3 Discussion of Results from Sensitivity Analyses

In this section of the report the results from the various sensitivity analyses conducted to date using PRO-LOCA will be discussed. Again, it should be remember that the results of these sensitivity analyses are based on using Version 3.5.30 of PRO-LOCA, with a release date of April 24, 2009.

4.3.1 Parametric Study

A detailed parametric study was conducted using Version 3.5.30 of PRO-LOCA to ascertain the effect that specific input parameters had on the resultant LOCA probabilities. As part of this study, a base case was developed for both BWRs and PWRs and then specific input parameters were changed to ascertain the effect those specific changes had on the resultant LOCA probabilities. The objectives of this study were two-fold: (1) a sanity check to ascertain whether the specific input parameter changes had a logical effect on the resultant LOCA probabilities and (2) to ascertain the major drivers associated with the resultant probabilities. A major outcome of these sanity checks was to identify any coding errors associated with PRO-LOCA.

4.3.1.1 Base Case Results – Figures 3.18 and 3.19 show the base case results for the BWR and PWR base cases, respectively. As would be expected the probabilities decrease for the larger LOCA categories. Of further note from these figures are the decreases in slope of the probability versus time curves that occur in both figures every 10 years (120 months). These changes in slope are an artifact of the inspections that occur every 10 years. As inspections are performed, and flaws discovered and subsequently removed from the analysis, the rate that which the LOCA probabilities are occurring decreases (reduction in slope of the probability versus time plot). This is to be expected.

4.3.1.2 Effects of Loads and Stresses on Resultant LOCA Probabilities - Figures 3.20 and 3.31 show the effects of the static global bending stress on the BWR and PWR LOCA probabilities, respectively. As can be seen in these figures increasing the static global bending stress resulted in higher LOCA probabilities for both plant types. The effect was most pronounced for the larger LOCA categories, i.e., Category 3 LOCAs, where, increasing the global bending stress 2 ½ times

from 20 MPa (3 ksi) to 50 MPa (7 ksi) caused almost a 3 order of magnitude increase in the LOCA3 probabilities for the BWRs. Similarly, doubling the global bending stress from 117 MPa (17 ksi) to 235 MPa (34 ksi) caused about a 1 ½ order of magnitude increase in the LOCA3 probabilities for the PWRs. Of further note from Figure 3.31 is that the through-wall crack probability and LOCA2 probability are nearly identical for the higher static bending stress case for the PWRs. For this case the higher static bending stresses were high enough such that once a through-wall crack occurred, it immediately grows to a Category 2 LOCA size.

In a similar vein, increasing the inside surface weld residual stress caused an increase in the BWR and PWR LOCA probabilities, see Figures 3.21 and 3.32, respectively. Contrary to the global bending stress results where the larger category results were most affected, the most pronounced effect on the break probabilities for the weld residual stress case occurred for the through-wall cracks. (The effect of the weld residual stresses on the larger LOCA sizes was not that significant. Weld residual stress does not affect stability. The main effect of higher weld residual stress would be to increase the rate of occurrence of crack initiation and crack growth which would have a larger effect on the through-wall crack probabilities than on the larger category LOCAs.) Increasing the inside surface weld residual stresses from 70 MPa (10 ksi) to 210 MPa (30 ksi) for the BWRs caused an increase in the through-wall crack LOCA probabilities of slightly less than one order of magnitude, see Figure 3.21. Similarly for the PWRs, increasing the inside surface weld residual stresses from 35 MPa (5 ksi) to 200 MPa (29 ksi) resulted in an increase in the PWR through-wall crack probabilities of slightly less than one order of magnitude. One small question with these plots is the LOCA Category 3 results for the BWRs, see Figure 3.21. As can be seen in this figure, the higher inside surface weld residual stress resulted in slightly lower probabilities for the BWR case. (Note, this was not the case for the PWR case, see Figure 3.32.) A couple possible reasons for this behavior were put forward. One was that the higher inside surface weld residual stresses caused the cracks to grow faster resulting in higher through-wall crack probabilities, which led to slightly higher Category 2 LOCAs early in the life (within the first 50 months). As a result more cracks were being detected and removed from service, either by periodic in-service inspections or through the plant's leakage detection system, and replaced with non-susceptible material such that fewer crack were available to grow to a Category 3 LOCA size. In order to check this hypothesis another set of analyses were conducted for which the inspections and leakage detection limit were turned off. The results of those analyses are shown in Figure 4.4.

As can be seen in this figure the Category 3 LOCA probabilities are still slightly lower for the higher inside surface weld residual stress case. A third set of analyses were then conducted for which the inside surface weld residual stresses were further reduced such that they were a factor of 10 less than the higher stress case, i.e., 21 MPa (3 ksi) versus 210 MPa (30 ksi). For these analyses both leakage detection and inspections were again turned off. The results from those analyses are shown in Figure 4.5. Early in the life (within the first 150 months), the results are as would expected where the LOCA probabilities consistently increase with an increase in the inside surface weld residual stresses, much like was the case for the PWRs. Later in life, the probabilities for the Category 2 and 3 LOCAs tend to merge together. For this case, with no inspections and no leakage detection, even at the lower level of weld residual stresses, the through-wall crack probabilities are approaching unity at the end of life (60 years). Even at 20 years, the probability of a through-wall crack occurring is about 25 percent for the low stress state for this case where there were no inspections. As a result, at these lower levels of weld residual stresses, the stresses are great enough to cause these resultant through-wall cracks to continue to grow to a size to cause a Category 2 or 3 LOCA. The same is true for the higher stress case, except at the higher stress state, the cracks are growing faster earlier in life, resulting in higher probabilities of not only through-wall cracks occurring but also Category 2 and 3 LOCAs

occurring. Then, as these cracks for the higher stress state grow and result in Category 2 and 3 size LOCAs, fewer cracks remain in the analyses for this higher stress state than do for the lower stress state. As a result, later in life more cracks are available to continue to grow in size for the lower stress state such that with time the probabilities for the two cases begin to merge.

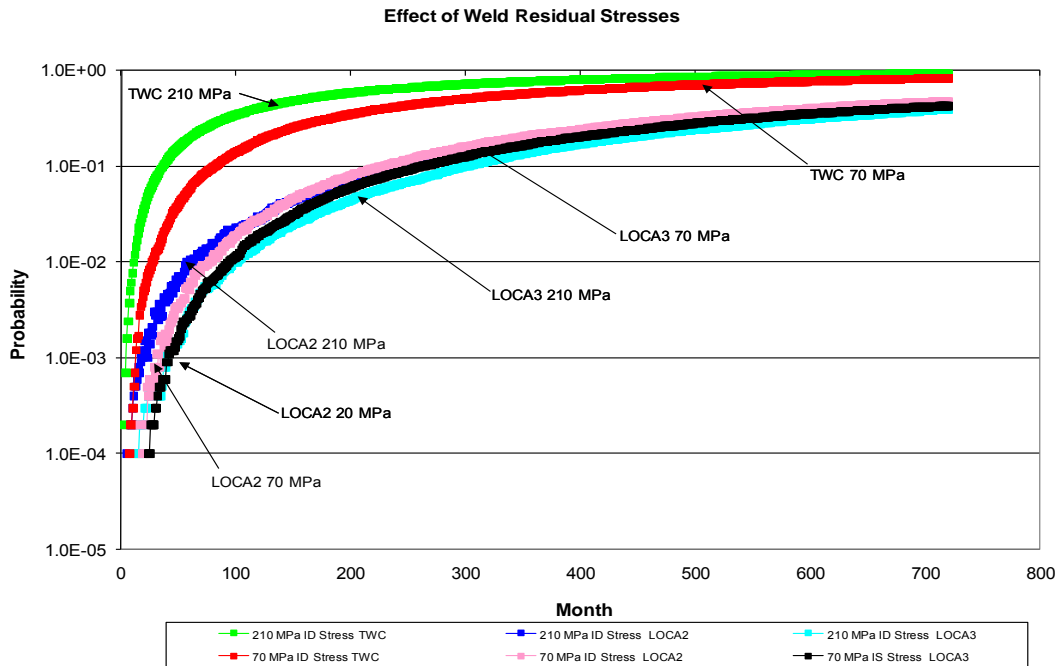


Figure 4.4 Results comparing the effect of weld residual stresses on the BWR LOCA probabilities for the case where the in-service inspections and leakage detection limit were turned off

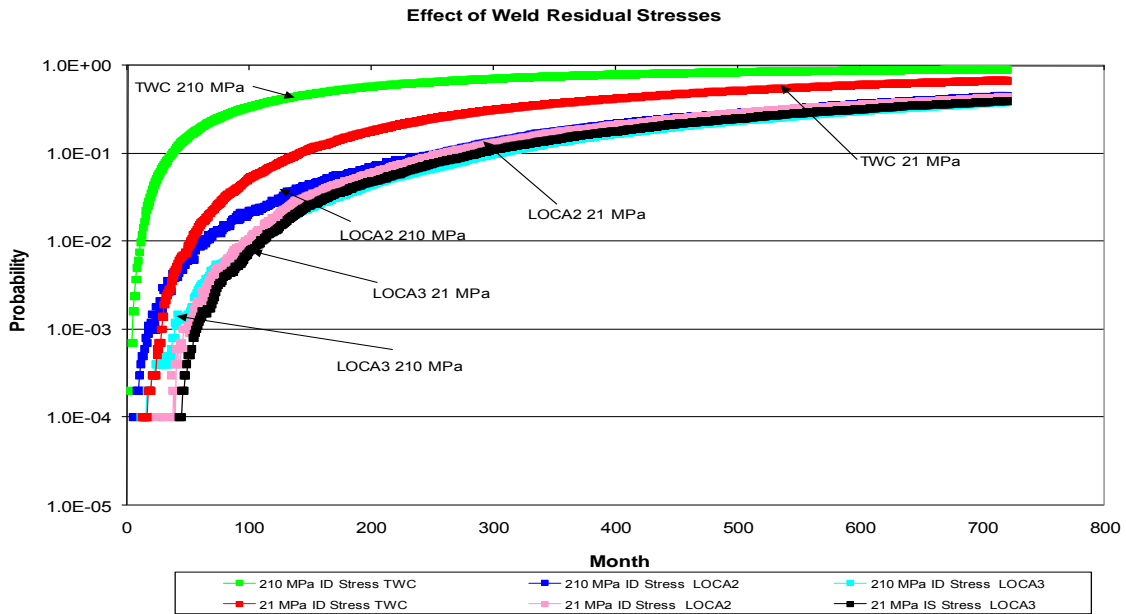


Figure 4.5 Comparison of BWR LOCA probabilities for the cases where the inside surface weld residual stresses were 210 MPa (30 ksi) and 21 MPa (3 ksi)

Figures 3.22 and 3.23 show the effects of zero, one, and two transients on the BWR LOCA probabilities. Increasing the number of transients had no effect on the through-wall crack probabilities and minimal effect on the larger LOCA categories. There was a slight increase in the Category 2 LOCAs with additional transients and less of an effect for the Category 3 LOCAs. For the PWRs there was a more pronounced effect of adding an earthquake to the load history. Adding an earthquake to the PWR load history increased in the through-wall crack and Category 2 LOCAs by approximately one order of magnitude, see Figure 3.33. It was originally thought that this increase may have been too substantial. However, the magnitude of this earthquake was quite severe. The earthquake magnitude was 140 MPa (20 ksi), which when added to the static bending stress of 117 MPa (17 ksi) resulted in a combined normal plus seismic stress of 257 MPa (37 ksi). The ratio of the normal plus seismic stress to the design stress intensity (S_m) for the stainless steel base metal (Type 304) was approximately 2.2. (The ASME Code design stress intensity for the Type 304 stainless steel at 288 C (550 F) is 117 MPa [17 ksi].) In looking at probability of exceedance curves for 27 PWRs in Figure 4-4 of Reference 4.12, the probability of exceedance for this magnitude of loading ranged from a low of approximately 2×10^{-8} per year to a high of 5×10^{-6} per year. As a point of reference, the probability of occurrence used in the analysis for which Figure 3.33 is based on was 2.5×10^{-2} per year, which is 5,000 times higher than the highest probability of exceedance for the 27 plants reflected in Figure 4-4 of Reference 4.12 for a stress ratio of 2.2. Thus, it is probably safe to assume that if an earthquake with more representative stresses was assumed in the analysis, that the effect would have been less.

Increasing the number of cycles in the earthquake had almost no effect on the through-wall crack and Category 2 LOCAs, see Figure 3.34. On the other hand, increasing the number of cycles in the earthquake caused about a half order of magnitude increase in the Category 3 LOCA probabilities. In a similar vein increasing the magnitude of the earthquake caused an increase in the LOCA probabilities, see Figure 3.35.

In all of these cases increasing the applied stress, whether it be the global static bending stress, transient stress, or earthquake stress, consistently increased the BWR and PWR LOCA probabilities, as should be expected.

One final note with regards to the applied stresses: as was demonstrated in Figure 3.46, the resultant LOCA probabilities are the same whether one inputs the loads in terms of stress or equivalent moments.

4.3.1.3 Effect of Environment on the Resultant LOCA Probabilities - Figure 3.25 shows the effect of water chemistry on the BWR LOCA probabilities. Changing from normal water chemistry to hydrogen water chemistry had a significant effect on the LOCA probabilities. Of all the effects considered for the BWRs, water chemistry had the most significant effect on the LOCA probabilities. Similarly, another environmental parameter, operating temperature, had the most significant effect on the PWR LOCA probabilities, see Figure 3.30. Both of these environmental parameters impact the crack initiation and crack growth properties of the problem. The implications being that crack initiation and growth have a significant influence on the resultant LOCA probabilities for both the BWRs and PWRs, probably more so than the other deterministic models embedded in PRO-LOCA, e.g., stability, leak rate, and inspection. In particular, since changes in environment (including temperature) had a more significant effect of the resultant LOCA probabilities than any changes in the transients (i.e., number of transients/earthquakes or the magnitude of those transients/earthquakes), it is probably the safe to say that it is the stress corrosion cracking initiation and growth models, more so than the fatigue initiation and growth models, that have the most significant affect on the resultant LOCA probabilities, at least for the

cases considered in these analyses, i.e., large diameter recirculation lines for BWRs and large diameter hot legs for PWRs.

4.3.1.4 Effect of Inspections on the Resultant LOCA Probabilities - As can be seen in Figure 3.24, increasing the inspection interval (less frequent inspections) resulted in an increase in the LOCA probabilities for the BWR case. Increasing the inspection interval from 10 to 20 years resulted in about a half order of magnitude increase in the Category 2 and 3 LOCAs for the BWRs. Furthermore, for the first 10 years, prior to the first inspection, there was absolutely no difference in the Category 2 and 3 LOCA probabilities. This increase in inspection interval also had almost no effect on the through-wall crack probabilities. For the PWRs, increasing the inspection interval from 10 to 20 years resulted in about an order of magnitude increase in the resultant LOCA probabilities for not only the Category 2 and 3 LOCAs, but also for the through-wall cracks, see Figure 3.38. Conversely, improving the quality of the POD curve resulted in only a slight reduction in the resultant LOCA probabilities, see Figure 3.39, however, the improvement in the POD curve was not that dramatic, see Figure 3.40. In order to further examine the effect of the quality of the POD curve on the resultant LOCA probabilities, another set of analyses were conducted for which the probabilities of detection were reduced by a factor of 4. The results of those analyses are shown in Figure 4.6. As can be seen in this figure the effect of the POD curve was much more pronounced than was evident in Figure 3.39.

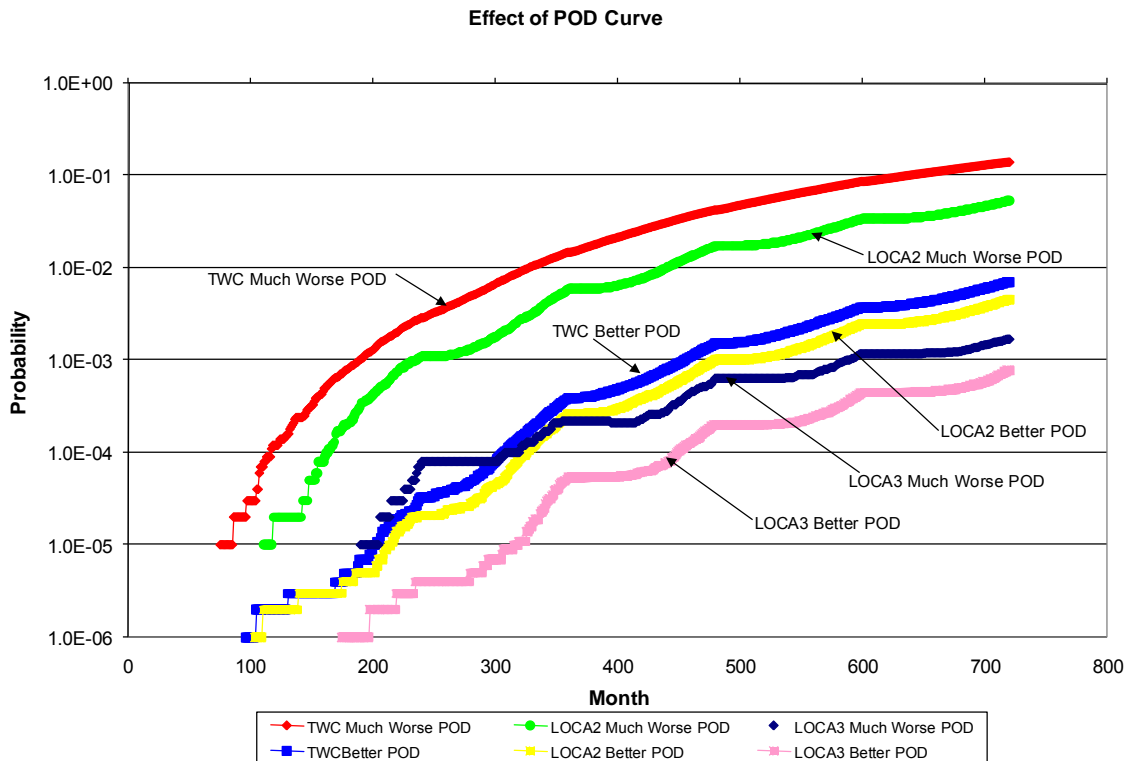


Figure 4.6 Effect of a much worse POD curve on the resultant PWR LOCA probabilities

4.3.1.5 Effect of Material Properties on the Resultant LOCA Probabilities - Changes in the material properties were also considered in this parametric study. Figures 3.36 and 3.37 show the effect of changing the material strength and toughness, respectively, on the resultant PWR LOCA probabilities. As can be seen in these two figures, the effect was very minor. From a toughness perspective, the nominal toughness case (570 kJ/m² [3,250 in-lbs/in²]) was tough enough such

that stability would be governed by limit load conditions and increasing the toughness by almost a factor of 20 would have little impact on stability, i.e., stability is independent of fracture toughness. As such, a second analysis was conducted in which the fracture toughness was reduced by a factor of 20 (28.5 kJ/m^2 [163 in-lbs/in^2] versus 570 kJ/m^2 [$3,250 \text{ in-lbs/in}^2$]) to see if the lower toughness had any impact on the LOCA probabilities. The results from that analysis are shown in Figure 4.7. As can be seen in Figure 4.7, lowering the fracture toughness by a factor of 20 did not significantly alter the resultant LOCA probabilities, except for the larger Category 3 LOCAs, for which the lower toughness resulted in slightly less than one order of magnitude increase in the LOCA probabilities. In this case the toughness was probably low enough that elastic plastic fracture mechanics (EPFM), not limit load, conditions govern. As a result fracture toughness plays a role in stability. As such this decrease in the LOCA probabilities is probably to be expected. Similarly, increasing the material strength had a minimal effect on the resultant LOCA probabilities, see Figure 3.36. In this figure the higher strength case had a yield strength that was approximately 25 percent higher than the nominal case and an ultimate strength that was approximately 35 percent higher than the nominal case. As can be seen in this figure, the effect on the resultant LOCA probabilities was insignificant. These findings tend to support the notion that stability may not be as critical a parameter as crack initiation and growth in the overall assessment of the LOCA probabilities. Note, yield strength may play a role in crack initiation and crack growth in that many of the weld residual stress distributions embedded in PRO-LOCA are yield strength dependent. However, the cases considered in Figure 3.36 were based on the user defined weld residual stress distribution which is independent of yield strength.

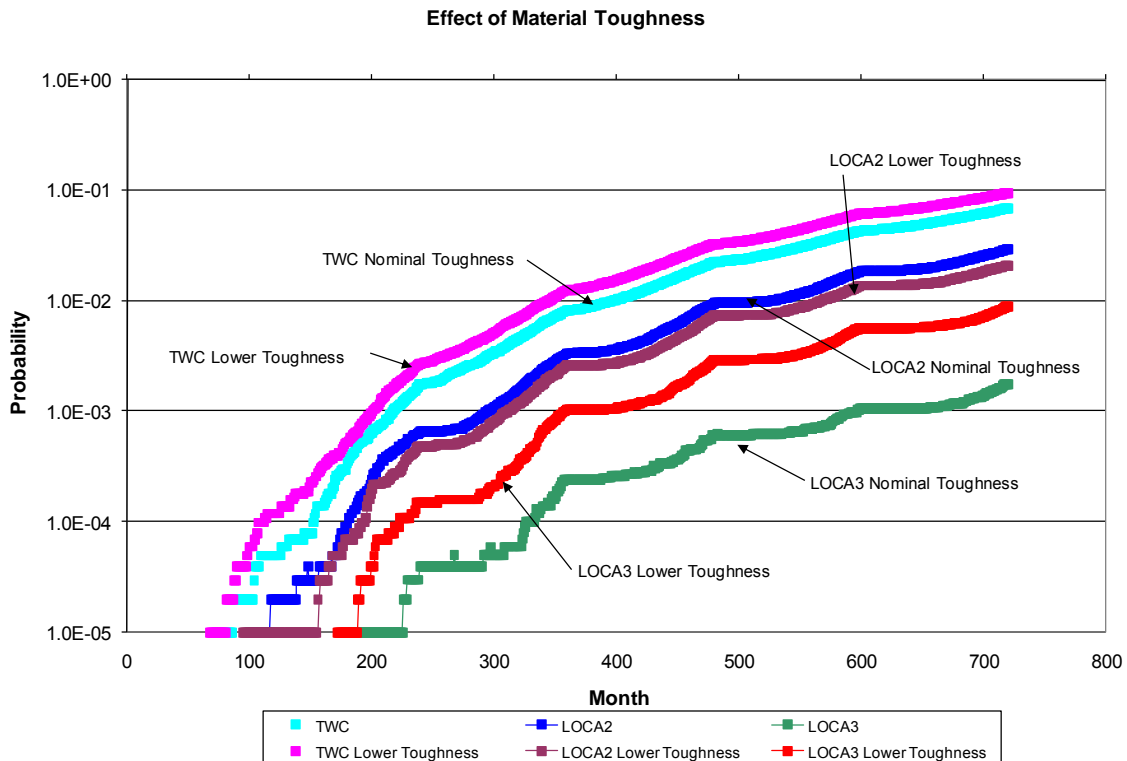


Figure 4.7 Effect of lowering the fracture toughness on the PWR LOCA probabilities

4.3.1.5 *Effect of Crack Initiation Model on the Resultant LOCA Probabilities* - Figure 3.28 shows the effect of the crack initiation model (single versus multiple crack initiation) on the BWR LOCA probabilities. Since the same initiation time and crack size distributions were used

in both cases, one would not expect much of a difference in the LOCA probabilities unless multiple cracks linked up causing slightly higher LOCA probabilities for the larger break sizes. As can be seen in Figure 3.28 the multiple crack initiation model resulted in a very slight increase in the Category 2 LOCAs and a slightly larger increase in the Category 3 LOCAs. However, early in life (in the first 200 years), the through-wall crack probabilities were very slightly higher for the single crack analysis. Figure 3.43 shows a similar, albeit more pronounced effect for the PWR through-wall crack probabilities. For the PWR case, this increase in LOCA probabilities for the single crack analysis is carried over to the Category 2 and 3 results as well. The one possible explanation for this apparent discrepancy is that for the single crack analysis, the initiated crack is always centered on the maximum bending stress plane, whereas for the multiple crack analysis, the initiated cracks are randomly distributed around the pipe circumference.

Figure 3.29 shows the effect of the arrival rate on the BWR LOCA probabilities. The higher arrival rate case (1 crack/year) resulted in higher LOCA probabilities than did the lower arrival rate case (0.01 cracks/year). This is a trend that would be expected. However, for the PWR case, the reverse was found to be the case, see Figure 3.44. In this case, the lower arrival rate case (0.01 cracks per year) resulted in higher LOCA probabilities than did the higher arrival rate case (0.05 cracks per year). However, when one examines the probability of crack initiation for this set of analyses, see Figure 4.8, one sees that the higher arrival rate resulted in higher crack initiation probabilities, as one would expect. One possible explanation offered for the apparent discrepancy observed in Figure 3.44 is that those results may be being unnecessarily complicated by the in-service inspections and leakage detection limit. Thus, another set of analyses were conducted for which inspections and leakage detection were turned off. The results of those analyses are shown in Figure 4.9. As can be seen in this figure, the higher arrival rate consistently resulted in higher LOCA probabilities, as one would expect.

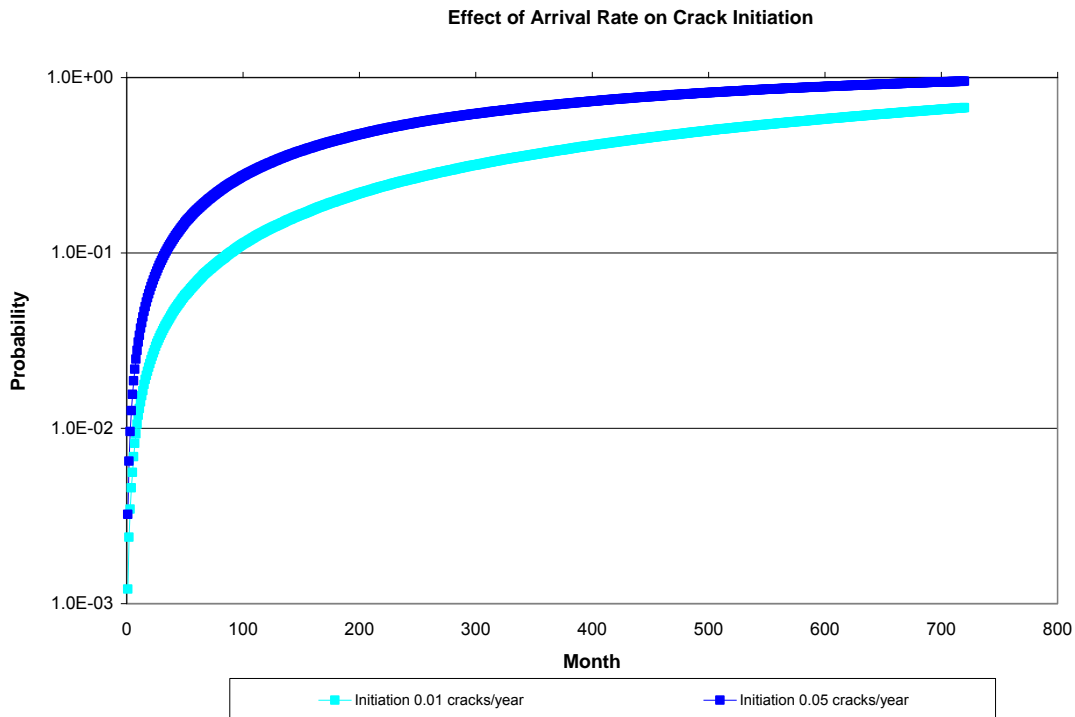


Figure 4.8 Effect of arrival rate on crack initiation probabilities

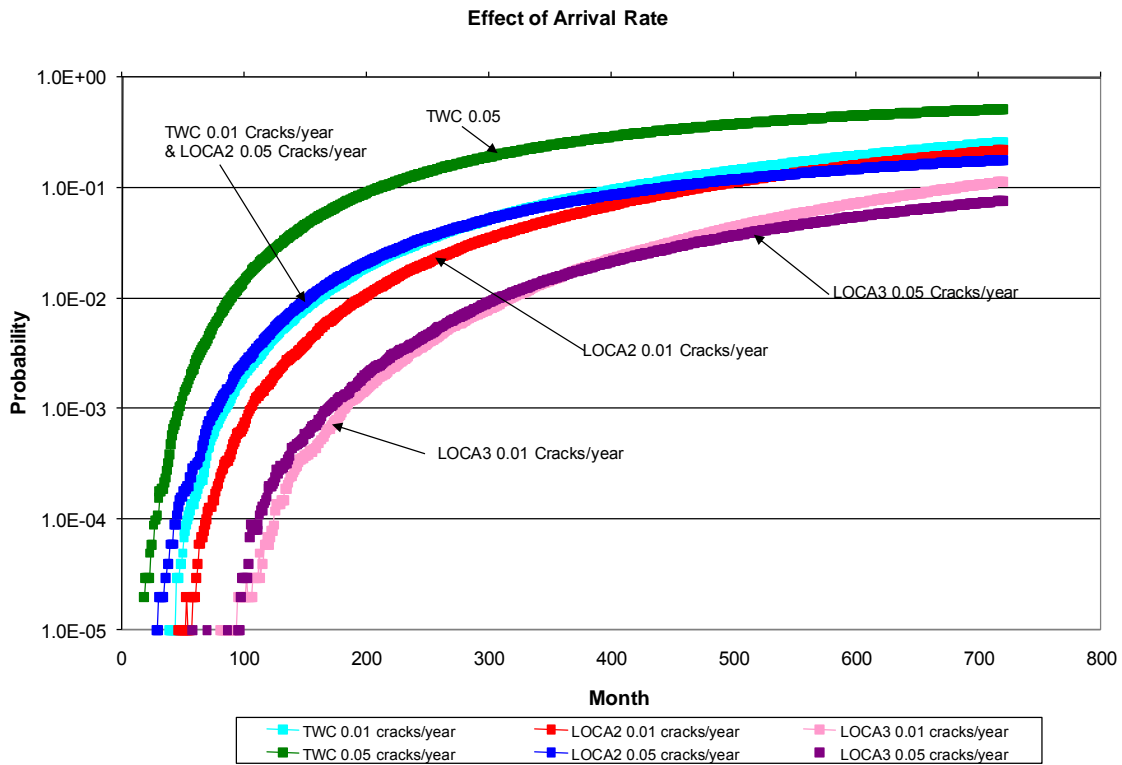


Figure 4.9 Effect of arrival rate on PWR LOCA probabilities when inspection and leakage detection were turned off

4.3.1.6 *Effect of Leak Rate on the Resultant LOCA Probabilities* – Figures 3.26 and 3.27 show the effect of leak rate detection limit on the BWR LOCA probabilities. Figure 3.26 is for the case of hydrogen water chemistry while Figure 3.27 is for the case of normal water chemistry. As would be expected the leakage detection limit had no effect on the through-wall crack probabilities since by definition there is no leakage prior to the occurrence of the first through-wall crack. For both cases the lower leakage detection limit resulted in higher Category 2 LOCA probabilities and lower Category 3 LOCA probabilities. The higher Category 2 LOCA probabilities are somewhat surprising in that one would expect that with the lower leakage detection limit more flaws would be detected and subsequently removed from service before they could grow to a size sufficiently large to support a Category 2 LOCA. Conversely, the lower Category 3 LOCA probabilities for the lower leakage detection limit is as one would expect, i.e., the lower leakage detection limit results in more through-wall flaws being detected and removed from service before they can grow to a size sufficient to result in a Category 3 LOCA.

Figure 3.41 shows the effect of leak rate detection limit on the PWR LOCA probabilities. As can be seen in this figure increasing the leakage detection limit from 1.89 lpm (0.5 gpm) to 1,890 lpm (500 gpm) had no effect on the through-wall crack, Category 2, or Category 3 LOCA probabilities. To further examine the effect of leakage detection limit additional analyses were conducted spanning a greater range of leakage detection limits, i.e., from 1.5 lpm (0.4 gpm) to 50,000 lpm (13,000 gpm). For these analyses the in-service inspections were turned off. The effect of varying the leakage detection limit from 1.5 lpm (0.4 gpm) to 50,000 lpm (13,000 gpm) are shown in Figure 4.10 to Figure 4.12 for the through-wall crack, LOCA2, and LOCA3

probabilities, respectively. In each case the two higher leakage detection limits, 7,500 lpm (2,000 gpm) and 50,000 lpm (13,000 gpm), resulted higher LOCA probabilities than for the other leakage detection limits considered. The fact that the Category 2 and 3 LOCA probabilities were higher for these higher leakage detection limits is what one would expect. What was somewhat surprising was the fact that the LOCA probabilities were identical for the two higher leakage detection limits. They were also identical for the 5 lower leakage detection limits considered. The only exception was that the LOCA probabilities were lower still earlier in the life for the lowest leakage detection limit considered, 1.5 lpm (0.4 gpm). Then after about 300 months, the LOCA probabilities for this lowest leakage detection limit equaled those of the higher leakage detection limits. What is especially disconcerting are the results for the through-wall crack probabilities shown in Figure 4.10. As can be seen in this figure the through-wall crack probabilities change with leakage detection limit. Since there is no leakage prior to the occurrence of the first through-wall crack, the through-wall crack probabilities should be independent of leakage detection limit. Consequently, leakage detection limit seems to be one parameter which deserves further scrutiny.

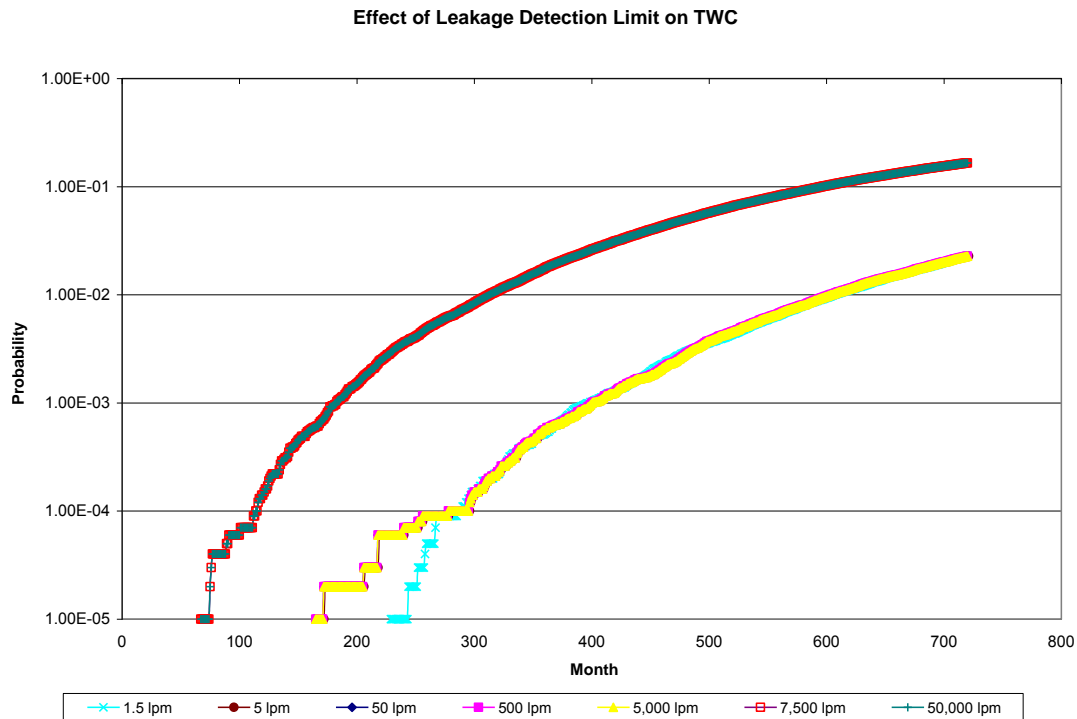


Figure 4.10 Effect of varying the leakage detection limit from 1.5 lpm (0.4 gpm) to 50,000 lpm (13,200 gpm) on the PWR through-wall crack probabilities

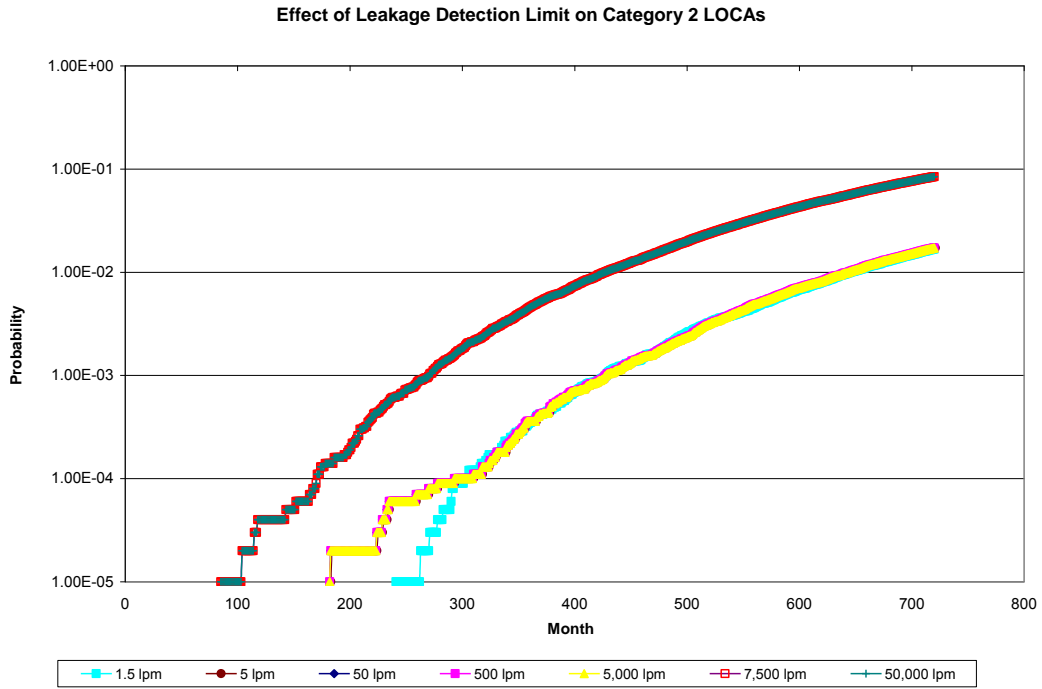


Figure 4.11 Effect of varying the leakage detection limit from 1.5 lpm (0.4 gpm) to 50,000 lpm (13,200 gpm) on the PWR LOCA2 probabilities

Effect of Leakage Detection Limit on Category 3 LOCAs

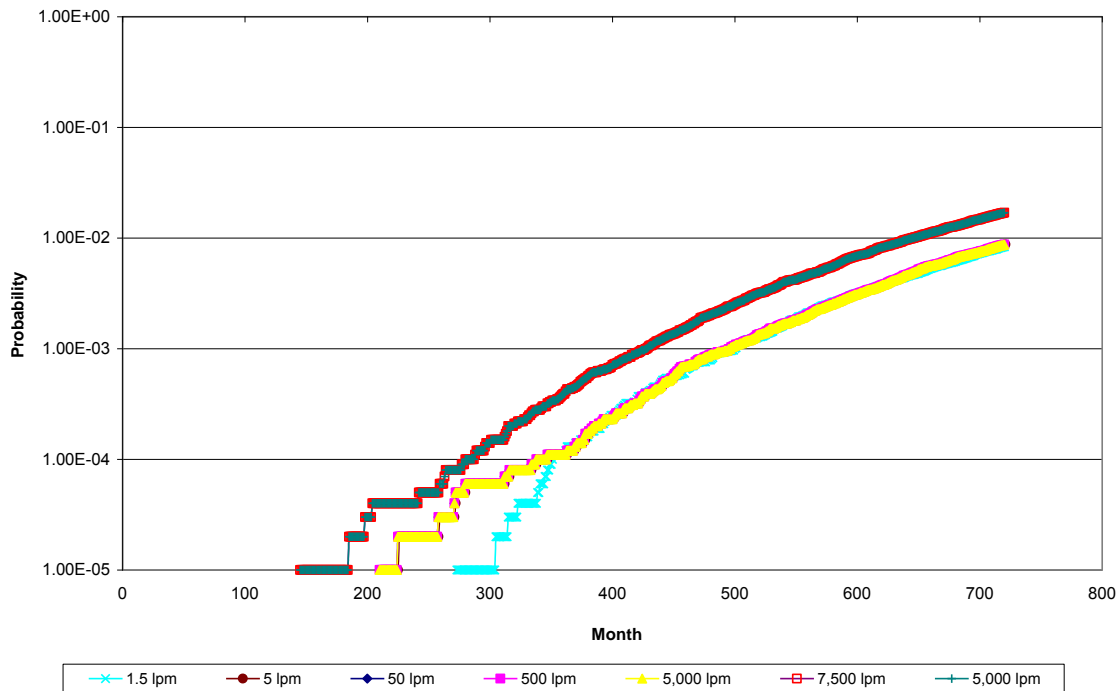


Figure 4.12 Effect of varying the leakage detection limit from 1.5 lpm (0.4 gpm) to 50,000 lpm (13,200 gpm) on the PWR LOCA3 probabilities

Figure 3.42 shows the effect of crack morphology on the PWR LOCA probabilities. As can be seen in this figure the smoother crack surface resulted in lower Category 3 LOCAs. Smoother crack faces should result in more leakage (easier to detect) for the same crack opening area and same thermal-hydraulic conditions (i.e., fluid temperature and pressure). Since cracks are easier to detect, one would expect that the resultant LOCA probabilities should decrease. The fact that there is no effect on the through-wall crack probabilities makes sense in that up to the first occurrence of a through-wall crack there is no leakage and the crack morphology is not a parameter of concern. The fact that there is little or no effect on the LOCA2 probabilities is more difficult to discern. However, when one considers that the leakage detection limit for these cases was set to 1,890 lpm (500 gpm), the Category 2 LOCA threshold may be below this limit such that the Category 2 LOCA probabilities are unaffected by leakage much in the same way that the through-wall crack probabilities are not. As a result, if the Category 2 LOCA probabilities are independent of leakage detection, they will also be independent of crack morphology.

4.4 Key Parameters Affecting LOCA Probabilities

Two parameters which seem to have a large effect on the LOCA probabilities are water chemistry for the BWRs and operating temperature of the PWRs. The operating temperature of the PWR was especially significant where a 22 C (40 F) drop in temperature resulted in a 3 to 4 order magnitude decrease in the LOCA probabilities. Both of these parameters (water chemistry and temperature) effect both crack initiation and crack growth. Static bending stress, which also affects the crack initiation and growth characteristics, also had a significant effect on the LOCA

probabilities. For the BWRs, increasing the static bending stress from 20 MPa (3 ksi) to 50 MPa (7 ksi) resulted in a 1 ½ order of magnitude increase in the Category 2 LOCAs and a 3 order of magnitude increase in the Category 3 LOCAs. Similarly, doubling the static bending stress for the PWRs resulted in a 1 ½ order of magnitude increase in the Category 2 LOCAs and almost a 2 order of magnitude increase in the Category 3 LOCAs.

While inspection parameters had an effect on the LOCA probabilities, their impact did not seem to be as significant as those parameters which affect crack initiation and growth. Increasing the inspection interval from 10 to 20 years caused an order of magnitude or less increase in the LOCA probabilities. In a similar vein improving the quality of the POD curve caused a reduction in the LOCA probabilities although the impact was not that significant. To achieve a comparable order of magnitude decrease in LOCA probability required reducing the probability of detection by a factor of four. When a more realistic reduction in POD was assumed, the effect on the LOCA probabilities was minor. A related parameter to inspection is leakage detection limit. The results for leakage detection limit are somewhat counter intuitive. For the analyses conducted as part of this effort, leakage detection limit does not seem to have that big of an effect on the resultant LOCA probabilities. This finding deserves further exploration.

In contrast to those parameters which affect crack initiation and crack growth, those parameters which affect crack stability did not seem to have much of an effect on the LOCA probabilities. Neither material strength nor toughness had much of an effect on the LOCA probabilities. Even when the fracture toughness was decreased by a factor 20, the effect on the LOCA probabilities was not that significant. Another parameter which would affect crack stability is an earthquake. The addition of an earthquake to the PWR load history resulted in about a one order of magnitude increase in the LOCA probabilities. While this seems significant, it was shown earlier that the magnitude of this earthquake was quite severe. With a more representative earthquake the effect of the earthquake would be expected to be much less.

4.5 Current Limitations and Shortcomings of PRO-LOCA

When PRO-LOCA was initially developed, the plan was to incorporate the latest state-of-art deterministic models into a probabilistic framework that could be used to help make regulatory assessments, such as assessing the NRC's revised emergency core cooling system requirements in 10 CFR 50.46. Older deterministic methods such as limit load analyses for crack stability were to be replaced by the latest, most up to date methods, such as J-estimate scheme routines based on elastic-plastic fracture mechanics principles. To facilitate and expedite this approach, the plan called for using legacy codes where available. As such, major sections of such legacy codes as SQUIRT, NRCPIPE and NRCPIPES were incorporated in their entirety into PRO-LOCA. While this sped up the developmental process, it did create a situation where a great deal of extraneous code was embedded within PRO-LOCA. This extraneous code has turned out to be somewhat problematic to the developmental process. Furthermore, some of the legacy variable definition has proved troublesome as the same parameter has a different variable name in different legacy codes. There have also been issues with some of the common block definitions. In retrospect, in the long run, it would have been better to rewrite these individual modules from scratch instead of using major sections of these previously developed legacy codes. New versions for some of these deterministic modules were developed as part of MERIT. For example, new versions of the LBB.ENG2 through-wall crack stability routine and the DPZP surface crack and through-wall crack stability routines were developed, but were not incorporated into PRO-LOCA due to

budgetary limitations. In addition, to creating coding problems, this unneeded legacy code is undoubtedly impacting the run times for PRO-LOCA. As part of the development process of the new LBB.ENG2 routine, it was found that the new routine was much quicker and more efficient than the legacy LBB.ENG2 routine currently incorporated in PRO-LOCA.

Furthermore, the plan is to rewrite the SQUIRT2 module, which is currently written in Quick Basic, into FORTRAN as part of a new NRC program. In rewriting SQUIRT2, much of the extraneous legacy code will be eliminated. In addition, the plan is to address a number of the technical limitations with SQUIRT. One such limitation is a limitation with the orifice flow model used in SQUIRT. Currently SQUIRT assumes a constant pressure up stream of the break. If the thermo-hydraulic conditions inside the pipe are subcooled and the break is large enough, the fluid will flash to steam and the pressure will eventually drop to the saturation pressure or below. As a result, the assumption embedded in SQUIRT of a constant upstream pressure will result in an over-prediction of the flow rate. One possible fix to address this issue is if the break opening exceeds a certain value, then SQUIRT would assume that the upstream pressure drops to the saturation pressure. In addition, the transition flow model (i.e., for the flow regime between where the Henry-Fauske tight crack model and the orifice flow model are valid) that was developed as part of MERIT has not yet been incorporated into PRO-LOCA. As part of this new NRC effort, that new transition flow model will be incorporated into PRO-LOCA.

Another limitation with PRO-LOCA is the level of quality assurance behind it. As described in Section 3.1, a number of the deterministic modules in PRO-LOCA were subjected to QA checks. However, the level of that QA is not to the level required by ASME NQA-1 (Ref. 4.13). Part I of NQA-1-2008, *Quality Assurance Requirements for Nuclear Facility Applications*, is organized as 18 separate requirements to mirror the 18-criteria structure of 10 CFR Part 50 Appendix B, *Quality Assurance Criteria for Nuclear Power Plants and Fuel Reprocessing Plants*, and, as such is intended to meet and implement the requirements of Appendix B. Some of the key requirements of NQA-1-2008 not formally implemented as part of the PRO-LOCA development process to date include:

- Requirements definition/documentation, including interface control documentation,
- Process design documentation,
- Test plans/procedures with acceptance criteria definition and documentation,
- Configuration management,
- Quality assurance plan documentation.

As such, PRO-LOCA in its current state of development is considered to be more of a research code than a regulatory tool. Furthermore, while PRO-LOCA represents a significant advancement in probabilistic analyses, the NRC is moving towards the development of a suite of new probabilistic codes, xLPR and the modular code, which may replace the PRO-LOCA code as the probabilistic tool of choice. The xLRP code, which stands for eXtremely Low Probability of Rupture, is the first code to be developed, scheduled for release in 2012, and will be used as a means to demonstrate compliance with the 10CFR50 Appendix A, General Design Criterion 4 (GDC-4) requirement that the primary system pressure piping exhibit an extremely low probability of failure. The goal being to address the current limitation with the NRC's Standard Review Plan 3.6.3 for leak-before-break (LBB) analyses which does not allow for the application of LBB to piping systems subjected to active degradation mechanisms, such as exists today with PWSCC in a number of PWR piping systems previously approved for LBB. While the xLRP code will focus primarily on piping, the NRC's new modular code will also address vessel and steam generator issues.

Another possible limitation with PRO-LOCA is how it handles uncertainty. This remains a point of debate within the technical community. PRO-LOCA handles all uncertainty the same while other codes treat aleatory uncertainty differently than epistemic uncertainty. Aleatory uncertainty, i.e., inherent randomness or variability, is uncertainty that cannot be reduced with further measurement, e.g., the time and magnitude of a seismic event. While epistemic uncertainty, i.e., lack of knowledge, is uncertainty that can be reduced if additional measurements or data are made available, e.g., weld residual stress thresholds for stress corrosion cracking. In some of these other codes, the epistemic uncertainty is modeled differently than the aleatory uncertainty. Whether this is an issue of significance remains to be seen.

Another limitation with PRO-LOCA is a lack of user experience. In comparing the development process of PRO-LOCA with that of SQUIRT, SQUIRT has been developed over the past 20 years and has been subjected to significant user experience. As a result of that user experience, a number of errors have been identified and subsequently addressed. PRO-LOCA on the other hand has not been exposed to nearly as wide an audience of users as SQUIRT, or for as long a time, and as such has not received this valuable feedback.

Finally, one possible observed limitation with PRO-LOCA that deserves further examination is the fact that for the sample cases considered in the sensitivity analyses discussed in Section 3 is that for each case the LOCA probabilities for the Category 4, 5, 6, and 7 LOCAs were all the same. Since these probabilities are threshold values, this implies that any large break which occurred immediately grew to a size that resulted in a Category 7 LOCA, and there were no LOCAs of a size that just met the Category 4, 5, or 6 thresholds. In other words, there were no LOCAs of a size in the bins between a Category 4 and 5 LOCA or between a Category 5 and 6 LOCA or between a Category 6 and 7 LOCA. This observation deserves additional scrutiny.

In all likelihood, many of these limitations and shortcomings will be addressed as part of the NRC's new xLPR and modular code development process. The new crack stability routines for through-wall cracks (LBB.ENG2 and DPZP) and surface cracks (DPZP) developed as part of MERIT will likely be incorporated into these new codes. In addition, the plan is to rewrite the SQUIRT2 module, which is currently written in Quick Basic, into FORTRAN. Other modules will undoubtedly be updated as well. Another program that may be used to help address some of these limitations is the PARTRIDGE program. PARTRIDGE, which stands for **P**robabilistic **A**nalysis as a **R**egulatory **T**ool for **R**isk **I**nformed **D**ecision **G**uidanc**E**, is a follow on to the MERIT program, with five distinct objectives:

- Provide a mechanism by which the international community can participate in the development process of the xLPR and modular codes,
- Enhancing the quality assurance basis for PRO-LOCA, and as such, the quality assurance basis for some of the deterministic modules in xLPR and the Modular code,
- Improving the efficiency of PRO-LOCA,
- Making improvements to the graphical user interface (GUI) for PRO-LOCA, and
- Providing additional user support for PRO-LOCA.

In retrospect one of the valuable lessons learned from this development process is the issue raised by the lack of formalized requirements documents, interface control documents, configuration management system, and acceptance criteria for verification and validation activities. As such, more upfront planning with formalized documentation will be a key part of the PARTRIDGE program, and hopefully of the xLPR and modular code development process.

Finally, with the initiated efforts to develop xLPR and the modular code, and the possible de-emphasis on PRO-LOCA, a natural question is how much investment is warranted for a code, such as PRO-LOCA, which may have a relatively short shelf life. While the NRC and US

industry are moving towards xLPR and the modular code, and away from PRO-LOCA, it should be recognized that both xLPR and the modular code are still several years from being ready for use. Current schedules indicate that xLPR will not be ready for release until sometime in 2012 while the modular code will not be ready until 2015. PRO-LOCA is available now, and with the effort proposed for PARTRIDGE, PRO-LOCA will fill the critical need for probabilistic pipe fracture analysis until the xLPR and modular codes are ready for use. In addition, improvements made to PRO-LOCA as part of PARTRIDGE have a good chance of finding their way into xLPR and the modular code. In addition, PRO-LOCA can be used in its current state of development to help guide the development process of xLPR and the modular code, especially in terms of identifying key models and parameters which affect LOCA probabilities most and the required inputs, though sensitivity analyses similar to those discussed earlier in this report.

4.6 References

- 4.1 Harris, D. O., and others, —Probability of Pipe Fracture in the Primary Coolant Loop of a PWR Plant, Vol. 5: Probabilistic Fracture Mechanics Analysis,” NUREG/CR-2189, Vol. 5, August 1981.
- 4.2 Harris, D. O., and others, —Theoretical and User’s Manual for pc-PRAISE, A Probabilistic Fracture Mechanics Code for Piping Reliability Analysis,” NUREG/CR-5864, July 1992.
- 4.3 Harris, D. O., and Dedhia, D., —WinPRAISE: PRAISE Code in Windows,” Engineering Mechanics Technology, Inc. Technical Report TR-98-4-1, 1998.
- 4.4 Tregoning, R., Abramson, L., and Scott, P., —Estimating Loss-of-Coolant Accident (LOCA) Frequencies Through the Elicitation Process,” NUREG-1829, April 2008.
- 4.5 Shack, W. J., —Environmentally Assisted Cracking in Light Water Reactors: Semiannual Report, July-December 1999,” NUREG/CR-4667 Vol. 29, 2000.
- 4.6 Shack, W. J., and others, —Measurement of Residual Stresses in Type-304 Stainless Steel Piping Butt Weldments,” EPRI Report NP-1413, June 1980.
- 4.7 Kumar, V., German, M., and Shih, C., —An Engineering Approach to Elastic-Plastic Fracture Analysis,” EPRI Report NP-1931, 1981.
- 4.8 Wilkowski, G. M., and Scott, P. M., —A Statistical Based Circumferentially Cracked Pipe Fracture Mechanics Analysis for Design or Code Implementation,” Nuclear Engineering and Design, Vol. III, pp. 173-187, 1989.
- 4.9 Giles, P., and Brust, F. W., —Approximate Methods for Fracture Analysis of Tubular Members Subjected to Combined Tension and Bending Loads,” Proceedings of the 8th OMAE Conference, Hague, The Netherlands, 1989.
- 4.10 Brust, F. W., and others, —Assessment of Short Through-Wall Circumferential Cracks in Pipes,” NUREG/CR-6235, April 1995.
- 4.11 Krishnaswamy, P., and others, —Fracture Behavior of Short Circumferentially Surface-Cracked Pipe,” NUREG/CR-6298, November 1995.
- 4.12 Chokshi, N., Shaikat, S., Hiser, A., DeGrassi, G., Wilkowski, G., Olson, R., and Johnson, J., —Seismic Considerations for the Transition Break Size,” NUREG-1903, February 2008.

4.13 —Quality Assurance Requirements for Nuclear Facility Applications,” ASME NQA-1-2008, March 2008.

5.0 CONCLUSIONS

The MERIT program was an internationally cooperative research program whose main goal was the further development of the PRO-LOCA probabilistic fracture mechanics code. While significant improvements have been made to PRO-LOCA as part of the MERIT program, it is still considered a research code and any use of PRO-LOCA must factor that into consideration.

The code was originally developed as part of the US NRC's Large Break LOCA program. It was originally envisioned that PRO-LOCA would be used to augment the expert elicitation process for redefining the emergency core cooling system (ECCS) requirements in 10 CFR 50.46 as documented in NUREG/CR-1829. Other possible uses for PRO-LOCA include helping to prioritize maintenance activities, including in-service inspection prioritization, and helping to make risk-informed estimates of the failure probability of a piping system if a crack is detected in service.

As part of the NRC's Large Break LOCA program many enhancements in the technology developed since some of the earlier probabilistic codes (e.g., PRAISE) were developed were incorporated into the PRO-LOCA code. These enhancements include improved crack stability analyses, improved leak rate models, and new material property data. In addition, new degradation mechanisms, including the addition of primary water stress corrosion cracking (PWSCC) for dissimilar metal welds (DMWs) in pressurized water reactors (PWRs) were added. Updates to the crack initiation and growth models, weld residual stress distributions, inspection and repair schemes were also included.

After its initial development as part of the Large Break LOCA program, PRO-LOCA was further updated during the MERIT program. Some of the enhancements made to PRO-LOCA as part of MERIT include:

- Providing more user defined input parameters, e.g., user defined weld residual stress distributions, user defined crack growth laws, user defined material data, user defined crack morphology parameters, and user defined random seed,
- Incorporating alternative crack initiation models, e.g., single versus multiple crack initiation analyses and arrival rate models,
- Incorporating alternative inspection and probability of detection (POD) routines,
- Allowing a variable stress distribution around the pipe circumference,
- Incorporating advanced probabilistic routines, e.g., discrete probability methods, including importance sampling, in addition to Monte Carlo simulation,
- Incorporating bootstrap methods for predicting confidence limits to provide insights into the variability of results, and
- Updating the graphical user interface (GUI) to reflect the most up-to-date changes to PRO-LOCA.

As part of this report a series of sensitivity analyses were presented and discussed. One of the key objectives of those analyses was to ascertain what parameters had the most significant effects on the resultant LOCA probabilities. Two parameters which seem to have a large effect on the LOCA probabilities are water chemistry for the BWRs and operating temperature of the PWRs. The operating temperature of the PWR was especially significant where a 22 C (40 F) drop in temperature resulted in 3 or 4 order magnitude decrease in the LOCA probabilities. Both of these parameters (water chemistry and temperature) effect both crack initiation and crack growth. Static bending stress, which also affects the crack initiation and growth characteristics, also had a significant effect on the LOCA probabilities. For the BWRs, increasing the static bending stress from 20 MPa (3 ksi) to 50 MPa (7 ksi) resulted in a 1 ½ order of magnitude increase in the

Category 2 LOCAs and a 3 order of magnitude increase in the Category 3 LOCAs. Similarly, doubling the static bending stress for the PWRs resulted in a 1 ½ order of magnitude increase in the Category 2 LOCAs and almost a 2 order of magnitude increase in the Category 3 LOCAs.

While inspection parameters had an effect on the LOCA probabilities, their impact did not seem to be as significant as those parameters which affect crack initiation and growth. Increasing the inspection interval from 10 to 20 years caused an order of magnitude or less increase in the LOCA probabilities. In a similar vein improving the quality of the POD curve caused a reduction in the LOCA probabilities although the impact was not that significant. To achieve a comparable order of magnitude decrease in LOCA probability required reducing the probability of detection by a factor of four. When a more realistic reduction in POD was assumed, the effect on the LOCA probabilities was relatively minor. A related parameter to inspection is leakage detection limit. The results for leakage detection limit are somewhat counter intuitive. For the analyses conducted as part of this effort, leakage detection limit does not seem to have that big of an effect on the resultant LOCA probabilities. This finding deserves further exploration.

In contrast to those parameters which affect crack initiation and crack growth, those parameters which affect crack stability did not seem to have much of an effect on the LOCA probabilities. Neither material strength nor toughness had much of an effect on the LOCA probabilities. Even when the fracture toughness was decreased by a factor 20, such that stability would be expected to be governed by elastic plastic fracture mechanics instead of limit load, the effect on the LOCA probabilities was not that significant. Another parameter which would affect crack stability is an earthquake. The addition of an earthquake to the PWR load history resulted in about a one order of magnitude increase in the LOCA probabilities. While this seems significant, it was shown that the magnitude of this earthquake was quite severe. With a more representative earthquake signature, the effect of the earthquake would be expected to be less.

While PRO-LOCA represents a significant advancement in the technology, there is still work to be done. When PRO-LOCA was initially developed, the plan was to incorporate the latest state-of-art deterministic models into a probabilistic framework. Older deterministic methods such as limit load analyses for crack stability were to be replaced by the latest, most up to date methods such as J-estimate scheme routines based on elastic-plastic fracture mechanics principles. To facilitate and expedite this approach, the plan called for using legacy codes where available. As such, major sections of such legacy codes as SQUIRT, NRCPIPE and NRCPIPES were incorporated in their entirety into PRO-LOCA. While this sped up the developmental process, it did create a situation where a great deal of extraneous code was embedded within PRO-LOCA. This extraneous code has turned out to be somewhat problematic to the developmental process. Furthermore, some of the legacy variable definition has proved troublesome as the same parameter has a different variable name in different legacy codes. There have also been issues with some of the common block definitions. In retrospect, in the long run, it would probably have been more advantageous to rewrite these individual modules from scratch instead of using major sections of these previously developed legacy codes. New versions for some of these deterministic modules were developed as part of MERIT. New versions of the LBB.ENG2 through-wall crack stability routine and the DPZP surface crack and through-wall crack stability routines were developed, but were not incorporated into PRO-LOCA due to budgetary limitations. In addition, to creating coding problems, this unneeded legacy code is undoubtedly impacting the run times for PRO-LOCA. As part of the development process of the new LBB.ENG2 routine, it was found that the new routine was much quicker and more efficient than the legacy LBB.ENG2 routine currently incorporated in PRO-LOCA.

A further general limitation with PRO-LOCA is the level of quality assurance behind it. For example, as described in Section 3.1 a number of the deterministic modules in PRO-LOCA were subjected to some QA. However, the level of that QA and the overall QA for PRO-LOCA are not

to the level required by ASME NQA-1. Part I of NQA-1-2008, *Quality Assurance Requirements for Nuclear Facility Applications*, is organized as 18 separate requirements to mirror the 18-criteria structure of 10 CFR Part 50 Appendix B, *Quality Assurance Criteria for Nuclear Power Plants and Fuel Reprocessing Plants*, and, as such is intended to meet and implement the requirements of Appendix B. Some of the key requirements of NQA-1-2008 not formally implemented as part of the PRO-LOCA development process to date include:

- Requirements definition/documentation, including interface control documents,
- Process design documentation,
- Test plans/procedures with acceptance criteria definition and documentation,
- Configuration management,
- Quality assurance plan documentation.

As such, PRO-LOCA in its current state of development is considered to be a research code and any use of PRO-LOCA must factor that into consideration.

Appendix A

Details of the Development of Geometric Specific Weld Residual Stress Distributions Included in PRO-LOCA

A.1 Introduction

In the FY04 version of the code, the only options available for considering the weld residual stresses were to assume the ASME code specified values or to provide a 4th order polynomial fit of a user defined residual stress solution. In FY05, new solutions, based on detailed finite element analyses, for the hot leg to reactor pressure vessel (RPV) nozzle dissimilar weld, the surge line to pressurizer nozzle dissimilar weld, and the pressurizer spray line to pressurizer nozzle dissimilar weld were all added to the PRO-LOCA code. In addition, two stainless-to-stainless weld solutions were included. The hot leg/RPV dissimilar weld and the stainless-to-stainless similar weld solutions were developed for both the case of with and without an ID repair weld. For the case of an ID repair weld, the last pass of weld material (~ 15 percent of the wall thickness) on the ID surface was ground out and weld metal was re-deposited in the ground out area. The surge line to pressurizer nozzle weld solutions were only for the case of an ID repair weld. Due to size limitations, the spray nozzle solutions were only for the case of no ID repair weld.

For each of the dissimilar weld cases, solutions were developed using the Nickel alloy weld tensile properties as well as the stainless and ferritic steel tensile properties. The Nickel alloy weld tensile properties were used for the analysis of the residual stresses in the weld and buttered regions. The stainless and ferritic steel tensile properties were used in the analysis of the heat-affected-zone and fusion line residual stresses. For each case, solutions were developed for the mean tensile properties as well as the means plus and minus two standard deviation tensile properties. For the weld metal cases, solutions were developed for weld centerline and along paths in the weld metal and buttered region where the residual stresses were the highest. For the stainless and ferritic steel cases, solutions were developed for both the heat-affected-zone (HAZ) as well as along the fusion line.

The maximum weld residual stress in the sensitized region for a particular component was incorporated into the PRO-LOCA code. For example, for the stainless steel recirculation line in a BWR, since the heat affected zone is the sensitized region, which is where stress corrosion cracks will initiated and grow, the maximum stress distribution through the thickness in the heat affected zone was incorporated into the PRO-LOCA code. For the dissimilar weld metal cases, the solutions incorporated into the PRO-LOCA code were the maximum stresses in the weld or buttered region, whichever was greater, which is where pressurized water stress corrosion cracks would most likely initiate and grow. In all cases, the weld residual stresses were normalized by the yield strength of the material and fit to a 4th-order polynomial, see Figure A.1. This normalization will allow the weld residual stresses to be random in nature.

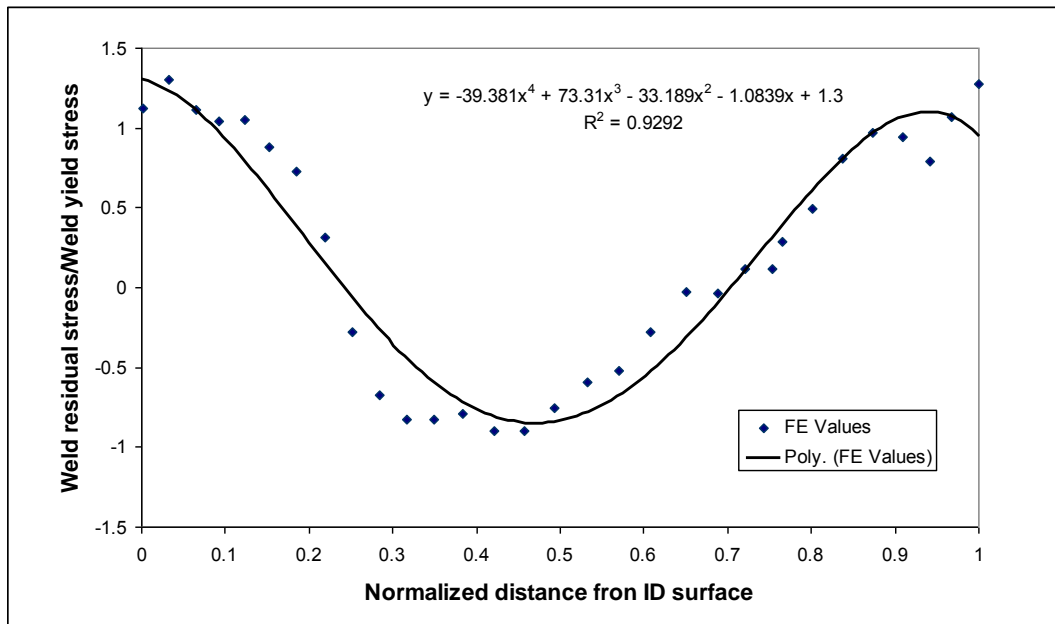


Figure A.1 Curve fit of weld residual stresses for inclusion into PRO-LOCA

A.2 Weld Analysis Procedure

Most computational weld models which are available commercially are mathematics and physics based modules; (i) thermal modules and (ii) structural models. The following is a description of the VFT™ (Ref. A.1) code, but other codes are similar (VFT™ is commercially available now). There are two main analysis modules, the thermal model and the structural model, that make up the weld process simulation models. The thermal model (CTSP) was developed based on superposition of complicated closed form analytical expressions and developed heat source theories. CTSP is very rapid and is used for large problems. Numerical thermal solutions based on a modification of Goldak theory are also used. The numerical solutions were used here since the analyses were made for axi-symmetric pipe welds. It is generally accepted that axi-symmetric analyses of girth welded pipe welds tend to produce conservative residual stress predictions compared with full three dimensional solutions. The structural model (UMAT) was developed based on ABAQUS commercial finite element codes by implementing a special materials module, which includes a constitutive law that permits stress relief due to weld melting/re-melting effects, strain hardening effects, large deformation mechanisms, rapid weld metal deposition features, phase transformation plasticity (based on the Leblond model [Ref. A.2]), etc. It is noted that experience clearly suggests that uncoupled thermal/structural solutions for weld problems is accurate in all weld models. Many more details of the VFT code, with many example solutions can be found in Reference A.3 and in the many references therein.

A.2.1 Geometry

Most bi-material welds consist of welding a ferritic pressure vessel steel nozzle to a stainless steel pipe with a Nickel alloy weld metal. There are many different geometries that have been used in actual PWR nuclear plants and there is no standard joint design. The weld residual stress distribution depends strongly on the geometry and the material properties. References A.4 and A.5 provide extensive details about the bimetallic weld modeling procedures used for the V.C.

Summer plant analysis and a new procedure to account for weld induced residual stresses on crack opening displacements. The general procedure of References A.4 and A.5 was followed here and further details can be found these references.

The geometries used for the hot leg, surge line, and spray lines were obtained from the literature and represent typical geometries that exist in PWR plants. Again, many geometries can be found in service and the residual stresses do vary significantly between them. Figure A.2 provides the geometry for the hot leg/RPV nozzle weld and the corresponding axi-symmetric finite element mesh used for the weld residual stress analyses. Note, the top figure in Figure A.2 shows a cross section of an actual cold leg/safe end bimetal weld from a Combustion Engineering plant, but it was thought to be fairly representative of the weld geometry for a hot leg/RPV nozzle weld for these purposes. As is typical of bimetallic welds that were used in nuclear power plants, the ferritic nozzle steel (A516 Grade 70 here but often A508) is first buttered with Alloy 182/82 weld metal and stress heat treated before making the weld. (Note, the RPV nozzle is typically fabricated from a vessel material such as A508, but more A516 Grade 70 tensile data was available for the statistical analysis of the means and standard deviations and the limited A508 data that was available was comparable to the A516 Grade 70 data.) The heat treat consists of heating the nozzle to 593 C (1,100 F) and holding for four hours. The corresponding stress relaxation is modeled via a creep algorithm within the material user routine. After the weld has cooled to room temperature, a hydro-test is modeled. The hydro-test load consists of applying an internal pressure of 1.4 times the normal operating pressure of 15.5 MPa (2,250 psi), i.e., 21.7 MPa (3,150 psi), and then releasing. Because the hot leg, surge line geometry, and spray line nozzle and pipe are very thick, the hydro-test does little to alter the weld induced residual stresses. However, it will be seen that for the stainless steel pipe geometry (discussed later) the hydro-test does modify the weld induced residual stresses. Note, the stainless steel case is for a higher R/t ratio pipe, which may explain this difference in behavior. The results needed for the PRO-LOCA code are the operating temperature residual stresses (324 C [615 F] for the bimetal welds and 288 C [550 F] for the stainless steel pipe).

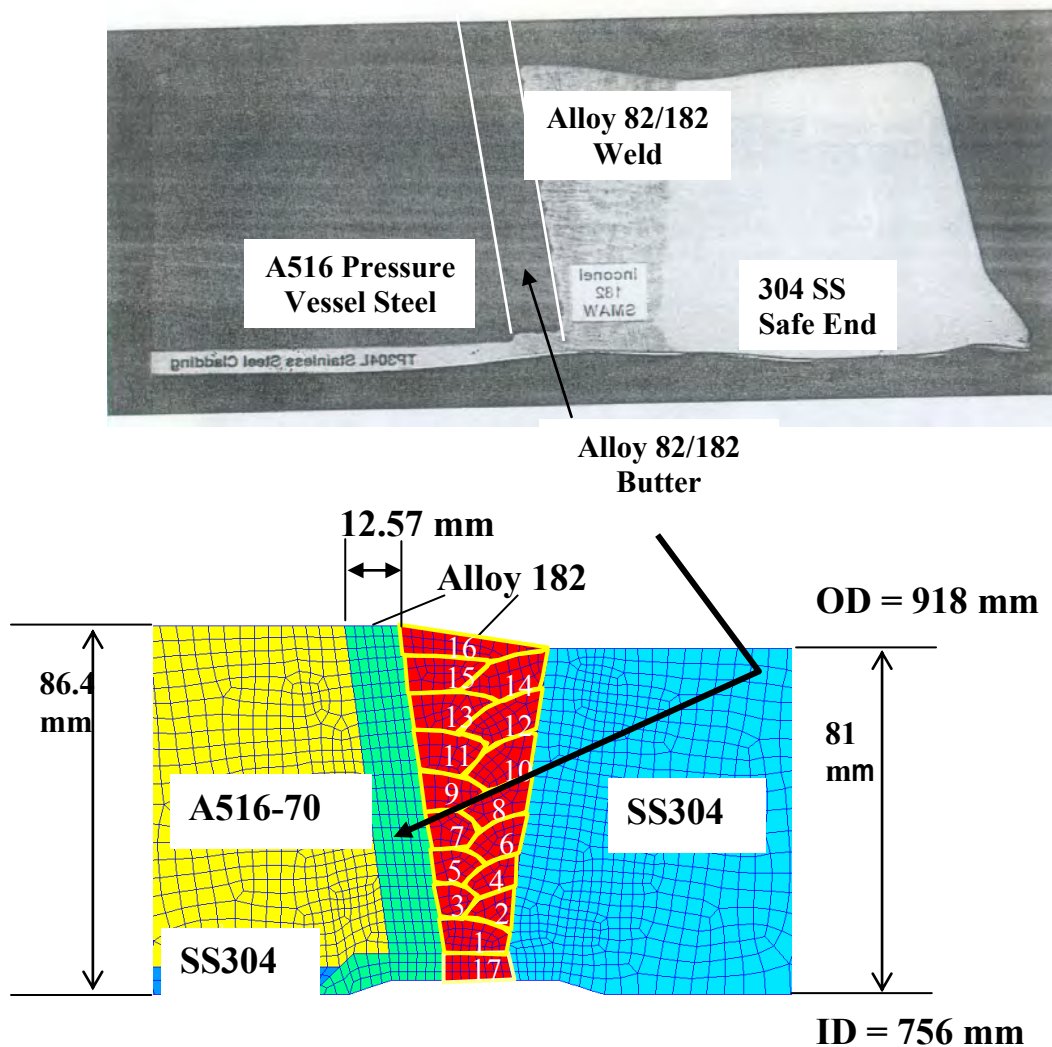


Figure A.2 Bimetal weld geometry used in hot leg/RPV nozzle weld residual stress analysis

The stresses at operating temperature with the internal pressure of 15.5 MPa (2,250 psi) applied are also provided and discussed. This is done because the current version of PRO-LOCA adds the operating loads (bending and pressure) to the weld residual stresses linearly. If the stresses at locations in the weld are at yield (equivalent stresses), then yielding will occur in these regions during load application. As such, the operating stresses used to predict PWSCC and IGSCC crack growth rates may be overestimated if the loads are applied linearly.

The geometry used for the hot leg/RPV nozzle analyses is as shown in Figure A.2. The geometry used for the surge line analysis has an inner radius of 128 mm (5.03 inches), an outer radius of 170 mm (6.68 inches) with a wall thickness of 42 mm (1.65 inches). The mean radius to thickness ratio (R_m/t) for the surge line is 3.5. The geometry for the spray line consisted of an inner radius of 63.9 mm (2.52 inches), outer radius of 90.2 mm (3.55 inches), a wall thickness of 26.2 mm (1.03 inches), and a mean radius to thickness ratio of approximately 3. Finally, the stainless steel pipe considered here had an inner radius of 285 mm (11.2 inches), an outer radius

of 315 mm (12.4 inches), a wall thickness of 30 mm (1.18 inches), and a mean radius to thickness ratio of 10. All of these geometries are rather thick pipes which leads to more complicated weld residual stress patterns.

A.2.2 Material Properties

The PRO-LOCA code is a probabilistic code which is being developed to permit risk informed predictions of loss of coolant accidents given certain inputs. For probabilistic predictions of primary water stress corrosion cracking (PWSCC), the weld residual stresses for the mean, plus two sigma, and minus two sigma material property data are required. For weld residual stress analyses, the material properties are required at temperatures that range from room temperature to melting. However, a statistical distribution of material properties is typically not available at all temperatures up to melting. In fact, for nuclear materials, a material data base is most likely only available at room temperature and at the normal operating temperature of 288 to 323 C (550 to 615 F). The material data base developed as part of this program is also incomplete in that plenty of data is available for some materials, but sparse for other materials.

With this in mind, the following section describes the procedure used to obtain material properties focusing on the Type 304 stainless steel data, recognizing that the data for the other materials were obtained in a similar fashion. From the database used, 23 sets of data are available for Type 304 stainless steel at room temperature and 32 sets of data are available at 288 C. As such, mean data (in the form of stress versus strain curves), $+2\sigma$, and -2σ curves could be estimated based on standard statistical analysis of the data sets. As an example, see Figure A.3. Here the mean curve, $+2\sigma$, and -2σ curves are shown for two temperatures (20 C and 288 C [68 and 550 F]). Figure A.4 shows the temperature dependent stress strain curves (i.e., 20 to 1100 C [68 to 2010 F] data) for Type 304 stainless steel used for the weld analyses. The method for obtaining this data was discussed in References A.4 and A.5. It turns out that this data is nearly mean stress-strain data.

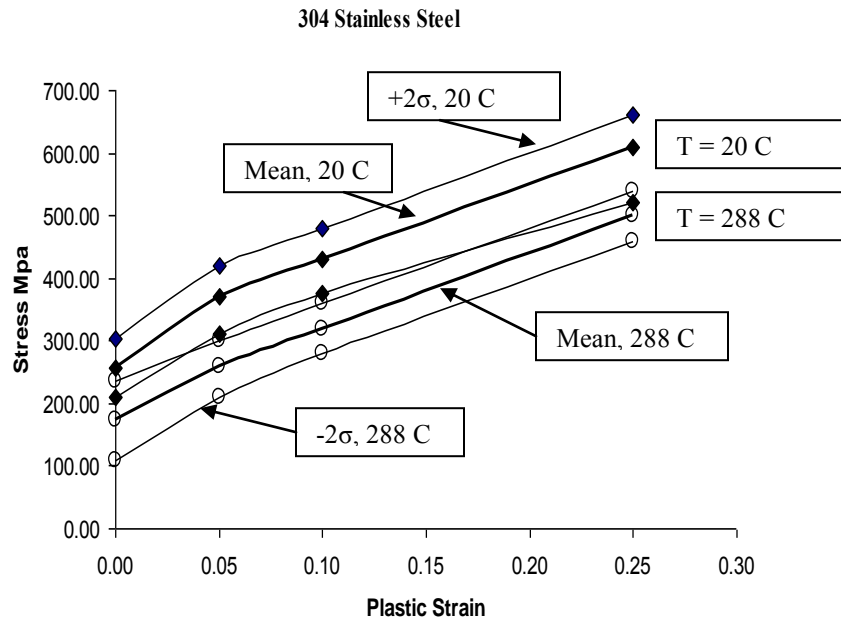


Figure A.3 Stress-strain data for Type 304 stainless steel from the database

In order to get this complete set of stress-strain curves from room temperature to melting (1,400 C [2,550 F]) the following procedure was used. The mean yield strength at 288 C (550 F) is 172.5 MPa (25.0 ksi), the $+2\sigma$ and -2σ yield strength values at 288 C (550 F) are 236 and 109 MPa (34.2 and 15.8 ksi), respectively. The ratio of $+2\sigma$ yield strength to mean yield strength is 1.37 (236/172.5) while the ratio of the -2σ yield strength to mean yield strength is 0.63 (109/172.5). To obtain the yield strength for the $+2\sigma$ data at 371 C (700 F) the yield strength of the mean data for 371 C (700 F) (Figure A.4) is multiplied by 1.37, and to get the -2σ yield strength at 371 C (700 F) the mean yield strength is multiplied by 0.63. From Figure A.4, the mean yield strength at 371 C (700 F) is 162 MPa (23.5 ksi). As such, the $+2\sigma$ and -2σ yield strength values at 371 C (700 F) are 221 and 102 MPa (32.0 and 14.8 ksi), respectively. This same procedure is used for each value of plastic strain where mean data is available. For instance, for a plastic strain value of 0.05, the ratio of $+2\sigma$, and -2σ stresses to mean stress at 288 C (550 F) is 1.15 and 0.81, respectively. As such, the $+2\sigma$, and -2σ stress values at 371 C (700 F) are 286 MPa (41.6 ksi), i.e., 1.15 times 249 MPa (36.1 ksi) from Figure A.4 at 371 C (700 F) for a plastic strain of 0.05, and 202 MPa (29.3 ksi), i.e., 0.81 times 249 MPa (36.1 ksi), respectively. This procedure was then used at all other temperatures. In the absence of statistical data for the $+2\sigma$ and -2σ stress strain data at all other temperatures this procedure appeared rational.

304 Stainless Steel

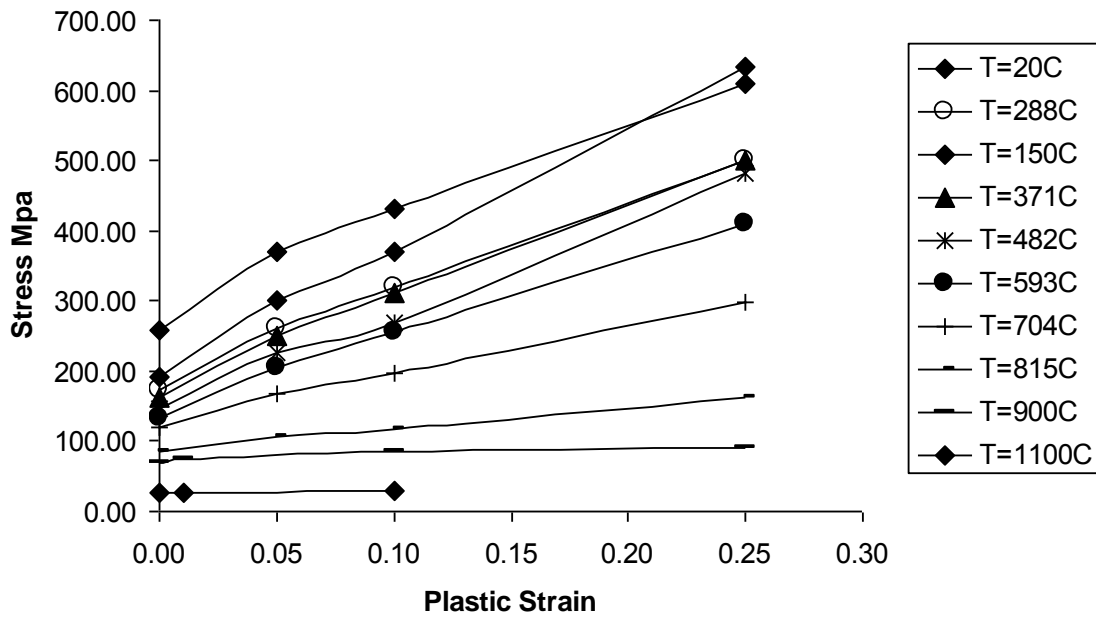


Figure A.4 Mean stress-strain curves for Type 304 stainless steel at various temperatures

Alloy 182/82 Weld Material

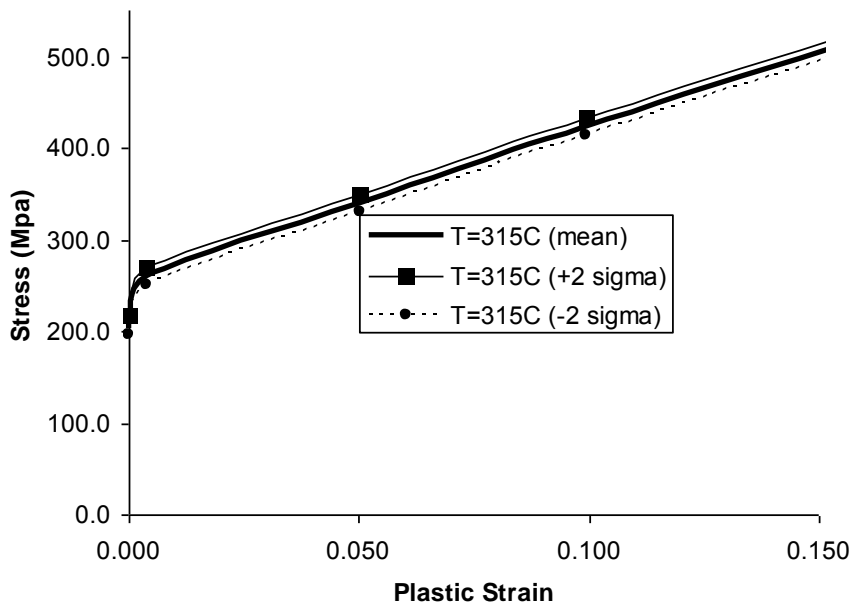


Figure A.5 Mean, +2σ, and -2σ stress strain curves for Alloy 182/82 material

For the other materials used, a similar procedure was used to estimate the $+2\sigma$ and -2σ material data for the weld residual stress analyses. For the A516 Grade 70 material, the baseline mean data is plotted in References A.5. From the material property database, there were 6 and 11 sets of data at 20 and 288 C (68 and 550 F), respectively. This data was used for the $+2\sigma$ and -2σ stress strain curves at these temperatures. The 'ratio' procedure was then used to estimate the $+2\sigma$ and -2σ stress strain curves at other temperatures and plastic strain values. For the Alloy 182/82 weld metal, only the (assumed) mean data were available from Reference A.5. In the database, there was no statistical data available for this material. However, there was data for Alloy 625 (only three sets of data were available). As such, the Alloy 182/82 weld metal was assumed to have the same statistical variation as the Alloy 625 data. Figure A.5 shows this data at 315 C (600 F). It is seen that there is not much statistical scatter in the $+2\sigma$ and -2σ data. This trend carried out throughout the data at all temperatures and plastic strains. This is why when the data is discussed later, there is less scatter in the predicted weld residual stresses in the weld and butter region than might be expected. This trend must be kept in mind as the results are discussed later in this section.

A.3 Dissimilar Metal Weld Results

For bimetal welds in pressurized water reactors (PWRs), primary water stress corrosion cracking (PWSCC) is a major concern. Referring to Figure A.2, PWSCC crack growth in the Alloy 182/82 weld material or buttering material is the main concern. In terms of PWSCC, stress solutions were developed for the butter material and the weld metal itself since the PWSCC crack growth constants may differ in these regions. Recall that the butter material is post weld heat treated prior to welding which may affect the microstructure and thus the PWSCC growth rates. Moreover, if a fluid path exists to the ferritic steel (A516 Grade 70 here), which may occur if the cladding is damaged or if PWSCC grows through the butter material, corrosion growth in the nozzle is possible. In the heat affected zone (HAZ) of the stainless steel (Figure A.2), stress corrosion cracking is possible as well. The PRO-LOCA computer code is being developed to be as general as possible. As such, stress solutions were developed for all potential stress corrosion crack growth paths.

In summary, weld residual stress solutions were developed for the (1) butter and (2) weld material (both axial and hoop residual stresses) for circumferential and axial crack growth predictions. In addition, weld residual stresses were tabulated in the A516 Grade 70 nozzle material adjacent to the butter region (axial stresses) and in the HAZ region of the stainless steel. This permits all potential forms of stress corrosion cracking to be considered in bimetal welds.

The PWSCC or SCC crack path will follow the maximum stress locations as the crack proceeds through the thickness of the pipe. This is illustrated in Figure A.6 where a schematic of a crack growing through the Alloy 182/82 weld material is shown. As such, for each of the four locations (discussed in the previous paragraph) the maximum stress through the thickness is compiled. Because of this, axial stresses may not be balanced through the pipe thickness (as they should since the ends of the pipe are free for the weld analysis). Keep this in mind when viewing the stress plots. Of course, the hoop stresses do not have to be self equilibrated.

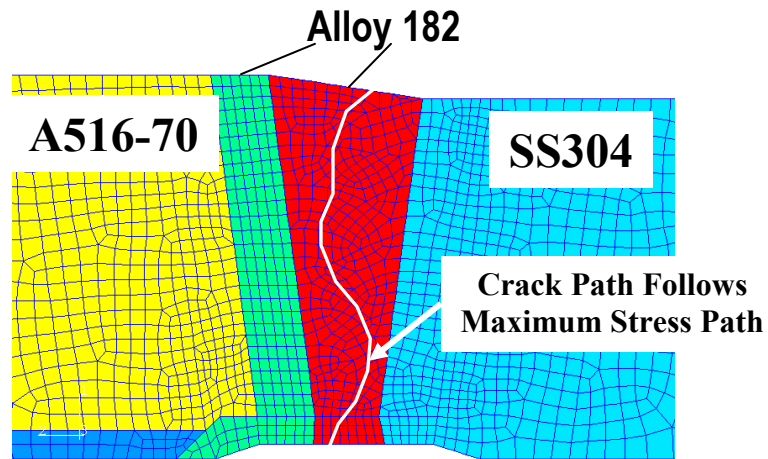


Figure A.6 Illustration of crack path following maximum stress location in weld

In most cases, the bimetal welds in the larger diameter pipe were completed and then the inner diameter (ID) region was ground out (~15% of the wall thickness) and a weld bead re-deposited. It turns out that this repair weld typically increases the tensile residual stresses in the ground out region. This effect is especially detrimental in thick pipe such as in the hot leg and surge line considered here. Figure A.7 illustrates this effect for the hot leg analysis and the mean tensile properties. The effect of the ID repair weld is dramatic. The maximum tensile stresses near the ID are increased along with increasing the maximum value of compressive stresses near mid thickness. For all of the cases considered here (hot leg, surge line, thick stainless steel pipe), the tensile stresses are markedly increased near the inner surface for the weld repair case. This of course suggests that PWSCC and IGSCC growth rates will increase as well. The hoop stresses are also significantly increased by the ID repair weld. The stresses in the A516 Grade70 and the stresses in the Type 304 stainless steel material are also altered by the repair weld, but to a lesser extent. All results presented from this point on include the effect the ID repair weld, except for the spray line where the diameter is too small to perform the ID repair weld.

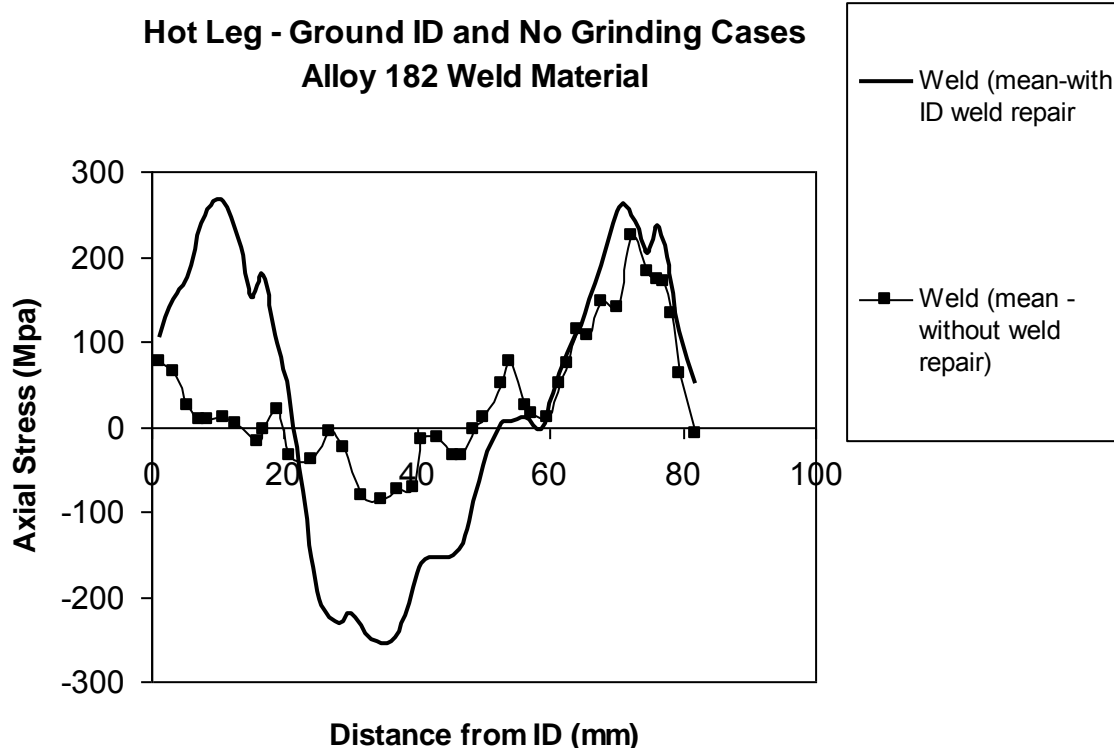


Figure A.7 Comparison of maximum weld residual stresses through the thickness for the hot leg pipe, with and without repair weld

Figure A.8 illustrates the maximum axial stresses in the weld region for the hot leg for the mean, $+2\sigma$, and -2σ analysis cases. Figure A.9 shows the corresponding hoop stresses. The variation in the axial stresses between the $+2\sigma$ and -2σ analysis cases depends on the location through the thickness, but can be in excess of 100 MPa (15 ksi). This is despite the fact that the statistical variation in the material properties for the Alloy 182/82 weld material is not significant here (see Figure A.5) because of the scarcity of data (only three sets of data for Alloy 625 material). As more data is collected, the variation in the stresses for the Alloy 182/82 material is expected to be greater. Figure A.10 shows the axial residual stresses in the hot leg pipe for the case which includes the ID repair welding at three locations: (i) maximum stress in the weld, (ii) maximum stress in the butter, and (iii) the actual stress at a cut directly through the center of the weld. It is seen that the axial stresses in the Alloy 182/82 weld material do vary somewhat significantly with location although the trends are comparable. The main differences appear to be near the ID and OD surfaces.

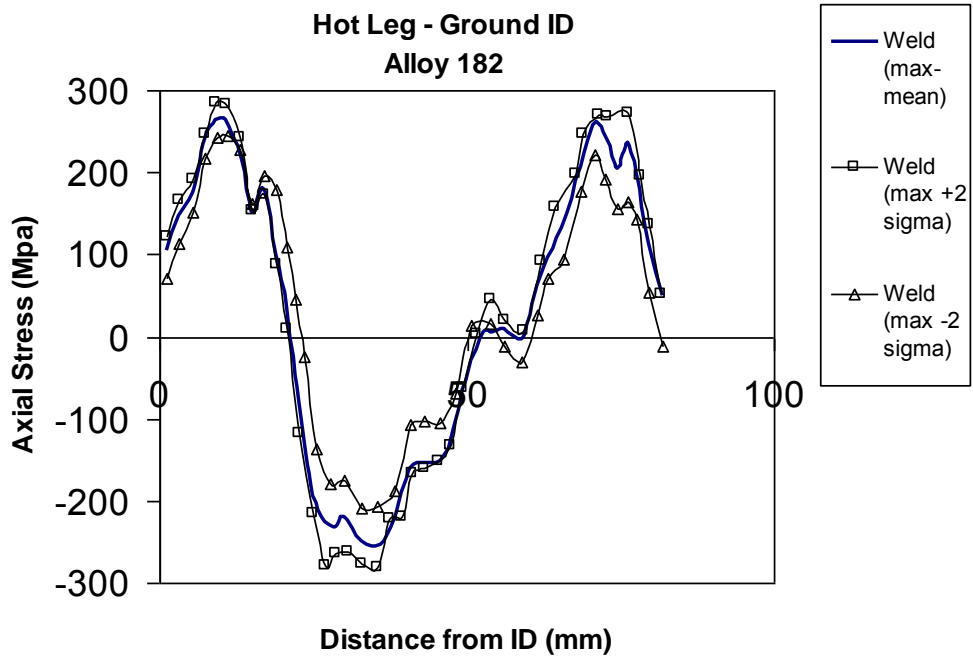


Figure A.8 Axial weld residual stress solutions for hot leg/RPV dissimilar weld with repair weld along the path through the weld region where the weld residual stresses were the highest for the case where the Alloy 182 weld tensile properties were used

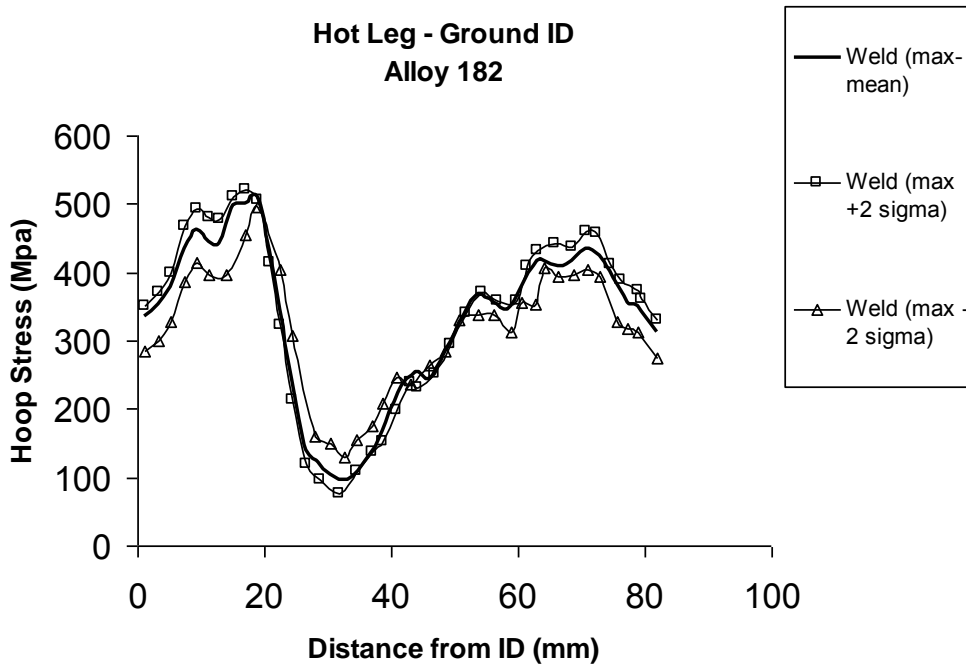


Figure A.9 Maximum hoop residual stresses for hot leg/RPV weld in the weld region

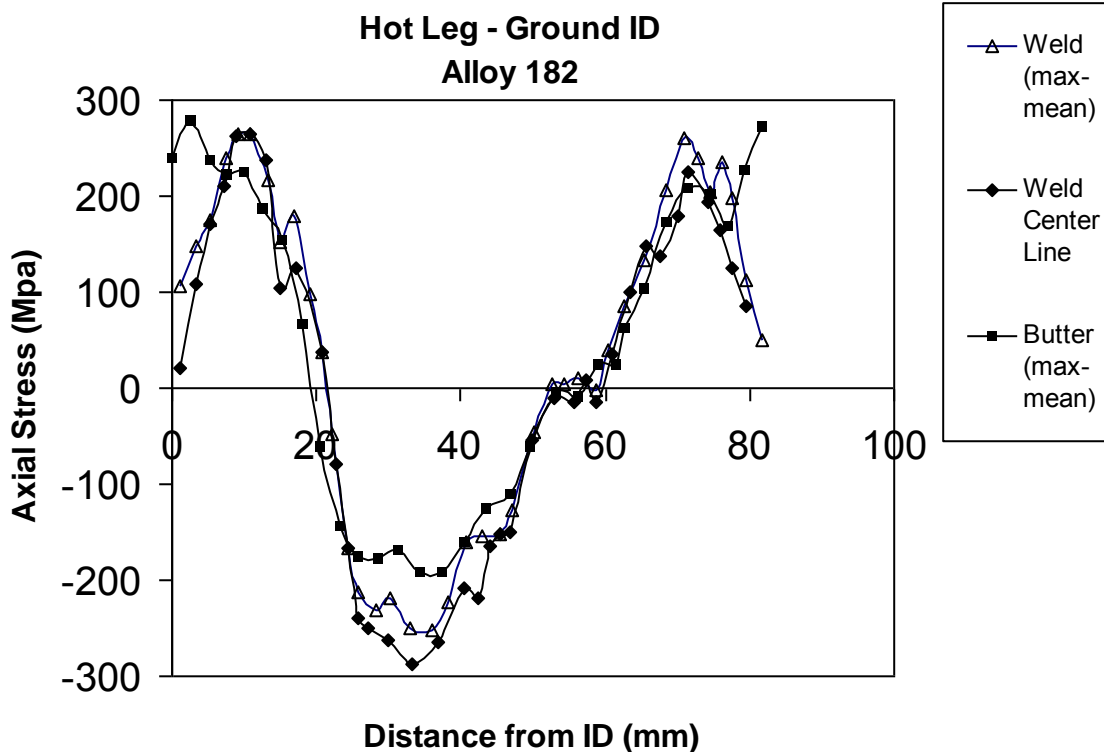


Figure A.10 Axial weld residual stress solution for hot leg/RPV dissimilar weld with repair weld at three locations: (1) at the weld centerline, (2) along the path in the weld where the stresses are highest, and (3) along the path in the buttered region where the stresses are highest

Figure A.11 is a plot of axial through-thickness stress gradients for the hot leg/RPV bimetallic weld in the heat affected zone (HAZ) of the Type 304 stainless steel. The stresses vary by more than 100 MPa (15 ksi) between the $+2\sigma$ and -2σ property variations. It is noted that other combinations of property variations are possible. For instance, it is possible that the A516 Grade 70 properties may have tensile properties that are at the low end (-2σ), the Alloy 182 weld metal may be at the high end ($+2\sigma$), while the Type 304 stainless may have mean properties. Of course there are many other combinations possible. Here, for this version of the PRO-LOCA code, all properties were at the same statistical level. For instance, when a $+2\sigma$ result is shown, it means that all properties (ferritic, weld, and stainless steel) all used tensile properties in the $+2\sigma$ range. These results may be modified to include other possible combinations in a future version of PRO-LOCA.

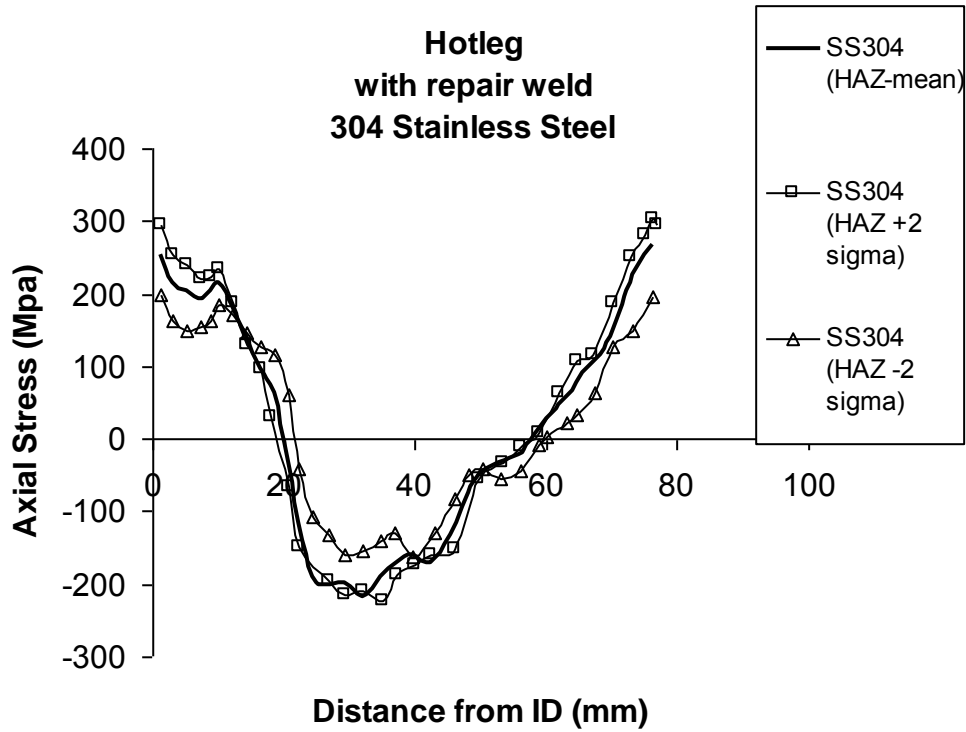


Figure A.11 Hot leg/RPV weld axial stresses in the Type 304 stainless steel HAZ

Similar results for the A516 Grade 70 steel are shown in Figure A.12. Notice that the difference in stresses between the different statistical variations of the tensile properties is somewhat less than that for the Alloy 182 weld and stainless steel. This is probably because the A516 Grade 70 steel is isolated from the weld deposition somewhat since the nozzle and buttered region are heat treated after the butter layer is deposited.

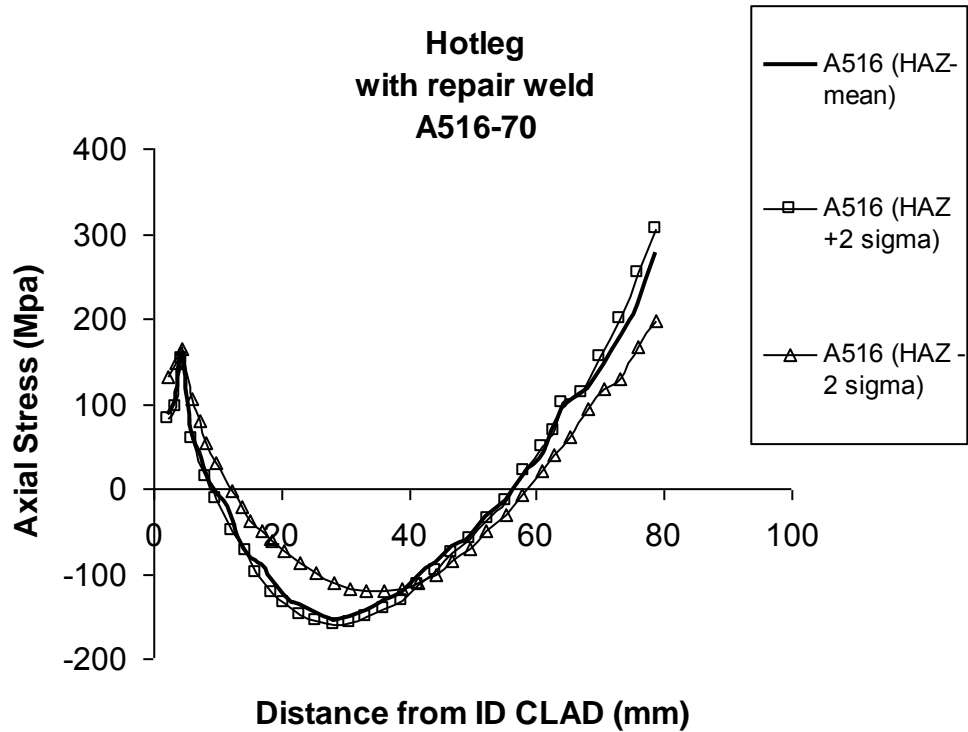


Figure A.12 Maximum hot leg/RPV stresses in the A516 Grade 70 steel

The axial stresses for the surge line/pressurizer nozzle weld are shown in Figure A.13 while the hoop stresses in the weld zone are shown in Figure A.14. The stresses for the surge line analysis, with a mean diameter of 298 mm (11.7 inches), appear to be less variable for the different statistical variations of tensile properties compared with the hot leg. The residual stress pattern is also different. The hoop stresses, which will lead to axial PWSCC cracks, as were found in the V.C. Summer hot leg/RPV weld, show more statistical variation compared with the axial stresses for this case.

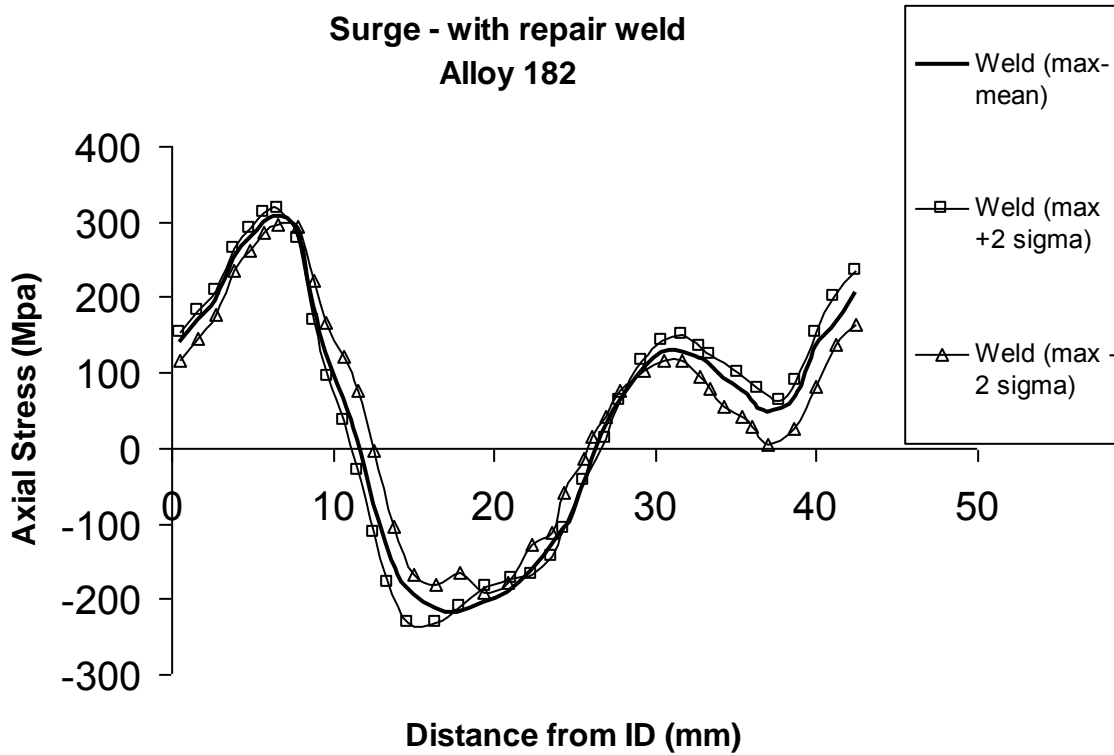


Figure A.13 Axial stresses in surge line/pressurizer nozzle weld

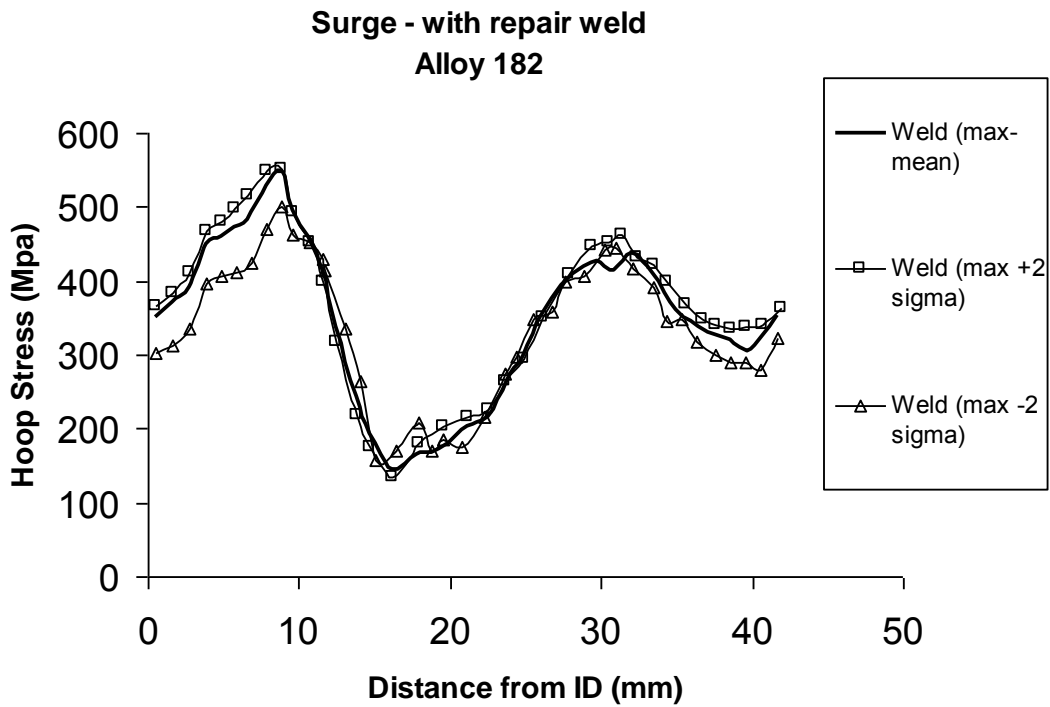


Figure A.14 Hoop stresses in the surge line/pressurizer nozzle weld

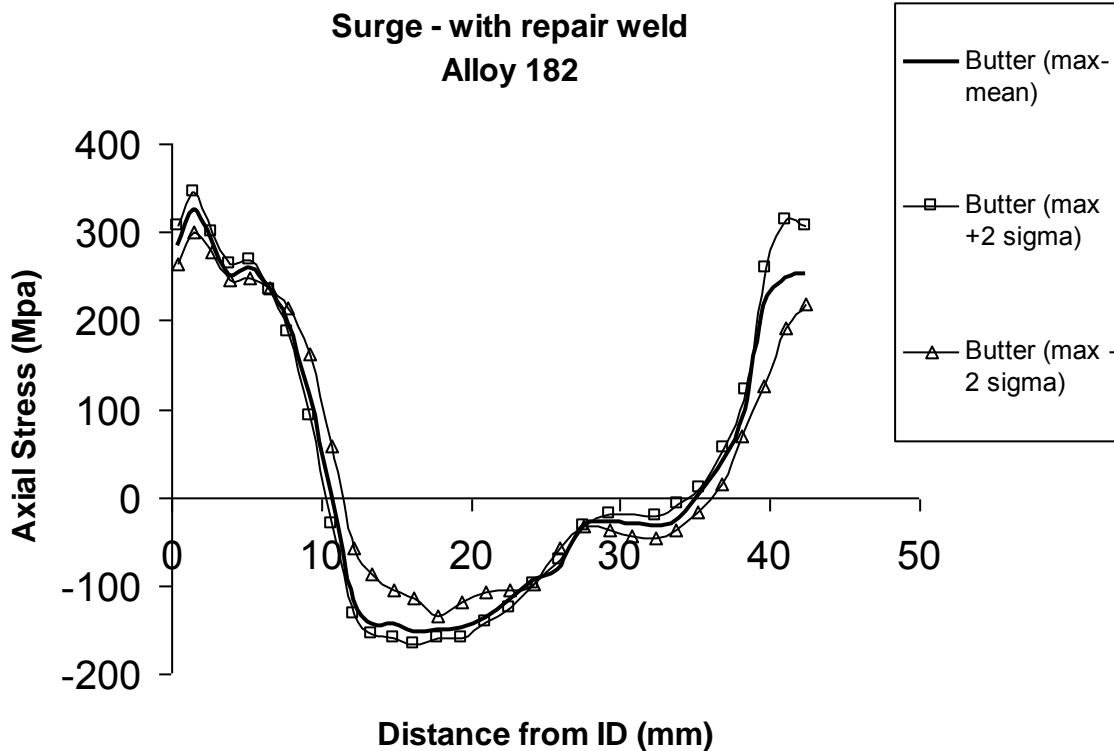


Figure A.15 Axial residual stresses in the buttered region for surge line to pressurizer nozzle weld

Figure A.15 shows the axial residual stresses in the buttered region for the surge line to pressurizer nozzle weld. Comparing Figure A.13 to Figure A.15 it is clear that the stresses in the buttered zone are higher than those in the weld, especially near the inner surface. Because of this, circumferential cracks are more likely to develop in the buttered region of the surge line/pressurizer nozzle weld compared with the weld zone.

The axial residual stresses for the Type 304 stainless steel and A516 Grade 70 ferritic steel for the surge line/pressurizer nozzle weld are illustrated in Figures A.16 and A.17, respectively. There is more than a 100 MPa (15 ksi) variation in stress at some locations between the $+2\sigma$ and -2σ variations in tensile properties for these two locations. It is important to note that such stress variations can have a significant effect on stress corrosion crack growth rates because the corrosion crack growth laws are nonlinear. It is important to point out that the axial weld residual stresses in this surge line case studied here are compressive along the ID for the case where there is no ID repair weld. Consequently, other surge line geometries must be considered on a case by case basis since the weld residual stresses depend strongly on the geometry of the bimetal weld.

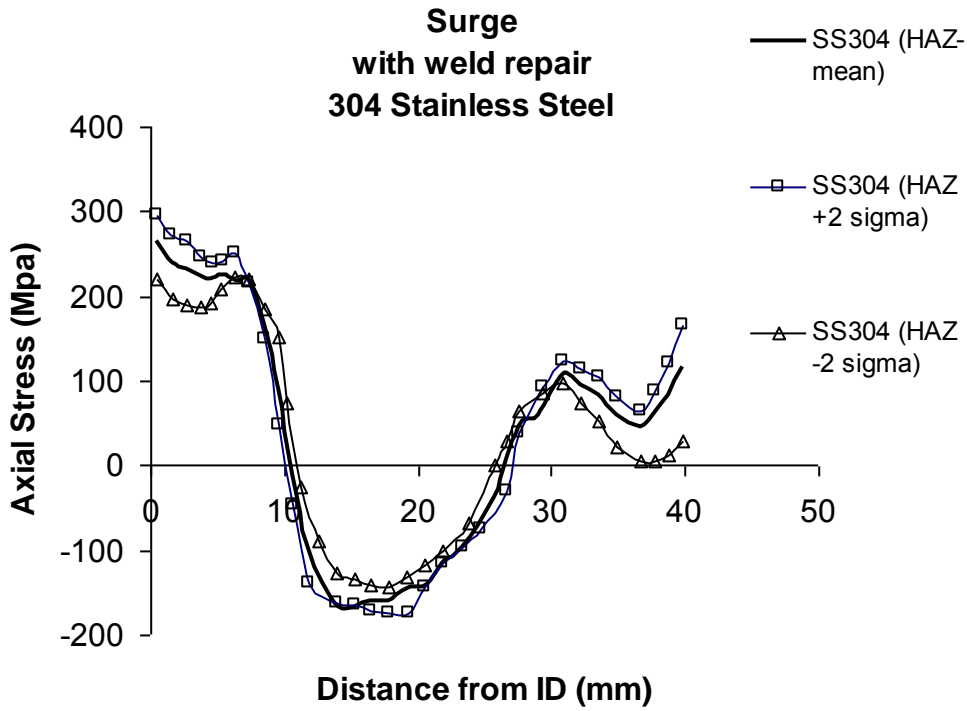


Figure A.16 Surge line/pressurizer nozzle axial weld residual stresses in the Type 304 stainless steel heat affected zone

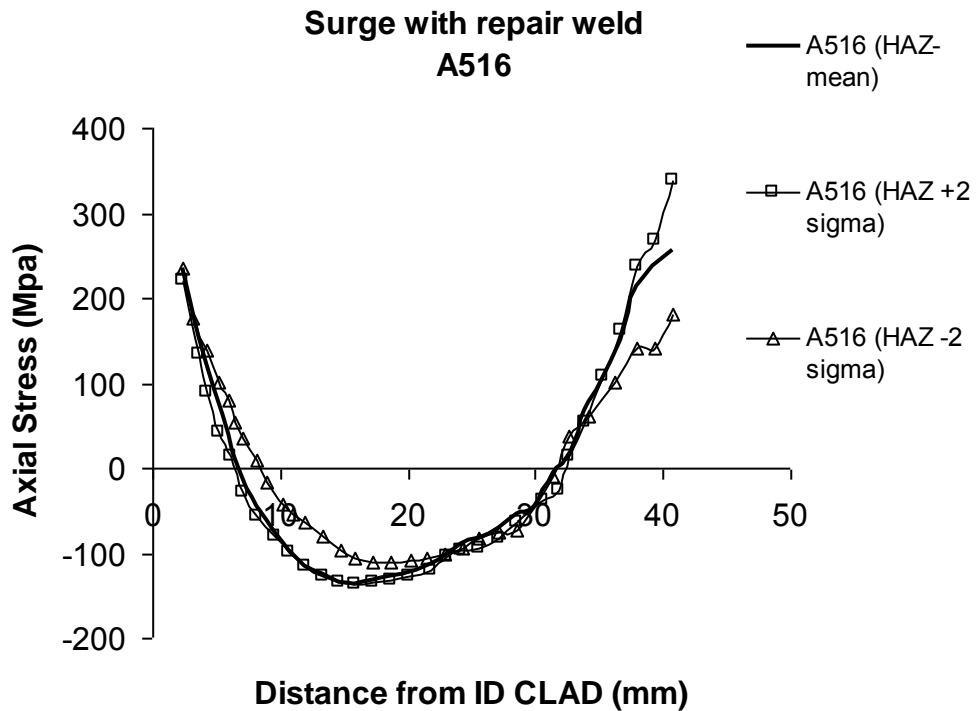


Figure A.17 Axial weld stresses in the surge line/pressurizer nozzle bimetal weld in the A516 Grade 70 material

For the spray line/pressurizer nozzle, which was a very thick geometry ($R/t = 3$), the axial stresses in the weld and butter for the Alloy 182/82 material are shown in Figures A.18 and A.19, respectively. It is seen that the axial stresses are only tensile for the -2σ tensile data near the ID in the weld (Figure A.18) and then the stresses quickly become compressive. A similar trend is observed for the axial stresses in the buttered region, see Figure A.19. This suggests that, for this spray line geometry, circumferential cracks are not expected to develop as a result of only weld residual stresses by themselves. These figures do not include the service load stresses. Recall that an ID repair weld cannot be performed on such a small diameter nozzle to pipe weld. The hoop residual stresses in the weld region are shown in Figure A.20 (similar results occur for the butter region). Axial PWSCC cracks should grow slowly at first.

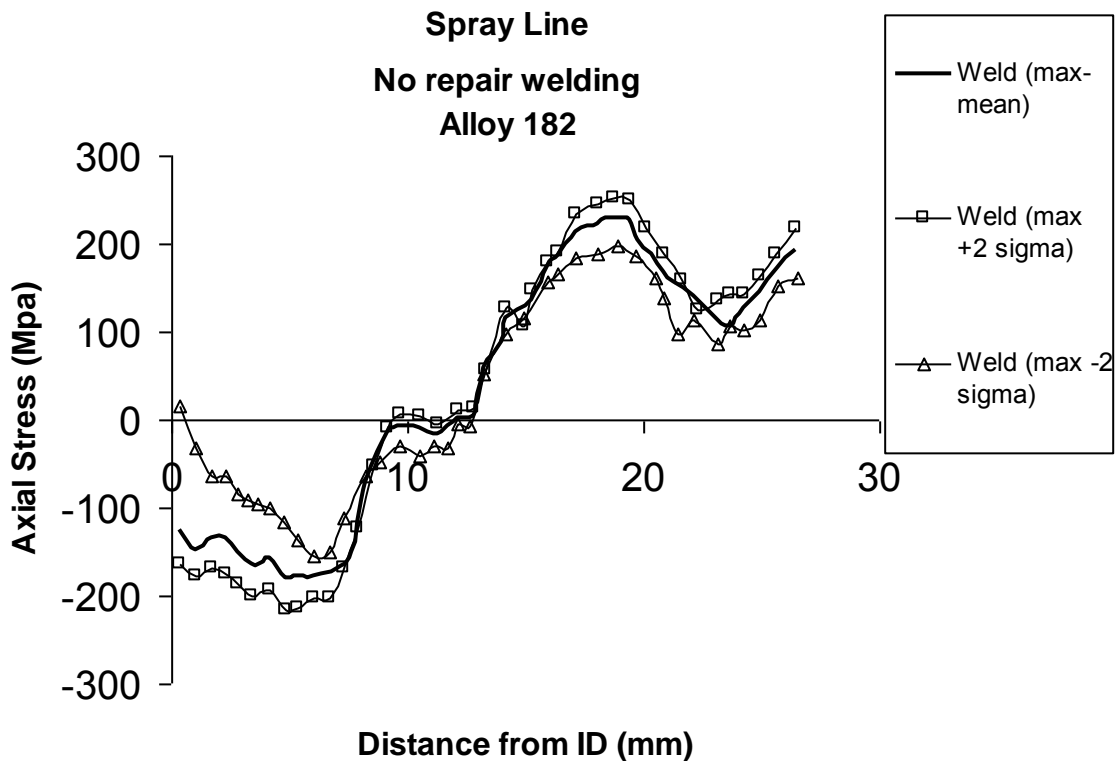


Figure A.18 Axial weld residual stress solutions for pressurizer spray line to pressurizer nozzle dissimilar weld with no ID repair weld along the path through the weld region where the weld residual stresses were the highest for the case where the Alloy 182 weld tensile properties were used

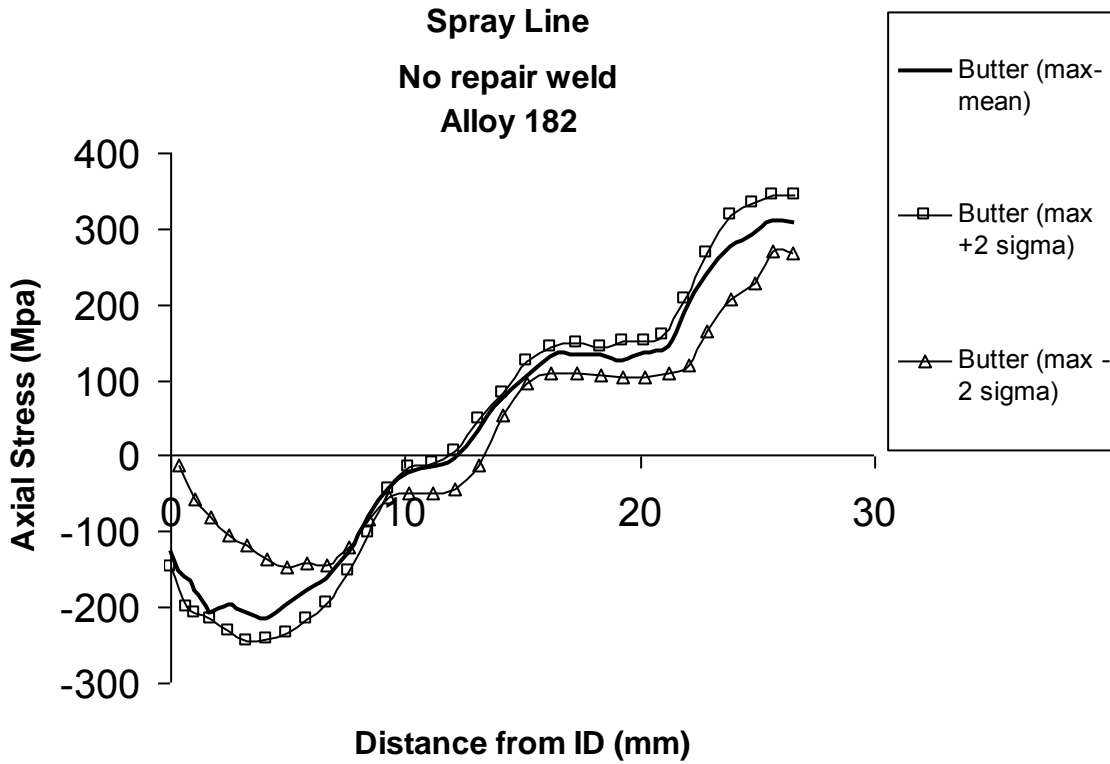


Figure A.19 Spray line axial residual stresses in the buttered zone

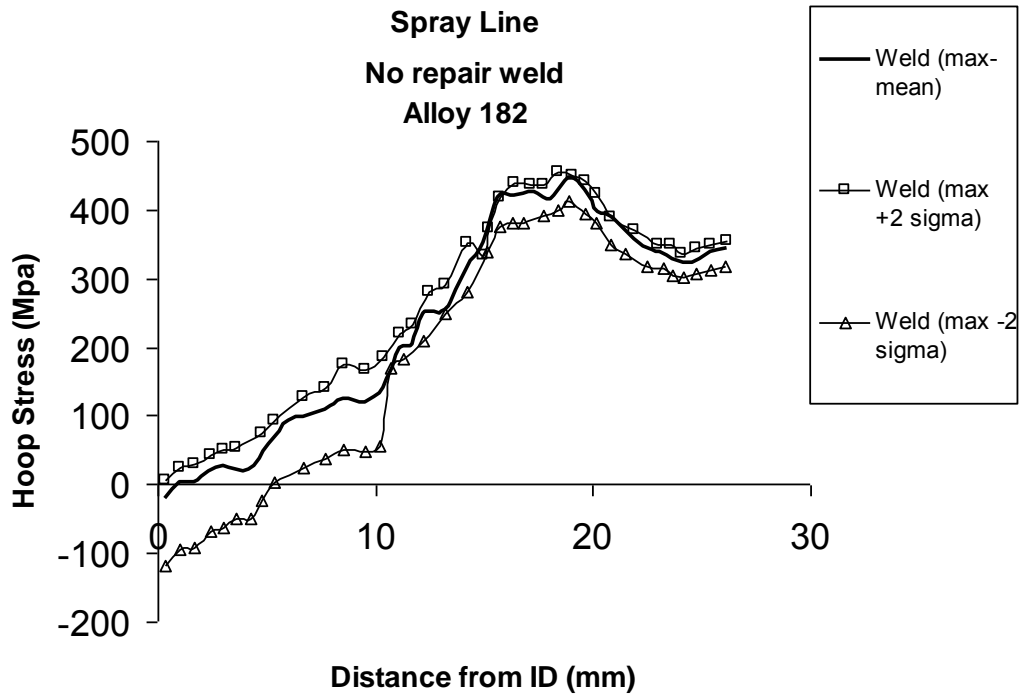


Figure A.20 Hoop residual stresses in weld region of the spray line/pressurizer nozzle weld

The axial weld residual stresses in both the Type 304 stainless steel and the A516 Grade 70 steel are compressive also, indicating SCC crack initiation/growth in these regions is unlikely.

In the PRO-LOCA code, the operating stresses caused by internal pressure and pipe bending loads are superposed on the weld residual stresses. This may not be entirely correct as discussed relative to the stainless steel results discussed next. The future versions of PRO-LOCA will better account for this effect. However, this superposition will most likely give conservative results.

A.4 Stainless Steel Weld Results

Weld residual stress results were also compiled for a rather thick (30 mm [1.18 inch]) pipe made of stainless steel. Only mean property solutions were compiled. The materials used were Type 316 stainless steel and Type 304 stainless steel. The pipe geometry chosen for this study represents a mock up weld that is discussed in detail in Reference A.5. The stainless steel pipe considered here had an inner radius of 285 mm (11.2 inches), outer radius of 315 mm (12.4 inches), a wall thickness of 30 mm (1.18 inches), and a mean radius to thickness ratio of 10. This is a rather thick pipe which leads to a more complicated weld residual stress pattern rather than the 'bending type' residual stresses discussed in Reference A.6. Since all of the bimetal nozzle to pipe welds discussed thus far were also rather thick pipe, it is interesting to compare the residual stresses in a single material weld. An example of the pipe geometry can be seen in Figure A.21.

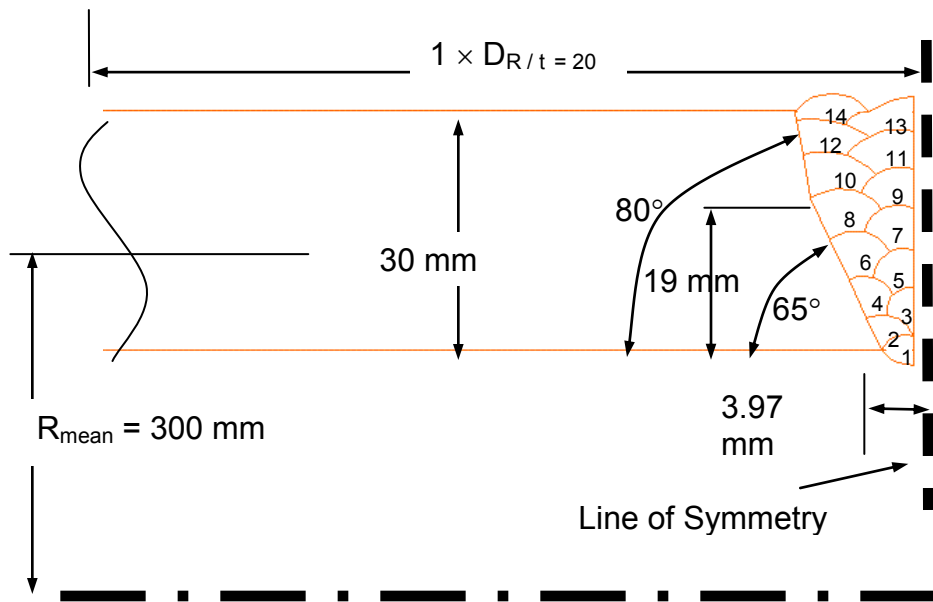


Figure A.21 Geometry of stainless steel pipe

Symmetry through the centerline of the weld was considered here. The temperature dependent material properties for the Type 304 stainless steel are shown in Figure A.4. The properties for the Type 316 stainless steel are shown in Figure A.22. The properties between these two grades

of stainless steel are similar although there are some differences in the yield strengths. The yield stress values for Type 304 stainless steel and Type 316 stainless steel are 254 and 283 MPa (36.8 and 41.0 ksi) at room temperature and 160 and 214 MPa (23.2 and 31.0 ksi) at 288 C (550 F), respectively.

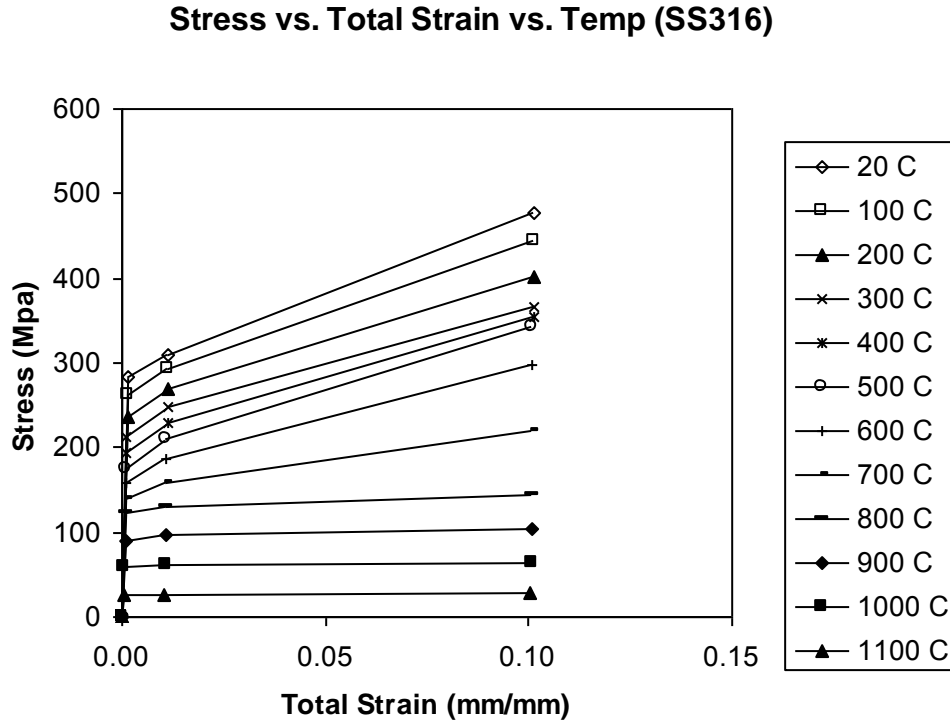


Figure A.22 Temperature dependent material properties for Type 316 stainless steel

In operating nuclear power plant piping systems, the piping system is typically hydro-tested at room temperature before being put into service. The hydro-test is performed at a pressure 1.4 times the normal operating pressure and the effect of end cap tensile pressure must be included. The hydro-test can have the important effect of reducing the weld induced residual stresses. Because the material in the weld and heat affected zone have experienced prior plastic straining due to the weld process, some of these elements already have equivalent stresses above yield due to the weld residual stresses. The hydro-test will further induce additional plastic straining in these elements. When the hydro-test pressure is removed, the stresses can reduce in a fashion analogous to the auto frettage process used sometimes to impart compressive stresses to cannon barrels. The process is more complicated than this discussion and the final residual stress state after hydro-test release depends on many factors related to the weld residual stresses. However, it should be clear that the hydro-test process must be modeled in order to have accurate weld residual stresses.

Figure A.23 shows predicted results at operating temperature (288 C [550 F]) for the proper case of modeling the hydro-test or neglecting this effect. Clearly, much higher stresses exist for the case where the hydro-test was neglected. Notice that these stresses are not in equilibrium since the maximum stress in the HAZ is plotted rather than the stress along a radial plane. The *change* in equivalent plastic strain from the end of welding to the end of the hydro-test (room temperature) is shown in Figure A.24. It is seen that more plastic straining occurs near the ID of

the pipe for this case. This additional plastic strain gradient, superposed on the weld residual stresses is what causes the reduction of residual stresses. The differential plastic strains are what lead to weld residual stresses and the proof that a hydro-test can modify these stresses depending on the situation.

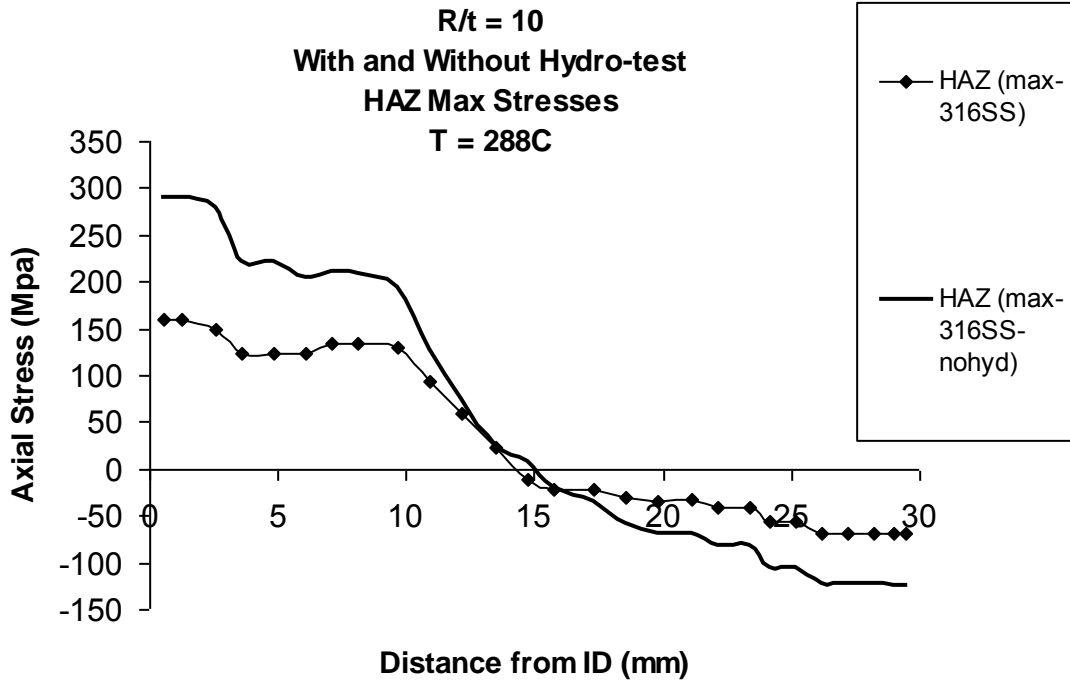


Figure A.23 Comparison of maximum axial weld residual stresses for the cases of with and without modeling the hydro-test (Type 316 stainless steel)

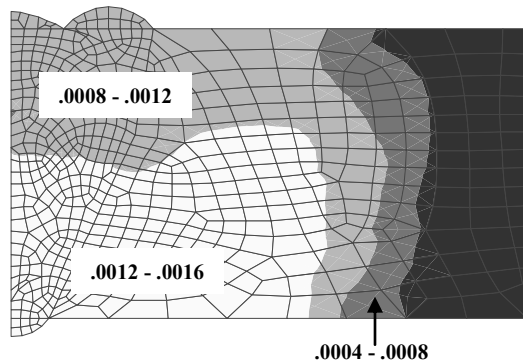


Figure A.24 Change in equivalent plastic strain contours from after welding to after completion of the hydro-test at room temperature

The maximum axial and hoop weld residual stresses for the Type 316 stainless and Type 304 stainless steel pipe in the weld and heat affected zone (HAZ) can be seen in Figures A.25 and A.26, respectively. These results are at operating temperature of 288C (550 F) with no applied load. At present in the PRO-LOCA code weld residual stress solutions are not available for all grades of steel. As such, if an analysis is being performed on a grade of material where the residual stresses are not in the database, an estimate of the residual stresses can be made knowing the ratio of the yield strength of that grade of material to yield strength of a similar grade of material for which weld residual stress data are available. For the two stainless steels considered here, the yield strength ratio $\{(yield\ strength\ of\ Type\ 316\ stainless)/(yield\ strength\ of\ Type\ 304\ stainless)\}$ at 288C (550 F) is 1.33. Figure A.27 shows the estimated results for the Type 316 stainless steel based on weld residual stresses for the Type 304 stainless steel in the HAZ. It is seen that the estimation procedure results in a fairly good approximation of the finite element predicted residual stresses and the predictions are conservative (i.e. the estimate of the Type 316 stainless steel results based on the Type 304 stainless steel results is higher residual stress values than the actual results). However, it is noted that with a probabilistic analysis, which is what PRO-LOCA provides, the deterministic portion of the analysis should be as accurate as possible. If the deterministic results used for a probabilistic assessment already have conservatism inherent in them, then the accuracy of the risk informed numbers are suspect. As such, it is best to have a set of weld residual stress data available for all materials that are of interest. The yield stress ratio estimates will only be used as needed in future versions of the PRO-LOCA code as more residual stress data is compiled.

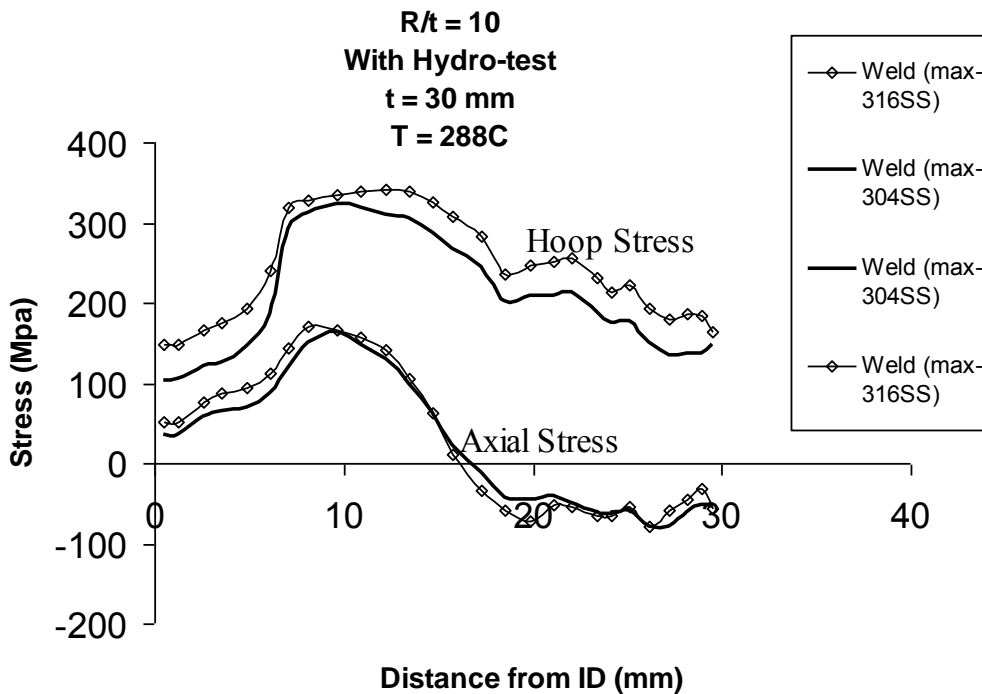


Figure A.25 Axial and hoop residual stresses in the weld for Type 304 and Type 316 stainless steel pipe

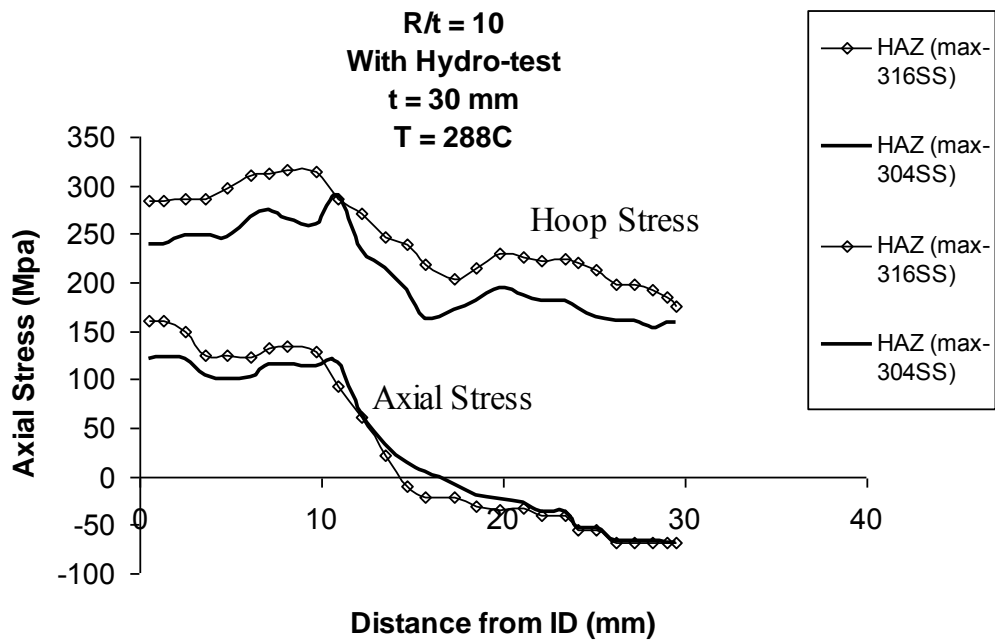


Figure A.26 Axial and hoop residual stresses in HAZ for Type 304 and Type 316 stainless steel pipe

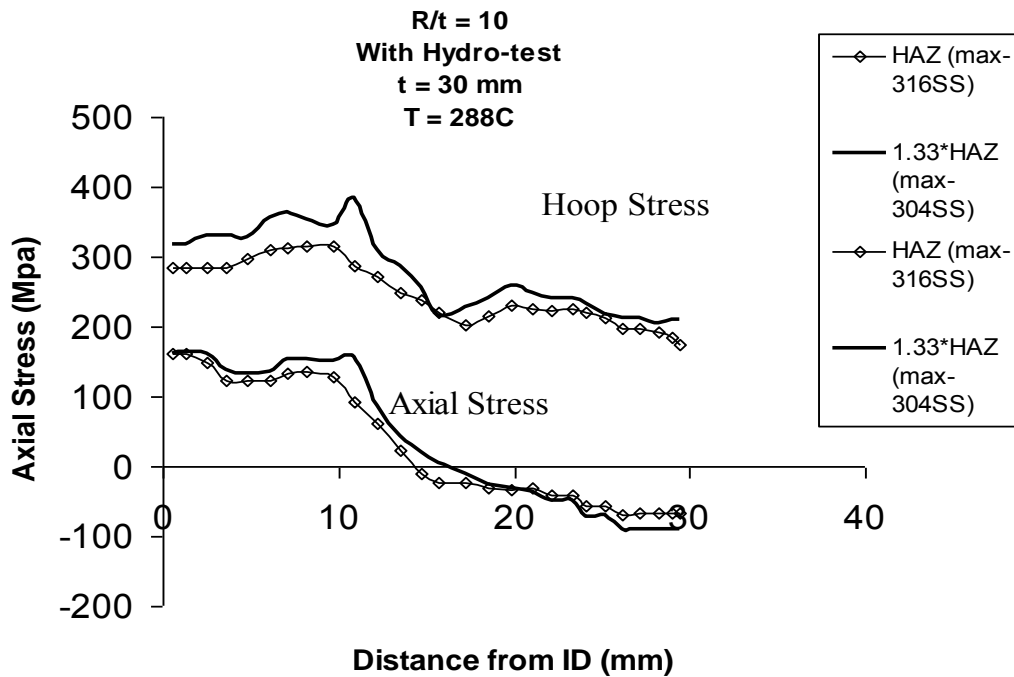


Figure A.27 Comparison of axial and hoop residual stress estimates for the Type 316 stainless steel determined by multiplying the Type 304 stainless steel results by the yield stress ratio (1.33) with the Type 316 stainless steel weld residual stress results from finite element analyses

The stress corrosion crack growth predictions made by the PRO-LOCA code require the stresses caused by the operating loads to be applied over the weld residual stresses. In service these loads arise from internal pressure, bending loads, and possibly thermal expansion and other load sources. The welding process itself leads to a nonlinear plastic strain state in the weld and HAZ regions. When the service loading is applied to the weld residual stress state, the response is not necessarily linear unless the weld residual stresses are quite low or are compressive and the loading stresses induce tension. In the current version of PRO-LOCA, the service load stresses are linearly superposed on the weld residual stresses because the interaction of these stresses is not known for all cases at present. Let us examine how good this estimate is for the Type 316 stainless steel pipe.

Figure A.28 represents the axial and hoop weld residual stresses plotted through the pipe thickness and the corresponding stresses after applying the pressure load. The pressure was applied to the weld model with all prior history included, i.e. the finite element analysis of the pressure was a fully nonlinear analysis which included the full history of the weld analysis. The nominal axial and hoop stresses caused by the pressure alone (15.5 MPa pressure [2,250 psi]) are 68.9 and 137.9 MPa (10.0 and 20.0 ksi), respectively. In Figures A.29 and A.30 the residual stress results from weld only solution were subtracted from the weld plus pressure solution. For fully linear analysis, this difference should be 68.9 and 137.9 MPa (10.0 and 20.0 ksi). Figures A.29 and A.30 show the error inherent in this assumption. For the future versions of PRO-LOCA, this effect will be studied in some detail so that a proper method for including service loads with the weld solution is included.

For the case of the bending stresses, this effect is more complicated and is not addressed here. This effect will be considered in the MERIT program so that more accurate and rational procedures exist in PRO-LOCA for determining the stresses for a stress corrosion cracking analysis.

Figures A.31 shows the effect of a surfaced repair weld on the maximum weld residual stresses in the heat-affected-zone, where IGSCC cracks typically initiate and grow, for Type 304 stainless steel. Figure A.32 is a similar plot except for Type 316 stainless steel. As can be seen from these two figures, the stresses through the inner half of the pipe wall are higher for the case of with repair weld than they are for the case of without the repair weld. Similar results were obtained for the maximum stresses in the weld zone.

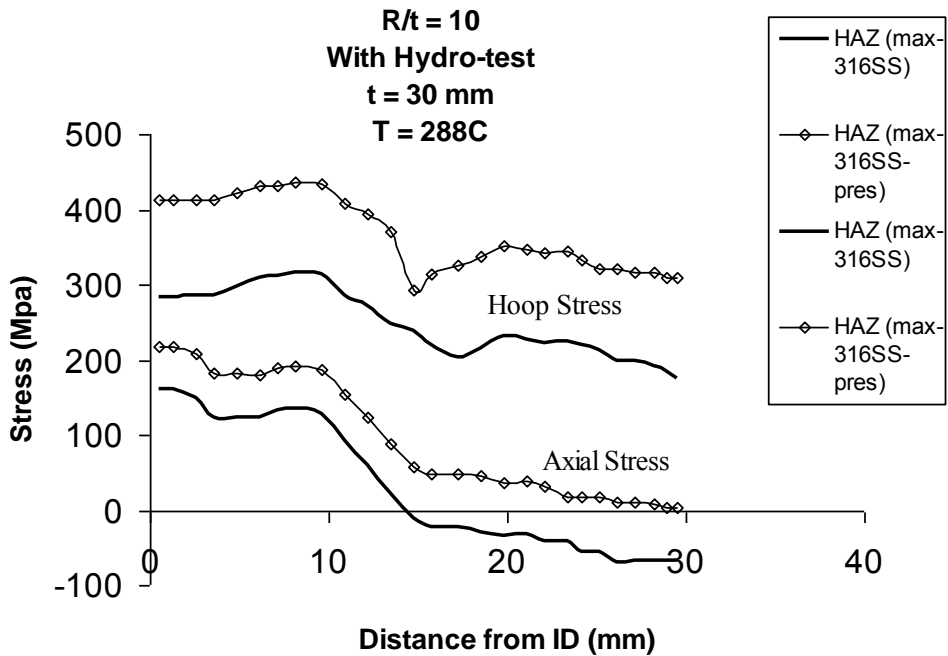


Figure A.28 Stresses in the Type 316 stainless steel pipe at 288 C (550 F). The solid curve represents the axial and hoop stresses from welding only. The diamond marked curves represent the operating stresses for pressure loading only

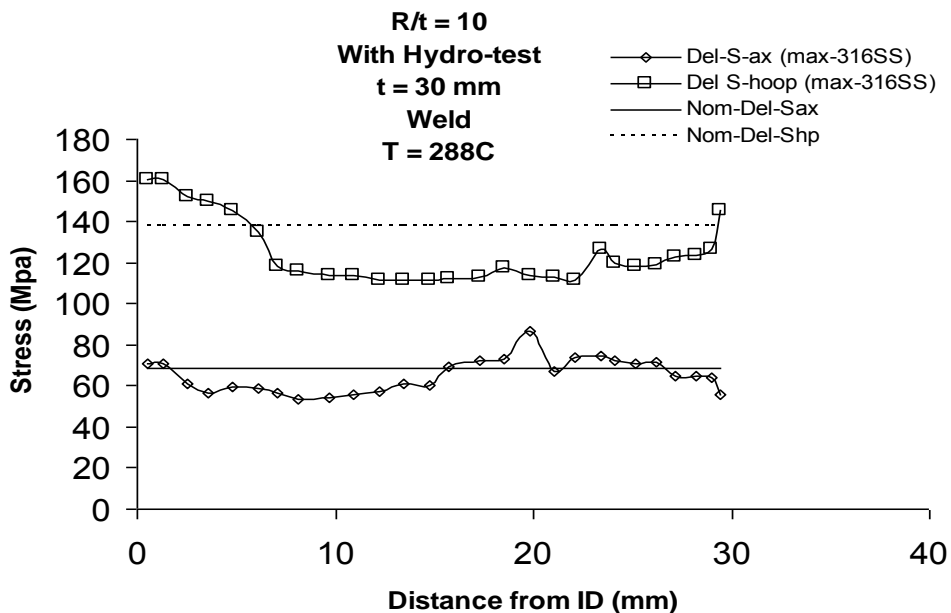


Figure A.29 The difference in stress between the weld plus pressure solution and the weld only solution in the weld

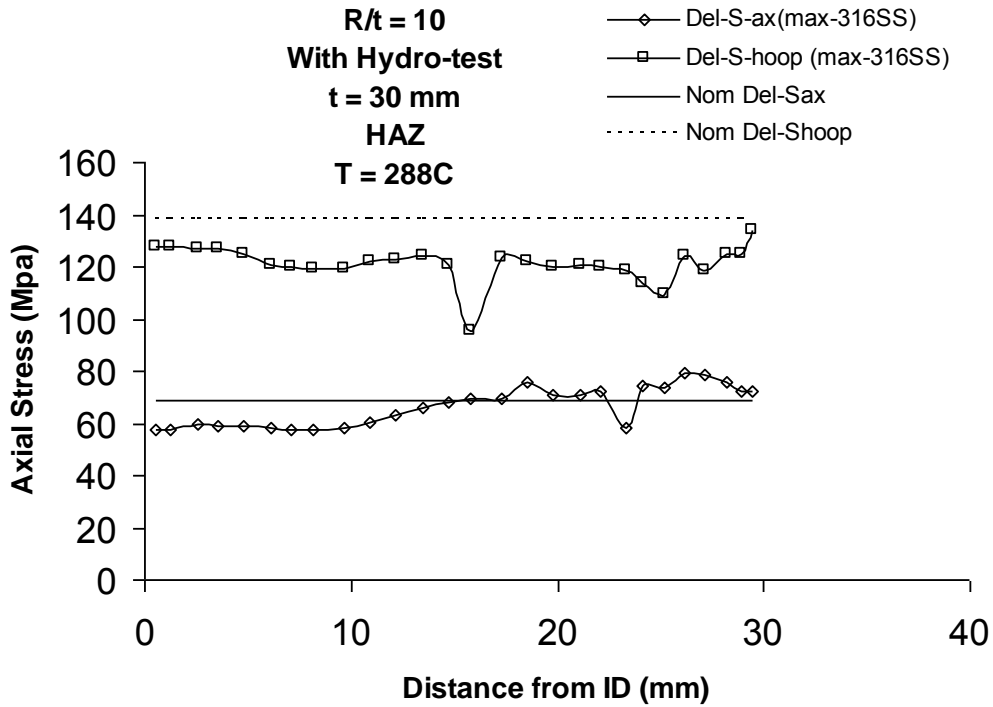


Figure A.30 The difference in stress between the weld plus pressure solution and the weld only solution in HAZ

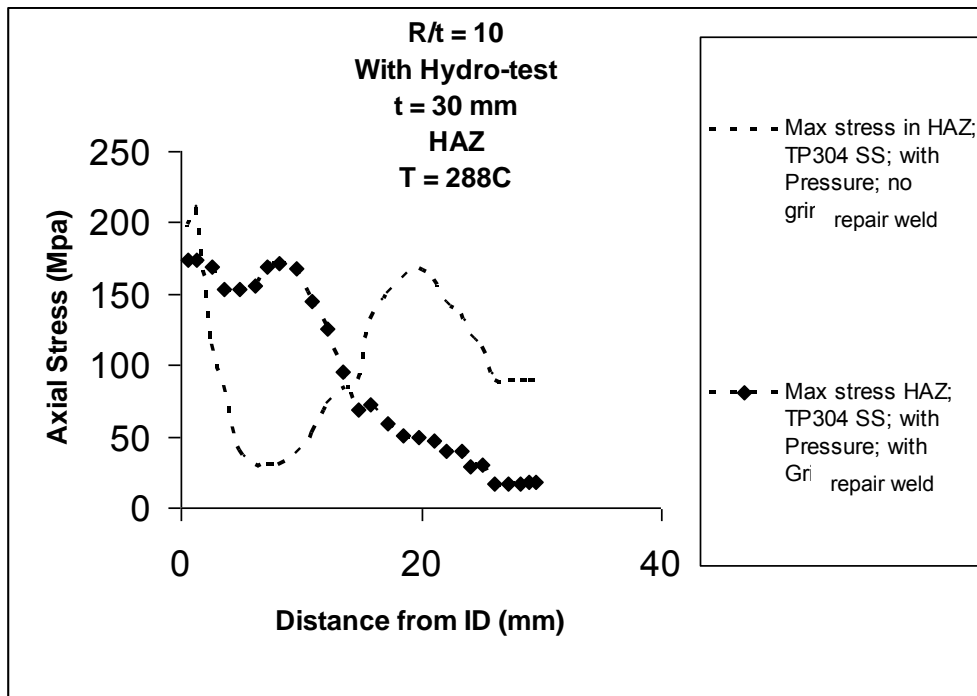


Figure A.31 Plot of maximum residual stress in HAZ for Type 304 stainless steel for cases of with and without ID repair weld

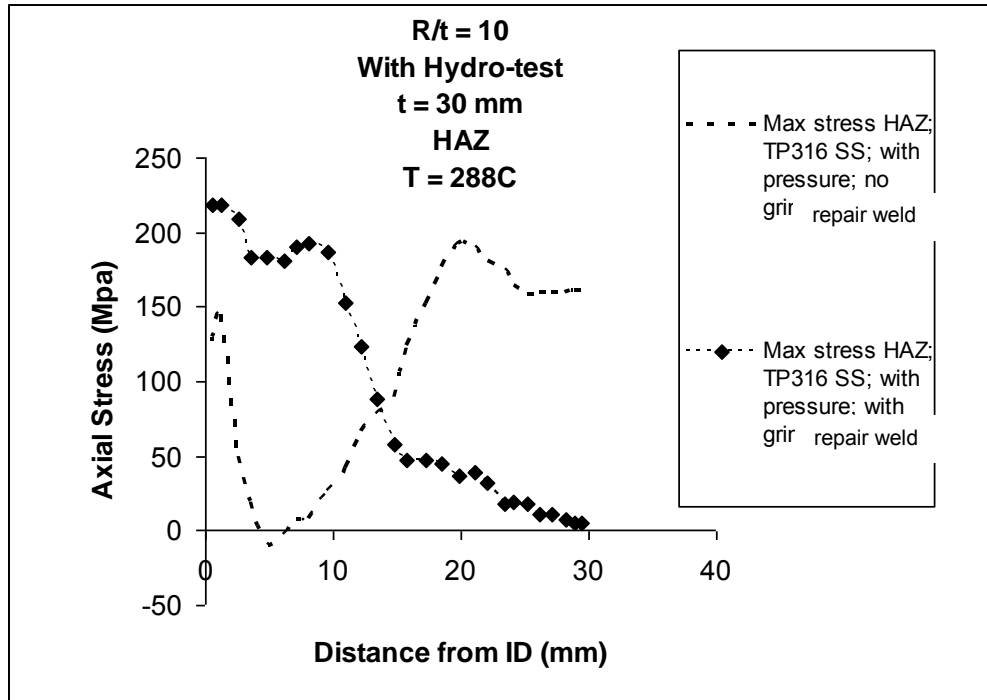


Figure A.32 Plot of maximum residual stress in HAZ for Type 316 stainless steel for cases of with and without ID repair weld

A.5 Summary of Results

A couple of points are worth noting from these results. For one, in looking at the weld residual stress values, there does not appear to be a large effect of the tensile properties on the residual stresses. However, it must be kept in mind that the statistical variation of the tensile properties in the Alloy 182 weld metal is not realistic because the data sample was only three tests and it was for Alloy 625 rather than Alloy 182/82 weld metal of concern here. However, even a 100 MPa (15 ksi) difference in stress between the +2 and -2 standard deviation data can have a marked effect on SCC growth rates since the laws are nonlinear. Secondly, the buttered region of the hot leg/RPV weld tends to have higher residual stresses than the weld region, especially on the ID surface, which are the stresses that will most contribute to crack initiation. Similar findings were apparent for other dissimilar weld cases. Third it can be seen that grinding out the last weld pass and re-welding results in higher residual stresses than the case where no repair weld is performed. Fourth, it can be seen that the weld residual stresses for the inner third of the wall thickness for the spray line to pressurizer nozzle weld remain compressive so that one may not expect cracks to initiate for this geometry from a stress corrosion cracking mechanism. Finally note that in many cases it appears that equilibrium is not satisfied. This is an artifact of the fact that the residual stresses are not for the same cross section through the weld or through the heat-affected zone. Instead, these figures show the maximum stress across the weld or heat-affected zone at various

normalized distances from the inside surface, where the distances are normalized to the wall thickness.

For inclusion into the PRO-LOCA the axial weld residual stress data were curve fit to the expression shown in Equation A.1. Equation A.1 shows the residual stresses normalized by the yield strength as a function of the normalized distance from the inside surface, where the normalizing parameter is the wall thickness of the component. Table A.1 shows the coefficients from the curve fitting exercise that are currently incorporated into PRO-LOCA. Figure A.33 is a plot of the normalized stresses as a function of the normalized distance from the inside surface.

$$\frac{\sigma_{WRS}}{\sigma_y} = \frac{\sigma_0}{\sigma_y} + \frac{\sigma_1}{\sigma_y} \left(\frac{x}{t} \right) + \frac{\sigma_2}{\sigma_y} \left(\frac{x}{t} \right)^2 + \frac{\sigma_3}{\sigma_y} \left(\frac{x}{t} \right)^3 + \frac{\sigma_4}{\sigma_y} \left(\frac{x}{t} \right)^4 \quad (\text{A.1})$$

where,

- σ_{WRS} = Weld residual stress,
- σ_y = Yield strength,
- $\sigma_0, \sigma_1, \sigma_2, \sigma_3,$ and σ_4 = Curve fitting coefficients, and
- x/t = Normalized distance from inside surface.

It should be noted that in this version of PRO-LOCA the variability in the welding residual stress is only addressed by the variability of the yield strength of the material. From the results presented in this section of the report, the actual variability may be larger than predicted with just the material variability.

From Figure A.33, the highest normalized stresses on the inside surface are for the surge line nozzle bimetal weld with ID repair weld and hot leg/RPV weld with ID repair weld. The surge line nozzle and hot leg/RPV weld stresses are slightly higher on the inside surface than the stainless steel weld with repair weld stresses, but they dissipate much quicker through the thickness than do the stainless steel weld with repair weld stresses. As discussed previously, it can be seen from Figure A.33 that the residual stresses through the inner half of the pipe wall are higher for the cases where ID repair welding was performed than the cases where it was not.

Table A.1 Coefficients from the curve fitting exercise used in PRO-LOCA

Weld Case Description	σ_0/σ_y	σ_1/σ_y	σ_2/σ_y	σ_3/σ_y	σ_4/σ_y	σ_y , MPa
Hot leg - Alloy 182 weld at 324 C (615F), using maximum stress in buttered region	0.75	-9.271	27.71	-32.91	14.98	213.3
Hot leg - Alloy 182 weld at 324 C (615F), using maximum stress in butter region, 15% ID repair weld	1.3	-1.084	-33.19	73.31	-39.38	213.3
Surge line - Alloy 182 weld at 324 C (615F), 15% ID repair weld	1.728	-5.494	-10.65	32.05	-16.53	213.3
Spray line - Alloy 182 weld at 324 C (615F), no ID repair weld	-0.5	-6.427	33.16	-41.32	15.73	213.3
Stainless steel weld at 288 C (550F), using maximum stress in HAZ, no ID repair weld	1.00	-14.04	48.04	-56.32	21.47	160.3
Stainless steel weld at 288 C (550F), using maximum stress in HAZ, ID repair weld	0.800	0.485	-5.007	3.314	0.00	160.3

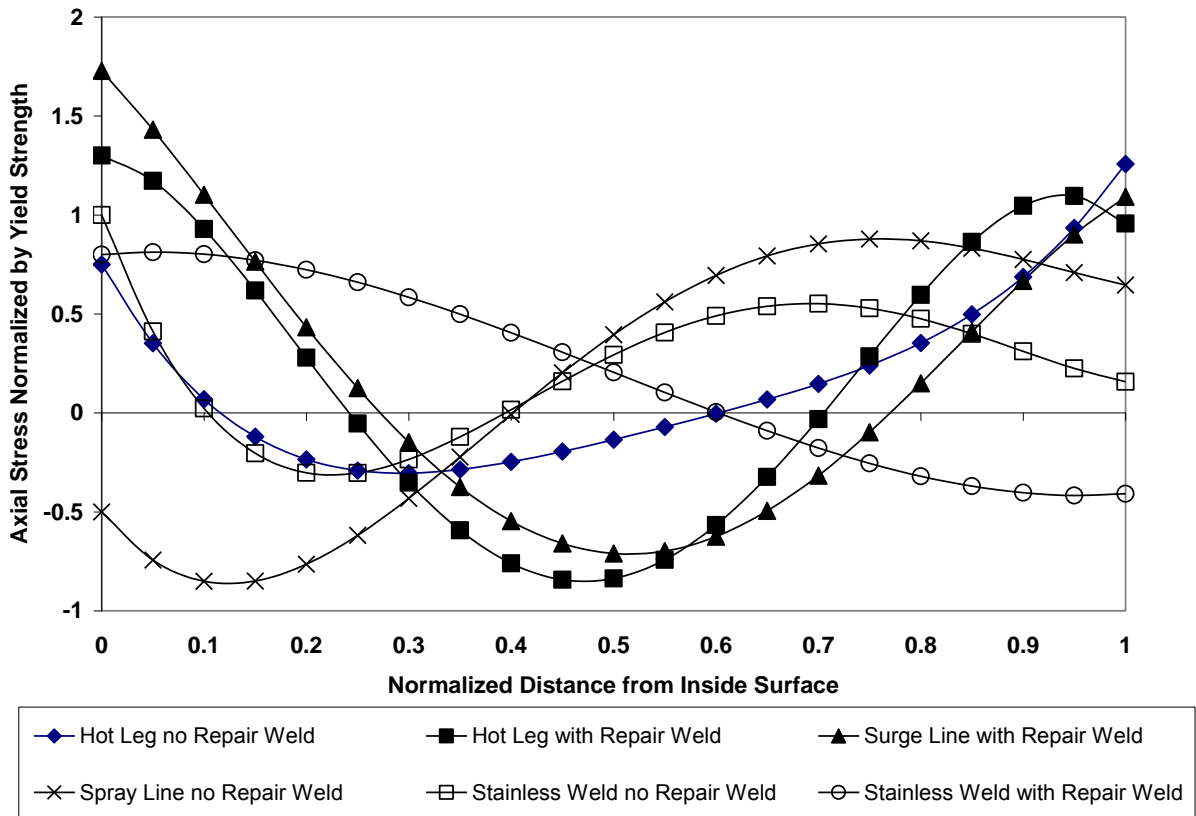


Figure A.33 Plot of the normalized stresses as a function of the normalized distance from the inside surface

A.6 References

- A.1 User Manual for VFT – Virtual Fabrication and Weld Modeling Software by Battelle Memorial Institute and Caterpillar Inc., February 2005.
- A.2 Oh, J., and Brust, F. W., ‘Phase Transformation Effects on Weld Distortion and Residual Stress Predictions’, in Proceedings of PVP2005, 2005 ASME Pressure Vessels and Piping Division Conference, July 17-21, 2005, Denver, Colorado USA, In *Welding and Residual Stresses*, edited by O’Dowd, N., Brust, F. W., Keim, E., Sherry, A., and Dong, P.
- A.3 Brust, F. W., Yang, Y. Y., Ezeilo, A., and McPherson, N., ‘*Weld Modeling of Thin Structures With VFT*’, Proceedings of ASME Pressure Vessel and Piping Conference, San Diego, CA, July, 2004, in *Residual Stress, Fracture, and Stress Corrosion Cracking*, Principal Editor, Y. Y. Wang, 2004.
- A.4 Brust, F. W., Scott, P. M., and Yang, Y., ‘*Weld Residual Stresses and Crack Growth in Bimetallic Pipe Welds*, Proceedings of SMIRT 17, Prague, Czech Republic, August, 2003.
- A.5 P. Scott, R. Olson, J. Bockbrader, M. Wilson, B. Gruen, R. Morbitzer, Y. Yang, Williams, F. W. Brust, L. Fredette, N. Ghadiali, G. Wilkowski, D. Rudland, Z. Feng, R. Wolterman, ‘The Battelle Integrity of Nuclear Piping (BINP) Program Final Report’, NUREG/CR 6837, Volumes I and II, June, 2005.
- A.6 Brust, F. W., and Dong, P., —‘Welding Residual Stresses and Effects on Fracture in Pressure Vessel and Piping Components: A Millennium Review and Beyond’, Transactions of ASME, Journal Of Pressure Vessel Technology, Volume 122, No. 3, August 2000, pp329-339.

APPENDIX B

OTHER MERIT DELIVERABLES

The major deliverable from MERIT was PRO-LOCA, along with its GUI (graphical user interface) and Users Manual. In addition to PRO-LOCA, the other MERIT deliverables include an updated version of the SQUIRT leak rate code and two databases, (1) an updated CIRCUMCK pipe fracture experiment database and (2) a leak rate experiment database, LEAKRATE.

B.1 Updated SQUIRT Leak Rate Code

As part of the MERIT program the SQUIRT leak rate code was updated. The major change was the addition of a transition flow model to address the flow regime between the single phase orifice flow model incorporated in SQUIRT and the two phase Henry-Fauske model. This transition flow model is described in detail in Section 2.11.1 of this report. This transition flow model is only included in the SQUIRT2 option if SQUIRT. It is not included in the SQUIRT4 option. Some of the other minor changes made to SQUIRT include:

- Added a message to inform the user if they input a path loss coefficient (number of turns) of zero. The message informs the user that the code has automatically changed the path loss coefficient from 0.0 to 0.01.
- Added air fatigue as a default option for defining the crack morphology parameters.
- Added a warning message that if the hydraulic diameter to global roughness is less than 3.65, then the user should use crack-opening displacement (COD) dependent crack morphology parameters.
- Added a note to the Thermal Hydraulics Option screen that when using a crack length based on units of length (inches or mm), then that length is at the mean diameter.
- Added the option whereby the user can append the output to an existing file.
- Added a note on the Thermal Hydraulics Input Parameters screen as to what the discharge coefficient should be and what it means.

B.2 Databases

A number of existing databases developed as part of the Short Cracks in Piping and Piping Welds program (e.g., CIRCUMCK, AXIAL_CK, etc.) were converted from Lotus 1-2-3 files to Excel files. In addition, additional circumferentially cracked pipe fracture data from India obtained from an open literature search were added to the CIRCUMCK database.

Also, a new database (LEAKRATE) was developed. LEAKRATE includes data from a number of leak rate measurement experimental programs conducted worldwide. In addition to the experimental data, the LEAKRATE database includes data from published crack morphology parameters for air fatigue, corrosion fatigue, IGSCC, and PWSCC cracks. LEAKRATE also includes sample photomicrographs for each of these cracking mechanisms.



2010:46

The Swedish Radiation Safety Authority has a comprehensive responsibility to ensure that society is safe from the effects of radiation. The Authority works to achieve radiation safety in a number of areas: nuclear power, medical care as well as commercial products and services. The Authority also works to achieve protection from natural radiation and to increase the level of radiation safety internationally.

The Swedish Radiation Safety Authority works proactively and preventively to protect people and the environment from the harmful effects of radiation, now and in the future. The Authority issues regulations and supervises compliance, while also supporting research, providing training and information, and issuing advice. Often, activities involving radiation require licences issued by the Authority. The Swedish Radiation Safety Authority maintains emergency preparedness around the clock with the aim of limiting the aftermath of radiation accidents and the unintentional spreading of radioactive substances. The Authority participates in international co-operation in order to promote radiation safety and finances projects aiming to raise the level of radiation safety in certain Eastern European countries.

The Authority reports to the Ministry of the Environment and has around 270 employees with competencies in the fields of engineering, natural and behavioural sciences, law, economics and communications. We have received quality, environmental and working environment certification.

Strålsäkerhetsmyndigheten
Swedish Radiation Safety Authority

SE-171 16 Stockholm
Solna strandväg 96

Tel: +46 8 799 40 00
Fax: +46 8 799 40 10

E-mail: registrator@ssm.se
Web: stralsakerhetsmyndigheten.se